DISSOLVED ORGANIC MATTER DYNAMICS FROM RIVERS TO THE SHELF SEA IN EAST ANGLIA (UK)

Chiara Cooper

Thesis submitted in fulfilment of the requirements
for the degree of Doctor of Philosophy

School of Environmental Sciences
University of East Anglia

August 2022

“Earth may be alive: not as the ancients saw her -a sentient Goddess with a purpose and foresight- but alive like a tree. A tree that quietly exists, never moving except to sway in the wind, yet endlessly conversing with the sunlight and the soil. Using sunlight and water and nutrient minerals to grow and change. But all done so imperceptibly, that to me the old oak tree on the green is the same as it was when I was a child.”

James Lovelock

I dedicate this thesis to my beloved rats past and present, who made this journey more enjoyable and whose love at the end of the day melts away any worry or difficulty.

I also dedicate it to my husband for being by my side at every step of the journey and for his invaluable emotional and practical help.

Abstract

Dissolved organic matter (DOM) plays an important role in the global carbon and nutrient cycles. DOM is one of the largest carbon pools, taking up and releasing carbon to and from the atmosphere, whilst also containing essential nutrients for the synthesis of organic molecules. In recent years, there has been an increasing number of studies on DOM transport across the land-to-ocean aquatic continuum, recognising the interconnection between terrestrial and marine ecosystems. Despite this, there remain major gaps in our understanding of DOM processing and dynamics as it is transported from rivers to seas, in particular the impact of tidal cycles and instream processing upon DOM composition and the fate of riverine DOM once it reaches the sea.

Through a combination of hourly to monthly-resolution sampling of two East Anglian rivers (River Yare and River Waveney) and the southern North Sea between November 2018 and July 2020, 309 water samples were collected and analysed for a range of variables (fluorescence spectra and indices, coloured DOM absorption, nutrients, chlorophyll-a, suspended solids) to determine DOM composition and dynamics.

Results revealed that the River Waveney (dominated by surface runoff) was characterised by terrestrial and biodegraded DOM, whilst DOM in the River Yare (groundwater dominated) was produced *in-situ*. In the estuary, DOM was biodegraded, photodegraded, adsorbed to the sediments, or released into the water column by tidal-induced sediment resuspension. Whilst dissolved organic carbon (DOC) was found to behave non-conservatively during some months, overall, DOC was transported conservatively through the rivers, whilst inorganic nitrogen was removed, and organic phosphorus was produced. The estuary exported a total of 3.20 ± 1.81 Gg yr^{-1} of DOC, 1.26 ± 0.89 Gg yr^{-1} of total dissolved nitrogen and 0.13 ± 0.06 Gg yr^{-1} of total dissolved phosphorus to the shelf sea, with 67.5% of DOM of terrestrial origin (3.09 ± 1.87 Gg yr^{-1}) and 32.5% produced and remineralised *in-situ* (1.49 ± 0.90 Gg yr^{-1}). After entering the North Sea, riverine DOM mixed with seawater, was photodegraded and biodegraded throughout the year until the terrestrial signature was lost offshore. In spring and summer, DOM was produced *in-situ* possibly due to riverine nutrient input.

Collectively, these results improve our understanding of DOM dynamics across the land-to-ocean continuum, providing important information to enhance biogeochemical modelling and predictions of climate change impacts upon carbon exported from land to the ocean.

Table of contents

List of Figures

List of Tables

Glossary

BCP	Biological carbon pump
BDOM	Bioavailable DOM
BFI	Baseflow Index
BGS	British Geological Society
BIX	Freshness Index
C	Carbon
C 1 – 6	Component 1 – 6
$CaCO_3$	Calcium carbonate
CDOM	Coloured dissolved organic matter
CEH	Centre for Ecology and Hydrology
CEND	Cefas Endeavour
CFA	Continuous Flow Analyser
Chla-*a*	Chlorophyll-*a*
CNC	Central North Sea Current
CO	Carbon monoxide
CO_2	Carbon dioxide
CP	Carbonate pump
CRM	Certified Reference Material
CSOs	Combined Sewer Overflows
CTD	Conductivity Temperature Depth
CV	Coefficient Variation
DC	Dooley Current
DCAA	Dissolved combined amino acids
DF	Degrees of Freedom
DIC	Dissolved inorganic carbon
DIN	Dissolved inorganic nitrogen
DIP	Dissolved inorganic phosphorus
DOC	Dissolved organic carbon
DOM	Dissolved organic matter
DON	Dissolved organic nitrogen
DOP	Dissolved organic phosphorus
EAP	East Anglia Plume
EEMs	Excitation-Emission Matrices
ER	Extracellular release
Ex/Em	Excitation / Emission
FC	Fair Isle Current
FDOM	Fluorescent dissolved organic matter
FI	Fluorescence Index
HDPE	High-density polyethylene
HIX	Humification Index
HMW	High molecular weight
HTCO	High-Temperature Catalytic Oxidation
ICOS	Integrated Carbon Observation System
iDOM	invisible DOM
IPCC	Intergovernmental Panel on Climate Change
KHP	Potassium hydrogen phthalate
KH_2PO_4	Potassium dihydrogen orthophosphate
KNO_3	Potassium nitrate
LOAC	Land-to-ocean continuum
LMW	Low molecular weight
MCP	Microbial carbon pump
MW	Molecular weight
N	Nitrogen
$NaNO_2$	Sodium nitrite

$NaNO_3$	Sodium nitrate
$Na_4P_2O_7$	Sodium pyrophosphate
$Na_5P_3O_{10}$	Sodium tripolyphosphate
NH_4	Ammonium
NH_4Cl	Ammonium chloride
$((NH_4)_2SO_4)$	ammonium sulphate
NMR	Nuclear Magnetic Resonance
NNR	National Nature Reserve
NO	Nitric oxide
NO_2	Nitrite
NO_3	Nitrate
NOM	Natural organic matter
NPOC	Non-Purgeable organic carbon
NRFA	National River Flow Archive
O_3	Ozone
P	Phosphorus
PAR	Photosynthetically Active Radiation
PARAFAC	Parallel Factor
PC	Principal Component
PCA	Principal Component Analysis
PIC	Particulate inorganic carbon
PMT	Photomultiplier tube
PO_4	Phosphate
POC	Particulate organic carbon
POM	Particulate organic matter
RCF	Relative Centrifugal Force
$RDOC_c$	Refractory dissolved organic carbon dependent on concentration
$RDOC_t$	Refractory dissolved organic carbon dependent on environmental context
RDOM	Recalcitrant dissolved organic matter
RMSE	Root Mean Squared Error
RV	Research Vessel
S	Spectral Slope
SAC	Special Area of Conservation
SC	Scottish coastal Current
SC 1 – 5	Sea Component 1 – 5
SD	Standard Deviation
SNC	Southern North Sea Current
SOP	Standard Operating Procedure
SP	Solubility pump
SPA	Special Protection Area
S_R	Spectral ratio
SSE	Sum of Squares Errors
SSS	Stock Standard Solution
SSSI	Site of Special Scientific Interest
SUVA	Specific UV Absorbance
TC 1 – 6	Tidal Component 1 – 6
TCC	Tucker Congruence Coefficient
TDN	Total dissolved nitrogen
TDP	Total dissolved phosphorus
TN	Total nitrogen
TOC	Total organic carbon
TSS	Total suspended solids
UTC	Universal Time Coordinated
UV	Ultraviolet
VIS	Visible
VLMW	Very low molecular weight
VOC	Volatile organic compounds

Acknowledgments

Firstly, I want to thank my five supervisors who supported me through this journey. I have learnt a lot from you, and I would not be at this point without all of you. Thanks to Dorothee Bakker for her invaluable guidance which kept me on point and for her encouragement to trust my work. I am grateful to Naomi Greenwood and Silke Kröger for their priceless advice and comments on this project. Thanks to Carol Robinson who was the last to join my supervisory team but whose knowledge and inputs were highly appreciated. I am thankful for the invaluable help from Andrew Mayes and his expertise which helped me navigate the waters of UV-visible and fluorescence spectroscopy.

To my sampling partner Richard Cooper, a heartfelt appreciation for our mini adventures on the Broads, for all the Sundays donated to me to collect water samples that have made this thesis possible.

A huge thank you to Tony Hinchcliffe, Rob Utting, Nick Garrard and Andy Macdonald for their time and assistance in the lab.

I am also very grateful for all the staff at Cefas that collected a great number of samples for me and without which my thesis would be less complete.

I want to express my gratitude to the organisers and the people of the Silent Zoom Writing Group (SZWG) and the Virtual Writing Retreat (WVR). Their company made me accountable, and it made the thesis writing more enjoyable and less of a 'mission impossible'.

Thanks also to Emma Cassar, an office mate become a dear friend amidst the joys and pains of the PhD, and to all the people I met along the way and with whom I shared a chat or a laugh and for those who taught me something, making this journey even more valuable.

Finally, I want to send appreciation and gratitude to my parents and my little sister who supported me all along, knowing too well that they would rarely see me during these long years.

Thank you for all of you that will make me remember my PhD journey with a smile!

Chapter 1

Introduction

Dissolved organic carbon (DOC), a major component of dissolved organic matter (DOM), is an important piece of the global carbon cycle and one of the largest carbon pools, constantly transferring to and from the atmosphere (Hansell and Orellana, 2021). DOM is highly important also for aquatic ecosystems as it regulates ecological processes (e.g. protecting organisms from UV radiation, affecting the pH, source of nutrients, influencing the depth of the solar radiation, etc) (Aiken, 2014; Stedmon and Nelson, 2015). The biogeochemical cycle of carbon involves its transfer between atmosphere, ocean, land and organisms by forming different inorganic and organic compounds. Terrestrial and marine systems play an important role in capturing and fixing carbon dioxide (CO_2), with 31% of atmospheric CO_2 fixed by land between 2010 – 2019, compared to 23% taken up by the ocean (Canadell et al., 2022). Until recently, terrestrial and marine ecosystems have been studied as separate entities and their interconnection is poorly understood (Xenopoulos et al., 2017; Regnier et al., 2022). This connection allows carbon to move from the land to the sea through rivers, estuaries and wetlands, with inland waters receiving ~ 2.9 Pg C yr^{-1} (Regnier et al., 2013) (Figure 1.1), and contributing to the lateral transport of a sizeable part of DOC into the coastal ocean (~ 0.2 Pg yr^{-1}) (Regnier et al., 2013; Painter et al., 2018), compared to 7 Pg yr^{-1} and 30 Pg yr^{-1} of DOC produced in the coastal and open ocean, respectively (Stein and Macdonald, 2004).

The interrelation between terrestrial and marine ecosystems is defined as the land-to-ocean aquatic continuum (LOAC) (Figure 1.1) and its importance has been recognised in the fifth assessment report of the Intergovernmental Panel on Climate Change (IPCC) (Ciais et al., 2014). This included the calculation of carbon fluxes from inland waters to the ocean in the global carbon budget. In addition, it was recognised that the carbon flux exchanged between terrestrial ecosystems and the atmosphere is also affected by processes occurring in inland waters and not only solely attributable to vegetation (Solomon et al. 2007; Ciais, et al., 2014). Bauer and Bianchi (2011) postulated that although the global flux of DOC and POC is not comparable in terms of size to that of other major global carbon fluxes (e.g., primary production and respiration), if the gross and net riverine export to the ocean are similar, then this would be comparable to the other net global carbon fluxes.

Depending on the source of DOM into inland waters, its characteristics, chemical properties, bioavailability, and the degree of degradability may change. In addition, depending on the aquatic environment transporting DOM, its biodegradability and

photodegradability as well as its reactivity can also change. As DOM is transported from rivers to the sea, DOM can be very labile (with a turnover of minutes to weeks) or semi-labile (turnover of months to years) (Carlson and Hansell, 2015), resulting into modifications of carbon pools, however small or big, with implications to the carbon cycle (Fellman et al., 2009; Lapierre and del Giorgio, 2014; Wurtsbaugh et al., 2019; Yang et al., 2022).
Despite the recognition of the active role of inland waters in the global carbon cycle, there are large gaps in our understanding of the magnitude and processes of carbon fluxes from land to sea, as well as a lack of high temporal and spatial resolution data covering the entirety of the LOAC (Regnier et al., 2022).

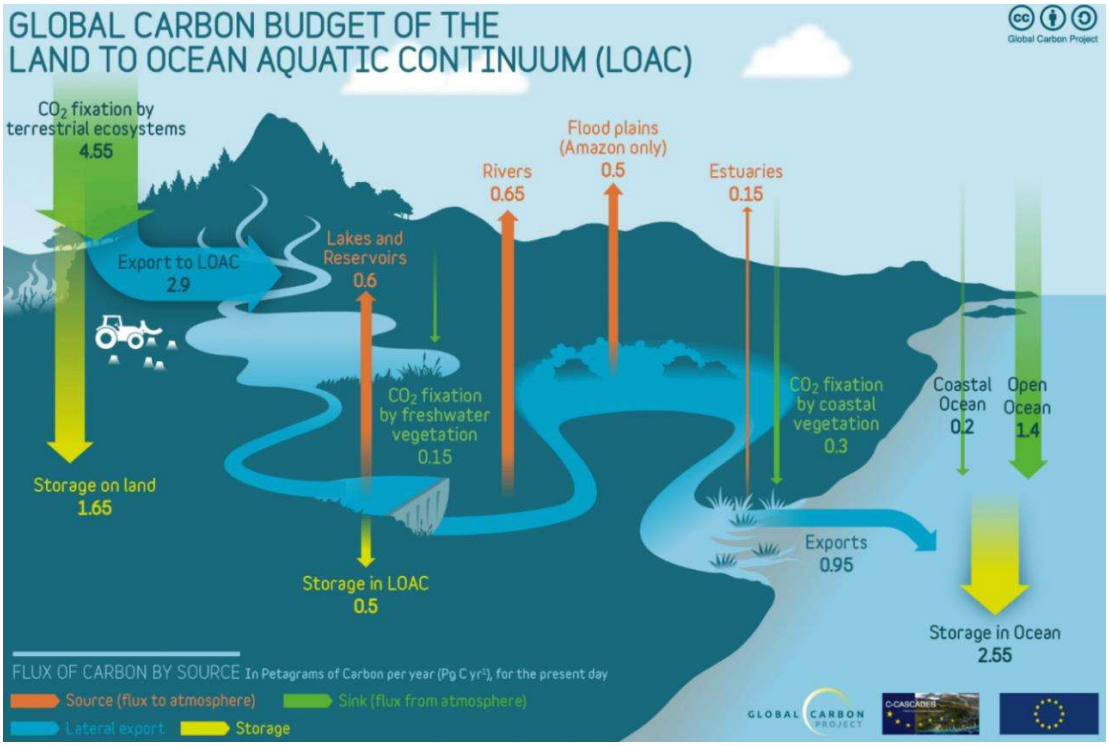

Figure 1.1. *Representation of the global carbon budget for the land-to-ocean aquatic continuum. From the Global Carbon Atlas of the Global Carbon Project (2022). The units for the fluxes are in Pg C* yr^{-1}.

As rivers, estuaries and coastal seas have already been heavily affected by human perturbation, a better understanding of the composition, processes and fluxes of DOM would allow improved prediction of the effects of climate change on the carbon fluxes across the land to ocean continuum (Little et al., 2017; Legge et al., 2020). Legge et al., (2020) highlighted a range of issues related to climate change likely to have an impact on the carbon fluxes on the North West European Shelf (which includes the shelf seas surrounding the UK). Amongst these issues is sea level rise, affecting transitional waters, the increase

in riverine nutrient inputs (linked to the increase in rainfall events in winter), the degradation of estuarine and coastal habitats due to destruction or conversion to other uses (exposing organic carbon to microbial degradation), the increase of atmospheric CO_2 resulting in indirect changes in aquatic pH, oxygen and temperature, as well as direct increase in water temperature, decrease in water oxygen and changes in the water circulation.

Although the issues related to climate change are widely known, major gaps remain in our understanding of DOM processing and dynamics as it is transported from rivers to seas, in particular the impact of tidal cycles and instream processing upon DOM composition and the fate of riverine DOM once it reaches the sea. Furthermore, as emphasised by Massicotte et al. (2017), most of the studies on DOM focus on specific sites or ecosystems, failing to resolve the uncertainties on the carbon fluxes of the land to ocean continuum. The same study suggested the need for integrative studies and this research aims at understanding the processes and fluxes of DOM from rivers to the sea, whilst at the same time complementing the research on DOM dynamics carried out by the LOCATE project (Williamson et al., 2021; García-Martín et al., 2021) across forty rivers and 13 estuaries in Great Britain.

1.1 Overview of DOM

DOC represents ~ 60% of total organic carbon (TOC) in rivers and over 95% of TOC in the ocean (Benner, 2003) and forms ~ 50% of the DOM (Dittmar and Stubbins, 2014). Other important components of DOM include dissolved organic nitrogen and phosphorus (DON and DOP, respectively). As organic matter can be either dissolved or particulate, the operational definition of DOM is the fraction able to pass filter pore sizes between 0.2 and 0.7 μm (Dittmar and Stubbins, 2014). DOM is dissolved in the water column, but it can be converted into particulate organic matter (POM) and settle in sediments, being exported from the water column. DOM can be composed of different organic molecules, such as humic and fulvic acids, lignin, aminoacids and peptides, nucleic acids, urea and polysaccharides (Carder et al., 1989; Opsahl and Benner, 1997; Søndergaard and Thomas, 2004; Jaffé et al., 2008 and references therein; Stedmon and Alvarez-Salgado, 2011; Dittmar and Stubbins, 2014; Zark and Dittmar, 2018).

Due to its properties, a portion of DOM is coloured and is defined as coloured dissolved organic matter (CDOM). CDOM has a “yellowish” appearance, a result of CDOM absorption of visible and UV (ultraviolet) light at different wavelengths, with a maximum absorbance in the UV-blue region (Bricaud et al., 1981; Coble, 2007). As a result, CDOM influences the penetration of solar radiation in seawater, for example reducing the

Photosynthetically Active Radiation (PAR) when its concentration is high (Coble, 2007; Gonçalves-Araujo et al., 2015). Furthermore, because of its optical properties, it is one of the most important sources of protection against the damages caused by UV radiation for phytoplankton and other organisms (Helms et al., 2008; Gonçalves-Araujo et al., 2015; Stedmon and Nelson, 2015).

A fraction of CDOM can also emit fluorescence (Stedmon and Cory, 2014) and is defined as fluorescent dissolved organic matter (FDOM). Only the humic and protein fractions of DOM are mostly investigated by fluorescence, and although only a portion of the natural organic matter (NOM) fluoresces, this optical property of DOM has been widely used to study DOM composition in aquatic ecosystems (Carstea, 2012; Coble, 2014; Aiken, 2014), for example through modelling the excitation-emission (Ex/Em) spectra of FDOM via PARAFAC (Parallel Factor) analysis (see section 2.3.1 of Chapter 2).

Depending on the compounds forming DOM, this has different molecular weights (MW) which can affect DOM reactivity and its bioavailability (Benner and Amon, 2015). It is widely recognised that DOM size and reactivity exist in a continuum defined as the size-reactivity continuum model (Benner, 2002) (Figure 1.2). This is used to describe the continuous flow of DOM molecular size and reactivity from more complex to less complex molecules as DOM is degraded and then produced again (Benner and Amon, 2015).

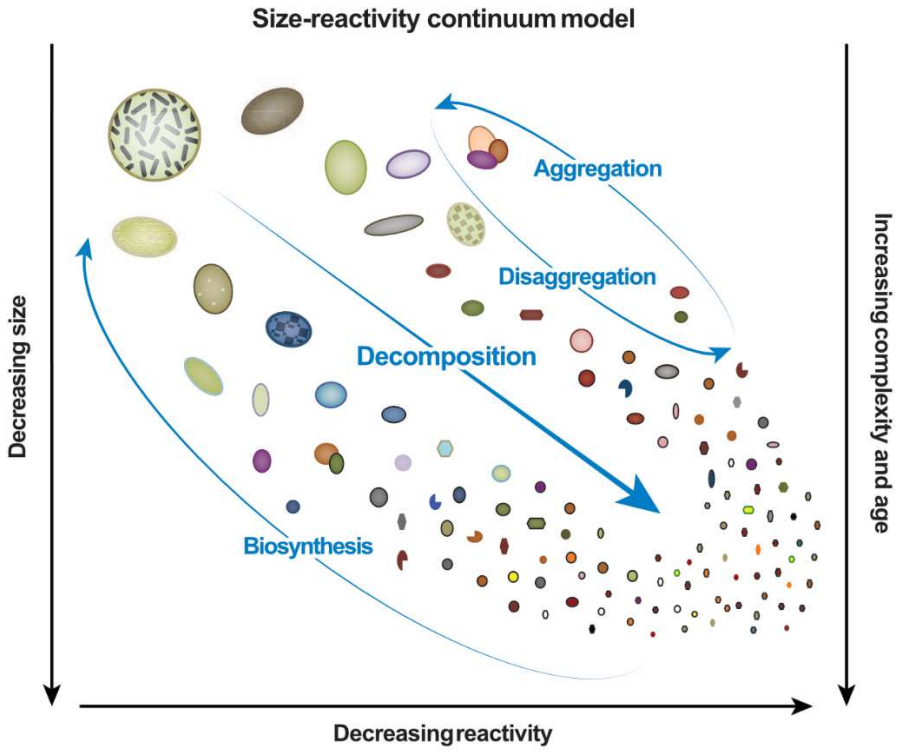

Figure 1.2. *Simplified representation of the size-reactivity continuum model showing the flow of DOM transformation between sizes, reactivity and age. From Benner and Amon (2015).*

Historically, DOM sizes have been determined according to its passage through a 1 nm membrane during ultrafiltration. As a result, DOM has been divided in high molecular weight (HMW), if it is retained by said membrane, that corresponds to > 1000 Da, and low molecular weight (LMW) if it is smaller than 1000 Da, with very low molecular weight (VLMW) as < 200 Da (Benner, 2002; Asmala et al., 2021). As reported by Asmala et al. (2021), DOM sizes, on average, change from land to sea from 50% of HMW in freshwater (1000 – 1500 Da) to 20% HMW in estuaries and coastal seas, with average sizes between 300 and 500 Da. In the ocean, about 22% of TOC is HMW, whilst about 77% is LMW (Benner and Amon, 2015). As previously mentioned, DOM molecular size is linked to its reactivity, with HMW generally more reactive than LMW, although Benner and Amon (2015) stated that it is mainly influenced by its chemical composition, which ultimately depend on the origin and processing of DOM.

1.2 Sources and processes affecting DOM composition

DOM in both freshwater and in marine water can be defined as allochthonous or autochthonous depending on its source. In freshwater and estuarine environments, allochthonous sources are soils and riparian zones (Takaki et al., 2022; Bauer and Bianchi, 2011), whilst in marine environments they are riverine inputs, groundwater and atmospheric deposition (Cauwet, 2002; Emerson and Hedges, 2008). Autochthonous DOM is defined as DOM produced *in-situ* by bacteria and viruses, phytoplankton degradation or extracellular release, by submerged aquatic vegetation or from animal excretions (Cauwet, 2002; Bertilsson and Jones, 2003; Mostofa et al., 2013). Additionally, sources from anthropogenic activities can contribute to DOM concentrations both in freshwater and seawater, such as road runoff and effluents from agricultural, sewage and industrial activities (Corbett, 2007; Mostofa et al., 2013; Kelso and Baker, 2022).

DOM consists of mixtures of aromatic and aliphatic hydrocarbon structures with several functional groups attached (Leenheer and Croué, 2003). Depending on its source and its carbon content, DOM can be more or less aromatic with riverine DOM containing between 30 and 51% of aromatic carbon (Mcknight et al., 2001; Mostofa et al., 2013), whilst microbially derived DOM contains 12 – 17% of aromatic carbon (Mcknight et al., 2001). Conversely, DOM produced *in-situ* is more aliphatic and richer in nitrogen compounds than terrestrially derived DOM (Mostofa et al., 2013). Lignin is an important fraction of riverine DOM, a key component of vascular plants, highly aromatic and with HMW, which provides a unique signature when studying DOM composition (Opsahl and Benner, 1998; Bauer and Bianchi, 2011; Stedmon and Nelson, 2015).

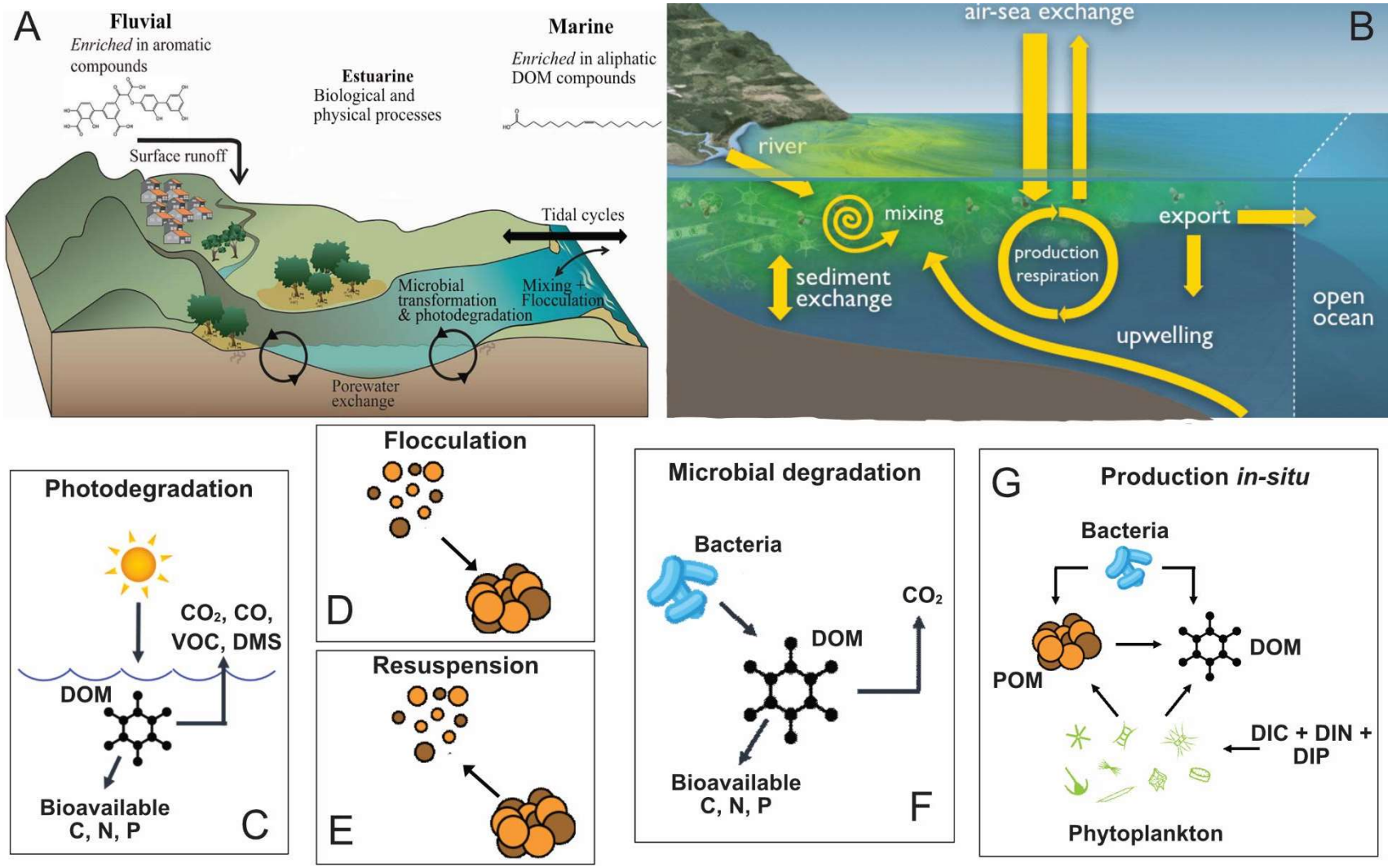

Figure 1.3. *(A) Generalised characteristics and processes of DOM from land to sea modified from Mori* et al. *(2019), (B) representation of processes affecting DOM in coastal ecosystems modified from NOAA PMEL Carbon Group (2022) and graphics of the main processes affecting DOM through the LOAC (C – G).*

Different processes can affect DOM as it travels through the LOAC, that can result in DOM increases to (sources) or removal from (sinks) the water column (Figures 1.3A and 1.3B). These processes affecting DOM both in freshwater and in seawater are summarised in Figure 1.3C – E, with photodegradation, flocculation and microbial degradation acting as sinks of DOM, whilst resuspension and *in*-situ production acting as sources of DOM in the water column. In addition, DOM can also mix conservatively between freshwater and seawater without being transformed (Bauer and Bianchi, 2011).

1.2.1 Photodegradation

Photodegradation (Figure 1.3C) is the process by which DOM is degraded by sunlight, releasing compounds such as CO_2, carbon monoxide (CO) and volatile organic compounds (VOC) as by products (which can be released into the atmosphere), and reducing the molecular weight of DOM, leaving smaller molecules rich in nitrogen and phosphorus, hence more bioavailable to the microbial community (Opsahl and Benner, 1998; Søndergaard and Thomas, 2004; Kitidis and Uher, 2008; Jones et al., 2015). Because of the exposure of marine ecosystems to solar radiation, photodegradation is the main sink of DOM in stratified surface waters, contributing to the transformation of terrestrial DOM once it enters the sea (Vodacek et al., 1997; Siegel et al., 2002). A study by Opsahl and Benner (1998) reported a reduction of 75% of riverine DOM after 28 days exposure to sunlight, with an accompanying transformation of DOM chemical composition, altering its terrestrial signature. This is in agreement with studies reporting a lack of terrestrial DOM in the open ocean (Spencer et al., 2009; Bauer and Bianchi, 2011; Fichot and Benner, 2012; Dittmar and Stubbins and references therein, 2014; Riedel et al., 2016; Clark et al., 2019).

1.2.2 Microbial degradation

Whilst photodegradation is the main sink of DOM in marine surface waters, microbial degradation (Figure 1.3F) is the main DOM sink where residence times are higher and sunlight exposure is reduced, such as in rivers and turbid estuaries (Opsahl and Benner, 1998; Seidel et al., 2015). Moreover, photodegradation which results in more bioavailable DOM compounds, can increase the contribution of the microbial community to DOM production. As reported by Søndergaard and Thomas (2004), DOM is widely utilised by the microbial community that is also capable of degrading terrestrial DOM, historically considered recalcitrant (Bauer and Bianchi, 2011; Barrón and Duarte, 2015; Schlesinger and Bernhardt, 2020) and thus thought to be exported passively into the open ocean (Liu et al., 2000).

DOM is defined as labile or recalcitrant depending on its bioavailability, and its reactivity can be affected by the residence time of water. Water bodies with long residence times can enhance the lability of DOM, whilst rivers with shorter residence times can export

terrigenous DOM with no or little transformation to the sea (Seidel et al., 2015; Kitidis et al., 2019), where it enters the oceanic microbial loop (Figure 1.4).

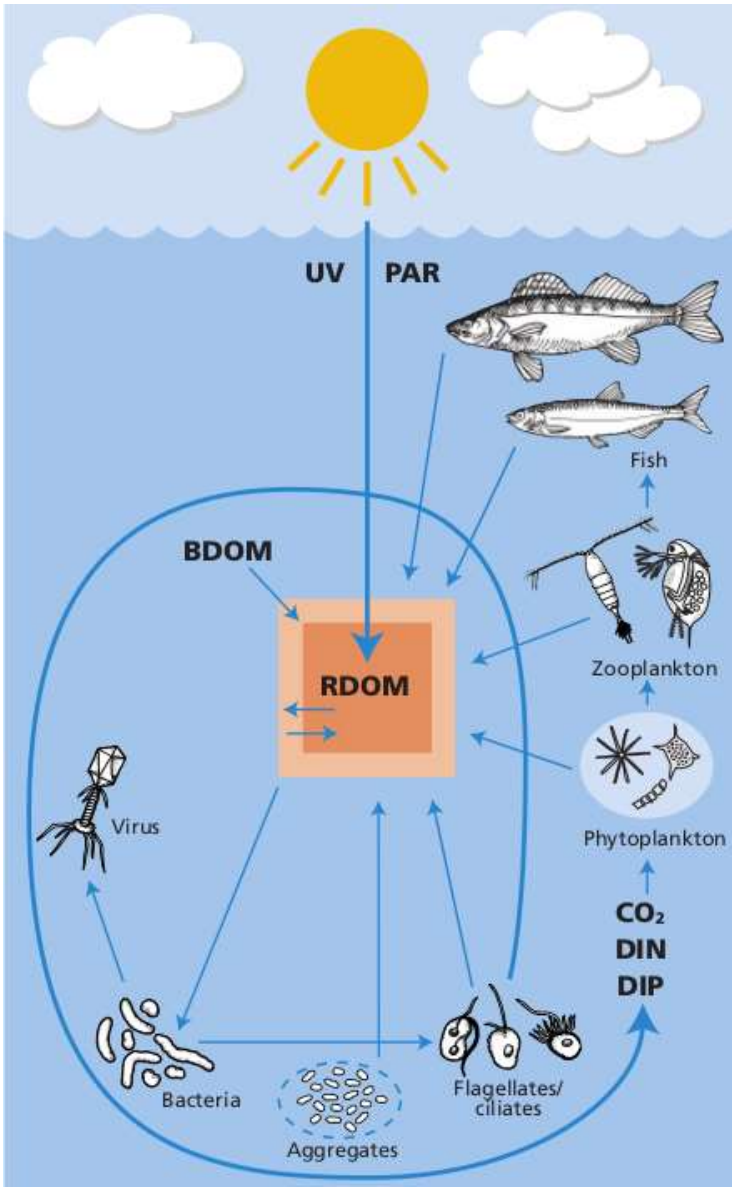

Figure 1.4. *Simplified representation of the food web model with fish, zooplankton and phytoplankton producing DOM. DOM is consumed and produced by bacteria and viruses in the microbial loop. RDOM is recalcitrant DOM, BDOM is bioavailable DOM, DIN is dissolved inorganic nitrogen and DIP is dissolved inorganic phosphorus. From Søndergaard and Thomas (2004).*

Labile DOM is the DOM fraction easily degraded by heterotrophic bacteria on timescales of minutes to a few days, resulting in an alteration of DOM composition (Dittmar and Stubbins, 2014). Approximately 5% to 7% of DOM produced by microbes is estimated to be recalcitrant and resistant to further remineralisation (Jiao et al., 2010; Hansen et al., 2016) as its reactivity decreases with increasing molecular complexity (Figure 1.2). However, research by Jiao et al. (2014) showed that marine DOM lability is more complex than

previously thought. The study introduced two types of refractory DOC, one linked to the environmental context ($RDOC_t$) and the other linked to its concentration ($RDOC_c$). $RDOC_t$ can be recalcitrant in a specific biogeochemical setting, but can be labile in a distinct one, with a different microbial community, whilst $RDOC_c$ can be unavailable to the microbial community because its concentration is too low. In addition, several studies reported that land use can influence the bioavailability of DOM in freshwater ecosystems (Molinero and Burke, 2009 and references therein; Asmala et al., 2013; Riedel et al., 2016; Lambert et al., 2017; Shi et al., 2020). In particular, Wilson and Xenopoulos (2009) showed that DOM delivered by rivers with agricultural land use is rich in nitrogen and phosphorus, has a lower molecular weight and it is more bioavailable to the microbial community, resulting in an increase of *in-situ* DOM production by the microbial community. Conversely, DOM from catchments characterised by natural forests and peatland is more complex, less labile, richer in carbon and potentially less susceptible to degradation and therefore able to be exported without much transformation to the sea (Molinero and Burke, 2009; Asmala et al., 2013; García-Martín et al., 2021).

1.2.3 *In-situ* production

As previously mentioned, the microbial community also contributes to the production of DOM in aquatic systems but to a lesser extent than phytoplankton (Søndergaard and Thomas, 2004). DOM production (Figure 1.3G) in rivers is mostly attributable to macrophytes followed by phytoplankton, whilst in estuaries and especially in coastal waters, phytoplankton is the main DOM source (Bauer and Bianchi, 2011; Massicotte et al., 2017). Phytoplankton and macrophytes release DOM during cellular growth and death and during herbivore grazing (Bertilsson and Jones, 2003). Viral lysis is another source of DOM, where there is a conversion of POM to DOM in the cell infected by the virus (Carlson and Hansell, 2015). Other sources include direct excretion by zooplankton, discharge of unassimilated molecules (egestion) and sloppy feeding (Bertilsson and Jones, 2003; Carlson and Hansell, 2015).

An interesting mechanism of DOM release from phytoplankton is through extracellular release (ER) which can contribute between 5% and 70% to DOM in natural waters (Mostofa et al., 2013). The reason for this is not clear, but two models have been identified, the 'overflow model' and the 'passive diffusion model' (Thornton, 2014; Carlson and Hansell, 2015). The overflow model is based on the inability of phytoplankton to stop photosynthesising when nutrients are unavailable, leading to a lack of cellular growth and the inevitable release of the photosynthate (organic carbon), which is not useful for the phytoplankton cells due to its nutrient deficiency (Thornton, 2014). The passive diffusion model reported by Bjørrisen (1988) involves a continuous passive leakage of DOM from phytoplankton cells to the environment. These leaked molecules are of LMW and the passive

diffusion is enhanced by the difference in concentration between the cells' interior and exterior environment with larger cells releasing more DOM (Bjørrisen, 1988; Carlson and Hansell, 2015). Although the causes of these mechanisms are still not clear some studies showed an increase in phytoplankton extracellular release during stressful conditions (higher temperatures, oligotrophic waters, low pH, etc) (Nagata, 2000; Thornton, 2014 and references therein), whilst others reported ER of DOM as a way for phytoplankton to interact with the environment or other organisms (allelopathy) (Legrand et al., 2003). Lastly, the ER of DOM could be a way for phytoplankton to acquire resources outside their cells or a signal that the cells had started the process of self-destruction, possibly as a response to adverse environmental conditions (Thornton, 2014).

DOM produced by both macrophytes and phytoplankton is typically more labile, rich in nitrogen and has more LMW than allochthonous DOM (Leenheer and Croué, 2003; Massicotte et al., 2017). Moreover, due to its molecular composition, its bioavailability decreases after exposure to sunlight, in opposition to terrestrial DOM, as previously discussed (Stedmon and Cory, 2014).

1.2.4 Flocculation, adsorption, sedimentation, resuspension, and desorption

Flocculation, sedimentation and resuspension are processes that play an important role especially in estuaries, although sedimentation and resuspensions also affect DOM in shallow coastal and shelf sea waters (Asmala et al., 2014; Niemistö and Lund-Hansen, 2019).

Flocculation (Figure 1.3D) is the process by which compounds, usually suspended solids, change from the dissolved phase to the particulate phase as a result of coagulation (Sholkovitz, 1976). Adsorption is a mechanism that causes flocculation and also plays an important role in nutrient cycling (see section 1.3). Adsorption results in the attachment of dissolved compounds (including trace metals and phosphorus) onto organic matter glued together through other particles, biofilms or organisms' exudates (Sholkovitz, 1976; Eisma, 1986). In addition to adsorption, dissolved compounds can flocculate when seawater meets freshwater. The high ionic strength of seawater is able to neutralise the negative surface charge of DOM, causing particles to aggregate and flocculate (Asmala et al., 2014; Asmala et al., 2021). Lastly, flocculation can also result from the collision of dissolved compounds carried by tidal motion or wave turbulence (Eisma, 1986).

DOM that has flocculated is into a particulate form and will settle out of suspension, therefore representing a sink for DOM (Dittmar and Stubbins, 2014). Thus, flocculation is important in aquatic systems as it prevents DOM in rivers and estuaries from entering the shelf sea and being exported to the open ocean, whilst also affecting the behaviour of DOM as it travels down rivers and mixes with seawater (Asmala et al., 2014).

Although flocculation and sedimentation remove DOM from the water column, resuspension and desorption can return organic matter into the water column (Eisma, 1986). While desorption is the opposite of adsorption, indicating the release of molecules from organic matter, resuspension is the opposite of sedimentation, where benthic solids become suspended through tidal cycles, wave motion or dredging activities. Resuspension (Figure 1.3E) can cause deflocculation of POM and desorption of molecules that then return to the water column (Eisma, 1986). The release of DOM and nutrients through sediment resuspension has been demonstrated in rivers, estuaries, coastal zones and open ocean (Fanning et al., 1982; Simon, 1989; Morin and Morse, 1999; Guo and Santschi, 2000; Komada and Reimers, 2001; Ortiz-Hernández et al., 2004; Fitzsimons et al., 2006; Niemistö and Lund-Hansen, 2019; Takasu et al., 2020; Lan et al., 2021; Liu et al., 2021; Wang et al., 2022), highlighting the importance of this process as a slow but steady source of DOC (and DOM) into the water column, being transformed from the particulate to the dissolved form (Komada and Reimers, 2001).

1.3 DON and DOP and their additional sources

DON and DOP contain nitrogen and phosphorus, respectively, which are important elements for the synthesis of organic molecules within organisms. DON compounds include urea, nucleic acids and dissolved combined amino acids (DCAA) (Sipler and Bronk, 2015), whilst DOP compounds include nucleic acids, phospholipids and amino phosphoric acids (Alam et al., 2021). DON and DOP can be degraded through bio- or photodegradation and then release inorganic compounds such as DIN and DIP (dissolved inorganic nitrogen and phosphorus, respectively), bioavailable to phytoplankton and microbial communities for fundamental biological processes. Nutrients utilised by organisms are fixed into organic compounds through photosynthesis and transformed again into the inorganic form through remineralisation by bacteria (as explained in section 1.2.2) (Figure 1.5). As DON and DOP are part of DOM, they both have a terrestrial and an aquatic origin (allochthonous and autochthonous, respectively). In addition to the sources mentioned in the previous sections, additional anthropogenic sources of nitrogen and phosphorus include agricultural fertilisers, animal waste, and sewage discharges (Søndergaard and Thomas, 2004) (Table 1.1).

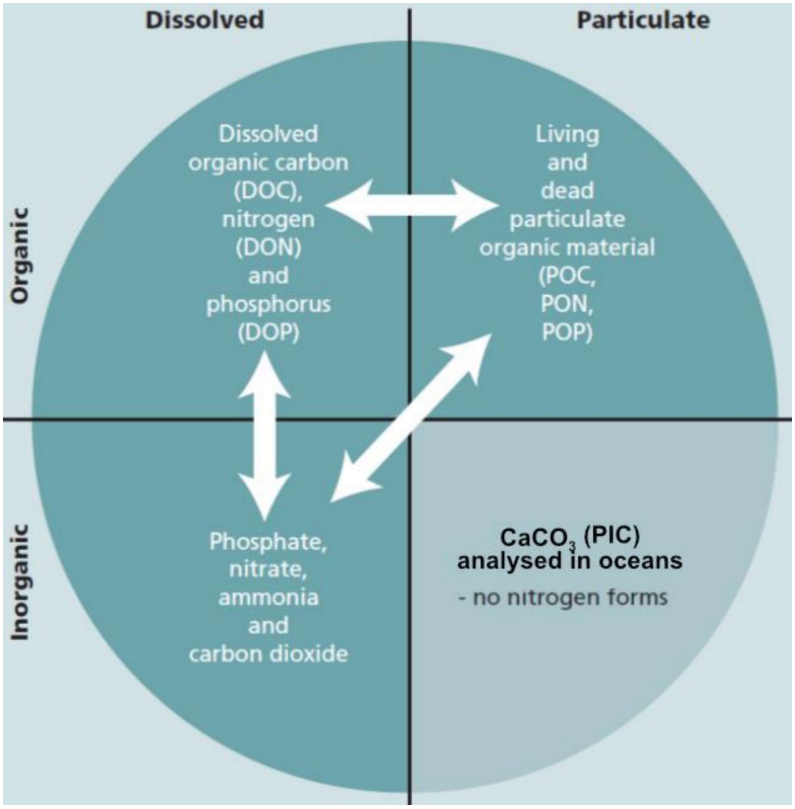

Figure 1.5. *Description of the different forms of carbon, nitrogen and phosphorus. $CaCO_3$ is calcium carbonate and PIC is particulate inorganic carbon. Modified from Søndergaard and Thomas (2004).*

Table 1.1. *Principal sources of nitrogen and phosphorus in aquatic systems. From Søndergaard and Thomas (2004).*

Sources		Nitrogen	Phosphorus
Natural	Primary	Atmosphere	Rocks
	Secondary	Soils, peat bogs, lakes and rivers	Soils, peat bogs, lakes and rivers
Anthropogenic			
Agriculture	Primary	Inorganic fertilisers (NO_3, NH_4, urea)	Inorganic fertilisers ($X\text{-}PO_4$)
	Secondary	Animal wastes, silage, runoff and groundwater	Animal wastes, silage, runoff and groundwater
Domestic		Sewage	Sewage
Industry		Various industrial wastes	Processing of phosphate rock

Generally, carbon (C), nitrogen (N) and phosphorus (P) are compared with the *Redfield ratio* of C : N : P that is 106 : 16 : 1 found in seawater and in phytoplankton cells linking biotic and abiotic processes (Redfield et al., 1963). The C : N and the C : P ratios are widely used as a proxy for substrate quality available to phytoplankton and bacteria. High ratios usually indicate poor nutritional value and are mostly associated with carbon enrichment due to a predominance of allochthonous material (Søndergaard and Thomas, 2004). Although this ratio was formulated for oceanic waters, it has been used for all aquatic systems, with large differences depending on the variability of the microbial communities and of the land use affecting the water body (Ptacnik et al., 2010). A study by Letscher et al. (2015) highlighted the uncertainty and imprecision of this proxy, stating that global DOM does not have a Redfieldian stoichiometry. Deviations from the Redfield ratio have been widely reported, as in a study on Baltic Sea measurements, where C : N : P ratios differed considerably from the 106 : 16 : 1 reference ratio, with values of C : N of 10, C : P of 125 and N : P between 11 and 12 (Kreus et al., 2015 and references therein). Islam et al. (2019) found consistent deviations from the Redfield ratio, especially during DOM decomposition. In addition, they stated that organisms can adapt their internal C : N : P ratios depending on nutrient availability and quality. This ability is important as freshwaters are considered P-limited, whilst coastal environments are N-limited (Nedwell et al., 2002; Mackenzie et al., 2011).

Nevertheless, with the increase in anthropogenic activities, aquatic systems experience a large increase in inorganic nutrients and a shift in the ratio between inorganic and organic nutrients. This was reported by Yates et al. (2019) for the UK, where concentrations of DON and DOP were larger in rivers draining catchments with little anthropogenic land use, compared to DIN and DIP, whilst the opposite was found in rivers draining agricultural catchments. The increase of inorganic nutrients in water bodies by agricultural activities has an influence on DOM processes, resulting in changes in the composition and therefore the bioavailability of DON and DOP (Wurtsbaugh et al., 2019). Yang et al. (2022) found that DOM from agricultural runoff had a different composition and was less bioavailable than DOM in water sampled upstream, as a result of increased microbial degradation of the agricultural runoff.

In water bodies affected by tidal intrusion, the mixing between freshwater and saline water can result in increased bioavailability of DON, due to an exchange of ions between DOM and saline waters. As salinity increases, humic compounds in DOM replace ammonium with salt ions, releasing highly bioavailable ammonium into the water column, a mechanism defined as *salinity-mediated release* (Bronk et al., 2010; Sipler and Bronk, 2015).

There is still limited information on the dynamics of inorganic and organic nitrogen and phosphorus, as the organic forms have not been measured until recently, also because

measurements of DIN and DIP are more common and still preferred (Benner, 2002; Yates et al., 2019; Yang et al., 2022).

1.4 Importance of DOM

As mentioned at the beginning of this chapter, DOC plays a major role in carbon uptake from the atmosphere. The processing of DOM in aquatic systems involves its transport through waters crossing terrestrial systems until it flows out to the sea. As stated in Ward et al. (2017), DOM dynamics are driven by water, highlighting the importance and the lack of DOM studies that include the hydrological connectivity between terrestrial and marine ecosystems, both in surface waters and in groundwater (Figure 1.6). When rainfall falls onto the soil, it permeates down until it reaches the saturated zone. This DOM enriched water can resurface in inland waters (rivers and lakes) as groundwater and form the baseflow of rivers. When soils have low permeability, rainfall water (and DOM) will move horizontally and will reach inland waters as overland flows. As the water moves through different environments, DOM undergoes compositional and reactivity changes as mentioned in section 1.3. Depending on the land use and the characteristics of the geology surrounding rivers and estuaries, the processes affecting DOM vary and influence the reactivity of the DOM reaching the sea. As an example, water residence times can affect the lability of DOM. Rivers with short residence times can deliver almost unaltered DOM to the sea, whilst DOM travelling through rivers with longer residence times is subject to microbial degradation and photodegradation that may result in a loss of up to 95% of DOM as CO_2 (Ward et al., 2017).

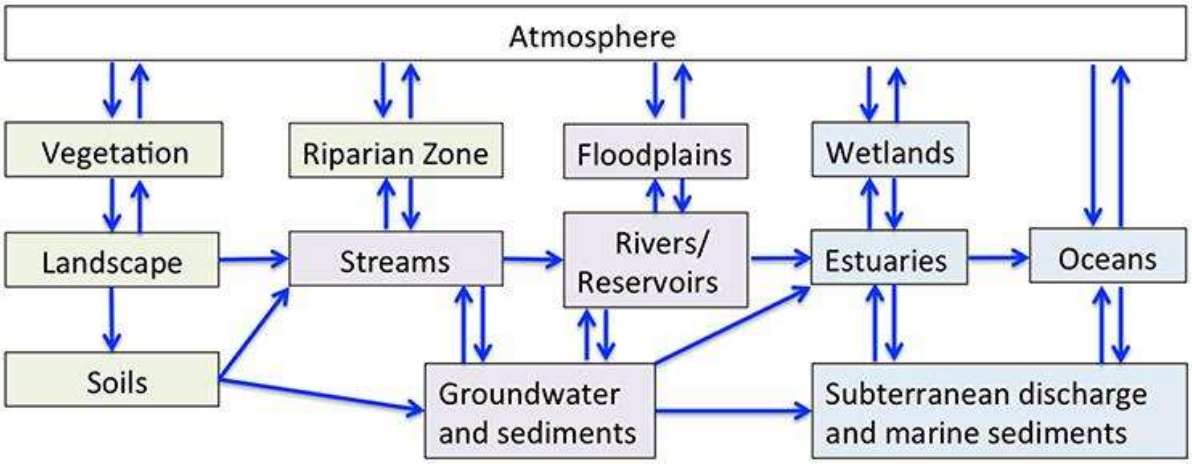

Figure 1.6. *Schematic representation of the water cycle through the atmosphere (white), terrestrial (green), freshwater (purple) and estuarine/marine ecosystems (light blue). The blue arrows represent the water cycle geochemical components. From Ward et al. (2017).*

When DOM reaches coastal waters, depending on its lability, it fuels the microbial community, and it undergoes further transformation (e.g., photodegradation). Coastal and shelf seas account for ~ 20% of the total oceanic organic matter production, although they cover only 7% of the oceanic surface area and are thus considered amongst the most productive areas in the ocean (Barrón and Duarte, 2015). DOC, DON and DOP exported into the coastal seas are subject to slightly different processes with DOC mainly being respired and exported, whilst DON and DOP can be incorporated into microbial food webs, or be deposited into sediments and subsequently being remineralised, with DON also undergoing denitrification (Søndergaard and Thomas, 2004) (Figure 1.7).

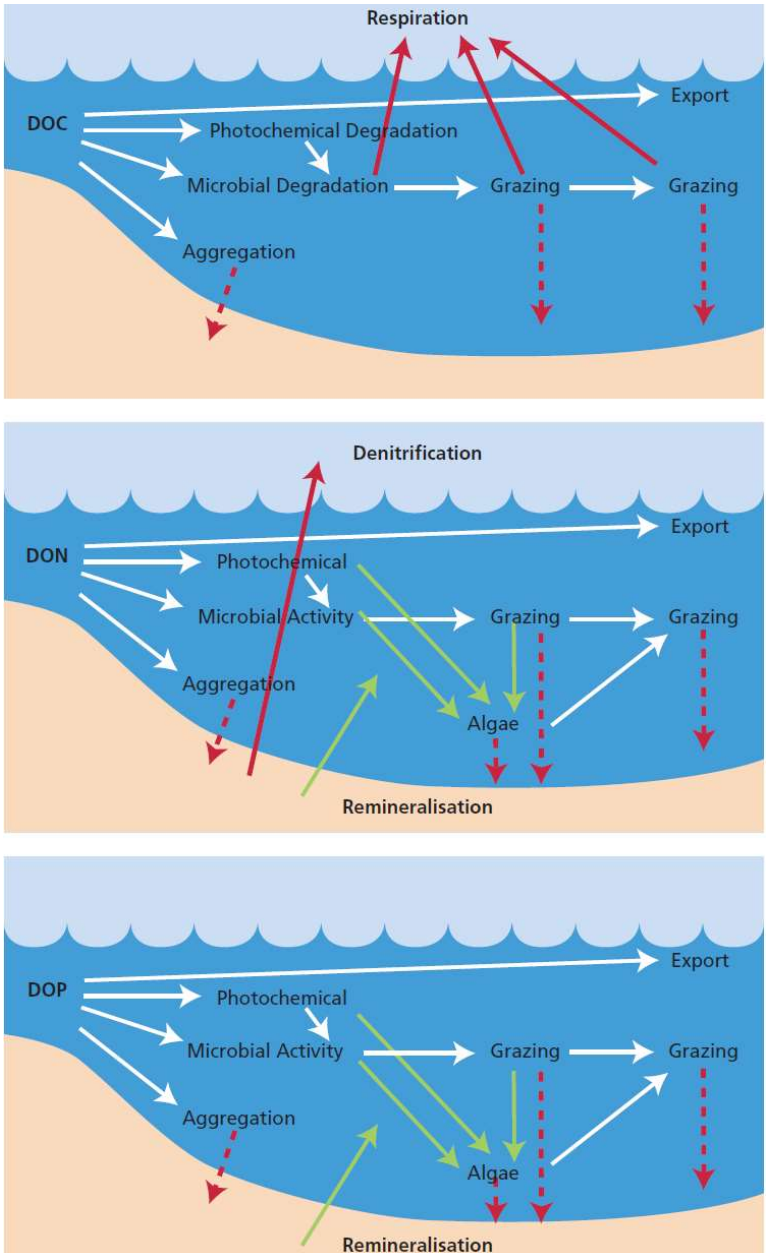

Figure 1.7. *Representation of the processes affecting DOC, DON and DOP in coastal and shelf seas. The solid red arrows indicate sinks and release to the atmosphere, the green arrows indicate processes resulting in DON and DOP bioavailability for phytoplankton and the dashed red arrows indicate losses due to sedimentation. From Søndergaard and Thomas (2004).*

The DOC in coastal zones and shelf seas that is either produced or not processed further, is exported to the open ocean (4.4 ± 1.0 Pg C yr^{-1} to 27.0 ± 1.8 Pg C yr^{-1}) (Barrón and Duarte, 2015), and sequestered into the deep sea through biological and non-biological mechanisms, defined as carbon pumps. The biological carbon pump (BCP) (Figure 1.8) is the mechanism through which DIC (dissolved inorganic carbon) is transformed into POM and DOM by phytoplankton and is vertically transported into the deep ocean by gravitation (POM), mixing and advection (DOM) or actively transported by zooplankton migration (Passow and Carlson, 2012). Organic carbon storage is defined as short-term (months to decades) or long-term (centuries to millennia) because throughout its journey it can be remineralised and be converted into DIC (Jiao et al., 2010; Passow and Carlson, 2012) and released back into the atmosphere. Another important carbon pump in the ocean is the microbial carbon pump (MCP) (Figure 1.8) which progressively converts labile DOM into recalcitrant DOM until it is not usable anymore and then may be stored into the deep ocean. Through continuous remineralisation of organic carbon during its descent, the MCP changes the ratios of C : N : P so that more carbon is stored as recalcitrant DOM, with ratios of ~3511 : 202 : 1, compared to ratios of 199 : 20 : 1 for labile DOM (Jiao et al., 2010; Jiao et al., 2014).

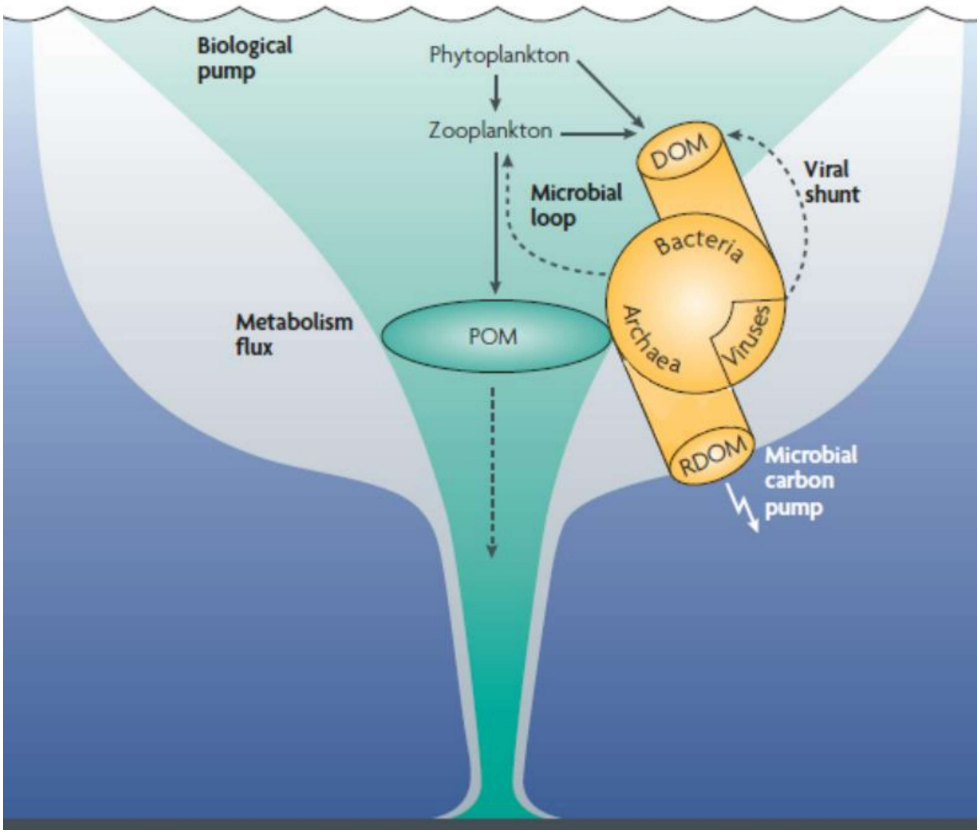

Figure 1.8. *Representation of the biological carbon pump (in green), with phytoplankton fixing atmospheric CO_2, which sinks by gravitation or through the vertical migration of zooplankton as POM and DOM. Representation of the microbial carbon pump (in yellow) where DOM is recycled and progressively transformed into recalcitrant DOM by bacteria and archaea, whilst cell lysis by virus returns POM to the DOM pool. The grey shading shows the total flux of carbon metabolism in the water column.*

Other carbon pumps are the solubility pump (SP) and the carbonate pump (CP). The solubility pump involves the dissolution of atmospheric CO_2 in the surface water, followed by its downward transport into deeper waters following overturning circulation (Bakker et al., 2014; Heinze et al., 2015; Legendre et al., 2015). The CP is based on the formation and precipitation of calcium carbonate ($CaCO_3$) mainly by marine organisms. This is accompanied by the formation of bio-mineral particles sinking together with calcium carbonate, as well as by the release of CO_2 (Legendre et al., 2015).

From precipitation, through rivers, to the open ocean, the biogeochemical processing and transfer of DOM through different water bodies contribute to maintain the efficiency of the BCP and the MCP (together with the SP and the CP). Understanding these interconnections is important given the anthropogenic land use change and the continuous increase of greenhouse gas emissions, with an estimated anthropogenic CO_2 atmospheric flux in 2020 of 10.2 ± 0.8 Gt C yr^{-1} with an increase of ~ 4.8% in 2021 (from preliminary data) (Friedlingstein et al., 2022).

1.5 Research aim and rationale

The aim of this research was to answer the question: ***What happens to DOM within rivers affected by tidal cycles as it travels downstream and enters the shelf sea?***

As explained in the previous sections, DOM plays an important role in the global carbon cycle and its dynamics from rivers to the open ocean are still unclear (Ward et al., 2017). As anthropogenic activities alter the fluxes of nutrients and carbon in rivers and estuaries, it can influence the amount and composition of DOM exported to the ocean. Regnier et al. (2013) estimated an additional flux of ~ 1.1 Pg C yr^{-1} is delivered to the land-to-ocean aquatic continuum due to anthropogenic activities, the main one being land use change. Of this additional flux of carbon, ~ 50% is retained in inland waters and sequestered into estuarine and coastal sediments, over 30% is converted to CO_2 and released back into the atmosphere, and less than 20% is exported to the open ocean. Moreover, Beusen et al. (2016) estimated an increase of nitrogen and phosphorus fluxes to rivers in the 20th century, from 34 to 64 Tg N yr^{-1} and from 5 to 9 Tg P yr^{-1}, leading to an increase in fluxes exported to the ocean from 19 to 37 Tg N yr^{-1} and from 2 to 4 Tg P yr^{-1}. Together with the anthropogenic activities, climate change is expected to affect DOM dynamics in the land-to-ocean continuum. With the increase in temperatures, precipitation and number of extreme rainfall events, there will be effects on freshwater runoff, DOM discharge in rivers and estuaries, and consequently to shelf seas and the open ocean (Watts et al., 2015; Wang et al., 2017; Xenopoulos et al., 2021). Xenopoulos et al. (2017) highlights a lack of knowledge of the

carbon cycle in tidal environments and in coastal regions, whilst Regnier et al. (2013) reports the need for estuarine studies at higher temporal resolution over a seasonal or annual cycles.

Therefore

1.6 Research objectives

The research objectives of this thesis are:

1. To study the effects of the tidal cycle on DOM composition and processes in two rivers (Chapter 3).
2. To determine changes in DOM composition, fluxes and processes within rivers from the freshwater endmember to the salinity endmember over an annual cycle (Chapter 4).
3. To investigate the fate and seasonal changes of DOM in the shelf sea after riverine export (Chapter 5).

These objectives were achieved through the analysis of DOM optical properties (coloured dissolved organic matter absorption and fluorescent dissolved organic matter), DOM chemical properties (DOC, DON and DOP), and the analysis of inorganic nutrients, chlorophyll-*a* and total suspended solids. The research was carried out in the UK rivers Yare and Waveney, their estuary and in the adjacent southern North Sea (Chapter 2). It included studies of a tidal cycle, annual riverine sampling and shelf sea cruises. The spatial and temporal dynamics of DOM in the rivers investigated in this research have never been systematically studied, therefore this research adds valuable knowledge to this field.

Chapter 2

Sampling and analytical methods

This chapter explains the study area, the sampling and analytical methods used. In order to understand the choice of the sampling locations, a description of the study area is presented. The chapter is divided into three sections. The first describes the study area, the second explains the sampling, storage methods and materials, and the third focusses on the analytical methodology.

2.1 Study area

The project is based on samples taken from two East Anglian rivers that flow into the southern North Sea and on samples collected in the southern North Sea. The first part of this section describes the area of the two rivers and the second part describes the North Sea.

The River Yare and the River Waveney

The Broadland Rivers Catchment is part of the Anglian River Basin District, an area of 27,900 km^2 delimited by the counties of Essex in the south, Northamptonshire in the west, Lincolnshire in the north and the East Anglian coast in the east. The Anglian River Basin District has 11 management catchments characterised by several water bodies, such as lakes, rivers, canals and estuaries. Several of these water bodies are natural, a small proportion are artificial, and the majority have been significantly altered (Environment Agency, 2015).

The Broadland Rivers Catchment is one of these 11 management catchments, covering an area of 3,200 km^2 that includes most of Norfolk and a small part of north Suffolk. This area is designated as a National Nature Reserve (NNR), a Special Protection Area (SPA), a Special Area of Conservation (SAC) and a Site of Special Scientific Interest (SSSI) and it is part of the EU Natura 2000 network (Environment Agency, 2014). The main rivers of The Broads are the Bure, the Yare, the Wensum and the Waveney flowing through the catchment and reaching the sea at Great Yarmouth (Broadland Catchment Partnership, 2014). This catchment provides drinking water to the public, as well as water to industries and for agricultural use (Broadland Catchment Partnership, 2014).

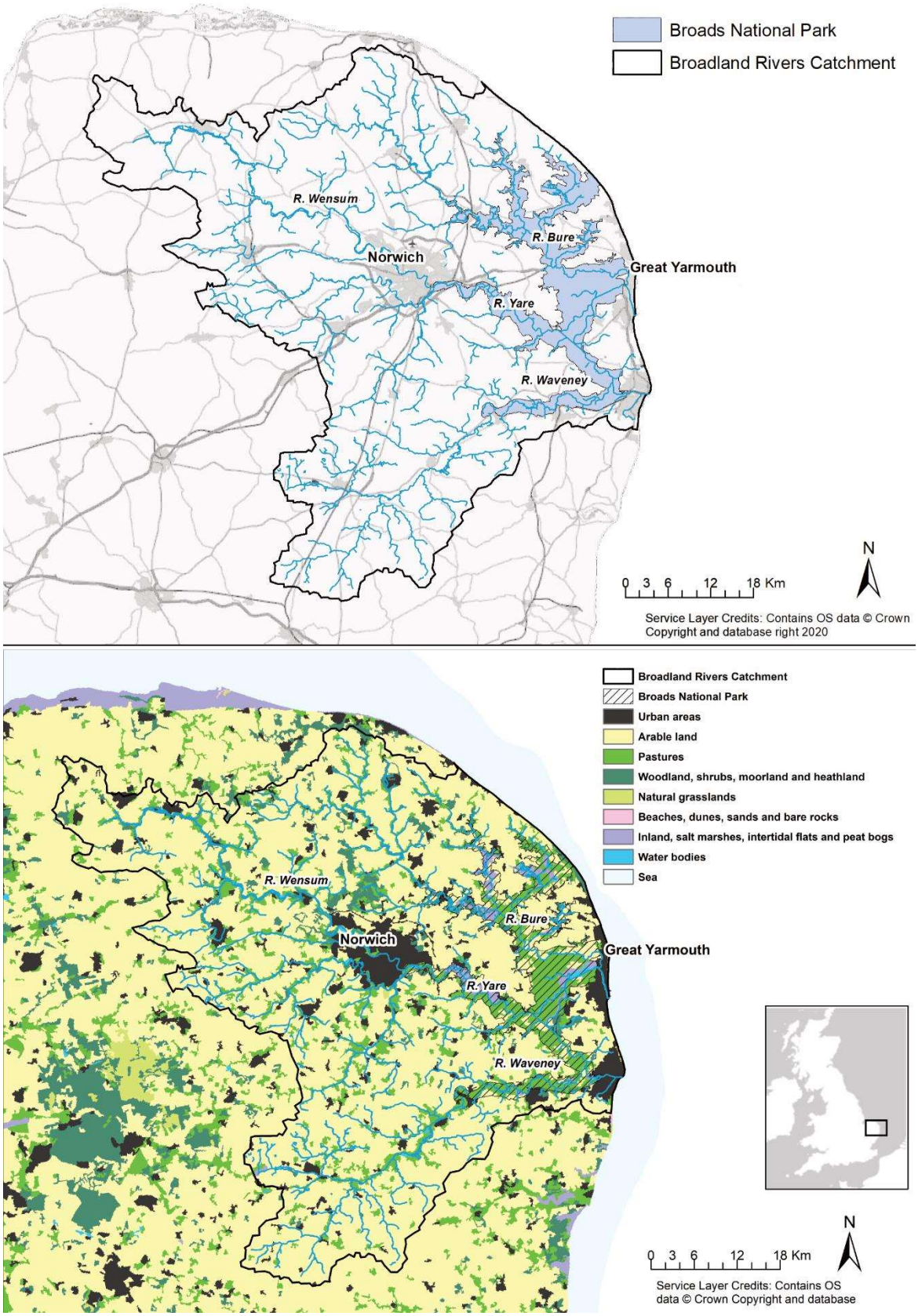

Figure 2.1. *Map of the Broadland Rivers Catchment with the Broads National Park highlighted (top) and land use for the Broadland Rivers Catchment (bottom). The maps contain data from the Environment Agency and Copernicus Land Monitoring Service 2018 (European Environment Agency, EEA).*

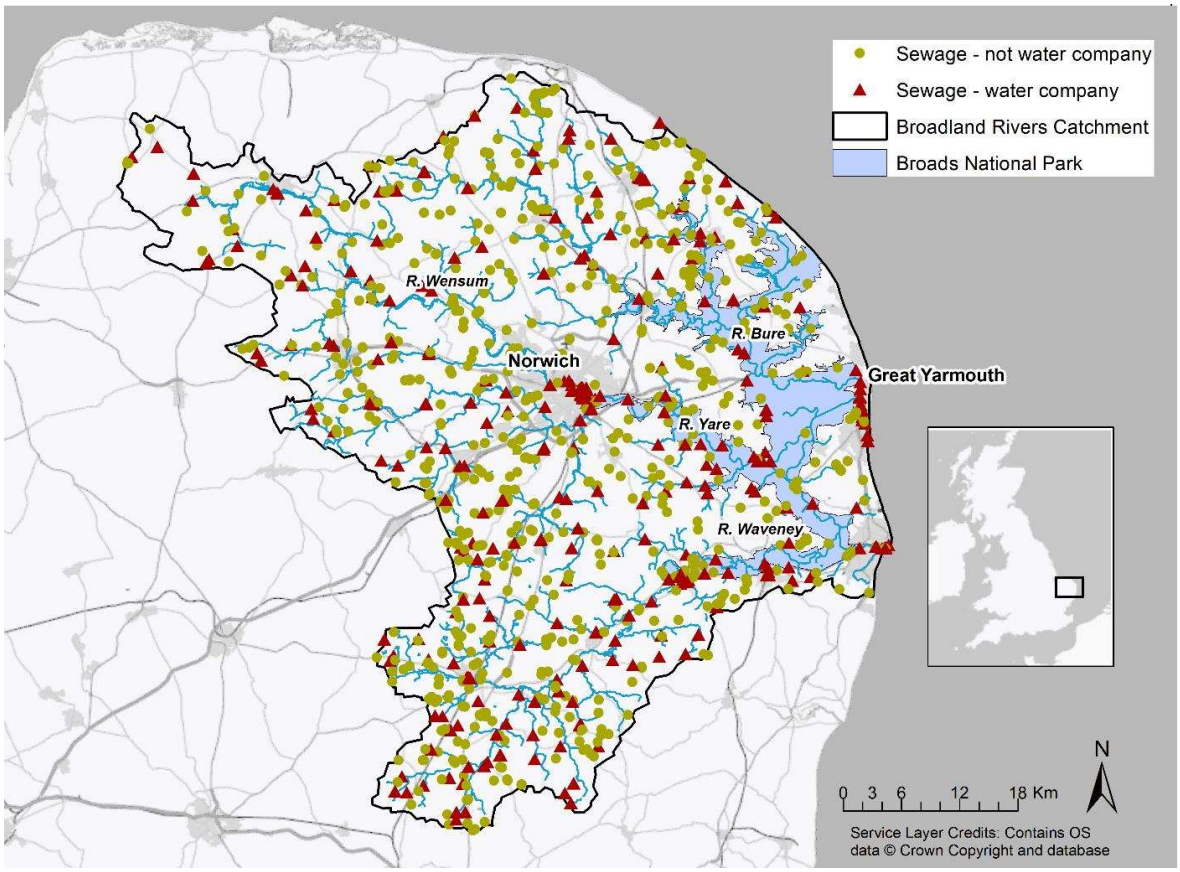

Figure 2.2. *Map of the Broadland Rivers Catchment with the Broads National Park highlighted and permitted wastewater discharges marked. The map contains data from the Environment Agency (2021).*

This project was carried out on two lowland, tidal rivers in East Anglia, UK, the River Waveney and the River Yare, which flow into the southern North Sea after passing through the Broads National Park (Figure 2.1 top). This is a river network managed by the Broads Authority which was established in 1988 (Pasquier et al., 2018). The Broads National Park is delimited by Great Yarmouth and Lowestoft in the east and by Norwich in the west and it is considered the most extensive wetland in Britain, with an area of 303 km^2 (Broads Authority, 2019). It is also considered ecologically important amongst Europe's wetlands (Broads Authority, 2019).This area has been shaped by medieval (12^{th}-14^{th} century) peat removal works, leaving depressions known as "broads" that were consequently flooded both by sea level rise and severe storms (Smith, 1966). These broads are surrounded by grazing marshes and a network of dykes (Broads Authority, 2019). There are more than 60 of these shallow lakes. Currently the waterways forming The Broads are fully navigable and they represent a tourist attraction, with over 7 million visitors every year (Broads Authority, 2017). The area is dominated by intensive arable agriculture and livestock grazing (Broadland Catchment Partnership, 2014) (bottom Figure 2.1).

The River Yare, is 83.5 km long, draining a catchment area of 757 km^2 (Environment Agency, 2015; Broadland Catchment Partnership, 2022b) with a mean annual discharge of 1.55 m^3 s^{-1} for the upper 30.5% of the catchment (UK National River Flow Archive, 2021). The source of the River Yare is near the village of Shipdam, south of Dereham (Environment Agency, 2014). The River Waveney is 95 km long, draining a catchment area of 943 km^2 (Environment Agency, 2015; Broadland Catchment Partnership, 2022a) and with a mean annual discharge of 1.75 m^3 s^{-1} for the upper 39% of the catchment (UK National River Flow Archive, 2021). The Redgrave and Lopham Fen National Nature Reserve is the source of the River Waveney (Environment Agency, 2014). These two rivers are subject to tidal cycles up to 20 km upstream, although salt water does not penetrate that far up the rivers (Holdway et al., 1978). Both rivers are susceptible to pollution from agriculture and livestock as well as run off from urban areas. The two rivers have been extensively channelised to increase land drainage and receive considerable domestic and industrial wastewater inputs from water recycling centres, once the wastewater is treated (Environment Agency, 2014) (Figure 2.2). A report summary by the (Broadland Catchment Partnership, 2014) stated that there are over 240 of these wastewater treatment plants in the Broadland Rivers Catchment which serve more than 700,000 people. In addition, untreated sewage is also released through Combined Sewer Overflows (CSOs), a mechanism that allows raw sewage to mix with rain-water runoff and be discharged into rivers during heavy rainfall events (Environment Agency, 2020). This practice contributes to the releasing of harmful pathogens and organic and inorganic pollutants into surface waters which impact rivers, coasts and bathing areas (Riou et al., 2007; Abdellatif et al., 2014; Anne-Sophie et al., 2015).

This whole area is characterised by surface deposits becoming older going from east to west as seen in Figure 2.3. The two rivers have differences both for the older bedrock geology and the younger superficial deposits. The bedrock underlying the River Waveney is composed of undifferentiated strata of gravel, silt, sand and clay dating back through the Quaternary and Neogene periods, about 23 million years ago (Mathers et al., 2014). This type of bedrock is evidence of shallow seas. The bedrock underlying the lower reach of the River Yare is partly the same as for the River Waveney, while the upper reach of the river is composed of chalk from the Cretaceous period, between 66 and 100 million years ago (Mathers et al., 2014). The chalk bedrock indicates an environment with warm shallow seas where carbonate originated from planktonic organisms, especially coccolithophores (British Geological Society, 2020). In terms of the superficial geology, the river valley of the Waveney is characterised by alluvium deposits which originated through the Quaternary period, over the past 2 million years. These deposits indicate the presence of rivers transporting detritus, gravel and sand, whilst clay and silt were left on the floodplains of

these rivers during flood events. These deposits are also evidence of estuarine and coastal environments (McMillan, 2002). The river valley of the Yare is characterised by intermittent outcropping of chalk and the same deposits described for the Waveney (McMillan, 2002). The current characteristic flat landscape of the Broadland Rivers Catchment has been partly shaped during the Holocene, by alternating periods of sea level rise and regression that also created rivers, estuaries (like Breydon Water) and wetlands.

In terms of weather, the area experiences a temperate maritime climate with a mean annual temperature of 10.1°C and mean annual rainfall of 674 mm for the period 1981-2010 (Met Office, 2022).

The geology of the Broadland Rivers Catchment influences the hydrology of the River Yare and the River Waveney, which will be discussed in Chapter 4.

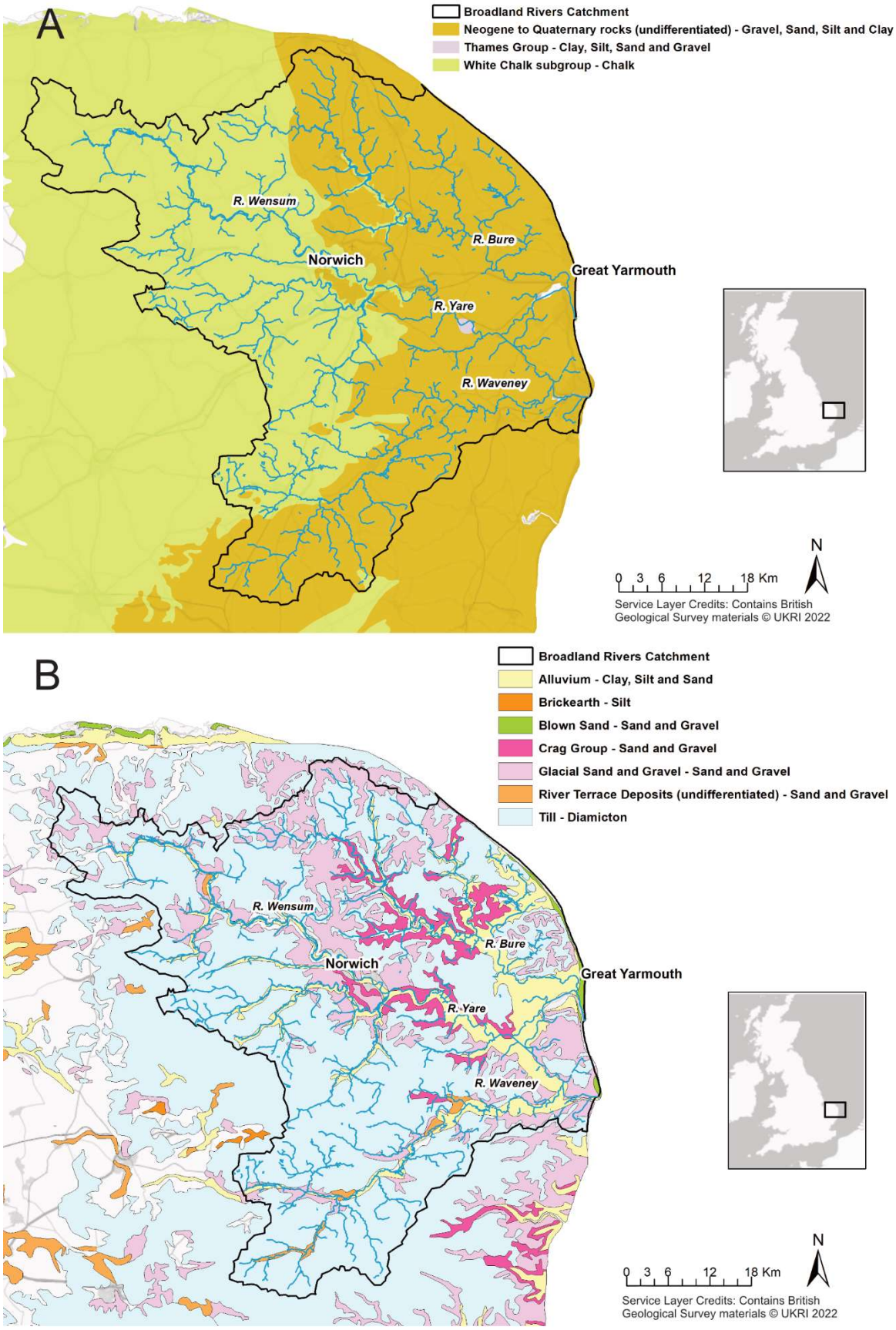

Figure 2.3. *Bedrock geology (A) and superficial geology (B) of the Broadland Rivers Catchment in Norfolk (UK). The maps contain data from the British Geological Society (BGS) (UKRI 2022).*

2.1.2 The North Sea

The North Sea basin is a shallow shelf sea with an average depth of approximately 90 m, although in some areas (such as the Norwegian Trench) the depth can reach 700 m. Situated in the north west of Europe, it is surrounded by several countries (Figure 2.4) and is connected to the north east Atlantic on its northern side and to the English Channel on its southern side (Ducrotoy and Elliott, 2008). Because of its varying depth, it can be divided into two zones at approximately 55°N (the location of the deposition area named Dogger Bank) (Chaichana et al., 2019). These two zones, the southern and the northern North Sea have different characteristics (Chaichana et al., 2019) (Figure 2.4).

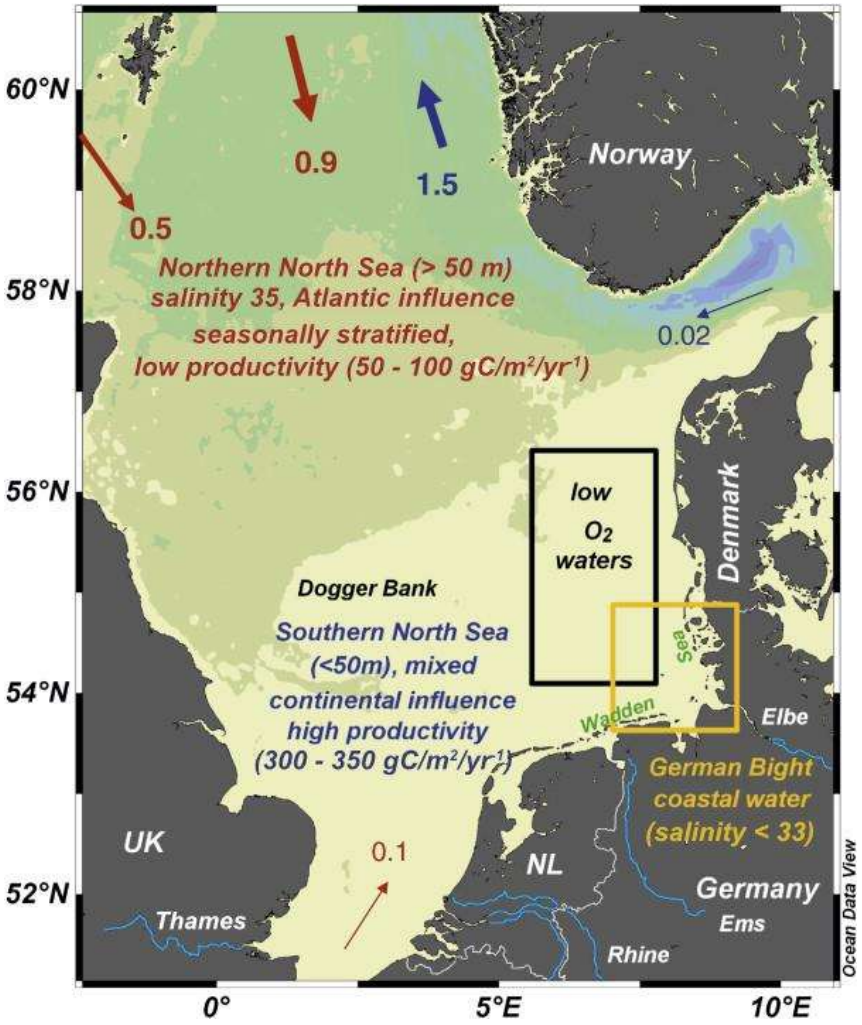

Figure 2.4. *Map of the North Sea and some of its characteristics. The arrows with numbers are the average water mass transports (Sv), inflows shown in red and outflows shown in blue. Modified from Emeis et al. (2015).*

The shallow southern North Sea is highly influenced by riverine inputs, with relatively low salinities and strong tidal currents. It is well mixed all year round as a result of its shallow depth and strong tidal currents (Jennings et al., 1999; Chaichana et al., 2019). The deeper

northern North Sea presents higher salinities, weaker tidal currents and seasonal stratification (Jennings et al., 1999; Chaichana et al., 2019). The North Sea is very productive due to its favourable environmental conditions (depth, water mixing, light availability, nutrients, etc.) (Ducrotoy and Elliott, 2008). Whereas the northern North Sea acts as a sink for atmospheric carbon dioxide for the whole year, the southern North Sea is a source for most of the year due to the well mixed column water (Bozec et al., 2005; Emeis et al., 2015). The North Sea as a whole is an efficient continental shelf pump, moving > 90% of all the carbon dioxide it draws from the atmosphere to the Atlantic Ocean (Thomas et al., 2005). The southern North Sea receives high riverine nutrient inputs, whilst the northern North Sea is considered nutrient limited (except in spring), relying on the North Atlantic as a nutrient source (Lenhart et al., 2004).

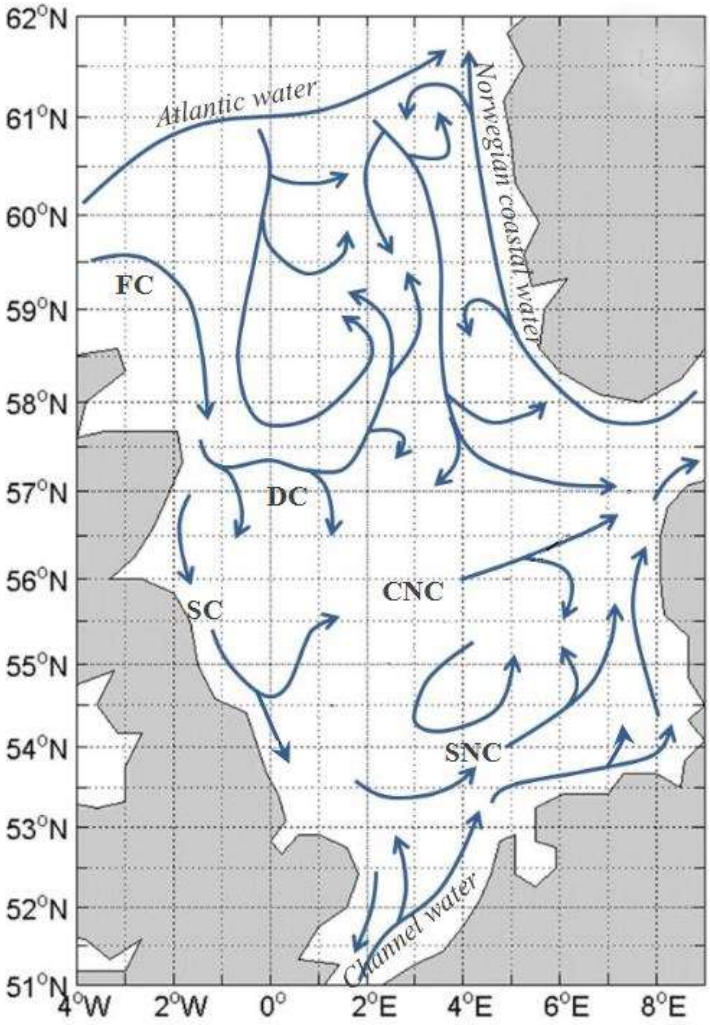

Figure 2.5. *Circulation pattern of the North Sea and name of currents annotated. FC (Fair Isle Current), SC (Scottish coastal Current), DC (Dooley Current), CNC (Central North Sea Current), SNC (Southern North Sea current). Adapted from Chaichana, 2017.*

The circulation of the North Sea is anticlockwise (Lenhart et al., 2004; Queste et al., 2016), where waters from the North Atlantic travel south and then turn east towards the Dogger Bank and waters from the English Channel (very small input) in the southern area travel along the eastern coasts, with finally all the water flowing out along the Norwegian coast (Thomas et al., 2005; Queste et al., 2016) (Figure 2.5).

2.2 Sampling and storage

This section describes the sampling procedures and storage for the samples collected during the surveys of the rivers and the shelf sea.

All plasticware and glassware (including the syringes used for filtering) were left to soak for 24 hours in a bath of 10% hydrochloric acid before any sampling or analysis (Table 2.1). Subsequently, they were rinsed 3-5 times with ultrapure water with a resistance of 18.2 MΩ at 25˚C and a total organic carbon content <0.001 mg L^{-1} (PURELAB Ultra, ELGA LabWater). Furthermore, the 125 mL amber glass bottles used to sample for fluorescent and coloured organic matter (FDOM and CDOM, respectively) were combusted at 450˚C for 6 hours to eliminate any organic compounds. A high-density polyethylene (HDPE) bucket was used to sample water from the rivers and was cleaned with Decon 90 and tap water, then rinsed 3-5 times with ultrapure water prior to any sample collection.

Table 2.1. *Containers used for sampling depending on analysis.*

Analysis	Type of container	Cleaning method
Fluorescent dissolved organic matter (FDOM) and coloured dissolved organic matter (CDOM)	125 mL amber glass bottles	24 hours 10% HCl acid bath + ultrapure water rinse + 450 °C combustion for 6 hours
Chlorophyll-*a*	1 L amber glass bottles	24 hours 10% HCl acid bath + ultrapure water rinse
Nitrate + nitrite, ammonium, dissolved organic phosphorus (DOP)	125 mL Nalgene bottles	24 hours 10% HCl acid bath + ultrapure water rinse
Dissolved organic carbon (DOC), dissolved organic nitrogen (DON)	125 mL Nalgene bottles	24 hours 10% HCl acid bath + ultrapure water rinse
Total suspended solids (TSS)	250 mL Nalgene bottles	24 hours 10% HCl acid bath + ultrapure water rinse

2.2.1 Sampling in the rivers

Water samples were collected along the River Waveney and the River Yare once a month from November 2018 to December 2019. Additional sampling was carried out during July 2020 on two days, one per river, with samples collected hourly from one site per river for 12 hours in order to cover a tidal cycle.

Sampling locations were characterised by different salinities with a freshwater endmember and a seawater endmember. Figure 2.6 shows the sampling locations for both rivers (see Figures A1-A11 in Appendix A for pictures of the sampling sites). Because the rivers share the same estuary and reach the sea at the same site, three estuarine sampling locations were the same for both rivers and were sampled twice every month. Table 2.2 below shows the range of salinity for the sampling locations. See Table A1 in Appendix A for sampling dates and weather conditions on the sampling days.

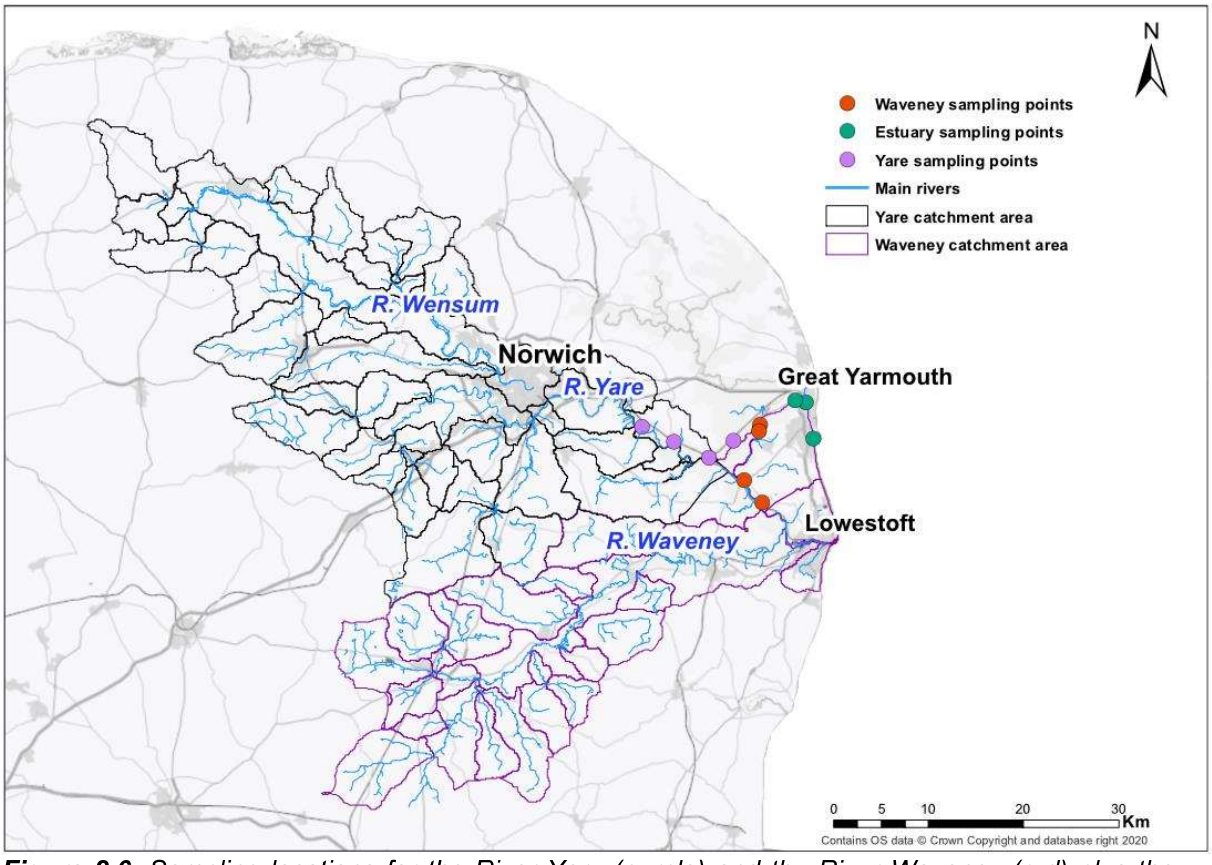

Figure 2.6. *Sampling locations for the River Yare (purple) and the River Waveney (red) plus the sampling points on the estuary (green) which were the same for the two rivers.*

Table 2.2. *Riverine sampling sites with their location and salinity range.*

Location	Sampling point	Coordinates lat. and long. (decimal degrees)	Salinity range	Sampling frequency
Estuary	SEA 1	52.57208 N, 1.73285 E	22.7 – 34.0	Twice per month
Estuary	SEA 2	52.60713 N, 1.72307 E	17.8 – 34.0	Twice per month
Estuary	SEA 3	52.60905 N, 1.70722 E	14.0 – 33.3	Twice per month
Waveney	WAVE 4	52.58780 N, 1.65115 E	10.7 – 20.8	Monthly
Waveney	WAVE 5	52.58165 N, 1.64877 E	4.5 – 19.8	Monthly
Waveney	WAVE 6	52.53670 N, 1.62182 E	0.7 – 2.0	Monthly
Waveney	WAVE 7	52.52475 N, 1.64731 E	0.7 – 1.2	Monthly
Yare	YAR 4	52.57448 N, 1.60807 E	10.3 – 27.7	Monthly
Yare	YAR 5	52.55927 N, 1.56778 E	0.5 – 17.7	Monthly
Yare	YAR 6	52.57643 N, 1.51463 E	0.4 – 3.1	Monthly
Yare	YAR 7	52.59180 N, 1.46606 E	0.3 – 0.4	Monthly

Tide times were checked prior to the sampling day, as it was preferable to sample during high tide when water was coming in because during low tide when the water was moving out to the sea some sampling locations did not have easy access to water for sampling (Figure 2.7). This is because the two sampled rivers are tidal and water levels are highly affected by tidal cycles. All river sampling was carried out from the river side throwing the bucket that was attached to a rope. The bucket was thrown as far as possible to sample towards the middle of the river.

Figure 2.7. *Sampling points WAVE5 and SEA3 at low tide.*

The following protocol was followed at each sampling site for each sampling event:

- The sampling site was photographed;
- *In situ* measurement of temperature and salinity before sampling;
- Completion of field log (Table 2.3) with the measurements and other metadata (weather conditions, direction of current, etc.);
- The bucket was rinsed three times in the river before the actual sampling;
- A clean plastic 60 mL syringe was used to take water from the bucket and filter it with a syringe filter (cellulose acetate, 0.45 µm pore size) into the bottles for subsequent analyses of FDOM, CDOM, DOC, DON and nutrients;
- The syringe was rinsed three times with water from the bucket;
- Before filling the bottles with the samples, all bottles were rinsed three times with the filtered water from the syringe;
- Samples for chlorophyll-*a* analysis were filtered through a 200 µm pore size mesh by pouring the water from the bucket;
- Bottles for total suspended solids analysis were filled with the water from the bucket and filtered afterwards in the laboratory;
- A field blank was also filtered using ultrapure water taken from the laboratory at UEA to account for the filter DOM content and any contamination from the sampling;

- After collecting the samples, the bottles were stored in a cool box filled with ice packs until the sampling was completed and the box returned to the laboratory;
- Routinely, one sample was collected for each analysis and occasionally 3 replicates were taken.

Table 2.3. *Field log used to collect information during sampling. The coordinates were recorded as latitude and longitude in decimal degrees, and the time was recorded as local time.*

RIVER SAMPLING FIELD LOG

River sampled:
Sampler name:

Date/time	Sample ID	Coordinates	Meteo conditions	Temperature (C°)	Salinity (PSU)	Conductivity (µS or mS)	Comments

A 556 MPS handheld multi-parameter probe developed by YSI (Figure 2.8) was used to measure temperature and salinity. For the calibration, the instrument was immersed in a tank containing artificial seawater alongside a Sea Bird Electronics 37-SM MicroCAT CTD and hourly salinity and temperature measurements were compared between the two instruments.

Figure 2.8. *556 MPS handheld multiprobe for measurements of salinity and temperature.*

Table 2.4. *Specifications for the YSI 556 handheld multiparameter instrument (YSI, 2009).*

Parameter specification	Range	Resolution	Accuracy
Dissolved oxygen (% air saturation)	0 – 500	0.1	± 6%
Air saturation (mg L^{-1})	0 – 50	0.01	± 6%
Temperature (°C)	-5 – +45	0.1	± 0.15
Conductivity (mS cm^{-1})	0 – 200	0.001 – 0.1***	± 0.001
Salinity (ppt)	0 – 70	0.01	± 0.1
pH	0 – 14	0.01	± 0.2
ORP* (mV)	-999 – +999	0.1	± 20
TDS** (g L^{-1})	0 – 100	4 digits	-
Pressure (mmHg)	-500 – + 800	0.1	± 3 †

*Oxidation Reduction Potential
**Total dissolved solids calculated from conductivity (variable constant, default 0.65)
***Range-dependent
†Within 10 °C temperature range from calibration point

The YSI multiparameter probe has a monitor to see the measurements in real-time whilst the probe is in the water. A summary of the specifications of this probe is given in Table 2.4. The multiprobe was calibrated every two months.

2.2.2 Sampling in the southern North Sea

Water was also collected offshore in the southern North Sea during cruises carried out by Cefas for the regular water quality monitoring programme on board the Research Vessel (RV) *Cefas Endeavour*. For this project, a total of 105 samples was collected during six cruises between November 2018 and July 2020. The sampling locations are shown in Figure 2.10.

Water samples on the ship were collected via the ship's underwater sampling system which allowed the collection of uncontaminated seawater at 4 m depth, through a plastic hose. Additionally, samples were taken from a Niskin Bottle Carousel which allowed water to be collected at different depths (Figure 2.9). Most of the samples were collected at 4 m depth, but some samples were collected at shallower or deeper depths as well. Therefore, the sampling depth ranges between 1.9 and 6 m.

Figure 2.9. *Niskin Bottle Carousel on board the RV Cefas Endeavour.*

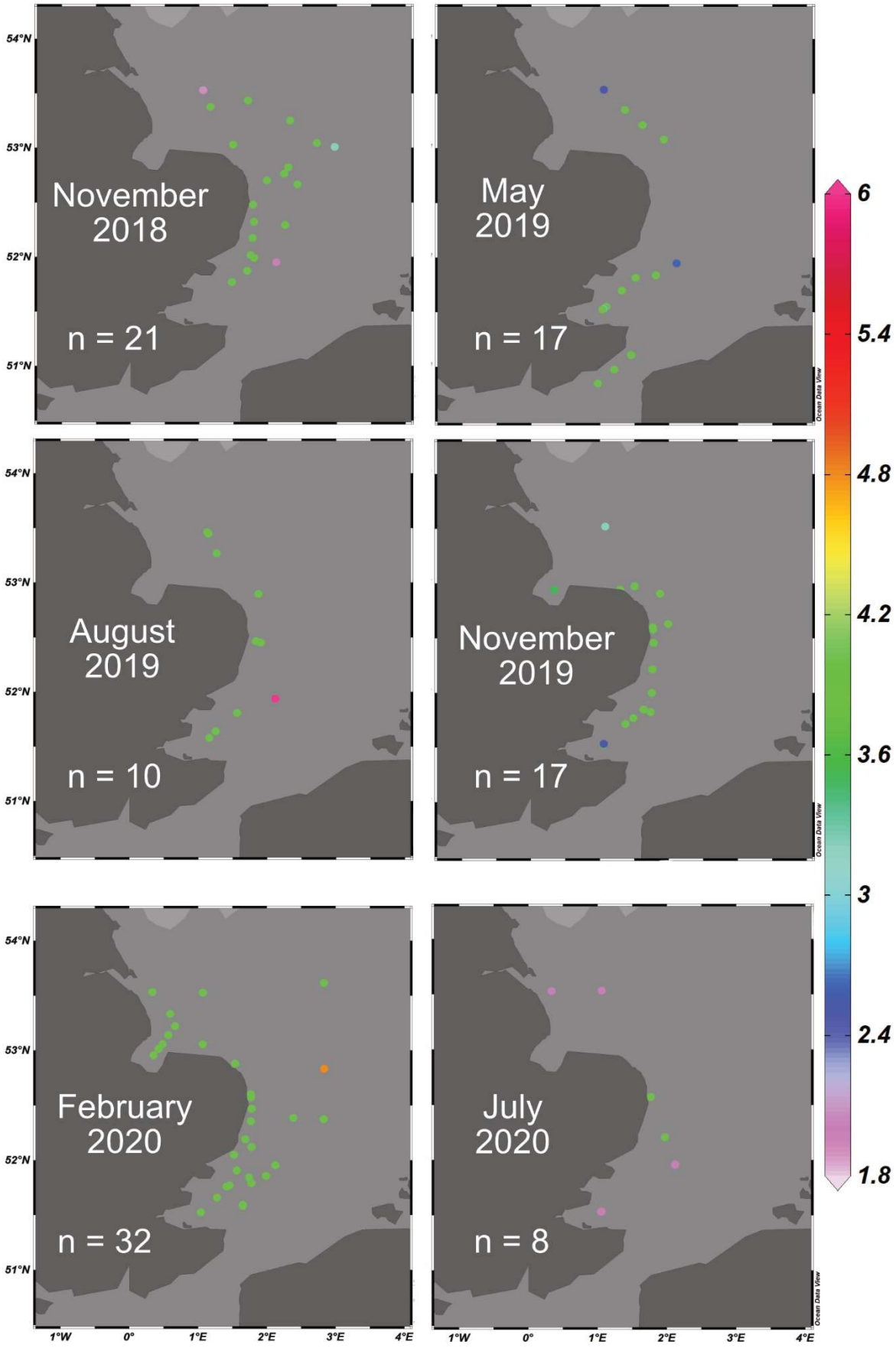

Figure 2.10. *Sampling locations for the water samples collected on the Cefas cruises and the number of samples collected on every cruise. The sampling points are coloured to highlight the depth in metres at which they were taken.*

2.2.3 Storage of samples

Water samples were stored differently depending on the analysis they were needed for (Table 2.5). Samples collected from the rivers and the shelf sea were stored in the same way.

- Samples to be analysed for dissolved organic carbon (DOC) and nutrients were stored in the freezer at -20 °C and in the dark;
- Samples for analysis of FDOM and CDOM, chlorophyll-*a* and total suspended solids were stored at 4 °C and in the dark;

Table 2.5. *Summary of the analysis type, volume collected, filter used, storage and number of all the samples in this thesis.*

Analysis	Volume collected	Filter used	Storage	Number of samples
FDOM	~ 50 mL	Syringe filter 0.45 µm, cellulose acetate	Dark and 4 °C	262
CDOM	~ 50 mL	Syringe filter 0.45 µm, cellulose acetate	Dark and 4 °C	283
Chlorophyll *a*	~ 500 mL	200 µm mesh + vacuum filtration onto 25 mm glass fibre filter	Dark and 4 °C	273
Nitrate + nitrite, ammonium, phosphate, total phosphorus	~ 70 mL	Syringe filter 0.45 µm, cellulose acetate	Dark and -20 °C	253
DOC, total nitrogen	~ 70 mL	Syringe filter 0.45 µm, cellulose acetate	Dark and -20 °C	260
Total suspended solids	250 mL	Vacuum filtration onto 25 mm glass fibre filter	Dark and 4 °C	220

2.3 Analytical methods

Prior to any analysis all the plasticware and glassware were cleaned to avoid any contamination (refer to section 2.2 for details). This section describes the methods used for the analysis of the water samples.

2.3.1 DOM fluorescence spectroscopy and PARAFAC

DOM fluorescence spectroscopy and PARAFAC (Parallel Factor) analysis explore the fluorescent properties of dissolved organic matter through the measurement of fluorescence Excitation-Emission Matrices (EEMs), in order to identify fluorophores or different components related to DOM with diverse characteristics and origin. Because of the optical properties of DOM (discussed in section 1.1 of Chapter 1), this technique can effectively identify the compounds which DOM is composed of. This analysis was previously used to analyse the coloured fraction of dissolved organic matter, CDOM and it is widely employed due to its efficiency, ease of use and time-effectiveness (Coble et al., 1990; Stedmon et al., 2003). It can be utilised to study DOM in freshwater, wastewater and marine water.

The theory underpinning this analysis is explained by Stedmon (2003), who states that "*when a molecule absorbs light (energy), an electron is excited and promoted to an unoccupied orbital. The energy difference between the ground (S_0) and excited singlet states (S_1, S_2 or higher) determines the wavelengths at which light is absorbed. Absorption (excitation) can result in a range of transitions to various vibrational sublevels of excited singlet states. This is the reason that molecular absorption spectra are often seen to consist of broad peaks. Excitation is then followed by non-radiative relaxation to the lowest sublevel of the S_1 state, via vibrational relaxation and internal conversion. Internal conversion, singlet-triplet intersystem crossing and fluorescence then compete for relaxation to the ground state (S_0). The wavelength of the fluorescence emission is determined by the difference in energy between S_1 and S_0 states. The greater the conjugation in the molecule, the lesser the difference in energy, resulting in a longer wavelength of fluorescence*" (p. 240) (Figure 2.11).

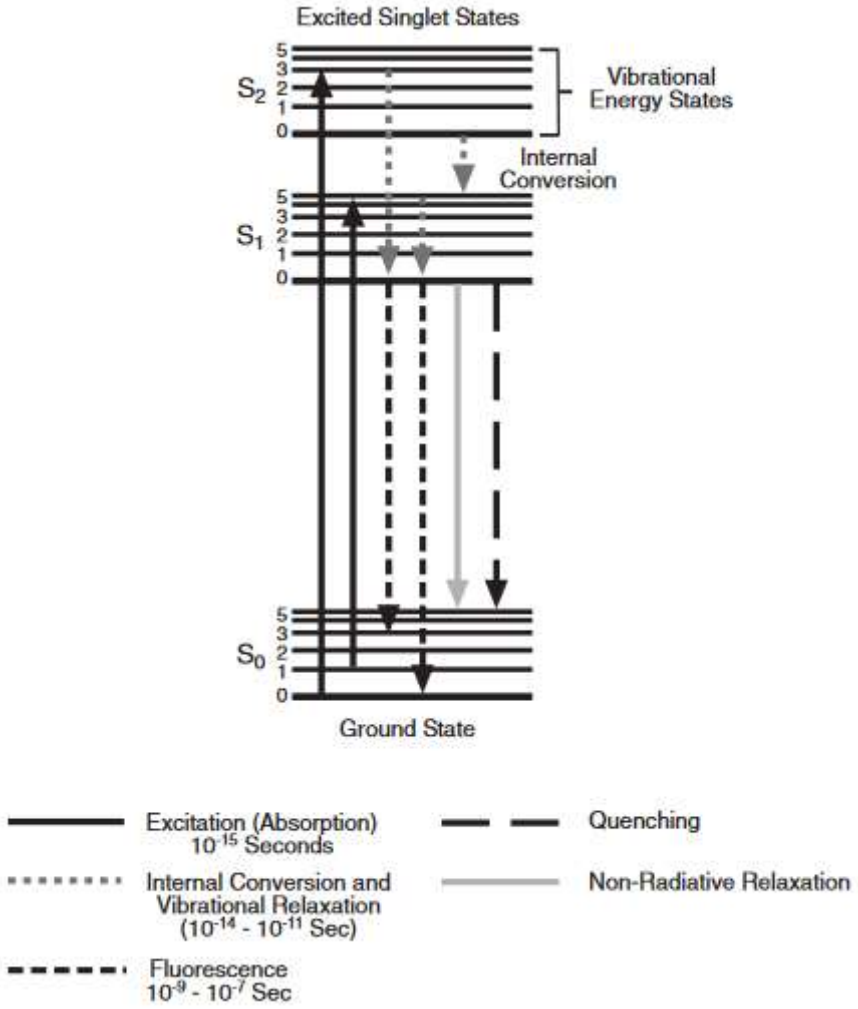

Figure 2.11. *Typical Jablonski diagram illustrating the physics of fluorescence. From Hudson et al., 2007.*

EEMs are matrices of excitation scans by emission scans ranging over different wavelengths. Depending on the molecular structure of the compounds in the sample, the intensity of the fluorescence changes allowing the identification of the possible composition of the compounds. Instruments used to measure DOM fluorescence can be set to determine a single pair of excitation-emission wavelengths, for specific compounds, setting a single excitation wavelength, or a single emission wavelength.

The analysis was carried out the day following the river sampling and within a week of the North Sea sampling, minimising the risk of DOM degradation as much as possible (Foden et al., 2008 and references therein). Prior to the analysis, water samples were allowed to reach room temperature in order to have the best fluorescence signal (Foden et al., 2008 and references therein). Starna 10 mm path length quartz cuvettes were used for the analysis and were soaked in 5% Decon 90 and then in 10% hydrochloric acid, followed by 3-5 rinses with ultrapure water before every analysis. Prior to every measurement the

cuvettes were rinsed three times with the water sample. Approximately 3 mL of the water sample (filtered at the time of collection) was needed for this method. Samples were analysed with a Jobin Yvon Horiba Fluorolog®-3 fluorometer (Figure 2.12) and FluorEssence software.

Figure 2.12. *Jobin Yvon Horiba Fluorolog®-3 fluorometer (Horiba, 2019).*

The settings for the EEMs were as follows: emission scans ranged between 280 – 600 nm wavelengths with a 2 nm increment, excitation scans ranged between 20 – 450 nm wavelengths with a 5 nm increment (Painter et al., 2018). The slit width for excitation and emission scans was 5 nm.

Slit widths are important in fluorescence spectroscopy and can affect the resolution and sensitivity of the analysis. Wider slits allow more light to pass through the emission and excitation spectrometers, causing an increase in the signal, but a decrease in resolution. Conversely, narrower slits give a higher resolution but a lower signal. The choice of the slit width depends on the nature of the substance analysed, but normally all emission spectra have peak intensities wider than 5 nm (Lakowicz, 2008).

Absorbance measurements from 230 to 800 nm at a 1 nm interval were also taken on a UV-VIS spectrophotometer (see details of the instrument in section 2.3.2) in order to correct for inner filter effects. This phenomenon can cause fluorescence intensity to decrease losing the proportionality to the concentration of the analyte (Kubista et al., 1994; Lakowicz, 2008). Blanks were measured using ultrapure water to identify water Raman scans. Two different emission scans for water Raman were measured from 285 to 450 nm

at the excitation wavelengths of 350 nm and 275 nm, with a 1 nm increment (Lawaetz and Stedmon, 2009).

The EEMs needed to be statistically processed. The statistical analysis used in this project is Parallel Factor Analysis (Stedmon et al., 2003; Stedmon and Bro, 2008; Murphy et al., 2013). PARAFAC was run in MATLAB using a series of toolboxes, N-way toolbox, DOMfluor, FDOM corr and drEEM (Murphy et al., 2013). This analysis required various steps: 1) Importing and assembling the dataset; 2) Pre-processing to remove noisy regions and scatter, and to eliminate outliers; 3) Exploring the data and running preliminary models; 4) Running the final, validated model with the components identified in the sample; 5) Exporting and interpreting the results (Murphy et al., 2013). A more detailed description of this statistical analysis is given in section 3.1.1.

2.3.2 Coloured dissolved organic matter absorption coefficients

The UV/VIS (ultraviolet/visible) absorbance of the water samples was analysed in order to correct EEMs for inner filter effects and to obtain more information about DOM composition. CDOM absorbs light at different wavelengths of the visible and ultraviolet spectrum, with maximum absorbance in the UV-blue region (Bricaud et al., 1981), causing its distinctive "yellowish" colour. By analysing its absorption, it is possible to extract information about composition and origin of the DOM.

Water samples were left to adjust to room temperature before the analysis. They were analysed with a dual beam Hitachi U-3000 UV-visible spectrophotometer over a range of 200 – 800 nm wavelengths at an interval of 1 nm and a 2 nm slit width. The same cuvette with a 10 mm path length was used as discussed in section 2.3.1. Ultrapure water was used to measure blanks that were subtracted from the spectra. The data obtained from the instrument were processed to convert the spectra from absorbance units A to absorption coefficients $\boldsymbol{\alpha}$ (m^{-1}) (Helms et al., 2008) through the following formula:

$$\boldsymbol{\alpha}(\lambda) = 2.303\left(\frac{A(\lambda)}{l}\right) \qquad equation\ 2.1$$

where $\boldsymbol{\alpha}$ is the absorption coefficient in m^{-1} at a specific wavelength λ, A is the absorbance at a specific wavelength λ and l is the optical path length of the cuvette in meters.

The spectra were then corrected for baseline offsets. These occur in particular when analysing seawater and using ultrapure water as reference, because of the difference in their refractive index or particle scattering (Green and Blough, 1994; Helms et al., 2008).

To correct for the offset, the average absorbance from 700 to 800 nm of every spectrum of the absorption coefficient α was subtracted from the whole absorbance of each spectrum.

2.3.3 Analysis of DOC and inorganic nutrients

This section contains the description of two methods for the analysis of nutrients in freshwater and seawater. The first method was used to analyse DOC and total dissolved nitrogen (TDN). The second method was used to measure the concentration of nitrate plus nitrite and ammonium, as well as of phosphate and total dissolved phosphorus (TDP). DON concentration was calculated from the combination of the two methods. Most of the samples were analysed at UEA and some of the analyses for the samples collected during the Cefas cruises (TSS and chlorophyll-*a*) were analysed at the laboratory at Cefas using the same methods.

- **High-Temperature Catalytic Oxidation method for DOC and TDN**

The High-Temperature Catalytic Oxidation (HTCO) method was used to determine the concentration of total organic carbon (TOC) in a sample by oxidising all the organic carbon CO_2. The samples analysed with this method filtered (0.45 µm pore size syringe filter) in order to remove particulate organic carbon, while leaving the dissolved organic matter. Therefore, these methods measure the concentration of DOC and TDN. Before the analysis, samples were left to adjust to room temperature.

In the instrument the samples were first acidified and then sparged with a flow of gas that was free of CO_2, in order to remove all the inorganic carbon. Subsequently, the organic carbon left in the samples was oxidised to CO_2 and the CO_2 concentration was determined by an IR (infrared) detector at 2.4 µm wavelength. The instrument was a Skalar Formacs^{HT} TOC/TN analyser (Figure 2.13) coupled with a Skalar ND20 detector, which allows the simultaneous measurement of the concentrations of TN (Total Nitrogen) and TOC. The instrument had a limit of detection of 0.08 mg L^{-1} for non-purgeable organic carbon (NPOC) and of 0.07 mg L^{-1} for TN, whilst the precision was ± 0.49 mg L^{-1} for NPOC and ± 0.20 mg L^{-1} for TN. TN was determined by pyrolytic oxidation of the total nitrogen to nitric oxide (NO) and then by quantification through a chemiluminescence detector. The detector was responsible for the reaction between NO and ozone (O_3) that forms excited nitrogen dioxide (NO_2*). This reaction emits light detected by a photomultiplier tube (PMT) that provided the concentration of TN.

Figure 2.13. *Skalar Formacs^{HT} TOC/TN analyser.*

This analysis required the preparation of a series of standards for a calibration curve that was then used to calculate the concentration of the analytes. A Stock Standard Solution (SSS) with a carbon concentration of 1 g L^{-1} was prepared by adding 1.0642 g of potassium hydrogen phthalate (KHP) (Thermo Scientific™) to ultrapure water to a final volume of 500 mL. A SSS with a nitrogen concentration of 1 g L^{-1} was prepared by adding 2.3585 g of ammonium sulphate ($(NH_4)_2SO_4$) (Thermo Scientific™) and 3.6095 g of potassium nitrate (KNO_3) (Thermo Scientific™) to ultrapure water to a final volume of 500 mL. From the SSS a range of five concentrations of carbon and nitrogen encompassing the expected sample concentrations were prepared (Table 2.6).

Table 2.6. *Concentrations of the five standards prepared for TOC and TDN analysis.*

Carbon		**Nitrogen**	
µM L^{-1}	**mg L^{-1}**	**µM L^{-1}**	**mg L^{-1}**
25	0.3	3	0.042
208.33	2.5	107.14	1.5
416.67	5.0	178.57	2.5
625	7.5	357.14	5.0
833.33	10.0	535.71	7.5

In order to analyse DOC by acid addition and then sparging with a gas flow, the non-purgeable organic carbon (NPOC) mode was selected from the instrument settings, before

starting the measurement. 2.5 M hydrochloric acid (37% extra pure, Fisher Chemical) was added in a default position in the carousel as per the instrument instructions, at the same time as the water to analyse (about 6 mL) was poured into the vials. In addition to the standards, CRMs (Certified Reference Material) from the Hansell Organic Biogeochemistry laboratory (Hansell, 2005) and ultrapure water for blanks were used.

Figure 2.14 shows the analytical procedure of this analysis: the measurements started with the automated acidification (100 µL of acid) of the samples by the instrument's syringe followed by a stirring and a sparging time of 180 and 240 seconds, respectively. The syringe then aspirated the sample to analyse, after having been flushed two times with the sample water itself and injected the sample into the high temperature TOC/TN reactor (set at 750 °C). The instrument carried out a minimum of two replicates (up to four) of the measurement, in order to reach a minimum coefficient of variation (CV) of 2%. Prior to the analysis, the carbon-free air entered a valve, a flow regulator (adjusting the flow to 240 mL min^{-1}) and a restrictor. The gas then flowed into the TOC/TN reactor where it was joined by the evaporated sample. The temperature of the carrier gas was reduced to 2 °C through a cooling coil, followed by a condensation trap where all the liquid was collected. Subsequently, the gas scrubber removed any halogens and the filter trapped any dust in the carrier gas. After this point, the gas moved to the infrared detector for CO_2 measurement, then to a flow meter before leading to the total nitrogen detector for the NO measurement.

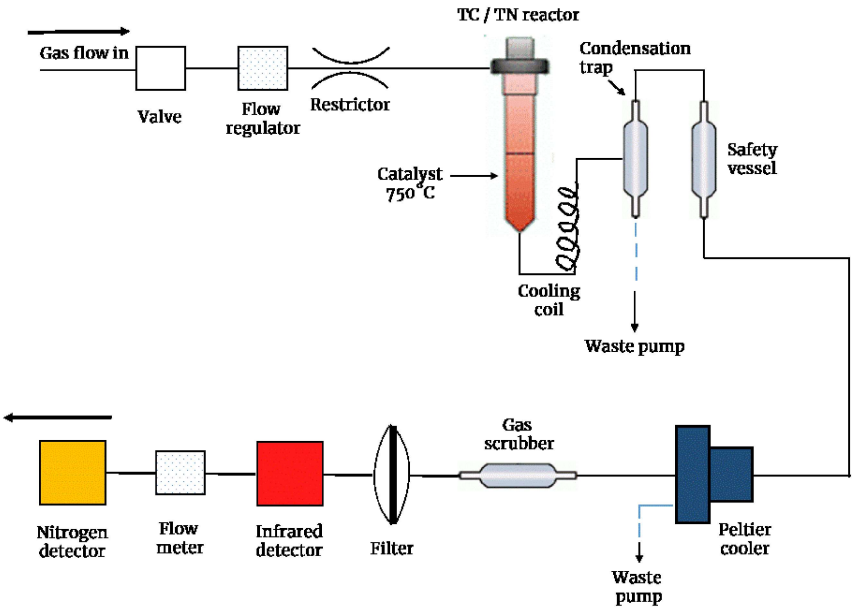

Figure 2.14. *Simplified diagram of the Skalar Formacs^{HT} TOC/TN analyser coupled with the Skalar ND20 detector.*

- **Nutrient autoanalyser**

A nutrient autoanalyser was used to determine nitrate plus nitrite, ammonium, phosphate and TDP. The concentration of DON was obtained by subtracting nitrate plus nitrite from TDN, determined with the HTCO method described above. The concentration of DOP was calculated by subtracting phosphate from total phosphorus. The analysis of the nutrients was carried out by Antony Hinchliffe from the Science Analytical Facility at the University of East Anglia.

The instrument used was a Skalar SAN++, also known as a Continuous Flow Analyser (CFA), which allowed the analysis of different species simultaneously (Figure 2.15). The limit of detection for the instrument was 1.0 µg N L^{-1} for nitrate plus nitrite, 6.0 µg N L^{-1} for ammonium, 4.0 µg P L^{-1} for phosphate and 1.0 µg P L^{-1} for total phosphorus. Samples were kept at -20 °C in the dark and left to thaw and adjust to room temperature before the analysis.

Prior to the analysis, standards for the calibration curve were prepared from standard stock solutions made for each species of nutrient. In particular, 6.1573 g of sodium nitrite ($NaNO_2$), 7.5852 g of sodium nitrate ($NaNO_3$), 4.7737 g of ammonium chloride (NH_4Cl), 5.4919 g of potassium dihydrogen orthophosphate (KH_2PO_4), 4.948719 g of sodium tripolyphosphate ($Na_5P_3O_{10}$) and 9.0009 g of sodium pyrophosphate ($Na_4P_2O_7$) were dissolved in separate volumetric flasks with ultrapure water to a volume of 250 mL, to obtain 500 mg L^{-1} concentration for each nutrient. The standard solutions prepared from the stock had concentrations of 10, 40, 80, 120, 160, 200, 300, 400 and 500 µg L^{-1} for nitrogen and phosphorus.

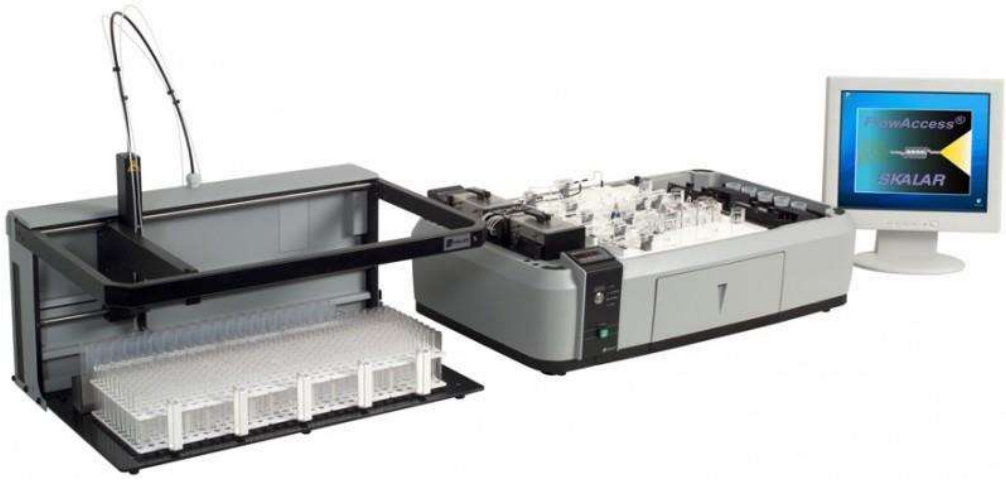

Figure 2.15. *Skalar SAN++ nutrient autoanalyser.*

To determine the nitrate plus nitrite concentration the instrument used the method based on cadmium reduction (SKALAR, 2009b). First nitrate was reduced to nitrite, then nitrite (consisting now of the nitrite originally present in the sample plus nitrate reduced to nitrite) was subjected to diazotisation, a reaction which resulted in the formation of an azo dye. The concentration of nitrite was then calculated using a spectrophotometer included in the autoanalyser, measuring the azo dye (which is highly coloured) at 540 nm. For the concentration of ammonium the autoanalyser used the method based on the Berthelot reaction which resulted in the formation of a green complex (SKALAR, 2009a). This was analysed at 630 nm by the instrument's spectrophotometer to determine the ammonium concentration.

The concentration of phosphate was determined by reactions which resulted in the formation of a blue complex (SKALAR, 2009c). To determine the phosphate concentration the blue complex was measured at 880 nm by the instrument's spectrophotometer. For the determination of total phosphorus, the method was the same as that for phosphate, apart from an additional step (either done by the instrument or manually) which digested all the forms of dissolved phosphorus to phosphate (SKALAR, 2012).

2.3.4 Determination of Chlorophyll-*a* by fluorescence analysis

This section provides a description of the fluorometric method used to determine the concentration of chlorophyll-*a* in water samples for this project (Arar, 1997; APHA, 1999b). The fluorometric method is easy to perform, requires small quantities of sample and is reasonably sensitive (Fargion and Mueller, 2000).

Phytoplankton not only include chlorophyll-*a*, but also other accessory pigments (chlorophyll b and c, phycobilins, xanthophylls and carotenes) that absorb and fluoresce light at some of the same wavelengths as chlorophyll-*a*. This happens also with some of the degradation products of chlorophyll-*a,* which are pheophytin-*a* and pheophorbide-*a*. To overcome this, usually water samples are analysed before and after acidification, with subsequent subtraction of the value measured after acidification. However, this modification is not recommended by some studies (APHA, 1999b; Stich and Brinker, 2005) which suggest that acidification alters the fluorescence wavelength emitted by some of the degradation products. This could cause an overlap of the fluorescence emission of the other pigments, resulting in an erroneous estimation of chlorophyll-*a* concentration. Therefore, in this project, the acidification correction was not used.

Water samples were filtered within 24 hours of collection both for the riverine and the North Sea samples, in order to minimise any alteration to the phytoplankton pigments.

The samples were filtered with a vacuum pump (pressure lower than 25 kPa) using Whatman GF/F glass fibre filters with 25 mm diameter, making a note of the volume of water filtered. After filtration, the filters were folded and placed into 15 mL polypropylene centrifuge tubes and kept at -20 °C in the dark until analysed, within one month. To carry out the extraction of the pigments, the centrifuge tubes were removed from the freezer and 5 mL of 90% acetone was added (diluted from 99.8% acetone, Thermo Scientific™). The filter was then ground with a glass rod taking care to avoid overheating the sample. Then another 5 mL of 90% acetone was added to the centrifuge tube, rinsing the glass rod at the same time, in order to wash out all the residues of the filter. The centrifuge tube with the slurry was shaken before being placed at 4 °C and in the dark for between 2 and 24 hours. The glass rod was always wiped with clean paper before proceeding with the extraction of the next filter.

Before the fluorescence analysis, the centrifuge tubes with the filters were centrifuged at 1000 RCF (Relative Centrifugal Force) for 5 minutes in order to concentrate the filter at the bottom and for the chlorophyll-*a* extract to become clear. The tubes were allowed to reach room temperature. Prior to the fluorometric analysis, an acetone blank was analysed using 90% acetone solution. 3 mL of the supernatant was aspirated using a pipette and moved into a Starna 10 mm path length quartz cuvette. This operation was repeated twice for every sample, first to rinse the cuvette and then for the actual sample transfer. The instrument for the analysis was the Jobin Yvon Horiba Fluorolog®-3 fluorometer (Figure 2.13) set to measure at an excitation wavelength of 430 nm and an emission wavelength of 663 nm (APHA, 1999b). In order to determine the concentration of chlorophyll-*a* from the fluorescence intensities, a calibration curve (Figure 2.16) was made.

The chlorophyll SSS was prepared using 1 mg powder of *Anacystis nidulans* algae from Sigma Aldrich. The concentration of the SSS was measured spectrophotometrically by Robert Utting at the University of East Anglia, as 1.97 mg L^{-1} of chlorophyll-*a*. A volume of 20 mL from the SSS was diluted to prepare calibration standards of 0.2, 1.0, 2.5, 5.0, 7.5, 10.0, 20.0 and 50.0 µg L^{-1} of chlorophyll-*a*.

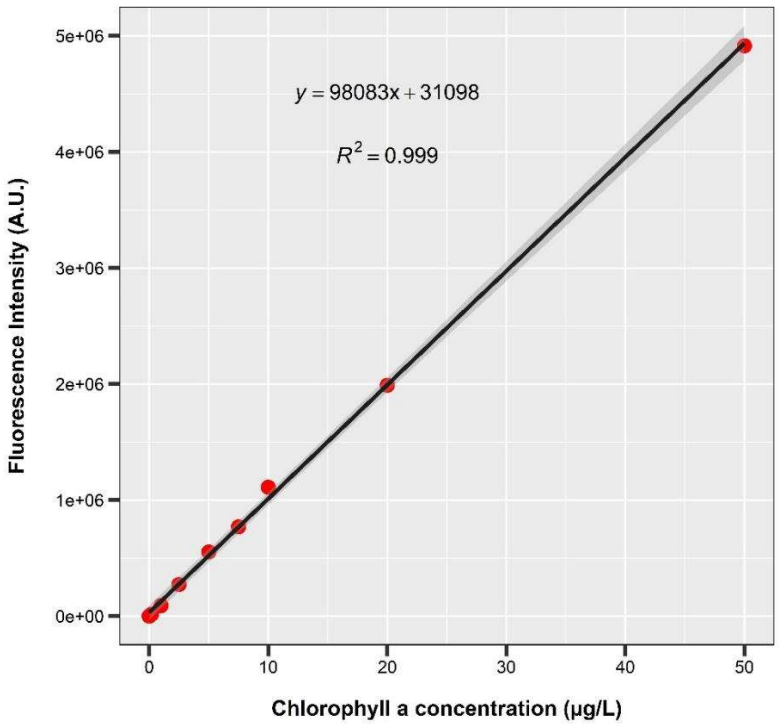

Figure 2.16. *Calibration curve for the determination of chlorophyll-a by fluorescence analysis.*

2.3.5 Total suspended solids determination

To determine the concentration of total suspended solids, water samples were filtered using a vacuum pump (pressure lower than 25 kPa), making a note of the volume of water filtered. Prior to the filtration, the filters were weighed in order to be able to subtract the filter weight from the overall weight of the solids plus the filter. Solids were retained onto a 25 mm diameter Whatman GF/F glass fibre filter and the filter placed in a glass container. After all the samples were filtered, the glass containers with the filters were moved into an oven and left to dry at 105 °C for 3-4 hours (APHA, 1999a; IAEA, 2005). The filters were left to reach room temperature before being weighed using an analytical scale that is calibrated and serviced every year by an external company appointed by the University of East Anglia (Nick Garrard, personal communication, 22 June 2022). To calculate the concentration of total suspended solids, the following formula was used:

$$TSS\ (mg\ L^{-1}) = \frac{(A\ (mg) - B(mg))}{sample\ of\ the\ volume\ filtered\ (ml)} \times 1000 \qquad equation\ 2.2$$

where A is the weight of the filter plus the solids retained on the filter after filtration of the water sample in mg, B is the weight of the filter prior to any filtration in mg.

Chapter 3

Dissolved organic matter properties during a tidal cycle in two UK lowland rivers

This chapter presents and discusses the results of two 12-hour sampling campaigns carried out on the River Yare and the River Waveney on 21 July 2020 and 26 July 2020, respectively. The aim of this chapter is to understand the changes and the behaviour of dissolved organic matter during tidal cycles. For this purpose, the following properties were studied:

i. The optical properties of dissolved organic matter (both absorption and fluorescence);
ii. The chemical properties of dissolved organic matter (organic nutrients);
iii. Chlorophyll-*a*, total suspended solids (TSS) and inorganic nutrient concentrations;
iv. The tidal cycle of the two rivers.

Through the above analyses the chapter aims to test the following hypothesis:

H1) DOC and CDOM concentrations decrease linearly at salinities above 0 when the tide is flowing in. This is because freshwater contains most of the DOC and CDOM, so dissolved organic matter is subjected to dilution when seawater and freshwater mix;

The chapter will also answer the following questions:

a) Does the fluorescence intensity of the components identified through PARAFAC follow the same pattern as DOC and CDOM?

b) Do the dissolved organic nutrients follow the same pattern as DOC and CDOM?

c) Does the behaviour of the dissolved inorganic nutrients through the tidal cycles inform on abiotic and biotic processes impacting DOM dynamics?

d) How does the TSS concentration vary with salinity?

e) Do the absorbance and fluorescence indices give an insight into the biogeochemical processes during the tidal cycle?

3.1 Additional methodology

A total of 24 samples was collected during two sampling campaigns in July 2020. The River Yare (n = 12) was sampled on 21 July 2020 and the River Waveney (n = 12) on 26 July 2020. The samples were collected every hour for a total of 12 hours to cover one tidal cycle per river, between 7:00 and 18:00 UTC. The sampling was carried out at one site per river and samples were collected at the same site every hour, where possible. Figure 3.1 shows the sampled sites which were YAR4, near Reedham for the Yare, and WAVE6 at St. Olaves for the Waveney (see section 2.2.1 for more details) and the position of the tide gauges used for this study. The tide gauges on the River Yare were located at Haven Bridge (Great Yarmouth) and at Reedham, whilst the ones on the River Waveney were located at Burgh Castle and at Haddiscoe (with Haddiscoe further upstream).

The methods used to analyse the samples are described in Chapter 2. Below a more in-depth explanation of the PARAFAC model and of the calculation and meaning of absorbance and fluorescence indices is given.

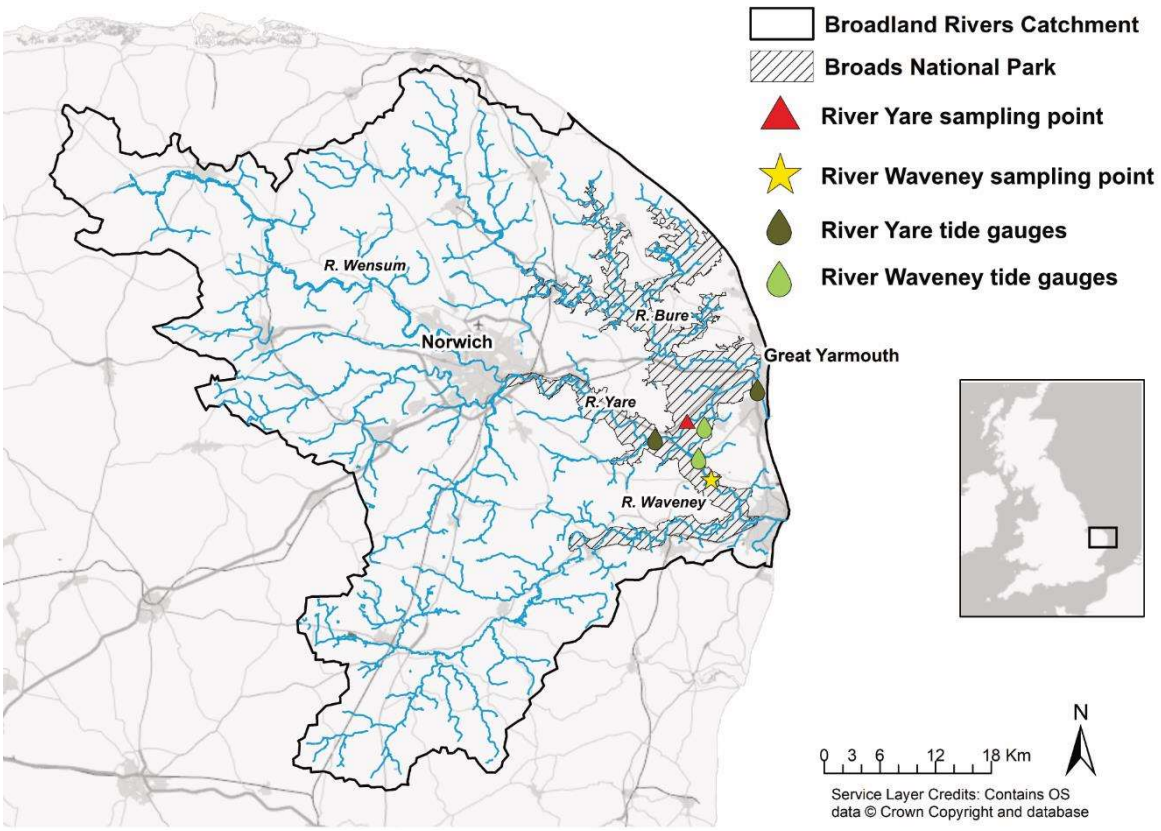

Figure 3.1. *Sampling points on the River Yare for 21 July 2020 and on the River Waveney for 26 July 2020, and the position of the tide gauges that recorded the tidal data used in this chapter. The map contains data from the Environment Agency (2021). The sampling sites are YAR4, near Reedham and WAVE6, at St. Olaves.*

3.1.1 DOM fluorescence spectroscopy and PARAFAC modelling

Analyses of the water samples were carried out with a fluorometer and fluorescence spectra were determined. This section focusses on the EEMs (emission excitation matrices) (discussed in section 2.3.1) and the results from the PARAFAC model with a brief explanation of this method. Further details of the methods are in section 2.3.1.

The PARAFAC analysis explores different models in order to find the one with the optimum least-squares fit to the data (Harshman, 1970; Harshman and Lundy, 1994). If the data X are arranged in a three-way array $i \times j \times k$ where i refers to the samples, the j refers to the emission wavelengths and the k refers to the excitation wavelengths, then the PARAFAC model can be mathematically written as

$$X_{ijk} = \sum_{f=1}^{F} a_{if} b_{jf} c_{kf} \, e_{ijk} \qquad equation\ 3.1$$
$$i = 1, \dots, I; j = 1, \dots, J; k = 1, \dots, K$$

where X_{ijk} represents the intensity of the ith sample at the jth emission wavelength at the kth excitation wavelength. F is the number of fluorophores or components, a_{if}, b_{jf}, c_{kf} are the parameters that describe the weight of the samples or variables to each component, and e_{ijk} represents the residuals and the variability the model could not compute (Bro, 1997; Andersen and Bro, 2003; Murphy et al., 2013). The matrices are decomposed by the model into fluorophores or chemical components (f) which are characterised by a score or concentration (a), emission (b) and excitation (c).

Following Murphy et al., 2013 the spectra were modelled using the *N-way* (Andersson and Bro, 2000) and the drEEM toolboxes in MATLAB R2020b. Before modelling the spectra, they were corrected for Raman and Rayleigh scatter as described in Bahram et al. (2006). Several models were run, and 5 outliers were removed in order to derive a better model. In addition, the model was constrained to be non-negative to avoid unreliable results as the spectra in this project were non-negative (Bro, 1997). After several runs, the final model with the number of components considered to be correct (Bro, 1997), was validated twice using the split-half analysis modality (Harshman, 1984; Stedmon and Bro, 2008). This mode divided the dataset into four quarters (A, B, C, D) randomly the first time and alternately the second time. The four quarters were then arranged in six sub-datasets (AB, CD, AC, BD, AD, BC), for the final validation. This was performed separately on the sub-datasets, three against the other three (AB vs CD, AC vs BD and AD vs BC) in order to obtain the same components with the lowest sum of squared errors (Bro, 1997) (Figure 3.2). The maximum fluorescence intensity was finally calculated for all the samples in the dataset, which include the samples excluded at the beginning.

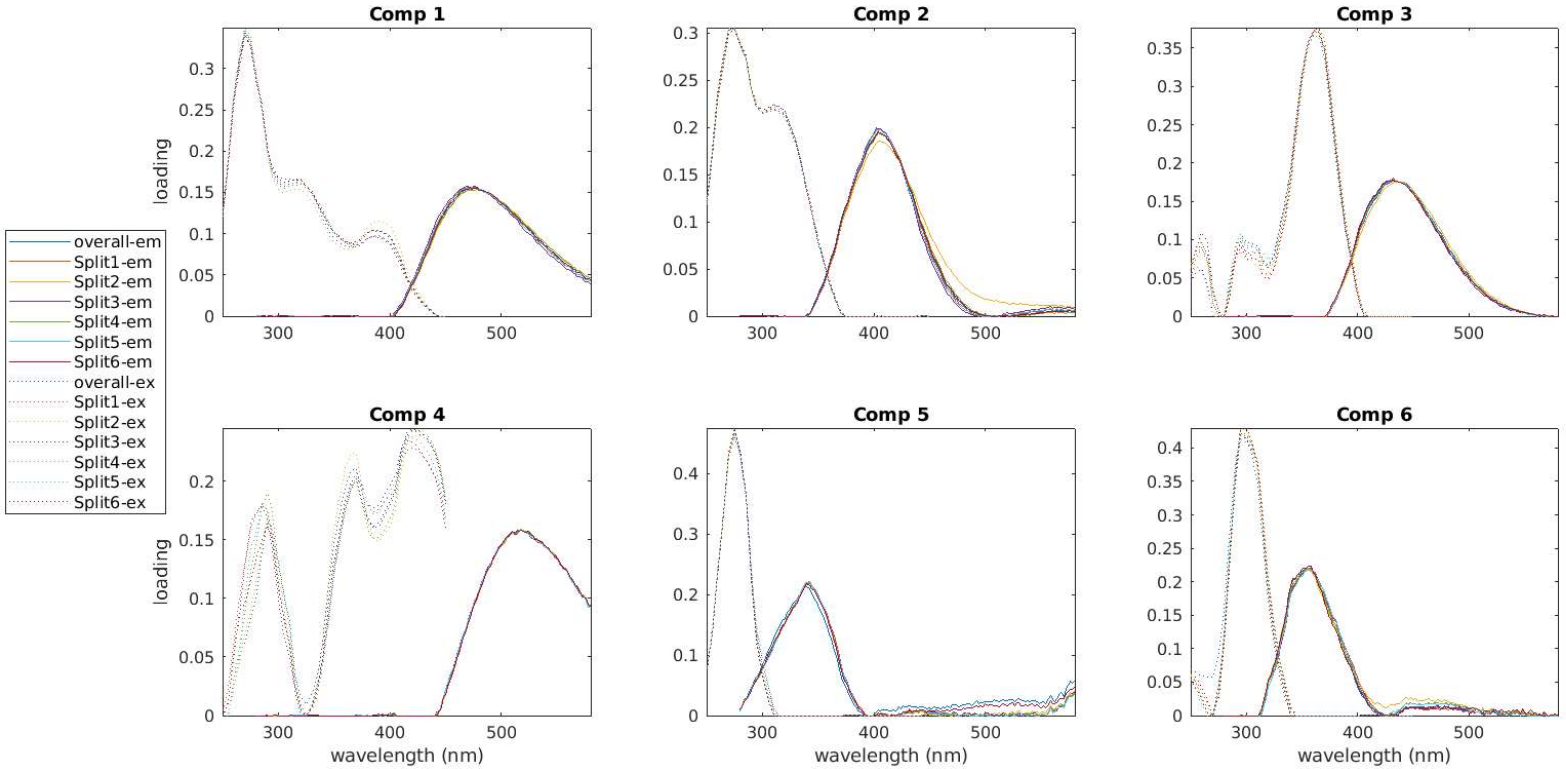

Figure 3.2. *Final validation of the model for six components identified through PARAFAC for the samples collected during the tidal cycles in the River Yare and Waveney (n = 24) at YAR4 on 21 July 2021 and at WAVE6 on 26 July 2020. The dashed lines indicate the excitation (ex) and the continuous lines indicate emission (em). The different colours indicate the different "splits" which the dataset was divided into. Every split has reached similar components and the model has been validated. See section 3.1.1 for further details.*

3.1.2 Absorbance and fluorescence spectral indices

Absorbance spectra were collected following the method discussed in section 2.3.2 and were processed to extract information (indirectly) on the molecular weight, source, photo- and bacterial degradation of CDOM (Table 3.1). The spectral slope coefficient S (Bricaud et al., 1981; Twardowski et al., 2004) was derived using the following formula:

$$\boldsymbol{\alpha}_{\lambda} = \boldsymbol{a}_{\lambda_0}\, e^{-\boldsymbol{S}(\lambda-\lambda_0)} \qquad equation\ 3.2$$

where $\boldsymbol{\alpha}_{\lambda}$ is the absorption coefficient in m^{-1} at a specific wavelength, $\boldsymbol{a}_{\lambda_0}$ is the absorption coefficient in m^{-1} for a wavelength of reference and $\boldsymbol{S}$ is the spectral slope in nm^{-1} which gives information about the steepness of the absorbance spectrum (Twardowski et al., 2004). To derive $\boldsymbol{S}$, equation 3.2 was fitted through nonlinear regression (Stedmon et al., 2000) for the wavelength ranges 275 – 295 nm and 350 – 400 nm as described in Helms et al. (2008). Values of S reflect the chemical characteristics of CDOM components such as molecular weight and aromaticity (Hansell *et al.*, 2009 and references therein). For $S_{275\text{-}295}$ and $S_{350\text{-}400}$ lower values are generally associated with more aromatic DOM and higher molecular weight (Helms et al., 2008; Hansen et al., 2016; Li and Hur, 2017). The decrease or increase of these spectral slope values have been also linked to biogeochemical processes such as biodegradation or photodegradation (Hansen et al., 2016; Li and Hur, 2017 and references therein). The Slope ratio S_R, was calculated by dividing $S_{275\text{-}295}$ by $S_{350\text{-}400}$, and gives information on CDOM molecular weight and degradation by solar radiation (Helms et al., 2008; Hansen et al., 2016). CDOM absorption coefficients were also used in combination with DOC concentration data to produce the Specific UV Absorbance at 254 nm wavelength ($SUVA_{254}$) (L mg-C^{-1} m^{-1}). This was obtained by dividing the absorbance at 254 nm wavelength (m^{-1}) by the DOC concentration (mg L^{-1}) (Weishaar et al., 2003). This parameter gives information about molecular weight and aromaticity as a result of studies that correlated it with carbon-13 Nuclear Magnetic Resonance (NMR) spectroscopy, allowing the differentiation between various sources of CDOM (Weishaar et al., 2003; Hansen et al., 2016).

Several fluorescence indices were calculated from the fluorescence spectra: the Fluorescence Index, the Freshness Index, the Humification Index and the peak T to peak C ratio (Table 3.1). The Fluorescence Index was calculated by dividing fluorescence emission intensity at 450 nm by the emission intensity at 500 nm, both excited at 370 nm (Mcknight et al., 2001). The Freshness Index was obtained by dividing the emission scans at 380 nm by those at 435 nm, both excited at 310 nm (Parlanti et al., 2000; Huguet et al., 2009; Wilson and Xenopoulos, 2009). The Humification Index was calculated by dividing

the emission intensity area between 435 - 480 nm by the emission intensity area between 300 - 345 nm, both excited at 254 nm (Zsolnay et al., 1999; Coble, 2014). Finally, the Peak T to Peak C ratio was calculated by dividing the maximum intensity at excitation 275 nm and emission at 350 nm (peak T), by the maximum fluorescence intensity of the excitation region between 320 – 340 nm and the maximum emission region 410 – 430 nm (Peak C) (Baker, 2001).

The Fluorescence Index gives insight into the origin of humic compounds that generally form most of DOM in freshwater, suggesting whether they have originated from soil or degraded plants, or from microbes like phytoplankton. It has been found to be linked to the C : N ratio with higher FI values corresponding to a lower ratio and vice versa (Gabor et al., 2014). The Freshness Index gives information on the "freshness" of DOM and the contribution of freshly produced versus more degraded (and therefore older) DOM. Some studies also found that the Freshness Index correlates with total dissolved nitrogen as inorganic nitrogen fuels microbial growth, therefore driving up BIX values (Wilson and Xenopoulos, 2009). Another index focussed on humic substances is the Humification Index which gives information on the H : C ratio and humification processes. As DOM becomes more humic the H : C ratio decreases, reflecting an increase in the carbon content and an increase in the HIX (Gabor et al., 2014; Hansen et al., 2016). The peak T : peak C ratio has been used to investigate water quality in terrestrial ecosystems more than marine ecosystems (Gabor et al., 2014). Peak T is associated with protein-like substances and freshly produced DOM, but some studies also showed a strong correlation with nitrate, phosphate and BOD (Biological Oxygen Demand), which can identify waters impacted by sewage or agricultural activities (Baker, 2001; Baker et al., 2003; Baker and Inverarity, 2004; Baker and Spencer, 2004; Hudson et al., 2007; Hudson et al., 2008). Conversely, peak C reflects humic-like compounds related to DOM from terrestrial sources and has been found to correlate to DOC in some studies (Gabor et al., 2014).

Table 3.1. *Description and calculation of spectral indices: spectral slopes, S_R, $SUVA_{254}$, FI, BIX, HIX, peak T : peak C.*

Spectral indices	Calculation	Use	Reference
Spectral slope S (nm^{-1}) (275-295, 350-400)	Non-linear regression fit of equation 3.2 for the absorbance over the chosen wavelength ranges	Higher values linked to lower molecular weight and to photodegradation	Bricaud et al., 1981; Stedmon et al., 2000; Twardowski et al., 2004; Helms et al., 2008
Spectral ratio S_R (nm^{-1})	S at 275-295 nm divided by S at 350-400 nm	Higher values linked to lower molecular weight. Also linked to photodegradation	Helms et al., 2008
Specific UV absorbance at 254 nm $SUVA_{254}$ ($L\ mg\text{-}C^{-1}\ m^{-1}$)	Absorbance at 254 nm divided by DOC concentration	Higher values indicative of high molecular weight and aromaticity	Weishaar et al., 2003
Fluorescence Index FI	Fluorescence emission at 450 nm divided by emission at 500 nm, both excited at 370 nm	Higher values linked to DOM of microbial origin and lower values linked to terrestrial DOM	Mcknight et al., 2001
Freshness Index BIX	Fluorescence emission at 380 nm divided by emission at 435 nm, both excited at 310 nm	Higher values indicative of freshly produced DOM and lower values indicative of more degraded DOM	Parlanti et al., 2000; Huguet et al., 2009; Wilson and Xenopoulos, 2009

Spectral indices	Calculation	Use	Reference
Humification Index HIX	Fluorescence intensity area between 435 – 480 nm divided by the emission area between 300 – 435 nm, both excited at 254 nm	Linked to the H : C ratio in DOM and the humification process. Higher values linked to higher aromaticity and carbon content	Zsolnay et al., 1999; Coble, 2014
Peak T to peak C ratio	Peak T (maximum fluorescence at excitation 275 nm and emission at 350 nm) divided by Peak C (maximum fluorescence intensity of the excitation region 310 – 340 nm divided by the maximum intensity of the emission region 410 – 430 nm)	Higher values correlated to freshly produced DOM indicative of agricultural activities and wastewater and lower values linked to terrestrial DOM	Baker, 2001

3.2. Results and discussion

3.2.1 PARAFAC components and OpenFluor database

The analysis of the 24 samples through PARAFAC resulted in the identification and validation of six components (Figure 3.8 and Table 3.2). The first component TC1 (Tidal Component 1) had excitation maxima at wavelengths (λ) of 270, 320 and 390 nm and an emission maximum at λ of 476 nm. TC1 is associated with humic-like substances of terrestrial origin, found across different aquatic environments (Lapierre and del Giorgio, 2014; Shutova et al., 2014; Dainard et al., 2019). TC2 (Tidal Component 2) had excitation maxima at λ of 275 and 310 nm and an emission maximum at λ of 404 nm. It is linked to humic-like substances that could be a result of microbial processing of organic matter of terrestrial origin, and they could be considered both allochthonous and autochthonous (Coble, 1996; Stedmon, 2003; Fellman et al., 2010; Amaral, et al., 2021; Du et al., 2021). TC3 (Tidal Component 3) had an excitation maximum at λ of 365 nm and an emission maximum at λ of 436 nm. TC3 has been linked to humic-like compounds found in waters impacted by wastewater or nutrient enrichment from agriculture (Murphy et al., 2011; Osburn et al., 2016; Amaral et al., 2021). TC4 (Tidal Component 4) had excitation maxima at λ of 420, 370 and 290 nm and an emission maximum at λ of 518 nm. It is probably indicative of humic-like compounds associated with soils, or waters near terrestrial sources, but since it has not been found in many studies its description is uncertain (Coble, 2014; Wagner et al., 2015; Chen et al., 2018; Hong et al., 2021). TC5 (Tidal Component 5) had an excitation maximum at λ of 275 nm and an emission maximum at λ of 340 nm and is associated with protein-like substances, in particular tryptophan-like compounds which are produced *in-situ* (see references in Table 3.2). The sixth component, TC6 (Tidal Component 6), had an excitation maximum at λ of 295 nm and an emission maximum at λ of 356 nm. This component is indicative of a mix of protein-like and humic-like compounds. The process involved in producing these complex components is microbial processing of autochthonous DOM, from either algae or plants or polyphenols derived from plants (Stedmon and Markager, 2005; Maie et al., 2007; Stedmon et al., 2007; Brym et al., 2014; Coble, 2014; Ren et al., 2021).

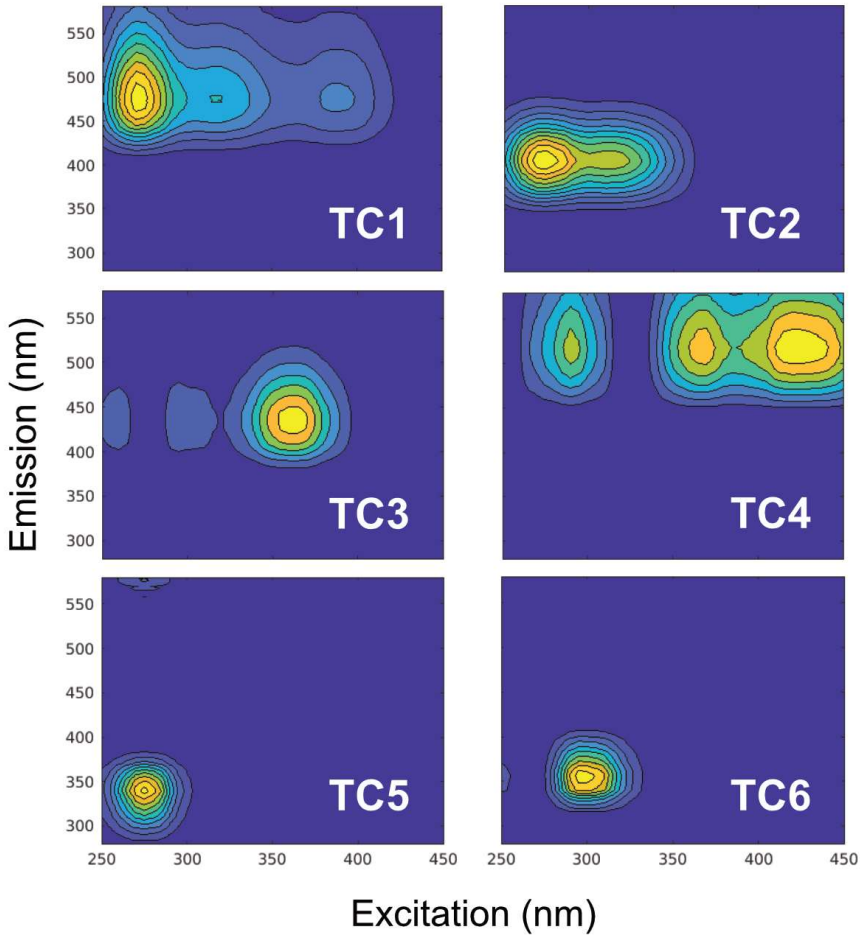

Figure 3.3. *Plots of the six components (TC1 – TC6) identified through the PARAFAC model for the 24 samples collected during tidal cycles in July 2020 for the River Yare and the River Waveney.*

The results of the PARAFAC model were input into the OpenFluor database (Murphy et al., 2014) which runs a comparison with other models and returns published studies that match the components fed into the database. The results are matched using the Tucker Congruence Coefficient (TCC) (Lorenzo-Seva and ten Berge, 2006). Table 3.2 shows some of the published studies matched with the dataset in this study with a TCC > 0.9, except for TC4 which had TCC > 0.8 – 0.9.

Table 3.2. *Description, spectral characteristics and comparison with the OpenFluor database of the six components identified and validated by the PARAFAC model for the 24 samples collected during the tidal cycle in July 2020 for the River Yare and the River Waveney.*

Component	Excitation/emission maxima λ (nm)	Description	OpenFluor database matches	Water type matches
TC1	270, 320,390 / 476	Humic-like of terrestrial origin with high aromaticity and molecular weight	Lapierre and del Giorgio, 2014; Shutova et al., 2014; Catalá et al., 2015; Amaral et al., 2016; Guéguen et al., 2016; Wünsch et al., 2017; Dainard et al., 2019; DeFrancesco and Guéguen, 2021; Imbeau et al., 2021; Smith et al., 2021	Boreal aquatic networks; Drinking water treatment plants; Dark ocean, >200 m depth; Shallow coastal lagoon, Uruguay; Estuarine system, Hudson Bay; Lakes, rivers and ocean waters; Polar mixed waters, Canada Basin; Arctic Ocean; Boreal and Arctic lakes; River to coastal waters, U.S.A
TC2	275, 310 / 404	Humic-like from microbial processing of organic matter of terrestrial origin	Kothawala et al., 2014; Shutova et al., 2014; Lambert et al., 2016; Sharma et al., 2017; Wünsch et al., 2017; Schittich et al., 2018; Amaral et al., 2021a, 2021b; Imbeau et al., 2021	Boreal lakes, Sweden; Drinking water treatment plants; River waters, Congo; Soil samples, Israel; Lakes, rivers and ocean waters; Groundwater aquifers, Bengal Basin; Estuarine and sediment pore waters; Boreal and Arctic lakes
TC3	365 / 436	Humic-like common in waters affected by wastewater and nutrient enrichment from agriculture	Murphy et al., 2011; Hambly et al., 2015; Osburn et al., 2016; Wünsch et al., 2017; Vines and Terry, 2020; Amaral et al., 2021	Water treatment plants; Recirculating aquaculture systems; Agro-urban coastal watershed; Lakes, rivers and ocean waters; Lake, river and water treatment plant; Estuarine water, Spain
Component	**Excitation/emission maxima λ (nm)**	**Description**	**OpenFluor database matches**	**Water type matches**

TC4*	420, 370, 290 / 518	Humic-like associated with soils or waters near terrestrial sources (uncommon)	Chen et al., 2018; Hong et al., 2021	Lake water, China; River water, Taiwan
TC5	275 / 340	Protein-like, particularly tryptophan-like from *in-situ* biological activity	Murphy et al., 2006; Yamashita et al., 2010; Stedmon et al., 2011; Dainard et al., 2015; Yu et al., 2015; Lee et al., 2018; Kida et al., 2019; Wang et al., 2020; Catalán et al., 2021; Sheng et al., 2021	Ballast waters from ships; Coastal waters, Liverpool Bay; Antarctic sea ice brines; Seawater, Beaufort Sea, North Atlantic; River, water treatment plant and algae; Algae; Lake and river waters, Antarctica; Lake waters, New York; River, algae, leaf leachates; Settled dust, China
TC6	295 / 356	Complex mix of substances with protein-like and humic-like. It is a product of microbial processing of plants, algae or polyphenols from senescent plants. Indicative of *in-situ* production.	Stedmon et al., 2007; Stedmon et al., 2011; Kowalczuk et al., 2013; Brym et al., 2014; Amaral et al., 2016; Chen et al., 2018; Schittich et al., 2018; Amaral et al., 2020a, 2020b; Ren et al., 2021	Sea ice, Baltic Sea; Antarctic sea ice brines; Atlantic Meridional Transect; River waters, North Carolina; Shallow coastal lagoon, Uruguay; Chukchi Sea, Arctic Ocean; Groundwater aquifers, Bengal Basin; Estuarine and sea waters, Spain; Lake waters, China.

*Studies matched shown for TC4 have a Tucker Congruence Coefficient (TCC) of 0.8 - 0.9.
The matches shown for the other components have TCC > 0.9.

3.2.2 Principal Components Analysis for both rivers

This section highlights similarities and differences between the two rivers through a principal component analysis (PCA) which allows the identification of the main drivers of DOM behaviour.

The PCA was run in the programming language R (R Core Team, 2020), but prior to the PCA, the one missing value in the dataset (for ammonium) was estimated using the R package missMDA which allows the determination of the impact of the estimated value on the PCA, hence the confidence of the imputed value (Josse et al., 2011; Josse and Husson, 2016). The PCA was performed using the R packages FactoMineR and factoextra (Lê, Josse and Husson, 2008; Kassambara and Mundt, 2020). The statistical significance of the PCA, the components and the loadings for the variables was tested using the R package PCAtest (Camargo, 2022) through permutation-based statistical tests (Figures B4 and B5 in Appendix B). The number of principal components (PCs or dimensions) to be considered were chosen based on the eigenvalues that contributed most to the variance in the dataset (Jolliffe, 2005). Figure 3.4 shows a *scree* plot which simplifies the choice of the principal components by choosing the number of components that explains most of the variability. In this study two principal components were chosen as in both PCAs run they explained most of the variance in the dataset.

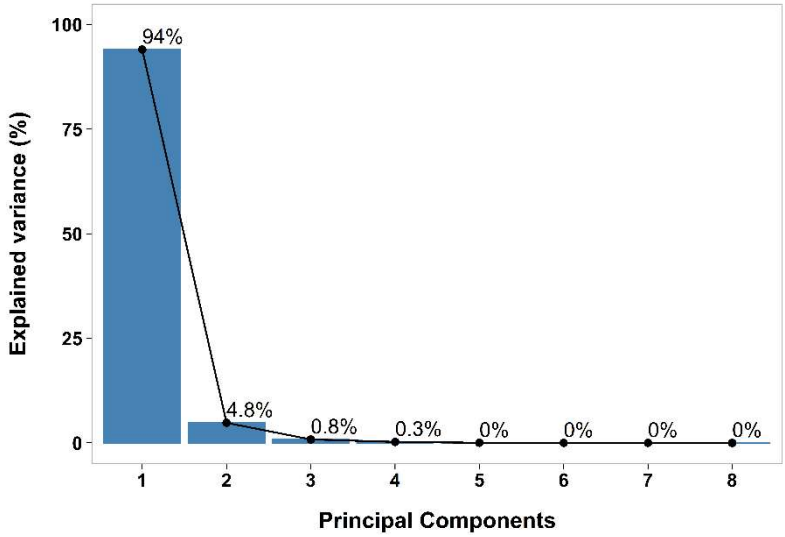

Figure 3.4. *Scree plot of the principal components and their variance in percentage for the sampling campaigns of the River Yare and Waveney on 21 and 26 July 2020 for the PCA analysis on the quantitative data of DOM.*

Two separate PCAs were run, one with CDOM, DOC and the fluorescent components as primary variables, whilst nutrients, chlorophyll-*a*, TSS, air temperature, solar radiation, salinity and the tide were input as supplementary variables. The second PCA was run with the spectral slopes, the spectral ratio, $SUVA_{254}$, BIX, FI, peak T to peak C and HIX

as primary variables, and the same variables as supplementary as in the second PCA, mentioned above. The purpose of the first PCA is to understand what the drivers of the data of quantitative DOM are (e.g., DOC concentration, CDOM, etc.), whilst the second PCA allows for greater insight into qualitative DOM data (e.g., $SUVA_{254}$, fluorescent ratios, etc.). In addition, adding non-DOM variables as "supplementary" allows to understand how the behaviour of DOM data compares to variations of non-DOM variables.

The quality of the variability explained by the principal components is obtained by the correlation between the variables and the two components (Abdi and Williams, 2010). The higher the correlation, the better the variables are represented by the principal components, and the closer to the circumference when plotted (Figures 3.5, 3.6, 3.7 and 3.8). The correlation between the variables and the components also gives information on the relationship between the variables. Variables that are grouped together are positively correlated, whilst variables positioned in opposite quarters of the circle are negatively correlated (Cooper et al., 2022). In the first PCA (Figures 3.4 and 3.5), all the variables showed a high positive correlation (> 0.9) with the first component.

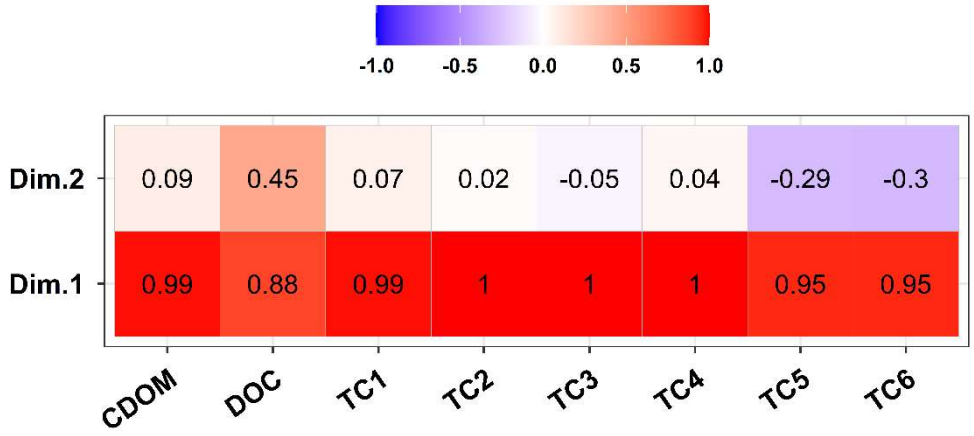

Figure 3.5. *Correlation between the variables of the quantity of DOM and the first two principal components chosen for the PCA. The numbers within the squares represent the correlation coefficients.*

The visualisation of the loadings (Figures 3.6A and 3.8A) of the variables and the score of the samples (Figures 3.6B and 3.8B) clarify which variables have the higher influence on the components and therefore on the dataset and the clustering of the samples. For the first PCA, Figure 3.6B shows two clusters for PC1 (left to right) and PC2 (top to bottom) characterising the two rivers, highlighting a difference between the rivers for these two sampling campaigns and for the quantitative DOM variables. The variables underlying this difference are visible in Figure 3.6A. On the right side of the plot in Figure 3.6A are the variables which content is higher in the River Waveney cluster (Figure 3.6B) than in the

River Yare cluster. The PCA highlighted a difference between the two rivers, with the River Waveney characterised by higher DOC (higher in less saline water), whilst the River Yare showed higher salinity and TSS and was negatively correlated to quantitative DOM variables. As explained previously, the closer the variables the more correlated and the larger the distance between them, the less correlated they are. If the variables are at a 90˚ angle there is no correlation. Note that in this dataset was negatively correlated to many variables in the study.

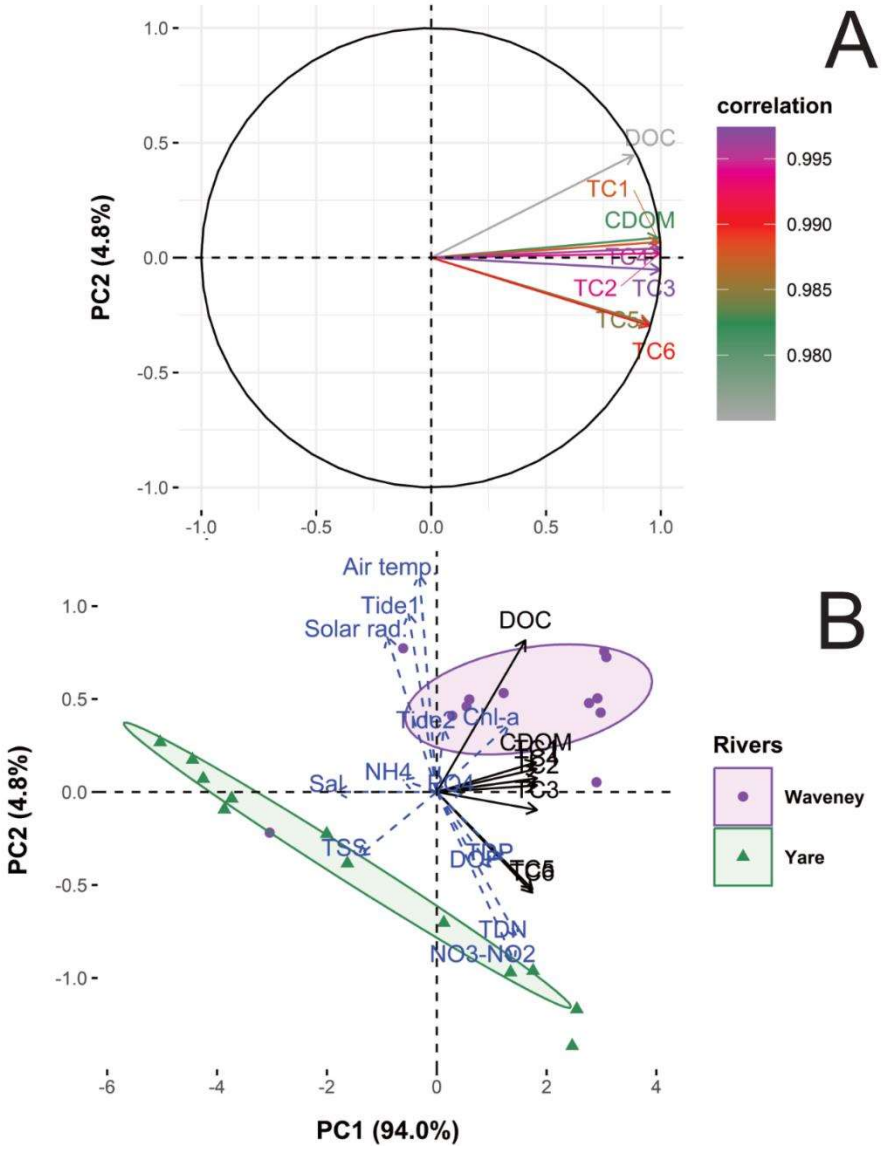

Figure 3.6. *Plot A represents the visualisation of the loadings of the variables analysed, coloured depending on how correlated they are to PC1 and PC2, whilst plot B represents the scores of the quantitative DOM data (black), plus the supplementary variables (blue) sampled in the River Yare on 21 July 2020 and in the River Waveney on the 26 July 2020 clustered by river (B) with ellipses representing 60% confidence assuming the dataset as a multivariate t-distribution.*

The second PCA was run with the two spectral slopes $S_{275\text{-}295}$ and $S_{350\text{-}400}$ and their ratio S_R, $SUVA_{254}$, BIX, FI, peal T to peak C and HIX as primary variables and nutrients, air temperature, tides, chlorophyll-*a*, salinity and TSS as supplementary variables. As in the

first PCA, the first two components explained most of the variance with 44.0% for PC1 and 29.8% for PC2.
The correlation between the variables of the quality of DOM and the two principal components (Figure 3.7) indicates a positive high correlation between the first component and peak T to peak C (0.9), whilst a high negative correlation between HIX and the first component (-0.9). The second component showed positive high correlation with $S_{350-400}$ (0.8) and negative high correlation with S_R (-0.8), which is expected given these two variables are usually negatively correlated.

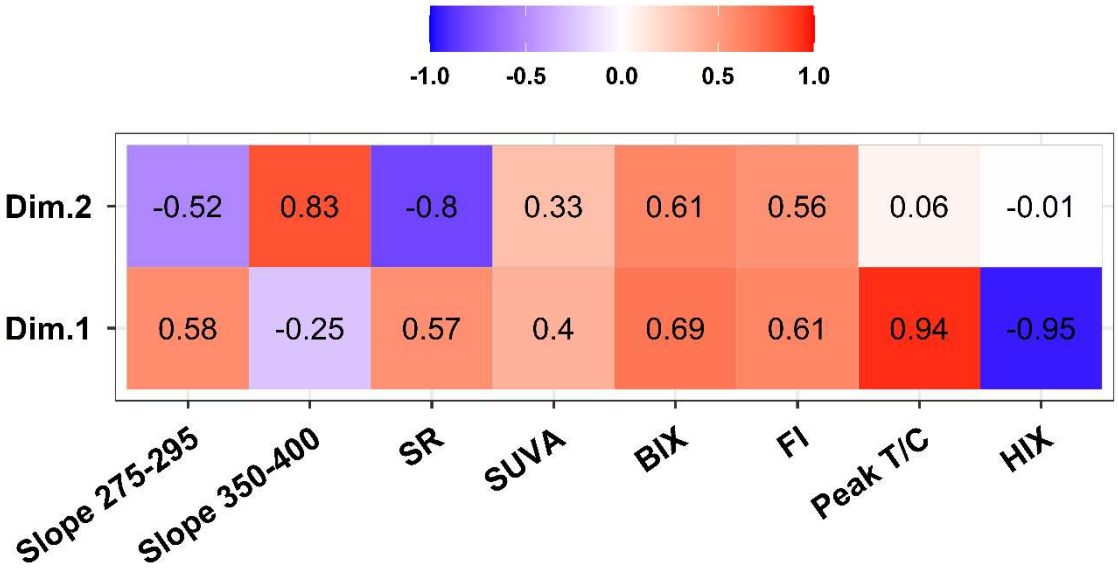

Figure 3.7. *Correlation between the variables of the quality of DOM and the first two principal components chosen for the PCA. The numbers within the squares represent the correlation coefficients.*

Figure 3.8A show the expected positive correlation between $S_{275-295}$ and S_R and the equally expected negative correlation between the mentioned spectral variables and $S_{350-400}$. In addition, also FI and BIX are positively correlated, whilst HIX is negatively correlated with all the variables, particularly with peak T to peak C (which gives an indication of freshly produced DOM). When the data are grouped by river (Figure 3.8B) the PCA shows a difference between the River Yare and the River Waveney, as in the first PCA, highlighting a difference in DOM characteristics. The River Waveney was characterised by more terrestrial DOM, with higher HIX values, whilst the River Yare is characterised by more microbial DOM, with higher BIX, FI and peak T to peak C values.

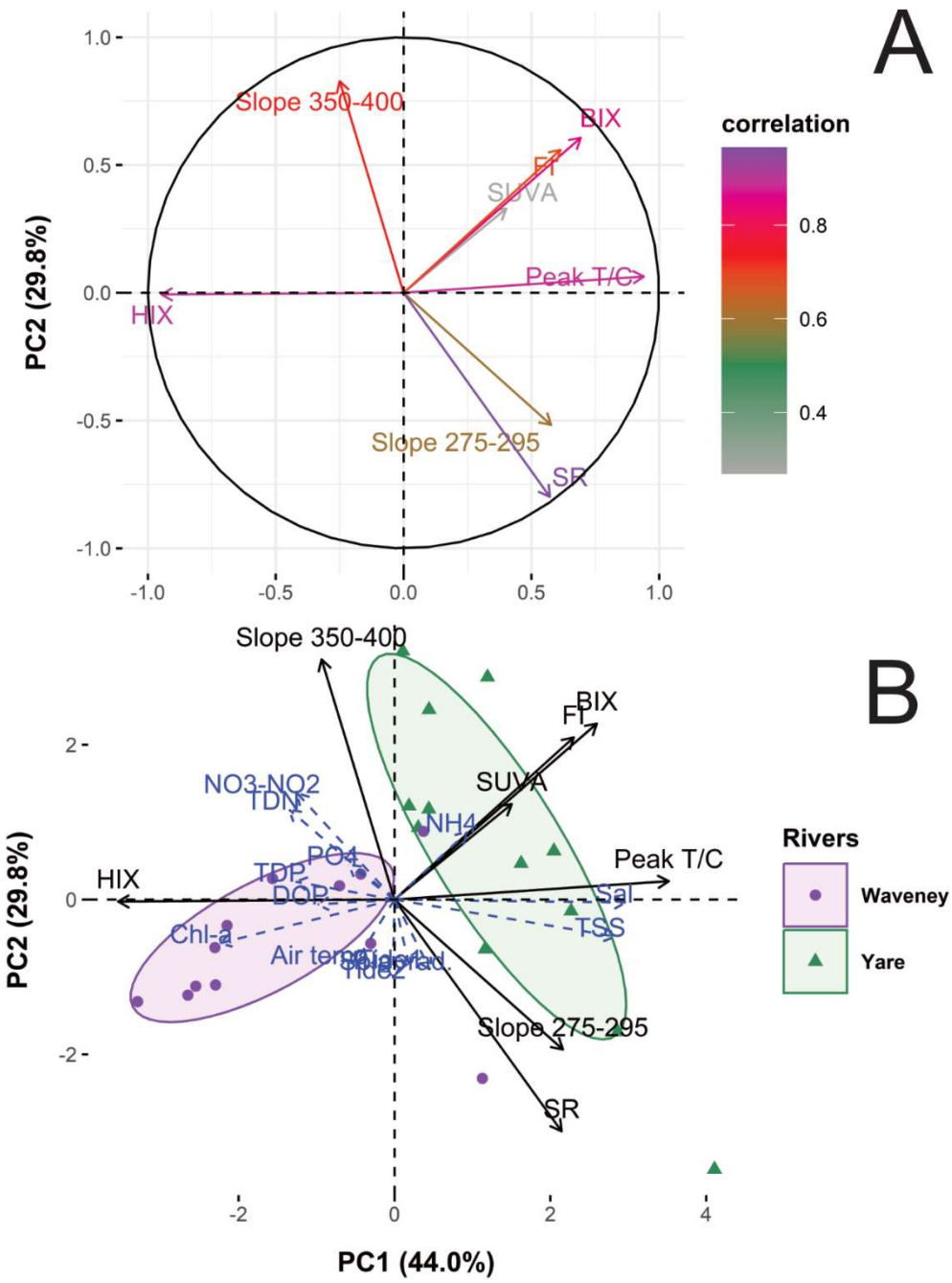

Figure 3.8. *Plot A represents the visualisation of the loadings of the variables analysed, coloured depending on how correlated they are to PC1 and PC2, whilst plot B represents the scores of the qualitative DOM data (black), plus the supplementary variables (blue) sampled in the River Yare on 21 July 2020 and in the River Waveney on the 26 July 2020 clustered by river (B) with ellipses representing 60% confidence assuming the dataset as a multivariate t-distribution.*

3.2.3 Sampling on the River Yare, 21 July 2020

This section shows the results and the tidal cycle for the sampling carried out on the River Yare, on the 21st July 2020. Samples were collected every hour between 7:00 and 18:00 UTC at the sampling site YAR4, near Reedham (see Figure 3.1). Spring tides occurred on 6 July and 24 July 2020, whilst neap tides occurred on 14 and 29 July 2020 (British Oceanographic Data Centre, 2021).

- Tidal cycle on the day of sampling

Figure 3.9 shows the tidal cycle of the day of sampling recorded by the two tide gauges (Figure 3.1) at Haven Bridge and at Reedham. The tide gauge at Haven Bridge is located approximately 8.5 km (straight line distance) downstream from the sampling location, whilst the tide gauge at Reedham is located approximately 3 km (straight line distance) upstream from the sampling location.

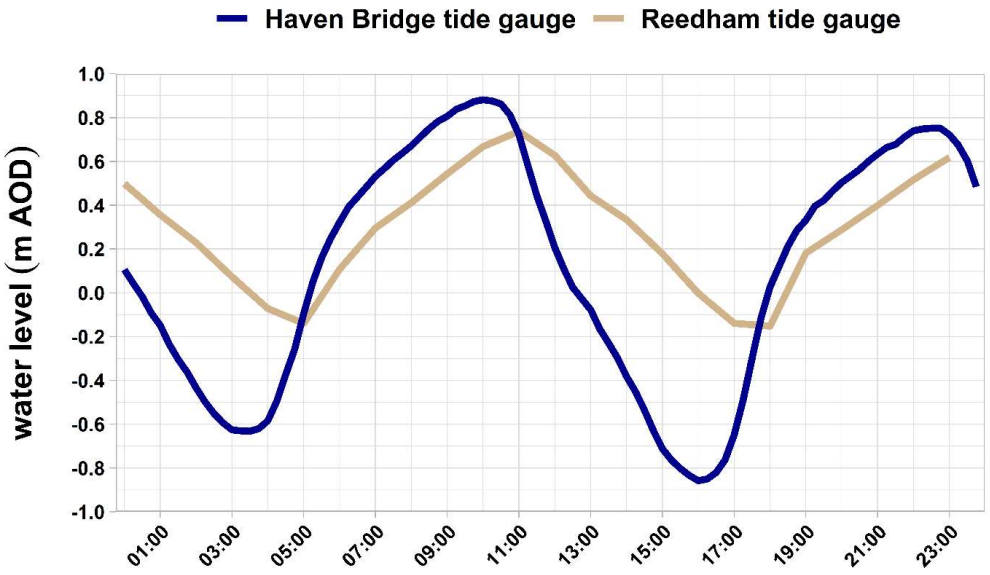

Figure 3.9. *Water level on the sampling day on the River Yare (21 July 2020) recorded by the tide gauges at Haven Bridge (Great Yarmouth) and Reedham. Times are in UTC.*

Figure 3.9 shows the tide was flowing in at the time of the collection of the first sample (7:00), then changing direction and ebbing at approximately 10:30 at Haven Bridge and at 11:00 at Reedham. Low tide was at 16:00 at Haven Bridge and approximately at 18:00 at Reedham.

- Salinity changes during the tidal cycle

Salinity reflected the tidal changes for most of the sampling day and it mirrored more strongly the tidal change at Reedham (closest to the sampling location). Although, as the

tide was ebbing at 14:00 salinity increased briefly, and then continued to decrease until 18:00, when the water level at Reedham reached its lowest height. Figure 3.10 shows the water level and the salinity for the sampling day, whilst Figure 3.11a provides the correlation between the water level at Reedham and salinity. Figure 3.11b shows the water level at Haven Bridge and salinity. There is a correlation between salinity (at YAR4) and the water level at Reedham (R^2 = 0.57), whilst there is no correlation between the water level at Haven Bridge and salinity at YAR4. This reflects the proximity of the tide gauge at Reedham with sampling location YAR4.

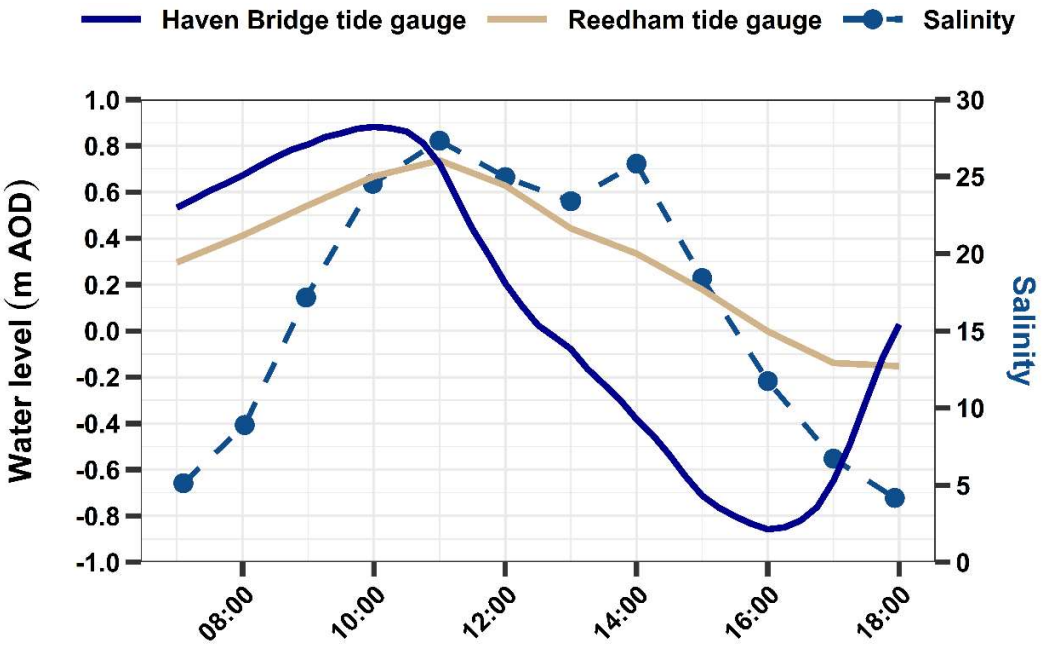

Figure 3.10. *Water level measured by tide gauges at Haven Bridge and Reedham and salinity measured at YAR4 through the tidal cycle between 7:00 and 18:00 on 21 July 2020. The points on the salinity curve represent the samples. Times are in UTC.*

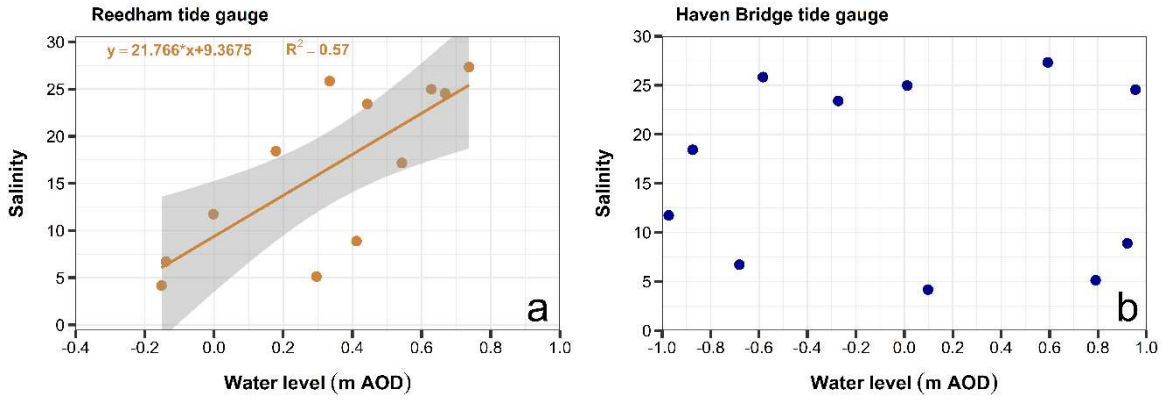

Figure 3.11. *Linear correlation between the water level at Reedham (a) and salinity, and the water level at Haven Bridge (b) versus salinity for the samples collected on 21 July 2020 at sampling site YAR4. The grey area indicates the 95% confidence interval for the linear correlation. p – value is < 0.01 for plot a. There was no correlation for plot b.*

- Behaviour of DOC and $CDOM_{\alpha 254}$ during the tidal cycle

Figure 3.12 shows the linear correlation between DOC and salinity, $CDOM_{\alpha 254}$ and salinity and the correlation between DOC and $CDOM_{\alpha 254}$, whilst Table 3.3 shows their range. In this study, both DOC and $CDOM_{\alpha 254}$ in the River Yare showed a strong linear anti-correlation with salinity with an R^2 of 0.98 for $CDOM_{\alpha 254}$ and R^2 of 0.99 for DOC. In addition, the correlation between DOC and $CDOM_{\alpha 254}$ was strong with an R^2 of 0.98, indicating a coupling of CDOM and DOC. Generally, low salinity water has a higher DOC and $CDOM_{\alpha 254}$ content, while saline water has a lower DOC and $CDOM_{\alpha 254}$ content (Álvarez-Salgado and Miller, 1999; Baker and Spencer, 2004; Bauer and Bianchi, 2011).

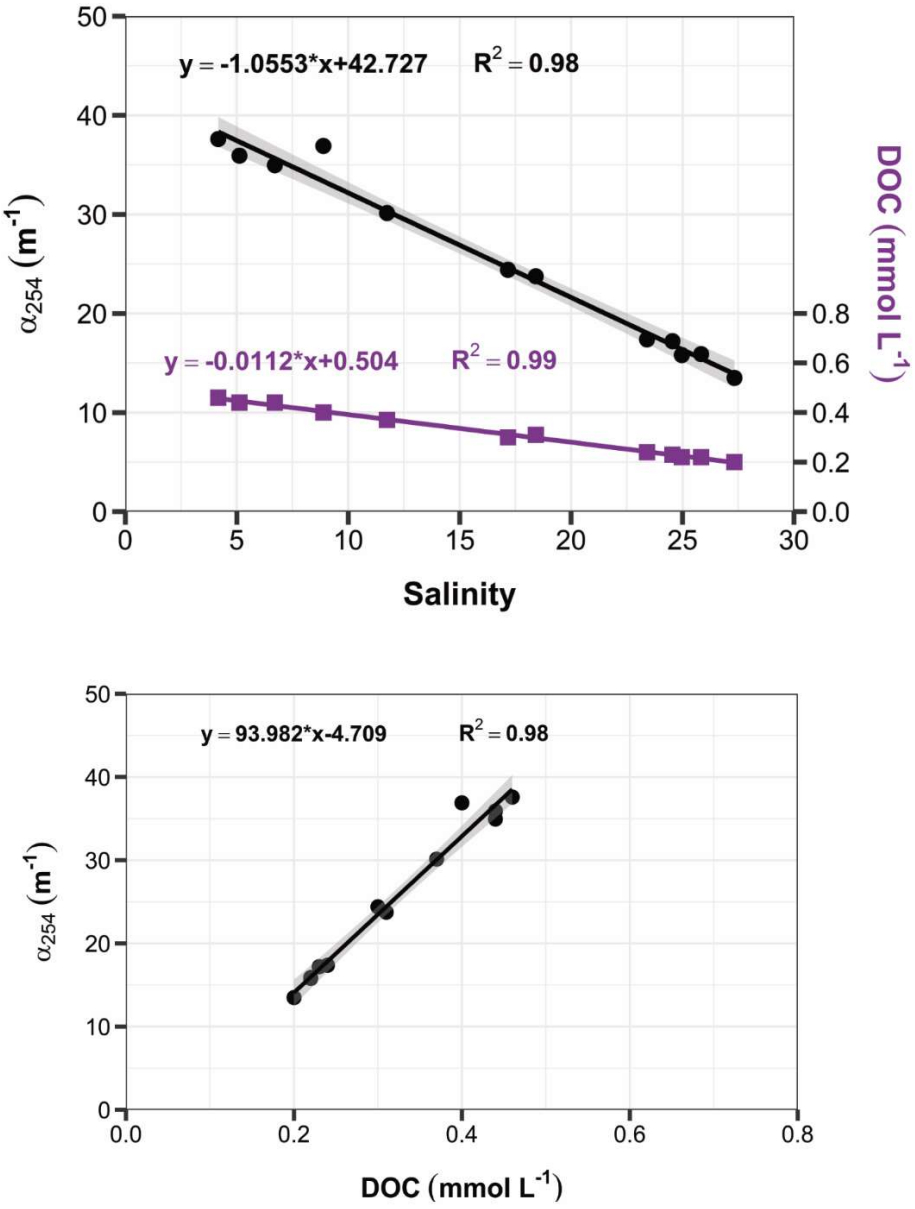

Figure 3.12. *Linear correlation between DOC (purple) and salinity, and $CDOM_{\alpha 254}$ (black) and salinity (top), and linear correlation between $CDOM_{\alpha 254}$ and DOC (bottom) for the samples collected on 21 July 2020 at sampling site YAR4. The grey area indicates the 95% confidence interval for the linear correlation. The significance for all the linear correlations is < 0.001.*

Table 3.3. *Minimum, maximum and average values for salinity, DOC concentration (mmol L^{-1}) and $CDOM_{\alpha 254}$ (m^{-1}) for the samples collected on 21 July 2020 at sampling site YAR4.*

Variable	Minimum	Maximum	Average
Salinity	4.17	27.33	16.53
DOC (mmol L^{-1})	0.20	0.46	0.32
$CDOM_{\alpha 254}$ (m^{-1})	13.58	37.60	25.29

- PARAFAC components dynamics

Figure 3.13 shows the six components identified through the PARAFAC model against salinity and Table 3.4 provides the equations and the R^2 for the linear correlations between the PARAFAC components and salinity. The fluorescence intensity of the six components decreased linearly with salinity. The fluorescence intensity is an indication of the concentration of the components. As DOC and $CDOM_{\alpha 254}$, FDOM (fluorescent DOM) was also influenced by the mixing of low salinity water rich in FDOM with saline water with a low FDOM. The range of fluorescence intensity of the six components is in Table 3.5.

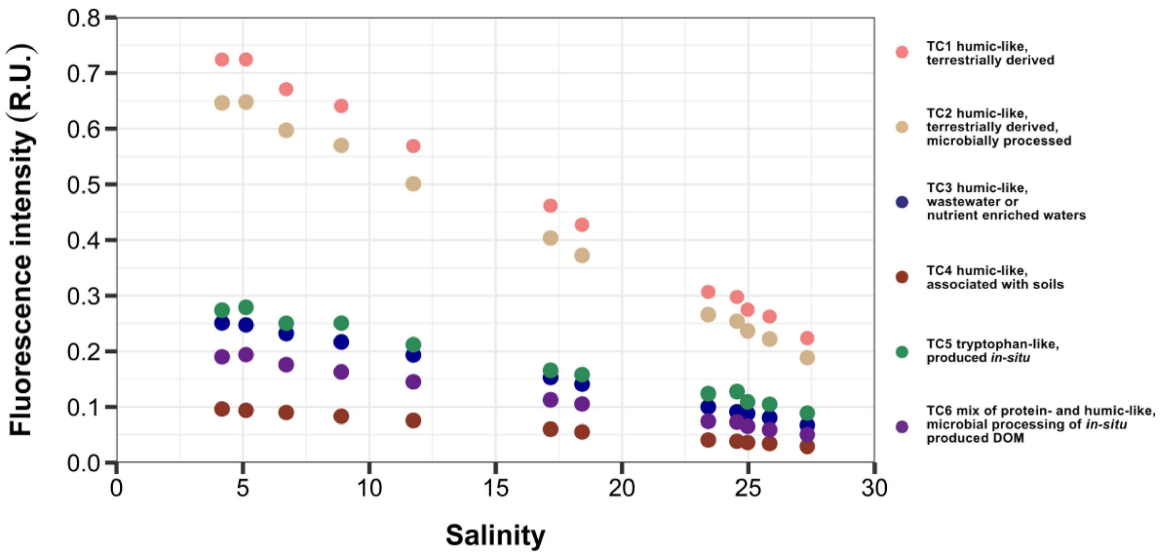

Figure 3.13. *The fluorescence intensity for the six components identified through the PARAFAC model as a function of salinity for the samples collected on 21 July 2020 at sampling site YAR4. The fluorescence intensity is in Raman units (R.U.).*

Table 3.4. *Equations and R^2 for the linear correlations between the components identified through the PARAFAC model and salinity, shown in Figure 3.8.*

Component	Equation linear correlation	R^2	Significance
TC1	$y = -0.0219x + 0.8273$	0.998	< 0.001
TC2	$y = -0.0201x + 0.7404$	0.998	< 0.001
TC3	$y = -0.0080x + 0.2867$	0.999	< 0.001
TC4	$y = -0.0029x + 0.1092$	0.999	< 0.001
TC5	$y = -0.0080x + 0.3111$	0.990	< 0.001
TC6	$y = -0.0061x + 0.2187$	0.997	< 0.001

Table 3.5. *Minimum, maximum and average fluorescence intensity in Raman units for the six components identified through the PARAFAC model for the samples collected on 21 July 2020 at sampling site YAR4.*

Components	Minimum fluorescence intensity (R.U.)	Maximum fluorescence intensity (R.U.)	Average fluorescence intensity (R.U.)
TC1	0.22	0.72	0.46
TC2	0.19	0.65	0.41
TC3	0.07	0.25	0.15
TC4	0.03	0.10	0.06
TC5	0.09	0.28	0.18
TC6	0.05	0.19	0.12

- Behaviour of chlorophyll-*a* and TSS

Components TC5 and TC6 found in the River Yare through the PARAFAC model were indicative of *in-situ* production, whilst TC4 was associated with soil and solids. Chlorophyll-*a* and total suspended solids (TSS) are shown as a function of salinity in Figures 3.14 and 3.15, whilst Table 3.6 shows the range of concentrations for the two variables. They are associated with primary production and particles including soil and sediments, respectively.

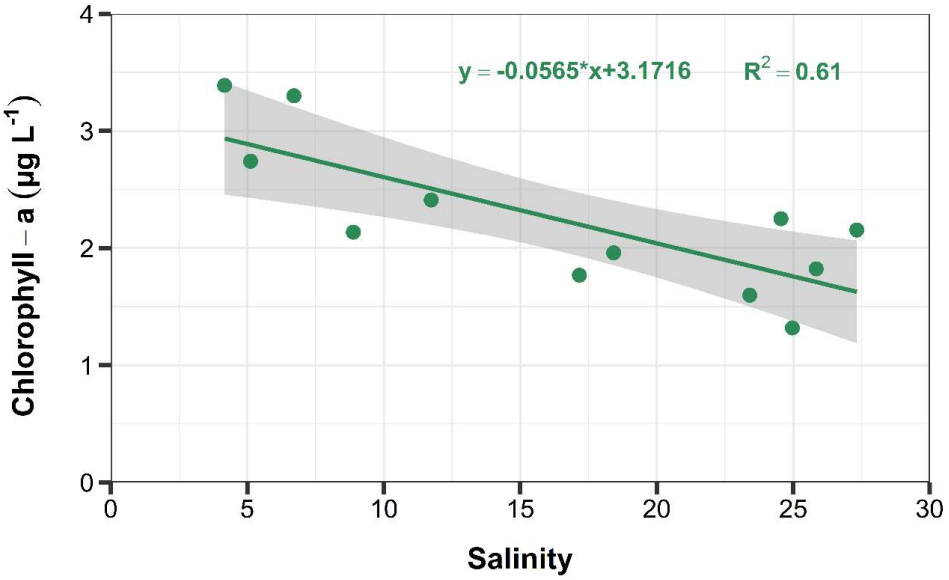

Figure 3.14. *Linear correlation between chlorophyll-a and salinity for the samples collected on 21 July 2020 at sampling site YAR4. The grey area represents the 95% confidence interval for the linear correlation. The significance of the correlation is < 0.01.*

Table 3.6. *Minimum, maximum and average concentrations for chlorophyll-a and TSS in µg L^{-1} and mg L^{-1}, respectively, for the samples collected on 21 July 2020 at sampling site YAR4.*

Variable	Minimum	Maximum	Average
Chlorophyll – a (µg L^{-1})	1.32	3.39	2.24
TSS (mg L^{-1})	91.46	241.20	136.95

Chlorophyll-*a* decreases with salinity, with the R^2 = 0.61 and the *p-value* below 0.01 indicating a moderate correlation The correlation between chlorophyll-*a* and salinity is weaker than that of DOC, $CDOM_{\alpha 254}$ and FDOM with salinity, with more variability along the mixing line. The variability along the correlation line could be explained by two overlapping processes: 1) higher concentration of chlorophyll-*a* at low salinity and lower concentration at high salinity and 2) increase in chlorophyll-*a* at high salinity due to coastal waters transported into the river through the tide.

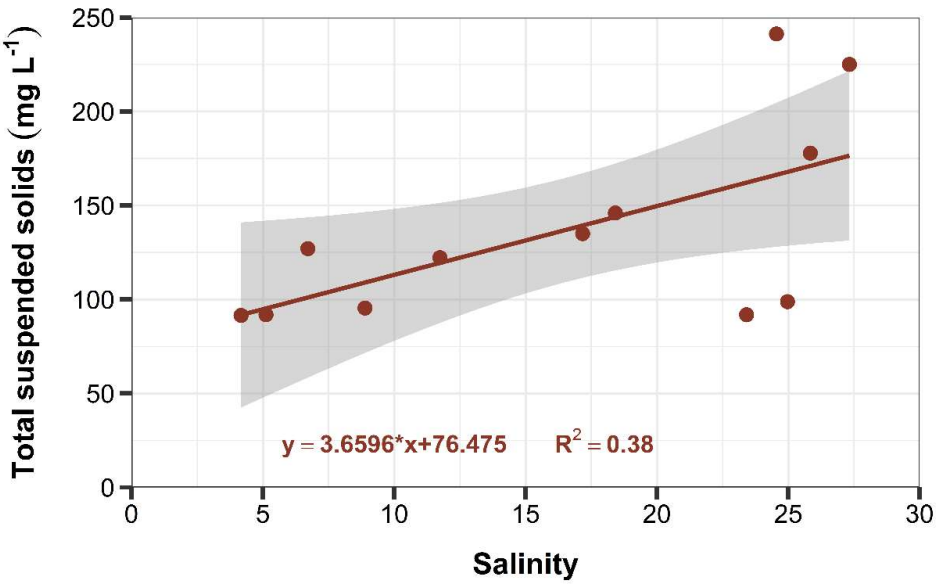

Figure 3.15. *Linear correlation between TSS and salinity for the samples collected on 21 July 2020 at sampling site YAR4. The grey area represents the 95% confidence interval for the linear correlation. The significance of the correlation is < 0.05.*

TSS generally increased with salinity, with some exceptions (Figure 3.15). This is in contrast with most published studies where TSS content is higher at low salinity and lower at high salinity linked to the river flow (Wisha and Ondara, 2017), although some studies found that TSS concentration is also affected by other factors such as strong tidal currents, strong winds, depth, topography and by the periodic tidal motion itself (Xiaohong et al., 2005; Park, 2007; Zhou et al., 2020). Note that the River Yare (and all the rivers within the Broads National Park) is frequented by boats, especially in summer, which contribute to the disruption of the natural current system of the river and to the resuspension of solids.

The variability along the correlation line in Figure 3.15 could be due to the settling of suspended solids during slack water, when the tide direction was changing, and the current velocity was near zero. This was reported by Pejrup and Edelvang (1996) for the Elbe estuary and by Winterwerp (1999), although the response of the suspended solids to the change in tide can vary depending on the location. In this study the TSS response to the change in tide was measured after ~ 1 - 2 hours of the tide reaching its maximum height at Reedham and ~ 1.5 – 2.5 hours after the maximum water level at Haven Bridge. The TSS increase with salinity could be also a result of cliff erosion or suspended solids coming from the North Sea with the tide.

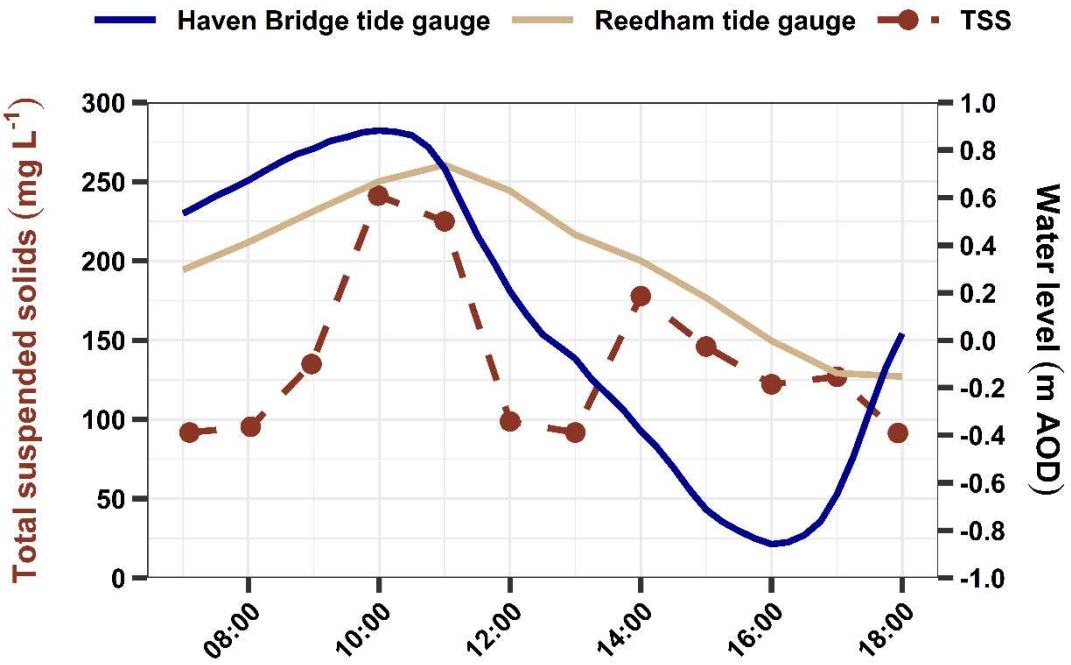

Figure 3.16. *TSS and water level through the tidal cycle between 7:00 and 18:00 on 21 July 2020 at sampling site YAR4. The points represent the samples. Times are in UTC.*

- Behaviour of nutrients

The following inorganic nutrients were measured in this study: total dissolved nitrogen (TDN), ammonium, nitrate plus nitrite, phosphate, and total dissolved phosphorus (TDP). From these measurements dissolved organic nitrogen (DON) and dissolved organic phosphorus (DOP) were derived by subtracting nitrate plus nitrite and ammonium from total dissolved nitrogen and by subtracting phosphate from total dissolved phosphorus, respectively. Figure 3.17 shows the linear correlation for the nutrients against salinity.

DON concentrations were negative for 22 of the 24 samples and therefore they are not included. Other studies have reported negative concentrations for DON due to its indirect estimation as a residual (Solinger et al., 2001; Lee and Westerhoff, 2005; Vandenbruwane et al., 2007). Especially when the concentrations of the inorganic forms of nitrogen are high, errors derived from the instrument can result in large uncertainties in the derived DON concentrations (Graeber et al., 2012; Sipler and Bronk, 2015). In addition, ammonium is a difficult chemical species to measure because it can be easily contaminated (Wurl, 2009). The range of concentrations for the nutrients is shown in Table 3.7 and values were comparable to those of a study from Neal and Robson (2000) for rivers with similar characteristics, although the concentrations in this study were lower for most of the parameters. This is highly likely due to the limited sampling in this dataset including data

collected only in July 2020, compared to the 6-year long sampling period used in the Neal and Robson (2000) study.

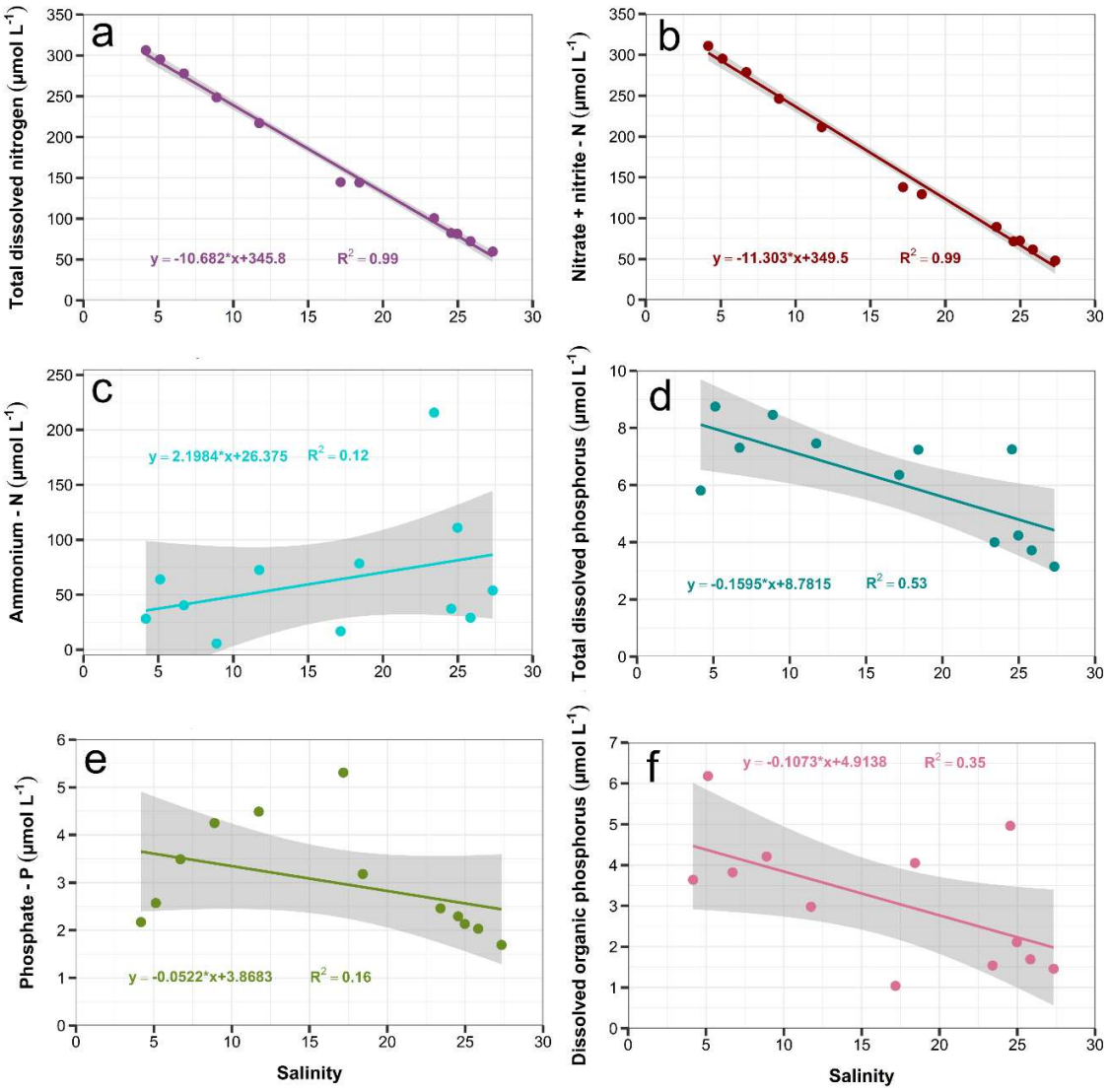

Figure 3.17. *Linear correlation of TDN, nitrate plus nitrite, ammonium, TDP, phosphate and DOP against salinity for the samples collected on 21 July 2020 at sampling site YAR4 (plots a-f). The grey area represents the 95% confidence interval for the linear correlation. The p-value was < 0.001 for linear correlations in plots* ***a*** *and* ***b****, < 0.01 for plot* ***d****, < 0.05 for plot* ***f*** *and 0.18 and 0.27 for linear correlations in plots* ***c*** *and* ***e****, respectively.*

Table 3.7. *Range of concentrations and average in µmol L^{-1} for TDN, nitrate plus nitrite, ammonium, TDP, phosphate and DOP for the samples collected on 21 July 2020 at sampling site YAR4.*

Variable	Minimum [µmol L^{-1}]	Maximum [µmol L^{-1}]	Average [µmol L^{-1}]
TDN	59.80	306.30	169.25
Nitrate + nitrite	47.90	311.00	162.73
Ammonium	5.70	215.70	62.71
TDP	3.15	8.75	6.14
Phosphate	1.69	5.31	3.00
DOP	1.04	6.18	3.14

The linear correlations for TDN and for nitrate plus nitrite indicate a strong riverine source and mixing of freshwater and seawater as the concentrations decreased linearly with the increase in salinity (Figure 3.17a and 3.17b), whilst the linear correlation for ammonium is not significant (*p*-value of 0.18) and indicates a more complex picture with concentrations increasing overall with salinity. The increase of ammonium with salinity could be due to the mechanism called *salinity-mediated release*, described by Bronk et al. (2010) and by Sipler and Bronk (2015). Due to the cationic nature of ammonium, it can form bonds with humic compounds and be replaced by salt ions once freshwater and saline water mix, releasing ammonium into the water column. Ammonium can also be released through desorption from sediments when solids are resuspended due to tidal currents or river flow (Simon, 1989; Morin and Morse, 1999; Fitzsimons et al., 2006; Porter et al., 2010; Duan and Kaushal, 2012). During this sampling day ammonium concentrations may have been impacted by both mechanisms, as evident from variability in both the correlation between ammonium and salinity (Figure 3.17c) and the correlation between ammonium and TSS (Figure 3.18). In addition, ammonium has a rapid turnover, and is not very stable.

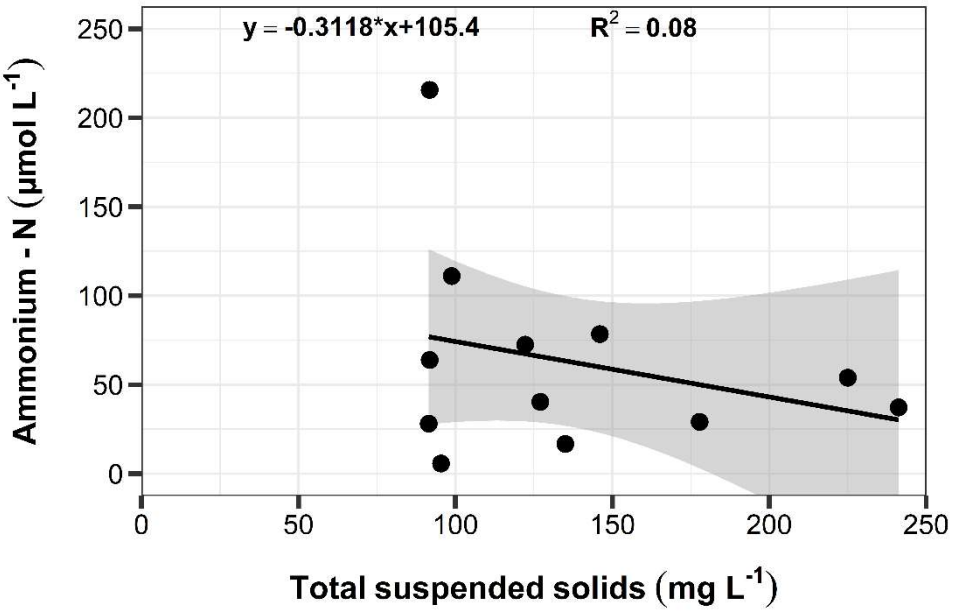

Figure 3.18. *Linear correlation between ammonium and TSS for the samples collected on 21 July 2020 at sampling site YAR4. The grey area represents the 95% confidence interval for the linear correlation. The p-value is 0.36.*

TDP, phosphate and DOP are negatively correlated with salinity (Figure 3.17d-f), although the correlation between salinity and phosphate is not significant (*p*-value = 0.27) and suggests the influence of processes in addition to linear mixing. The variability along the correlation line between TDP and salinity is a reflection of the variability of DOP and phosphate against salinity, given that TDP is the sum of the inorganic and organic forms of phosphorus, so only DOP and phosphate will be discussed. Generally, rivers have higher phosphorus content than seawater which decreases with an increase in salinity or by influence of coastal waters with less phosphorus content (Statham, 2012; Wang et al., 2022).

In general rivers also have higher suspended solids content than in seawater, which is not the case for the River Yare which has a lower concentration of suspended solids at low salinity and a higher concentration of suspended solids at higher salinity (as discussed in page 97, Figure 3.15). This can affect both inorganic and organic phosphorus concentrations, as suspended solids are transported upstream by the tide. The relationship of DOP and salinity in this study does not indicate simple linear mixing, although DOP overall decreased with an increase in salinity. Variability is also observed along the mixing line between phosphate and salinity. Phosphate does not correlate linearly with salinity between salinity 15 – 20, but above salinity 17.5 it decreased linearly, indicating linear mixing at higher salinities. The variability between DOP and salinity and the non-linear behaviour of phosphate with salinity could be explained by the mechanism of desorption from resuspended sediments due to the tidal currents (Roberts and Cooper, 2018; Li et al.,

2019; Liu et al., 2019; Wang et al., 2021), although the correlations between DOP and TSS and between phosphate and TSS are not very strong (Figure 3.19a and 3.19b). Another explanation could be the increased removal of phosphate from the water column with increased salinity reported by Wang et al. (2022) with greater adsorption when salinity is >15.

B

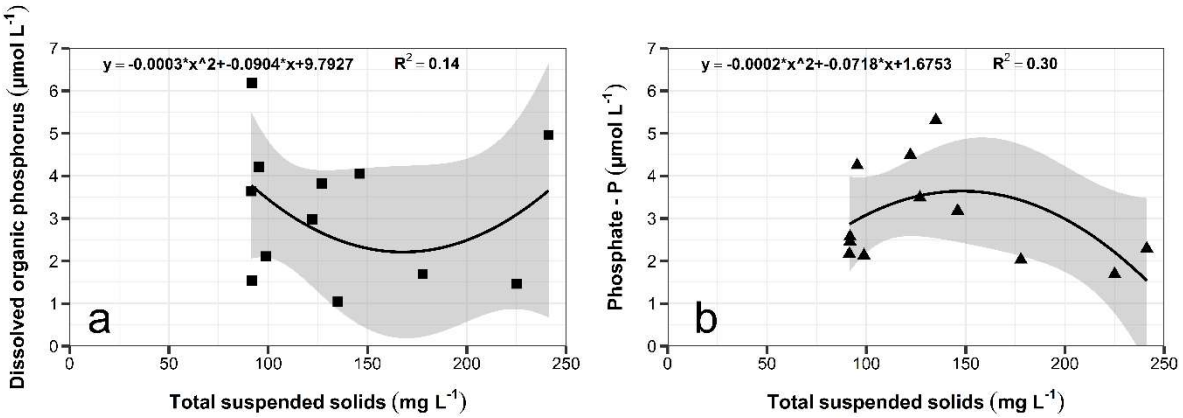

Figure 3.19. *Correlation between DOP and TSS (plot a), and between phosphate and TSS (plot b) for the samples collected on 21 July 2020 at sampling site YAR4. The grey area represents the 95% confidence interval for the linear correlation. The p-values are 0.5 for figure a, and 0.20 for figure b.*

A comparison between TSS, DOP and phosphate throughout the sampling day (Figure 3.20), shows DOP increasing following an increase in TSS at 10:00 and then following TSS behaviour but with a delay, whilst for phosphate, when TSS concentration was high between 10:00 and 11:00, the concentration of phosphate dropped. Note that between 7:00 and 10:00, DOP and phosphate show opposite trends. This could be due to the effect of bacterial remineralisation of DOP to phosphate or the consumption of phosphate by the microbial community producing DOP by exudation, excretion, cell lysis or death (Karl and Björkman, 2015). Phosphate is an important nutrient used by the microbial community and it can be readily taken up when it is released by resuspended sediments. In particular, as phytoplankton is transported upstream by the tide, where the phosphate concentration is higher than in seawater, it can stimulate their growth. Note that between 7:00 and 11:00 the tide was flowing in, moving saline waters into the river along with the coastal/marine microbial community.

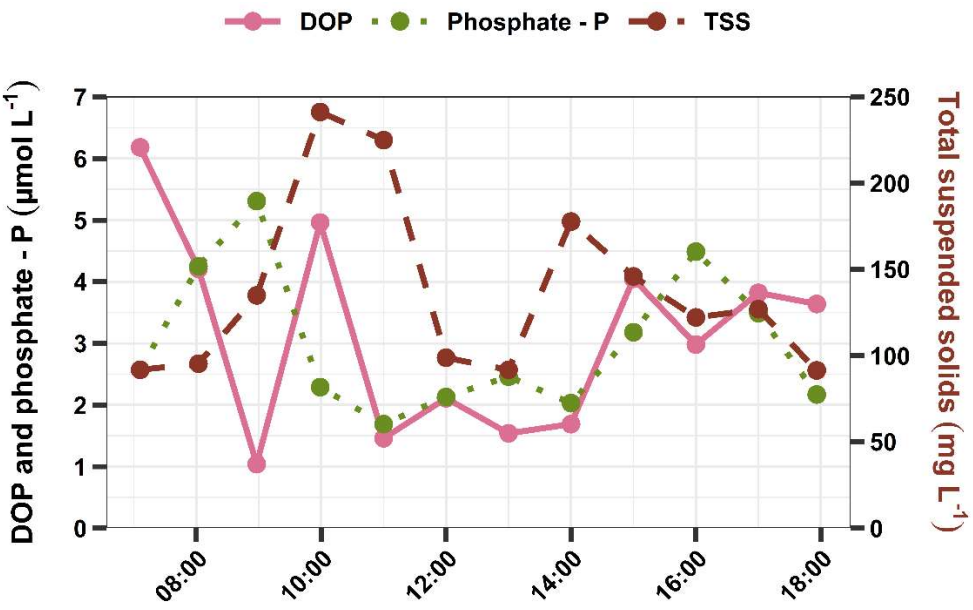

Figure 3.20. *DOP, phosphate and TSS through the tidal cycle between 7:00 and 18:00 of 21 July 2020 at sampling site YAR4. The points represent the samples. Times are in UTC.*

- Behaviour of absorbance and fluorescence indices

Figure 3.21 shows the spectral slopes $S_{275\text{-}295}$ and $S_{350\text{-}400}$ against salinity, whilst Table 3.8 shows the range of values for $S_{275\text{-}295}$, $S_{350\text{-}400}$ and S_R. The values for $S_{275\text{-}295}$ are in agreement with other studies for terrestrial and coastal ecosystems which are 0.012 – 0.023 nm^{-1} and 0.010 – 0.020 nm^{-1}, respectively (Helms et al., 2008; Pavlov et al., 2014; Hansen et al., 2016). The study conducted by Wagner et al. (2015) in the Florida Everglades, a system which includes freshwater, wetlands, estuarine waters and coastal waters reported values ranging between 0.005 and 0.032 nm^{-1} for $S_{350\text{-}400}$. The non-linear correlation between $S_{275\text{-}295}$ and salinity is weak (R^2 = 0.33) and not significant (*p*-value of 0.16). The non-linear correlation between salinity and $S_{350\text{-}400}$ is very weak (R^2 = 0.15) and not significant (*p*-value of 0.48). Previous studies reported an increase in $S_{275\text{-}295}$ when DOM molecular weight decreased, due to solar radiation, whilst $S_{350\text{-}400}$ values showed the opposite (Helms, et al., 2008; Hansen et al., 2016).

The variability of these values can be explained by the different processes characterising natural waters. Abiotic and biotic processes do not happen sequentially, but simultaneously, especially in rivers affected by tidal changes where water bodies are moved and mixed cyclically and by human activities. These simultaneous processes could impact the spectral slope values by masking one process over another, or by enhancing the signal of one process over another, hence the need for caution when interpreting these spectral slopes (Wagner et al., 2015; Hansen et al., 2016).

Table 3.8. *Range of concentrations and average in nm^{-1} for $S_{275-295}$, $S_{350-400}$ and S_R for the samples collected on 21 July 2020 at sampling site YAR4.*

Variable	Minimum (nm^{-1})	Maximum (nm^{-1})	Average (nm^{-1})
$S_{275-295}$	0.016	0.022	0.019
$S_{350-400}$	0.012	0.024	0.018
S_R	0.78	1.71	1.07

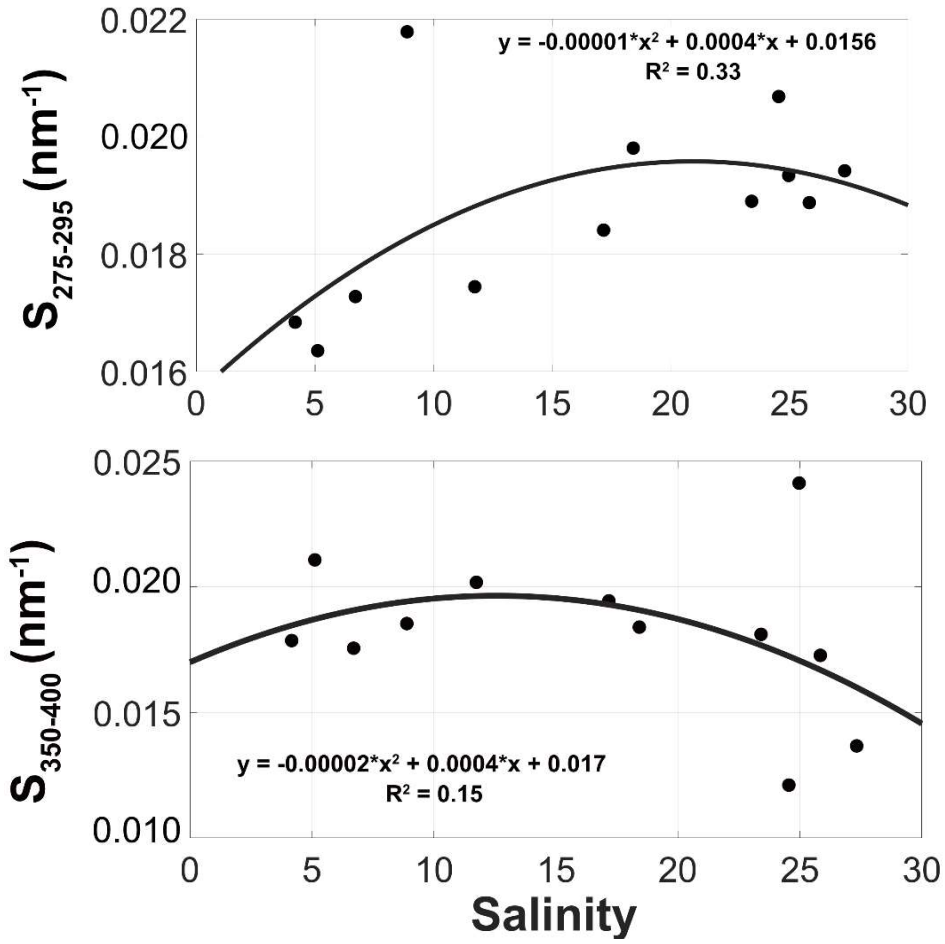

Figure 3.21. *Non-linear correlation between $S_{275-295}$ and salinity (top figure) and between $S_{350-400}$ and salinity (bottom figure) for the samples collected on 21 July 2020 at sampling site YAR4. Both correlations were non-significant with p-values of 0.16 and 0.48, respectively. The points represent the samples.*

Figure 3.22 shows the Spectral Ratio (S_R) between $S_{275-295}$ and $S_{350-400}$ against salinity. Previous studies reported values of ~ 0.71 for terrestrial ecosystems and ~ 1.10 for estuarine ecosystems, with higher values of ~ 1.5 reflecting marine waters and specifically the shelf break (Helms et al., 2008). The relationship between S_R and salinity indicates higher S_R values, hence DOM with lower molecular weight as the salinity increased with

some variability along the regression line. This variability could reflect the differences in molecular weights of DOM from freshwater and seawater.

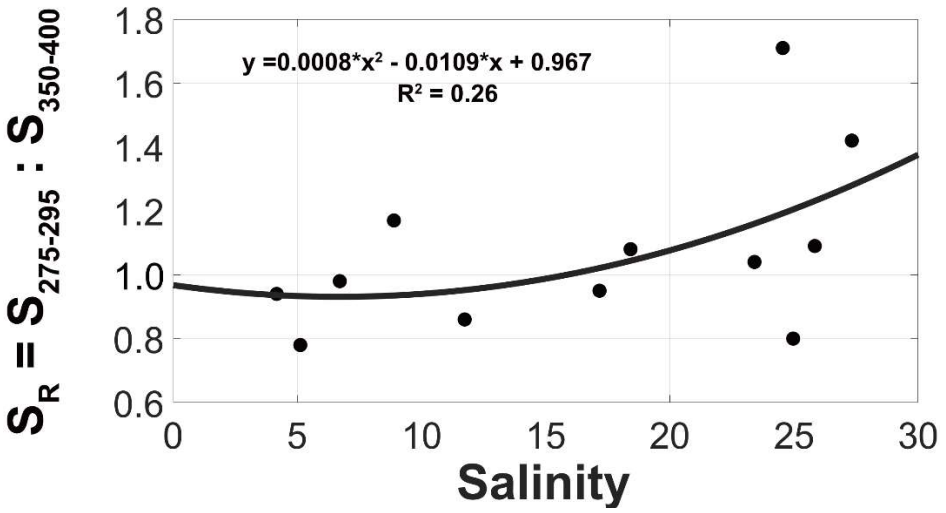

Figure 3.22. *Non-linear correlation between S_R and salinity for the samples collected on 21 July 2020 at sampling site YAR4. The p-value was 0.26. The points represent the samples.*

Figure 3.23 represents the non-linear correlations between $SUVA_{254}$, HIX, FI and peak T : peak C against salinity, whilst Table 3.9 shows their range in this study.

Both $SUVA_{254}$ and HIX significantly decreased with salinity as seen for CDOM and DOC, with values resembling those for waters with lower aromatic content (Figure 3.23a and 3.23b). Values for $SUVA_{254}$ have been reported by Hansen et al. (2016) for surface waters, ranging between 1.0 and 6.0 L mg-C^{-1} m^{-1} and by Kellerman et al. (2018) with a range of 0.6 – 4.9 L mg-C^{-1} m^{-1} with highest values from river samples and lowest values from groundwater and ocean waters. HIX values in this study are characteristic of waters with terrestrial inputs, as well as *in-situ* production. Huguet et al. (2009) reported HIX values from studies on several estuaries with HIX > 10 for waters with a strong terrestrial input, between 6 and 10 for waters mostly containing humic substances but also some material produced *in-situ*, a range of 4 – 6 for waters with a higher autochthonous character and less humic components and finally, HIX < 4 for waters strongly characterised by bacterial production.

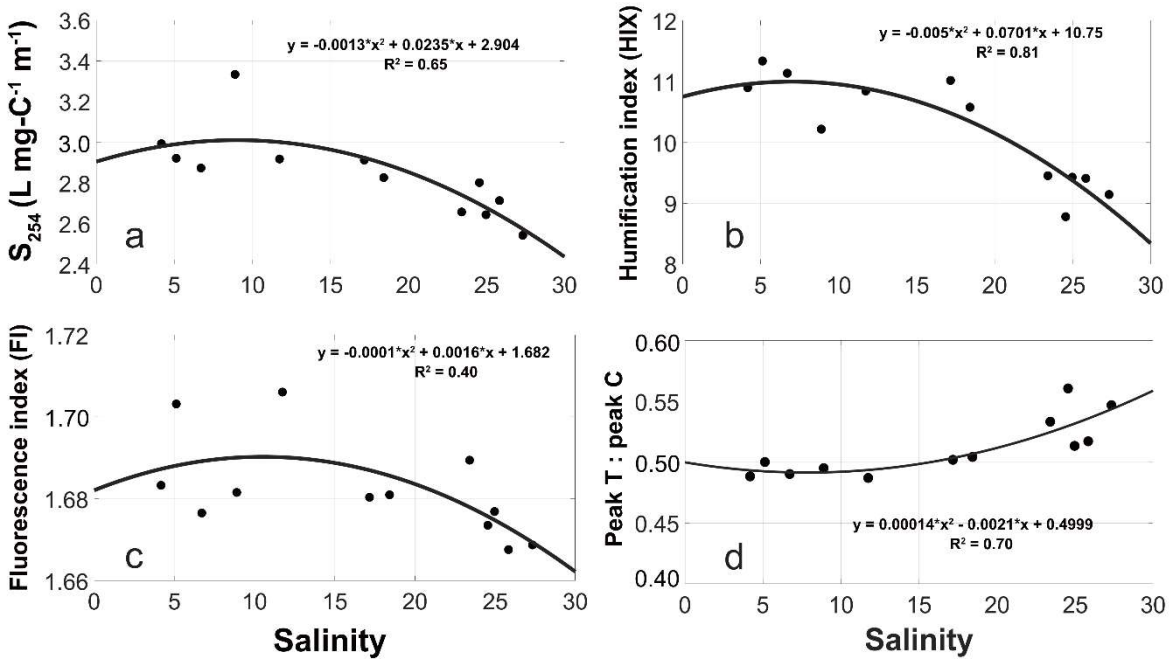

Figure 3.23. *Non-linear correlation between $SUVA_{254}$, HIX, FI and peak T : peak C and salinity (plots a-d) for the samples collected on 21 July 2020 at the sampling site YAR4. The p-value was < 0.01 for $SUVA_{254}$, < 0.001 for HIX, 0.1 for FI, < 0.01 and for peak T : peak C. The points represent the samples.*

FI also presented a negative relationship with salinity, although the variability along the mixing line is very high (R^2 = 0.40). FI gives information on the precursors of humic substances in DOM and it is correlated to the ratio of C : N in DOM with high FI values indicating low C : N and vice versa. Previous studies reported FI values ranging between ~1.2 to ~1.9 for rivers, lakes and ocean waters (Gabor et al., 2014; Kellerman et al., 2018), where the lower values indicate DOM which originated from terrestrial sources and higher values suggest DOM with a more microbial origin (DOM produced *in-situ*). The range of values for this study indicate that DOM originated both from terrestrial and microbial sources as indicated also by $SUVA_{254}$ and HIX.

The fluorescence indices in Figure 3.23d are representative of freshly produced DOM (see section 3.1.2) and depending on the land use of the catchment, values can vary between ~0.1 (upland catchments with a high peat content) and ~1 where the peak T and the peak C have equal intensity and are characteristic of sewage effluents (Baker, 2001; Hudson et al., 2007). In the study from Hudson et al. (2007) values from rivers impacted by urbanisation and intensive agriculture ranged from ~0.3 to ~0.9. In this study peak T : peak C values reflect the land use of the study area (urban and intensive agriculture) and increase with salinity, suggesting an increase either in the peak T (fresh DOM) or a decrease in peak C (terrestrial DOM) with salinity. In this case it can also be a mixture of the two as the river moves freshwater downstream (rich in aromatic DOM) and the tides bring saline waters upstream (richer in fresh DOM). This is confirmed by a positive correlation between the

water level at Reedham and peak T : peak C with R^2 = 0.59 and *p*-value < 0.01 (Figure B1 in Appendix B).

Table 3.9. *Range of values and average for $SUVA_{254}$, HIX, FI, peak T : peak C and BIX for the samples collected on 21 July 2020 at sampling site YAR4.*

Variable	Minimum	Maximum	Average
$SUVA_{254}$ L mg-C^{-1} m^{-1}	2.54	3.33	2.84
HIX	8.78	11.34	10.19
FI	1.67	1.71	1.68
peak T : peak C	0.49	0.56	0.51
BIX	0.74	0.79	0.77

3.2.4 Sampling on the River Waveney, 26 July 2020

This section shows all the results and the tidal cycle for the sampling carried out on the River Waveney, on the 26th July 2020. Samples were collected every hour between 7:00 and 18:00 at sampling site WAVE6 at St. Olaves (see Figure 3.1). As mentioned in section 3.2.2, spring tides occurred on 6 and 24 July, whilst neap tides occurred on 14 and 29 July (British Oceanographic Data Centre, 2021).

- Tidal cycle on the day of sampling

Figure 3.24 shows the tidal cycle of the sampling day and the water level recorded by the two tide gauges (Figure 3.1) at Burgh Castle and at Haddiscoe. The tide gauge at Burgh Castle is located approximately 0.4 km (straight line distance) downstream from the sampling location, whilst the tide gauge at Haddiscoe is located approximately 0.67 km (straight line distance) upstream from the sampling site.

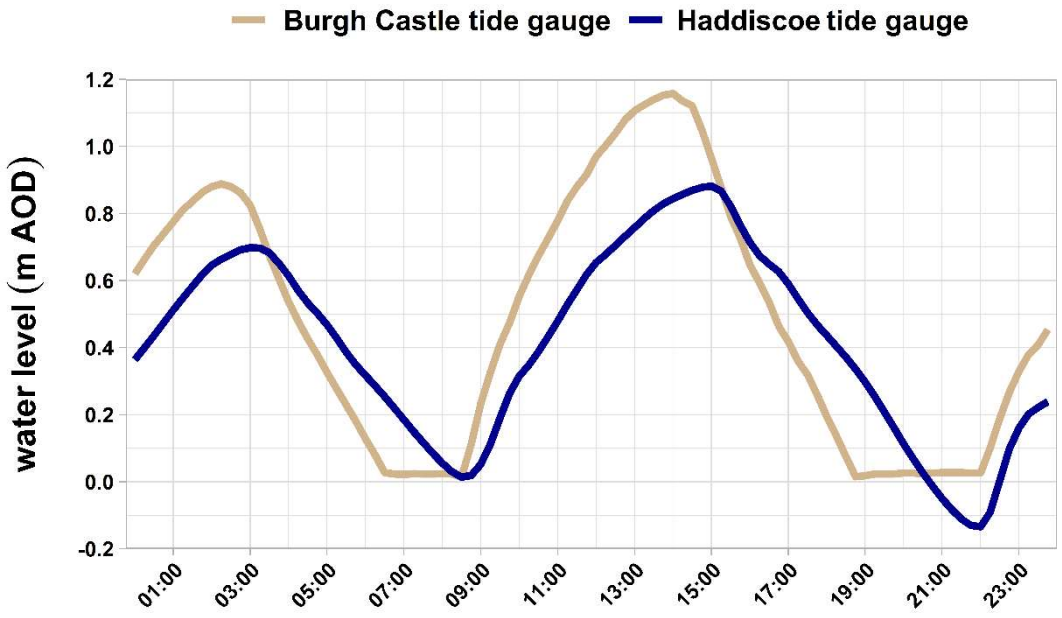

Figure 3.24. *Tidal cycle of the sampling day on the River Waveney (26 July 2020) recorded by the tidal gauges at Burgh Castle and Haddiscoe. Times are in UTC.*

At 7:00, when the first sample was collected, the tide was ebbing and changed direction at 8:30 at Haddiscoe. The low tide measurements for the tide gauge at Burgh Castle are not available, because the tide gauge did not record measurements below 0 m of the ordnance datum. The difference between the two tide gauges in terms of tidal range is about 1 hour, with the tide at the Haddiscoe gauge flowing in 1 hour later compared to the tide gauge at Burgh Castle. Therefore, if low tide was at 8:30 at Haddiscoe, it can be estimated that it was at 7:30 at Burgh Castle.

- Behaviour of salinity during the tidal cycle

Figure 3.25 shows salinity throughout the tidal cycle between 7:00 and 18:00. Salinity remained constant between 7:00 and 11:00, not responding to the tidal change at 8:30. Salinity had a rapid increase after 11:00 as the incoming tide was moving saline water upstream. The delay in the response of salinity to the tide could be due to a salt wedge characterised by less dense freshwater above the denser saline water. Salt wedges are not uncommon in this river as described by the Environment Agency (1999). Especially in summer, when the river flow is low (Hannaford and Buys, 2012; Cooper et al., 2020), the strength of the tide pushing upstream can form these salt wedges resulting in water stratification (Krvavica et al., 2017 and references therein).

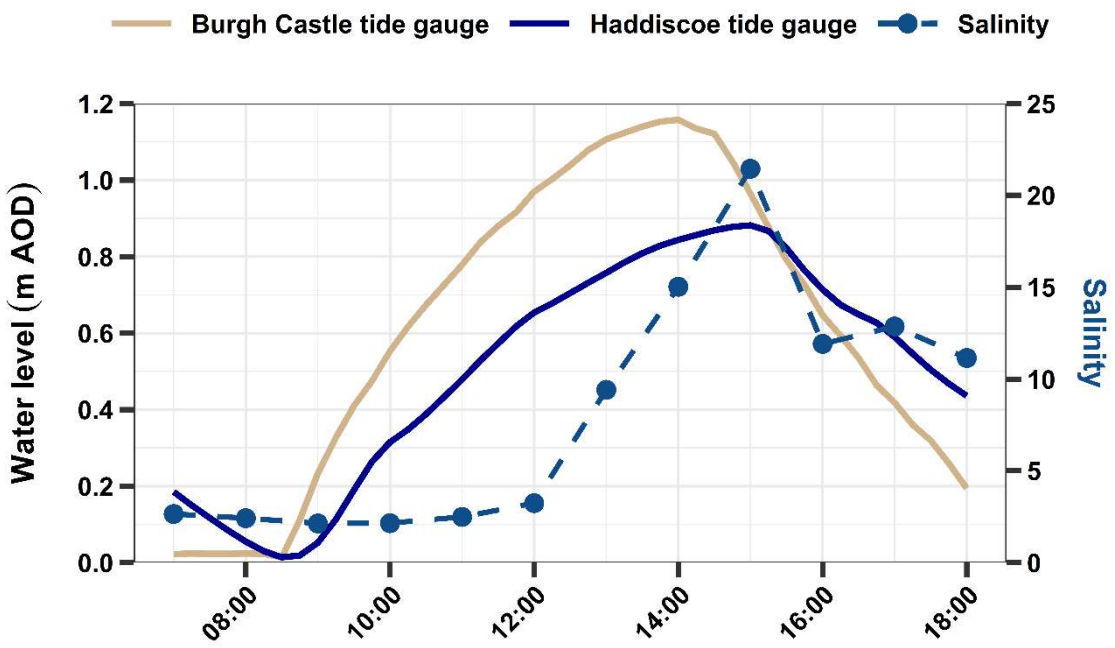

Figure 3.25. *Water level measured by the tide gauges at Burgh Castle and Haddiscoe with salinity measured at WAVE6 through the tidal cycle between 7:00 and 18:00 on 26 July 2020. The points on the salinity curve represent the samples. Times are in UTC.*

The correlations between salinity and the water level measured by the two gauges (Figure 3.26) show a higher correlation with the tide gauge at Haddiscoe (R^2 = 0.60), the more distant from the sampling location compared to the gauge at Burgh Castle (R^2 = 0.21). This could be a reflection of the salt wedge. As the saline water is moving underneath the freshwater, there was not an increase in salinity until later which resulted in a delay, reflected by the better correlation with the tidal gauge at Haddiscoe, the more distant to the sampling site.

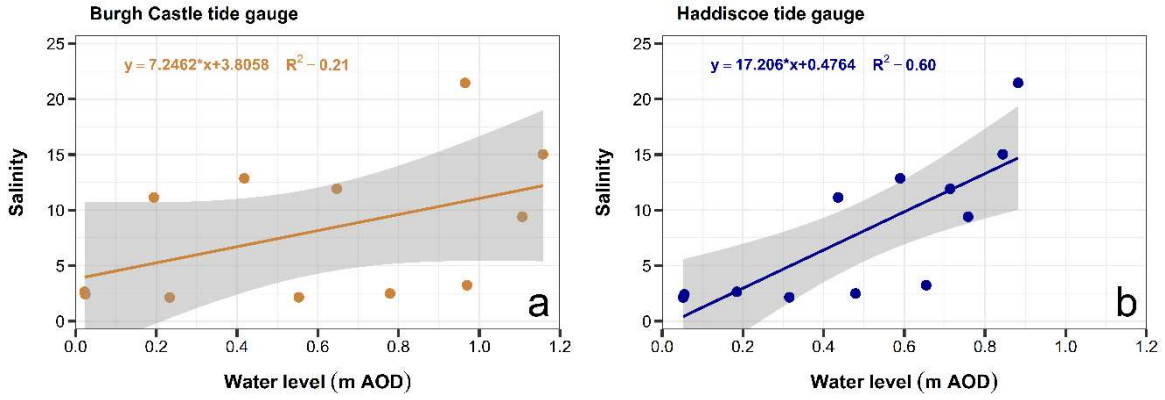

Figure 3.26. *Linear correlation between the water level at Burgh Castle and salinity (a), and the water level at Haddiscoe and salinity (b) for the samples collected on 26 July 2020 at sampling site WAVE6. The grey area indicates the 95% confidence interval for the linear correlation. p – values are 0.13 for plot a and < 0.01 for plot b.*

- Behaviour of DOC and $CDOM_{\alpha 254}$

Figure 3.27 shows DOC and $CDOM_{\alpha 254}$ versus salinity and Table 3.10 shows their range. As described in section 3.2.2, generally DOC and $CDOM_{\alpha 254}$ concentrations are higher in freshwater and lower in saline water. The correlation between $CDOM_{\alpha 254}$ and salinity is strong, even though the data points were not evenly distributed and did not fully cover the salinity gradient between 2 and 22. The correlation between DOC and salinity was not as strong as the one between $CDOM_{\alpha 254}$ and salinity, in particular due to the cluster of DOC concentrations at salinity below 5.

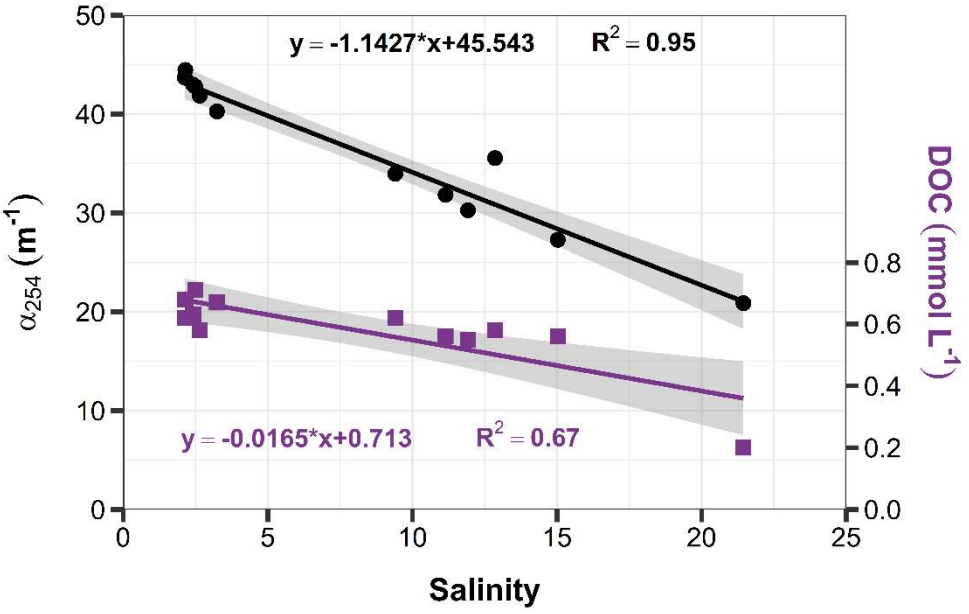

Figure 3.27. *Linear correlation between DOC (purple) and salinity, and $CDOM_{\alpha 254}$ (black) and salinity for the samples collected on 26 July 2020 at WAVE6 sampling site. The grey area indicates the 95% confidence interval for the linear correlation. The significance for the linear correlation is < 0.001 for both variables.*

This difference could be also explained by the difference between DOC and $CDOM_{\alpha 254}$. CDOM is the coloured fraction of DOM, whilst DOC also contains DOC fractions that are not coloured and invisible. As explained by Pereira et al. (2014) there is generally a strong correlation between CDOM and DOC such that CDOM is often used as a proxy for DOC concentration. Their research in a tropical rainforest in Guyana showed that the correlation between DOC and CDOM changed between the dry and the wet season which led them to coin the term *invisible DOM* (iDOM). Therefore, iDOM represents the fraction of DOM not detectable through UV absorbance because it is not coloured (Pereira et al., 2014). iDOM is thought to be non-humic and labile, although its bioavailability, its photo-lability and its drivers are still unknown (Pereira et al., 2014; Trojahn et al., 2019). In this study, the correlation between DOC and $CDOM_{\alpha 254}$ (Figure 3.28) was not as strong as reported in a study by Spencer et al. (2012) where the R^2 was over 0.9 for most of the thirty

rivers examined in the U.S.A. Song et al. (2017) also reported high correlations between CDOM and DOC for inland waters in China, although the correlations for waters impacted by anthropogenic activities were less strong. This could be due to the increase in iDOM which is labile and not coloured.

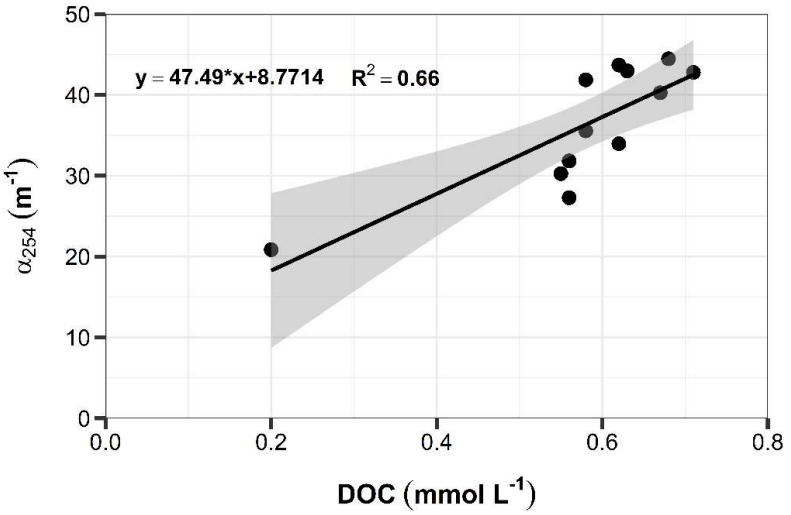

Figure 3.28. *Linear correlation between $CDOM_{\alpha 254}$ and DOC for the samples collected on 26 July 2020 at WAVE6 sampling site. The grey area indicates the 95% confidence interval for the linear correlation. The p-value is 0.001.*

Table 3.10. *Minimum, maximum and average values for salinity, $CDOM_{\alpha 254}$ (m^{-1}) and DOC concentration (mmol L^{-1}) for the samples collected on 26 July 2020 at sampling site WAVE6.*

Variable	Minimum	Maximum	Average
Salinity	2.13	21.45	8.07
DOC (mmol L^{-1})	0.20	0.71	0.58
$CDOM_{\alpha 254}$ (m^{-1})	20.86	44.47	36.31

- Behaviour of the PARAFAC components

Figure 3.29 and Table 3.11 show the fluorescence intensity of the six components identified through the PARAFAC model versus salinity, and the equations and the R^2 for the linear correlations in the figure, respectively. Table 3.12 shows the range of fluorescence intensity of the components. The fluorescence intensity of all the components showed a strong linear correlation with salinity, indicating a linear decrease of FDOM with salinity. The concentration of FDOM is higher at low salinity and lower at higher salinities, hence as the freshwater mixes with saline water due to the tidal cycle, FDOM concentration decreases. The terrestrially derived components TC1 and TC2 had the highest intensity at low salinity

and showed a decrease of 55% and 53% in intensity, respectively. The protein-like components TC5 and TC6 had the lowest decrease along the salinity gradient, of 41% and 47%, respectively (see Figure B2 in Appendix B).

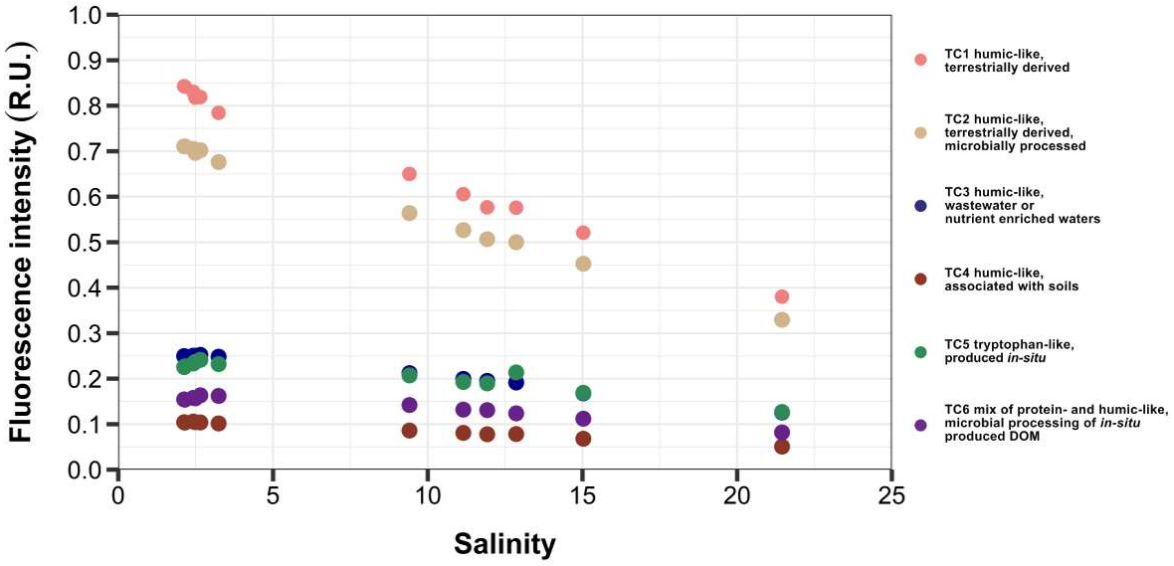

Figure 3.29. *Linear correlations between the fluorescence intensity (R.U.) for the six components identified through the PARAFAC model and salinity for the samples collected on 26 July 2020 at the sampling site WAVE6.*

The correlation coefficient between TC5 and salinity is lower than that for the other components. TC5 in Figure 3.29 shows some variability along the line with some lower values at the lowest salinity and an increase between salinity 12 and 13. Overall the correlations suggest linear mixing between freshwater and saline water throughout the tidal cycle of the sampling day, although with some variability.

Table 3.11. *Equations and R^2 for the linear correlations between the components identified through the PARAFAC model and salinity, shown in Figure 3.24.*

Component	Equation linear correlation	R^2	Significance
TC1	$y = -0.0240x + 0.8807$	0.994	< 0.001
TC2	$y = -0.0197x + 0.7492$	0.999	< 0.001
TC3	$y = -0.0063x + 0.2669$	0.990	< 0.001
TC4	$y = -0.0028x + 0.1111$	0.995	< 0.001
TC5	$y = -0.0049x + 0.2476$	0.885	< 0.001
TC6	$y = -0.0037x + 0.1690$	0.949	< 0.001

Table 3.12. *Minimum, maximum and average of fluorescence intensity in Raman units for the six components identified through the PARAFAC model for the samples collected on 26 July 2020 at sampling site WAVE6.*

Component	Minimum fluorescence intensity (R.U.)	Maximum fluorescence intensity (R.U.)	Average fluorescence intensity (R.U.)
TC1	0.38	0.84	0.69
TC2	0.33	0.71	0.59
TC3	0.12	0.25	0.21
TC4	0.05	0.10	0.09
TC5	0.13	0.24	0.21
TC6	0.08	0.16	0.14

- Behaviour of chlorophyll-*a* and TSS

There is a weak correlation between chlorophyll-*a* and salinity (Figure 3.30a) and there is high variability along the mixing line indicating that there is no linear decrease of chlorophyll-*a* with salinity. Figure 3.30b shows an increase in chlorophyll-*a* concentration as the salinity started increasing, between 11:00 and 13:00. This increase could be caused by the accumulation of chlorophyll-*a* in the freshwater layer at the surface as described by Sierra et al. (2002) and Falco et al. (2006). After the increase chlorophyll-*a* decreased as the salinity was still increasing, whilst there was also an increase of TSS concentration (Figure 3.31). The decrease of chlorophyll-*a* concentration could be a result of the TSS increase limiting the penetration of light through the water column as reported by Fanela et al. (2019). In this study there was no correlation between TSS and chlorophyll-*a* (R^2 = 0.03, see Figure B3 in Appendix B).

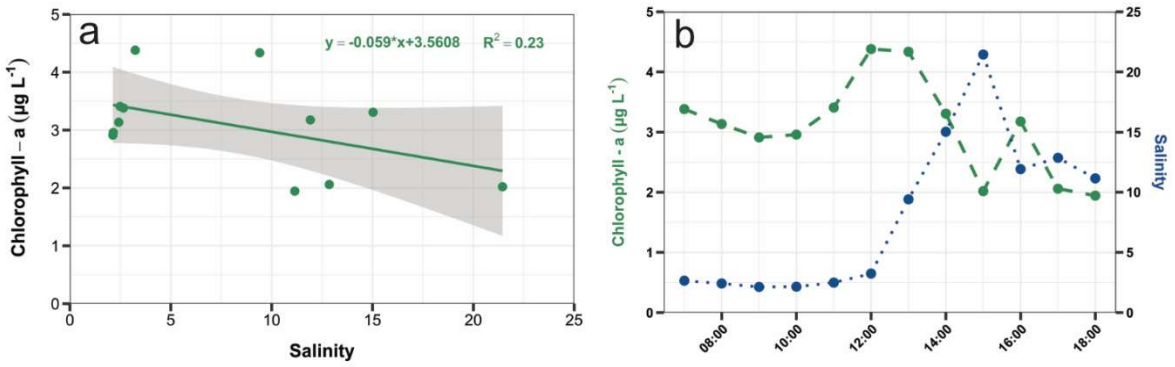

Figure 3.30. *Linear correlation between chlorophyll-a and salinity (a). The grey area represents the 95% confidence interval for the linear correlation and the p-value of 0.116. Figure b shows the salinity and chlorophyll-a through the tidal cycle between 7:00 and 18:00 on 26 July 2020 at sampling site WAVE6. Times are in UTC.*

The lack of correlation between chlorophyll-*a* and TSS could reflect different processes affecting chlorophyll-*a* and TSS. Chlorophyll-*a* accumulated in the freshwater layer on the surface (due to the salt wedge) might have decreased due to both an increase in TSS but also to the rise in salinity, resulting in cell lysis of the freshwater phytoplankton (Roegner et al., 2011). After the salt wedge broke down (at ~ 13:00), chlorophyll-*a* started showing a contrasting behaviour to salinity.

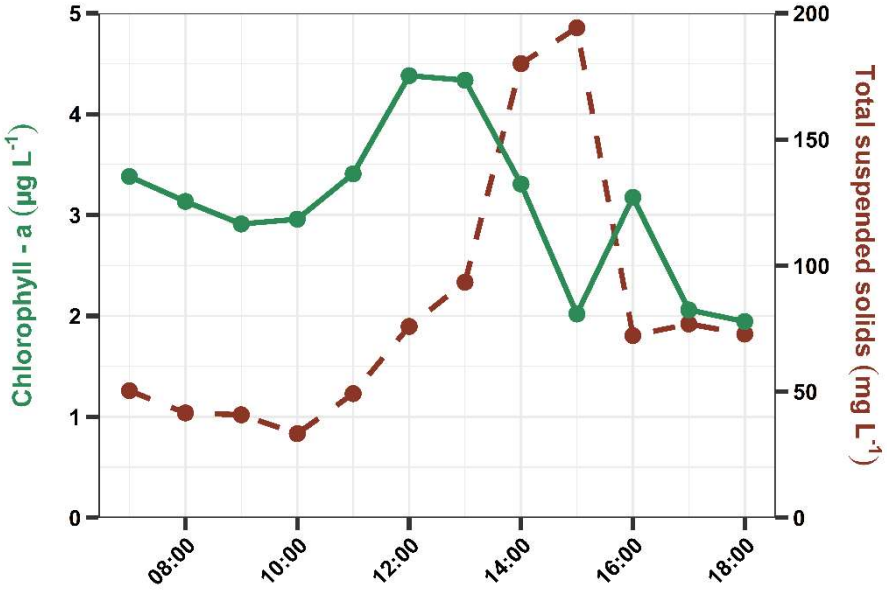

Figure 3.31. *Chlorophyll-a and TSS through the tidal cycle between 7:00 and 18:00 on 26 July 2020 at sampling site WAVE6. Times are in UTC.*

Table 3.13. *Minimum, maximum and average concentrations for chlorophyll-a and TSS in µg L^{-1} and mg L^{-1}, respectively, for the samples collected on 26 July 2020 at the sampling site WAVE6.*

Variable	Minimum	Maximum	Average
Chlorophyll – a (µg L^{-1})	1.94	4.38	3.08
TSS (mg L^{-1})	33.33	194.21	81.71

In Figure 3.32a TSS is shown as a function of salinity and its concentration increased with salinity, although there is some variability that could be due to the uneven distribution of the values along the line. This confirms the influence of salinity and TSS on chlorophyll-*a* concentration as salinity and TSS show a high correlation in this study. Figure 3.32b confirms the strong correlation between salinity and TSS as seen for the Yare in section 3.2.2.

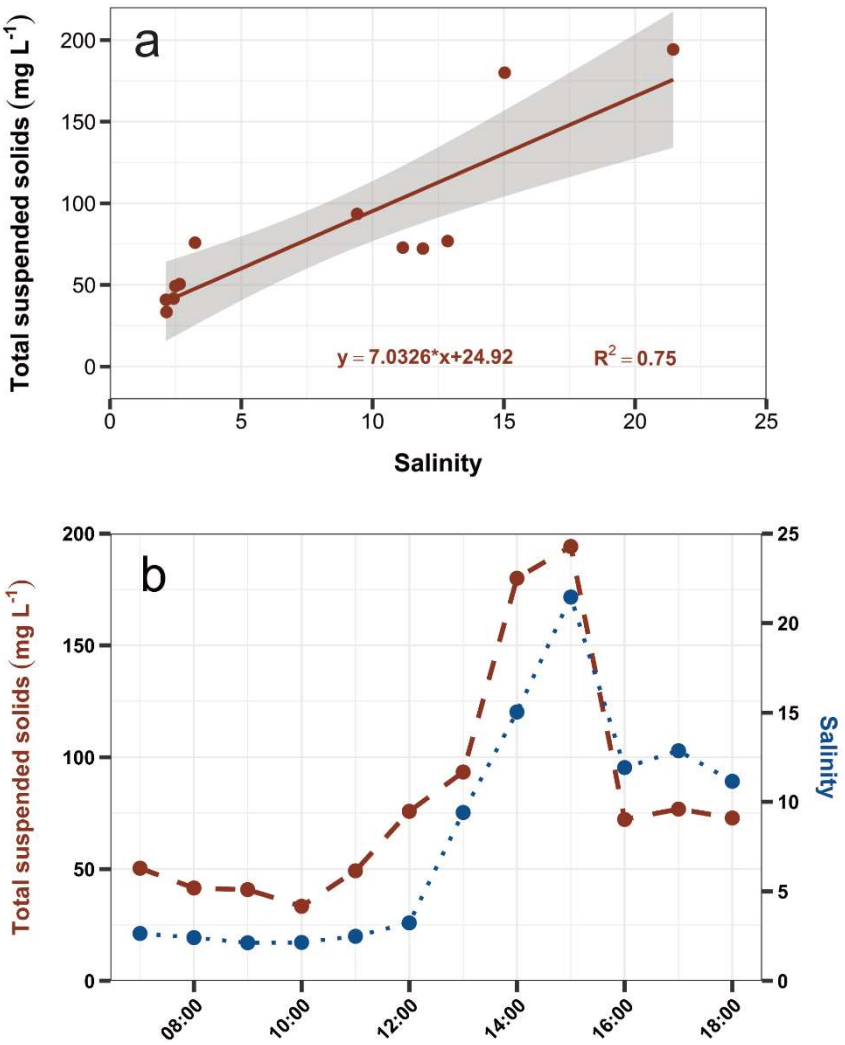

Figure 3.32. *Linear correlation between TSS and salinity (a). The grey area represents the 95% confidence interval for the linear correlation and the p-value is < 0.001. Figure b shows the salinity and TSS curves through the tidal cycle between 7:00 and 18:00 on 26 July 2020 at sampling site WAVE6. Times are in UTC.*

- Behaviour of nutrients

As described in section 3.2.2 for the Yare, DON concentrations for the Waveney are not included in this study because only two values were positive. Also, the ammonium concentration measured for the sample collected at 8:00 was negative and not included in this study. Figure 3.33 shows the nutrient concentrations as a function of salinity, whilst Table 3.14 shows the range of their concentrations.

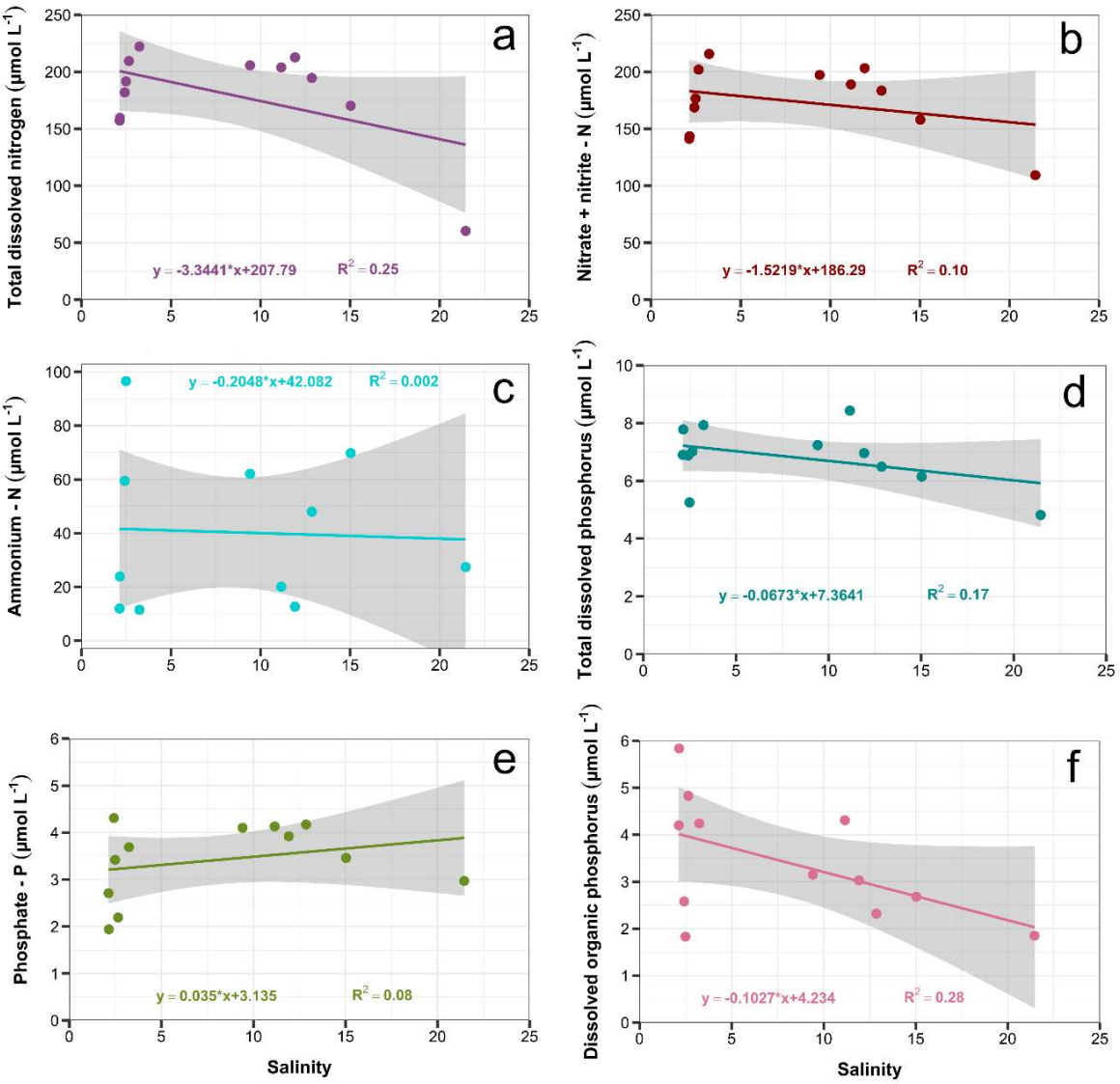

Figure 3.33. *Linear correlation of TDN, nitrate plus nitrite, ammonium, TDP, phosphate and DOP against salinity (plots a – f) for samples collected on 26 July 2020 at WAVE6 sampling. The grey area represents the 95% confidence interval for the linear correlation. The p-value = 0.10 for* ***a****, p-value = 0.32 for* ***b****, p-value = 0.89 for* ***c****, p-value = 0.18 for* ***d****, p-value = 0.37 for* ***e*** *and p-value = 0.08 for* ***f****.*

The relationship between the inorganic nutrients and DOP versus salinity is not linear (Figure 3.33), indicating other processes other than mixing for these variables. As stated previously, the values do not cover the whole of the salinity gradient, influencing the correlations and the trends in Figure 3.33. TDN, nitrate plus nitrite, TDP and DOP have a similar pattern versus salinity. They show high variability at salinity between 0 and 5 and then a decrease starting from salinity above 10. This could be due to the salt wedge and the accumulation of less dense freshwater on the surface. As described in the previous section, nutrient concentrations are higher in freshwater than seawater, hence the decrease with salinity, as described also by Sierra et al. (2002). However, the variability at low salinity could be a result of microbial consumption and release through biodegradation of these nutrients accumulated on the surface. In order to investigate any influence from the tides, correlations between TDN, nitrate plus nitrite, TDP and DOP versus water levels measured at Burgh Castle and Haddiscoe have been calculated (Table B1 in Appendix B). No significant correlation has been found between the water levels and these variables. Figure 3.34 shows the variability discussed above between 0 and 5 salinity (between 7:00 and 12:00) and a decrease of TDN, nitrate plus nitrite, TDP and DOP after the salt wedge dissipated (after 12:00) and the salinity started increasing, indicating mixing of freshwater and salt water.

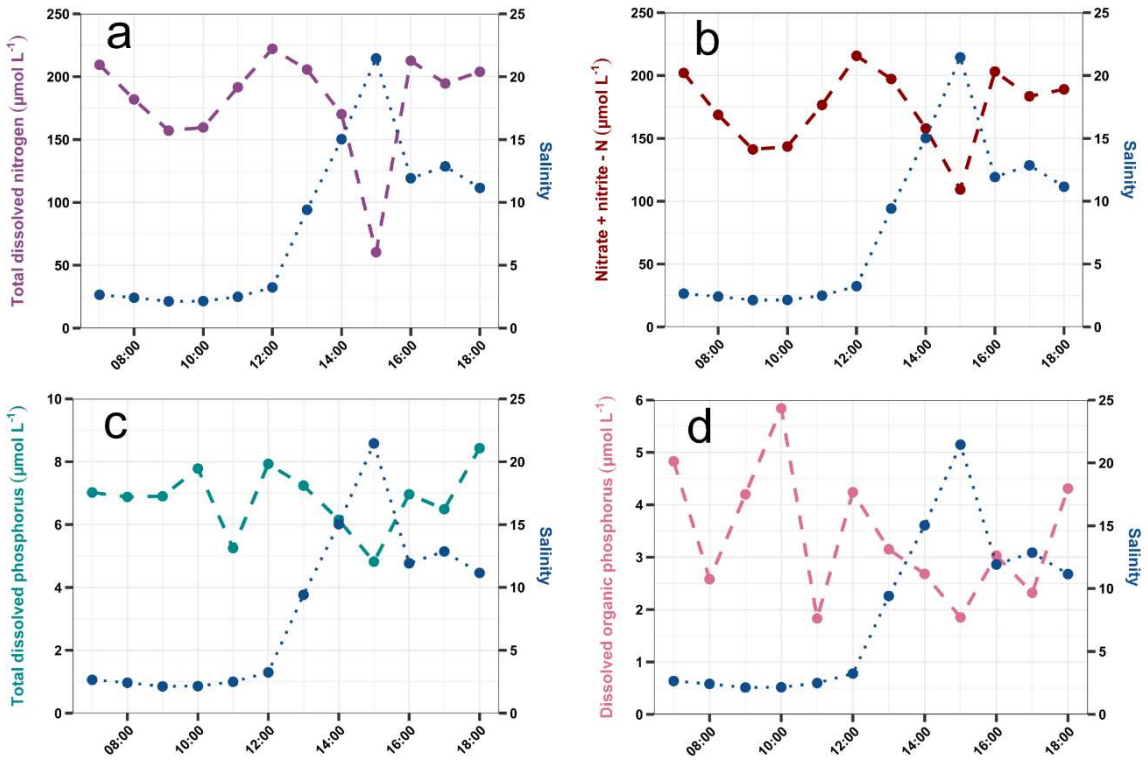

Figure 3.34. *Curves of TDN, nitrate plus nitrite, TDP and DOP through the tidal cycle between 7:00 and 18:00 on 26 July 2020 (plots a-d) at sampling location WAVE6. The points represent the samples. Times are in UTC.*

Table 3.14. *Range of concentrations and averages in µmol L^{-1} for TDN, nitrate plus nitrite, ammonium, TDP, phosphate and DOP for the samples collected on 26 July 2020 at sampling site WAVE6.*

Variable	Minimum [µmol L^{-1}]	Maximum [µmol L^{-1}]	Average [µmol L^{-1}]
TDN	60.40	222.20	180.78
Nitrate + nitrite	109.30	215.70	174.00
Ammonium	11.50	96.60	40.33
TDP	4.82	8.43	6.82
Phosphate	1.94	4.31	3.42
DOP	1.83	5.84	3.40

The relationship between phosphate and salinity in Figure 3.33e shows no correlation and the same high variability at salinity between 0 and 5 observed for the other nutrients. However, as salinity increased, the phosphate concentration was high, probably due to its release from suspended sediments as discussed in the previous section for the Yare. Figure 3.35a shows phosphate concentration as a function of TSS with a positive correlation up to 100 mg L^{-1} of suspended solids, and a decrease in phosphate concentration at higher TSS concentrations. This could be due to the consumption of phosphate by microorganisms (see previous section). Figure 3.35b shows an increase in phosphate between 10:00 and 13:00, coinciding with an increase in TSS. The drop in phosphate concentration might be a delayed response to the increase in chlorophyll-*a*, indicating its uptake from microbial organisms.

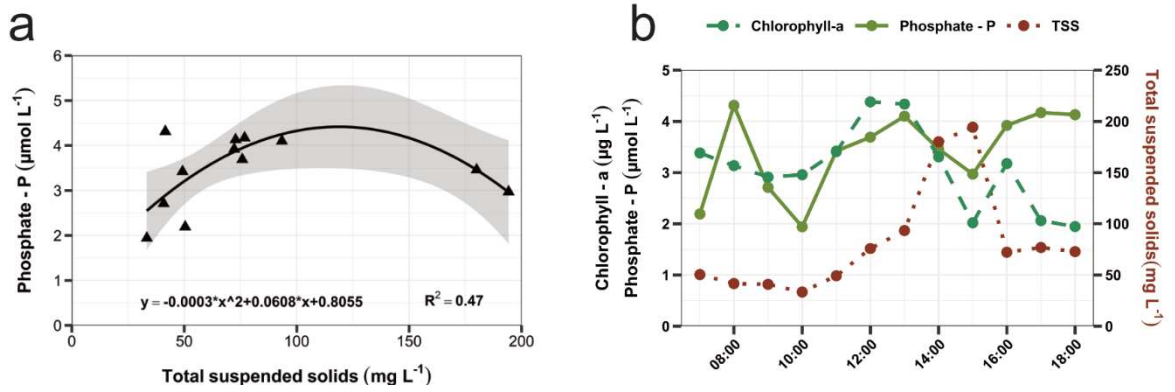

Figure 3.35. *Correlation between phosphate and TSS (plot a) and chlorophyll-a, phosphate and TSS through the tidal cycle between 7:00 and 18:00 on 26 July 2020 at sampling site WAVE6 (plot b). The points represent the samples. Times are in UTC.*

There is no correlation between ammonium and salinity with variability at both low and high salinities. As described previously, ammonium has a rapid turnover, and it can be

released by sediments and remineralised by microbial organisms. Ammonium is consumed by microorganisms and a study by Twomey et al. (2005) reported ammonium as the preferred form of nitrogen taken up by the microbial community. These overlapping processes could mask any correlation between ammonium and salinity.

- Behaviour of absorbance and fluorescence indices

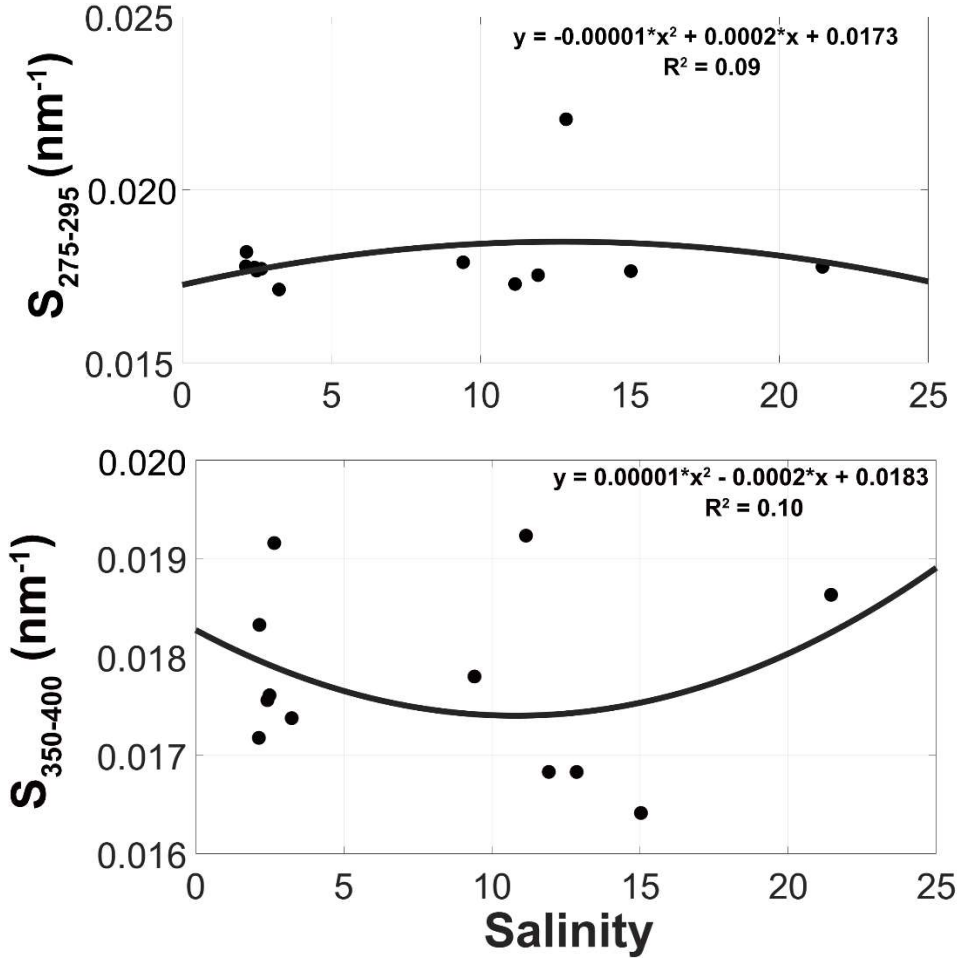

Figure 3.36. *Non-linear correlation between $S_{275-295}$ and salinity (top figure) and between $S_{350-400}$ and salinity (bottom figure) for samples collected on 26 July 2020 at sampling site WAVE6. The p-values are 0.65 for $S_{275-295}$ against salinity and 0.63 for $S_{350-400}$ against salinity. The points represent the samples.*

Correlations between the spectral slopes and salinity are not significant (Figure 3.36). Their range (Table 3.15) is small, and this implies not much change in the molecular weight of DOM. Some studies have reported shallow spectral slopes as indicative of waters rich in organic carbon with a terrestrial origin, usually very aromatic and with high molecular weight (Kowalczuk et al., 2003; Wagner et al., 2015), which is in line with other variables for the River Waveney.

The relationship between S_R and salinity (Figure 3.37) is not significant with values characteristic of a mixture of estuarine and terrestrial waters (as described in section 3.2.2).

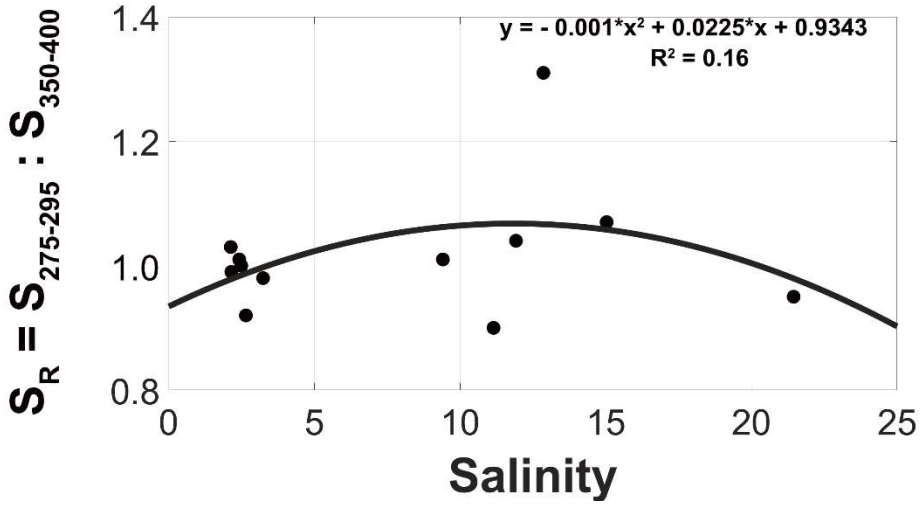

Figure 3.37. *Non-linear correlation between S_R and salinity for the samples collected on 26 July 2020 at sampling site WAVE6. The p-value is 0.46. The points represent the samples.*

Table 3.15. *Range of values and averages in nm^{-1} for $S_{275-295}$, $S_{350-400}$ and S_R for the samples collected on 26 July 2020 at sampling site WAVE6.*

Variable	Minimum (nm^{-1})	Maximum (nm^{-1})	Average (nm^{-1})
$S_{275-295}$	0.017	0.022	0.018
$S_{350-400}$	0.016	0.019	0.018
S_R	0.90	1.31	1.02

Figure 3.38 shows the fluorescence indices as a function of salinity and Table 3.16 shows the range of these variables. $SUVA_{254}$ and HIX show different trends, with the latter decreasing with salinity, although with some variability corresponding to the salinity wedge (salinity 0-5),whilst $SUVA_{254}$ shows a sharp increase due to one sampling point. As discussed at the beginning of this section, the correlation between DOC and CDOM was not as high as expected (R^2 = 0.66) and as $SUVA_{254}$ is the ratio between CDOM and DOC, it has an impact on the $SUVA_{254}$. HIX values indicate waters with a mixture of humic and *in-situ* produced material and although the values are clustered around salinity 0-5 and salinity 9-15, the correlation is significant (p < 0.001) indicating a decrease of aromaticity along the salinity gradient. Figure 3.39 shows this decrease as salinity increased after the saline water mixed with freshwater. The variability between salinity 0 and 5 could be a result of microbial

degradation shifting the aromaticity and the molecular weight of DOM (Fasching et al., 2015).

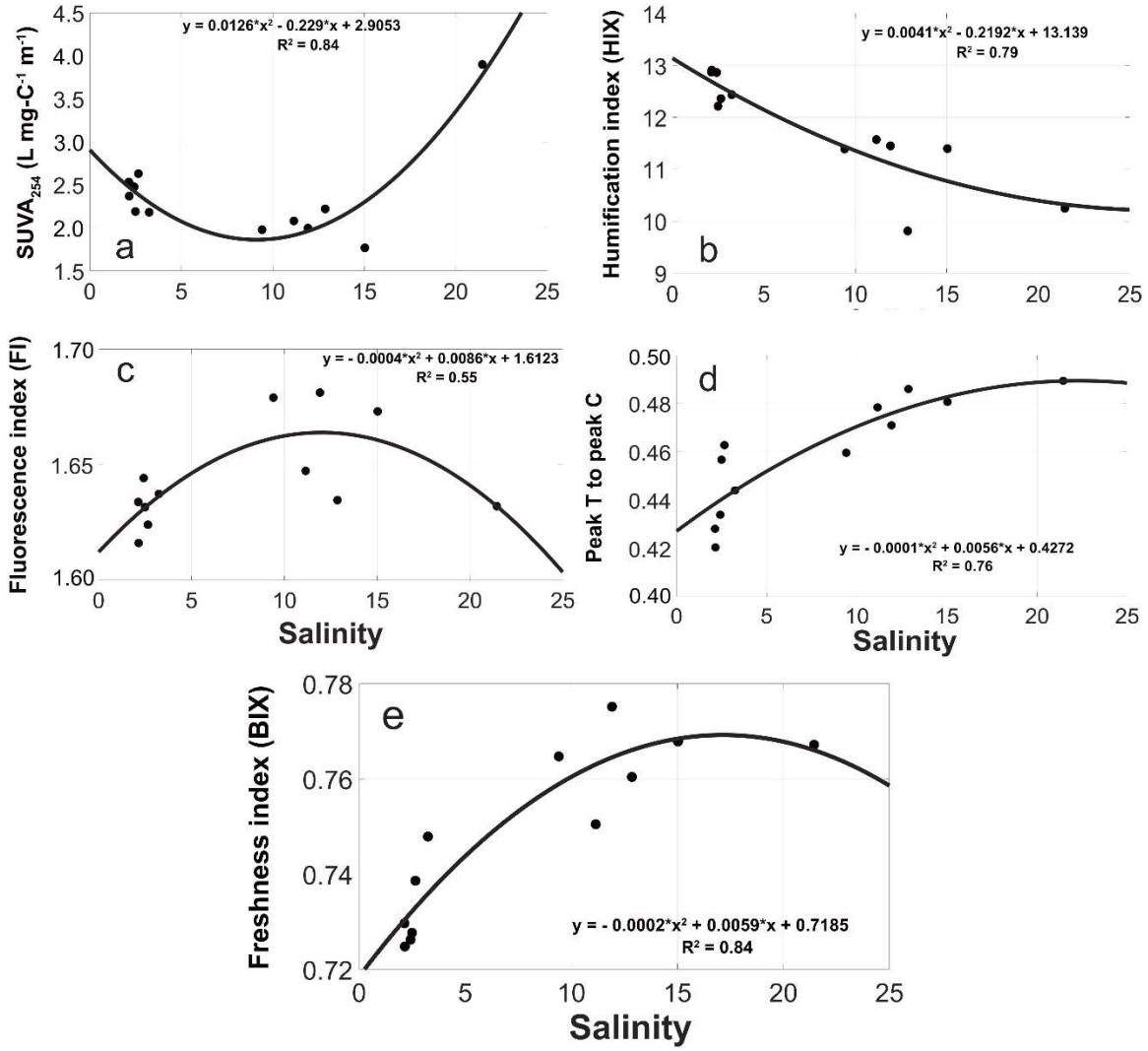

Figure 3.38. *Non-linear correlations between $SUVA_{254}$, HIX, FI, peak T : peak C and BIX with salinity (plots a-e) for the samples collected on 26 July 2020 at sampling site WAVE6. The p-values are < 0.001 for $SUVA_{254}$, HIX, and BIX, whilst < 0.05 for FI and peak T : peak C. The points represent the samples.*

The correlation for FI also shows variability between 0 and 5 salinity with an increase in values at higher salinities, an indication of DOM from both terrestrial and microbial sources. A confirmation of microbial activity during the stratification between salinity 0 and 5 is visible in Figure 3.38d and 3.38e. Both peak T : peak C and BIX increased with salinity, indicating a larger quantity of "fresh" DOM at high salinity, whilst their variability at low salinity could indicate DOM degradation. As previously discussed, the trend in peak T : peak C could be due to an increase in peak T (autochthonous DOM) or a decrease in peak C (allochthonous DOM). Because of the trend in the fluorescent index BIX it is possible to conclude that there was a rise in peak T.

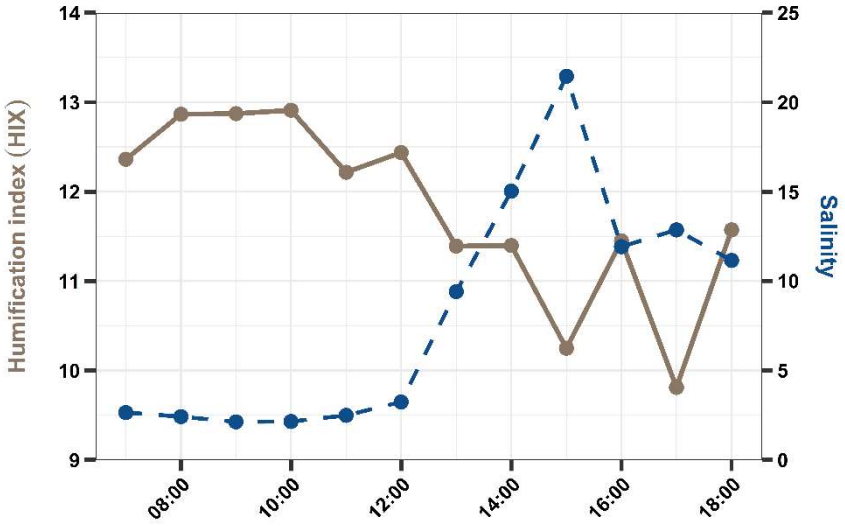

Figure 3.39. *Curves of HIX and salinity through the tidal cycle between 7:00 and 18:00 of 26 July 2020 at sampling location WAVE6. The points represent the samples. Times are in UTC.*

Table 3.16. *Range of values and average for $SUVA_{254}$, HIX, FI, peak T : peak C and BIX for the samples collected on 26 July 2020 at sampling site WAVE6.*

Variable	Minimum	Maximum	Average
$SUVA_{254}$ L mg-C^{-1} m^{-1}	3.90	1.77	2.36
HIX	12.91	9.81	11.79
FI	1.68	1.61	1.64
peak T:peak C	0.49	0.42	0.46
BIX	0.77	0.72	0.75

Table 3.17. *List of the range of variables discussed in this study highlighting similarities and differences between the sampling in the River Yare (21 July 2020) and the sampling in the River Waveney (26 July 2020).*

Variable	Yare	Waveney	Notes
Salinity	Range 4.17 – 27.33. It follows the tidal cycle.	Range 2.13 – 21.45 The water column was stratified due to a salinity wedge.	The distribution of the salinity points for the Waveney is poor, due to clustering around salinity <5.
DOC	Range 0.20 - 0.46 mmol L^{-1}. High correlation with salinity, $R^2 = 0.99$.	Range 0.20 - 0.71 mmol L^{-1}. Medium correlation with salinity, $R^2 = 0.67$.	For the Waveney, CDOM and DOC did not correlate strongly, probably due to iDOM which is not coloured.
CDOM	Range 13.58 – 37.60 m^{-1}. High correlation with salinity, $R^2 = 0.98$.	Range 20.86 – 44.47 m^{-1}. High correlation with salinity, $R^2 = 0.95$.	
TC1	Range 0.22 – 0.72 R.U. High correlation with salinity, $R^2 = 0.998$.	Range 0.38 – 0.84 R.U. High correlation with salinity, $R^2 = 0.994$.	
TC2	Range 0.19 – 0.65 R.U. High correlation with salinity, $R^2 = 0.998$.	Range 0.33 – 0.71 R.U. High correlation with salinity, $R^2 = 0.999$.	
TC3	Range 0.07 – 0.25 R.U. High correlation with salinity, $R^2 = 0.999$.	Range 0.12 – 0.25 R.U. High correlation with salinity, $R^2 = 0.990$.	
TC4	Range 0.03 – 0.10 R.U. High correlation with salinity, $R^2 = 0.999$.	Range 0.05 – 0.10 R.U. High correlation with salinity, $R^2 = 0.995$.	
TC5	Range 0.09 – 0.28 R.U. High correlation with salinity, $R^2 = 0.99$.	Range 0.13 – 0.24 R.U. Medium correlation with salinity, $R^2 = 0.88$. High intensity during salinity stratification due to high microbial activity.	

Variable	Yare	Waveney	Notes
TC6	Range 0.05 – 0.19 R.U. High correlation with salinity, R^2 = 0.997	Range 0.08 – 0.16 R.U. Strong correlation with salinity, R^2 = 0.949.	
Chla-*a*	Range 1.32 – 3.39 µg L^{-1}. Moderately strong correlation with salinity, R^2 = 0.61.	Range 1.94 – 4.38 µg L^{-1}. Weak correlation with salinity, R^2 = 0.23.	
TSS	Range 91.46 – 241.20 mg L^{-1} Weak correlated with salinity, R^2 = 0.38. TSS variability due to the settling during slack waters.	Range 33.33 – 194.21 mg L^{-1} Moderately strong correlation to salinity, R^2 = 0.75.	
TDN	Range 59.80 – 306.30 µmol L^{-1}. Strong correlation with salinity, R^2 = 0.99.	Range 60.40 – 222.20 µmol L^{-1}. Poor correlation with salinity, R^2 = 0.25. Variability at salinity < 5 due to microbial activity. Linear decrease at salinity > 10.	
NO_3 + NO_2	Range 47.90 – 311.00 µmol L^{-1}. Strong correlation with salinity, R^2 = 0.99.	Range 109.30 – 215.70 µmol L^{-1}. Weak correlation with salinity, R^2 = 0.10. Variability at salinity < 5 due to microbial activity. Linear decrease at salinity > 10.	
NH4	Range 5.70 – 215.70 µmol L^{-1}. No correlation with salinity, R^2 = 0.12. Affected by *salinity-mediated release* and by the resuspension of solids.	Range 11.50 – 96.60 µmol L^{-1}. Not correlated with salinity, R^2 = 0.002.	
TDP	Range 3.15 – 8.75 µmol L^{-1}. Medium correlation with salinity, R^2 = 0.53.	Range 4.82 – 8.43 µmol L^{-1}. Weak correlation with salinity, R^2 = 0.17. Variability at salinity < 5 due to microbial activity. Linear decrease at salinity > 10.	

Variable	Yare	Waveney	Notes
PO_4	Range 1.69 – 5.31 µmol L^{-1}. No correlation with salinity, R^2 = 0.16. Affected by the resuspension of solids and microbial consumption.	Range 1.94 – 4.31 µmol L^{-1}. No correlation with salinity, R^2 = 0.08. Affected by the resuspension of solids and microbial consumption.	
DOP	Range 1.04 – 6.18 µmol L^{-1}. Weak correlation with salinity, R^2 = 0.35. Affected by the resuspension of solids and remineralisation by microbes.	Range 1.83 – 5.84 µmol L^{-1}. Weak correlation with salinity, R^2 = 0.28. Variability at salinity < 5 due to microbial activity. Linear decrease at salinity > 10.	
$S_{275-295}$	Range 0.016 – 0.022 nm^{-1}. No significant correlation with salinity, R^2 = 0.24. Decrease of molecular weight with salinity.	Range 0.017 – 0.022 nm^{-1}. Not correlated with salinity, R^2 = 0.03.	
$S_{350-400}$	Range 0.012 – 0.024 nm^{-1}. No significant correlation with salinity, R^2 = 0.08.	Range 0.016 – 0.019 nm^{-1}. No significant correlation with salinity, R^2 = 0.005.	
S_R	Range 0.78 – 1.71. No significant correlation with salinity, R^2 = 0.24. Decrease of molecular weight as the salinity increased.	Range 0.90 – 1.31. No significant correlation with salinity, R^2 = 0.04.	
$SUVA_{254}$	Range 2.54 – 3.33 L mg-C^{-1} m^{-1}. Moderately strong correlation with salinity, R^2 = 0.56.	Range 1.77 – 3.90 L mg-C^{-1} m^{-1}. Not correlated with salinity, R^2 = 0.09.	This variable is affected by the medium correlation between CDOM and DOC for the Waveney.
HIX	Range 8.78 – 11.34. Moderately strong correlation with salinity, R^2 = 0.74. Linear decrease with salinity.	Range 9.81 – 12.91. Moderately strong correlation with salinity, R^2 = 0.76. Values decrease due to both microbial degradation and mixing of saline and freshwater.	

Variable	Yare	Waveney	Notes
FI	Range 1.67 – 1.71. Weak correlation with salinity, R^2 = 0.32. The range of values confirms mixing of waters and microbial processes.	Range 1.61 – 1.68. No significant correlation with salinity, R^2 = 0.17. Affected by the degradation and remineralisation of terrestrial DOM by microbes.	
Peak T to peak C ratio	Range 0.49 – 0.56. Moderately strong correlation with salinity, R^2 = 0.63. Confirms mixing of fresh and saline water.	Range 0.72 – 0.77. Moderately strong correlation with salinity, R^2 = 0.72. Confirms the increase of microbial activity at salinity < 5.	
BIX	Range 0.74 – 0.79. Weak correlation with salinity, R^2 = 0.10. High fresh DOM at low salinity and high variability of DOM at high salinity.	Range 0.72 – 0.77. Moderately strong correlation with salinity, R^2 = 0.72. Confirms the increase of microbial activity at salinity < 5.	

3.3 Conclusions

This section provides a summary of the previous results analysis and a discussion linked to the hypothesis and questions posed at the beginning of the chapter.

H1) DOC and CDOM concentrations decrease linearly at salinities above 0 when the tide is flowing in. This is because freshwater contains most of the DOC and CDOM, so dissolved organic matter is subjected to dilution when seawater and freshwater mix

The chapter will also answer the following questions:

a) Does the fluorescence intensity of the components identified through PARAFAC follow the same pattern as DOC and CDOM?

b) Do the dissolved organic nutrients follow the same pattern as DOC and CDOM?

c) Does the behaviour of the dissolved inorganic nutrients through the tidal cycles inform on abiotic and biotic processes impacting DOM dynamics?

d) How does the TSS concentration vary with salinity?

e) Do the absorbance and fluorescence indices give an insight into the biogeochemical processes during the tidal cycle?

3.3.1 River Yare

For the sampling day and at the sampling location in this study, DOC, CDOM, the six components identified through PARAFAC, TDN, nitrate plus nitrite and TDP decreased linearly with increasing salinity, indicating mixing of freshwater and seawater and dilution as the dominant driver. Amongst the organic nutrients, only DOP could be reported in this study, and it presented a negative correlation with salinity during the tidal changes. This variable is affected by both sediment resuspension and microbial remineralisation and production. The same processes were found to affect phosphate which did not show a linear relationship with salinity. Ammonium was also affected by resuspension of sediments due to tidal currents and also by an abiotic process which increases ammonium concentration with increase in salinity (salinity-mediated mechanism).

The TSS concentration was greater at high salinity than at low salinity, resulting in transport of TSS upstream when the tide was flowing in. The optical measurements of absorbance and fluorescence indices confirmed both the water mixing due to the tidal cycle and the processes discussed for the nutrients, such as the release of phosphate from resuspension of solids and the release of ammonium through the increase in salinity. In summary, the tidal cycle affected the River Yare at the sampling location YAR4 on 21 July 2020. The transport of saline waters into the river and the subsequent transport of freshwater into the coastal sea allow DOM of different origins to mix and allow nutrients to be remineralised and become bioavailable. Although the tidal change has been found to affect several variables in this study, overall DOM exhibited a conservative behaviour which suggests that the main driver for this sampling day was water mixing.

Although DOM had a conservative behaviour for this river in this study, PCA highlighted DOM with more microbial characteristics which could be due to saline water transported into the Yare through the tidal cycle resulting in an increase of remineralisation and/or DOM production by the microbial community.

3.3.2 River Waveney

During the sampling in the River Waveney on 26 July the results showed stratification of the water column with the freshwater layer on top of the saline layer and because of this, the values were not homogeneously distributed along the salinity gradient. This salt wedge impacted most of the variables investigated in this study. As hypothesised, CDOM and DOC decreased with salinity, although there were differences between the two variables. These differences have been attributed to the difference in the composition of CDOM and DOC, the latter containing also DOM substances which are not visible. The salt wedge did not affect CDOM, but it did have an impact on the linear decrease of DOC with salinity. During the stratification of the water column the freshwater layer remained at the surface (richer in nutrients and DOM), fuelling the growth of the microbial community and DOM degradation. This is also true for the fluorescence intensity of the six components identified by the PARAFAC model. They followed the pattern of CDOM and DOC and decreased along the salinity gradient, although TC1 and TC2 (terrestrial origin) showed the highest decrease and TC5 and TC6 (microbial origin) showed the lowest decrease along the salinity gradient.

The salt wedge had an effect also on the nutrients which showed a similar pattern to DOC with variability between salinity 0 and 5, in particular for TDN, nitrate plus nitrite, TDP and DOP. Ammonium and phosphate were affected by the increased microbial degradation due to the water stratification, but also by suspended sediments which release these nutrients into the water column. TSS were highly correlated to salinity and showed higher concentrations at high salinity and lower at freshwater endmember.

The absorbance indices did not correlate with salinity, although S_R confirmed DOM molecular weight shifting due to biodegradation. Moreover, the increased biodegradation of DOM (due to the water stratification) was confirmed by the fluorescence indices, especially the FI, BIX and peak T : peak C.

In summary, the tidal cycle investigated on the 26th July 2020 at the sampling location WAVE6 created a salt wedge which affected DOM degradation during the 12 hours of sampling. Although the values did not cover the whole salinity gradient, it is possible to conclude that the freshwater layer on top of the saline layer allowed DOM biodegradation by the microbial community, also as a result of the higher nutrient concentrations at low salinity. When the stratification broke down and freshwater and saline water were able to mix, most variables showed a decrease with salinity, indicating water mixing as the main driver.

Although the salt wedge increased DOM production, the characteristics of DOM in this river remained mainly terrestrial.

This research emphasises the need to incorporate the specific study of the influence of tidal cycles on DOM dynamics from rivers to sea, especially for those systems highly influenced by tidal changes. Despite the increase in the number of studies on the magnitude and the drivers of the processes DOM is subject to in its journey from rivers to the sea, there are still gaps, and one of the aspects which has not been extensively investigated is the influence of tidal cycles on the composition and dynamics of DOM.

Chapter 4

Riverine and estuarine spatial-temporal dynamics and fluxes of DOM from two catchments in East Anglia

This chapter explains and discusses the results of the monthly sampling carried out on the River Waveney and the River Yare between November 2018 and December 2019. In particular, the aim is to investigate the composition, optical and chemical properties of dissolved organic matter in these two tidal rivers and to estimate the quantity of DOM entering the shelf sea throughout the year. The aim is achieved through the following objectives:

i. Determine the spatial and temporal variability in optical (absorption and fluorescence) and biogeochemical (carbon, nitrogen and phosphorus) properties of DOM in the two rivers;
ii. Determine the drivers of this variability;
iii. Determine the fluxes of DOM from the two rivers to the southern North Sea.

In addition, the chapter aims to answer the following questions:

a) Is there a difference in DOM composition between the two rivers?
b) Is there a seasonal change in DOM composition and concentration?
c) How does DOM change with salinity, between the rivers and the estuary?
d) What processes DOM is exposed to along the salinity gradient?
e) What are the riverine and estuarine fluxes of DOM?
f) What are the sources of DOM to the shelf sea? Are they linked to the land use of the catchments?

4.1 Additional methodology

A total of 178 river water samples were collected at monthly intervals along a salinity gradient between November 2018 and December 2019 on the River Waveney (n = 48) and between December 2018 and December 2019 on the River Yare (n = 50). Three sampling sites in the estuary were the same for both rivers, so samples were collected at these sites twice a month (n = 80) (section 2.2.1 of Chapter 2 for sampling locations). River water was grab sampled 2-3 metres away from the riverbanks using a bucket (section 2.2.1 of Chapter 2). Sampling was carried out during high tide for those locations where it was difficult to sample when the tide was low (SEA3, WAVE4 and WAVE 5). Figures 4.2 and 4.3 show the condition of the tide for every sampling day. See section 2.2 for the sampling procedure and storage of the samples collected and section 2.3 for analytical methods.

It is worth clarifying the definition of '*Estuary*' used for this study (Breydon Water in Figure 4.1), based on the characteristics of the study area and proposed by Potter et al. (2010). This is a general definition which can be adopted for estuaries characterised by different types of tidal cycles: "*An estuary is a partially enclosed coastal body of water that is either permanently or periodically open to the sea and which receives at least periodic discharge from a river(s), and thus, while its salinity is typically less than that of natural sea water and varies temporally and along its length, it can become hypersaline in regions when evaporative water loss is high and freshwater and tidal inputs are negligible* (p. 499).

Figure 4.1. *Modified aerial photograph of Breydon Water with rivers highlighted. Copyright Anthony Parkes.*

Following page: ***Figure 4.2.*** *Tidal cycles of the River Waveney on the sampling days between November 2018 and December 2019. The white arrow pointing up reflects that the tide was rising when samples were collected whilst the arrow pointing down reflects that the tide was falling when samples were collected. The location of the tide gauges is shown in Figure 3.1 of Chapter 3.*

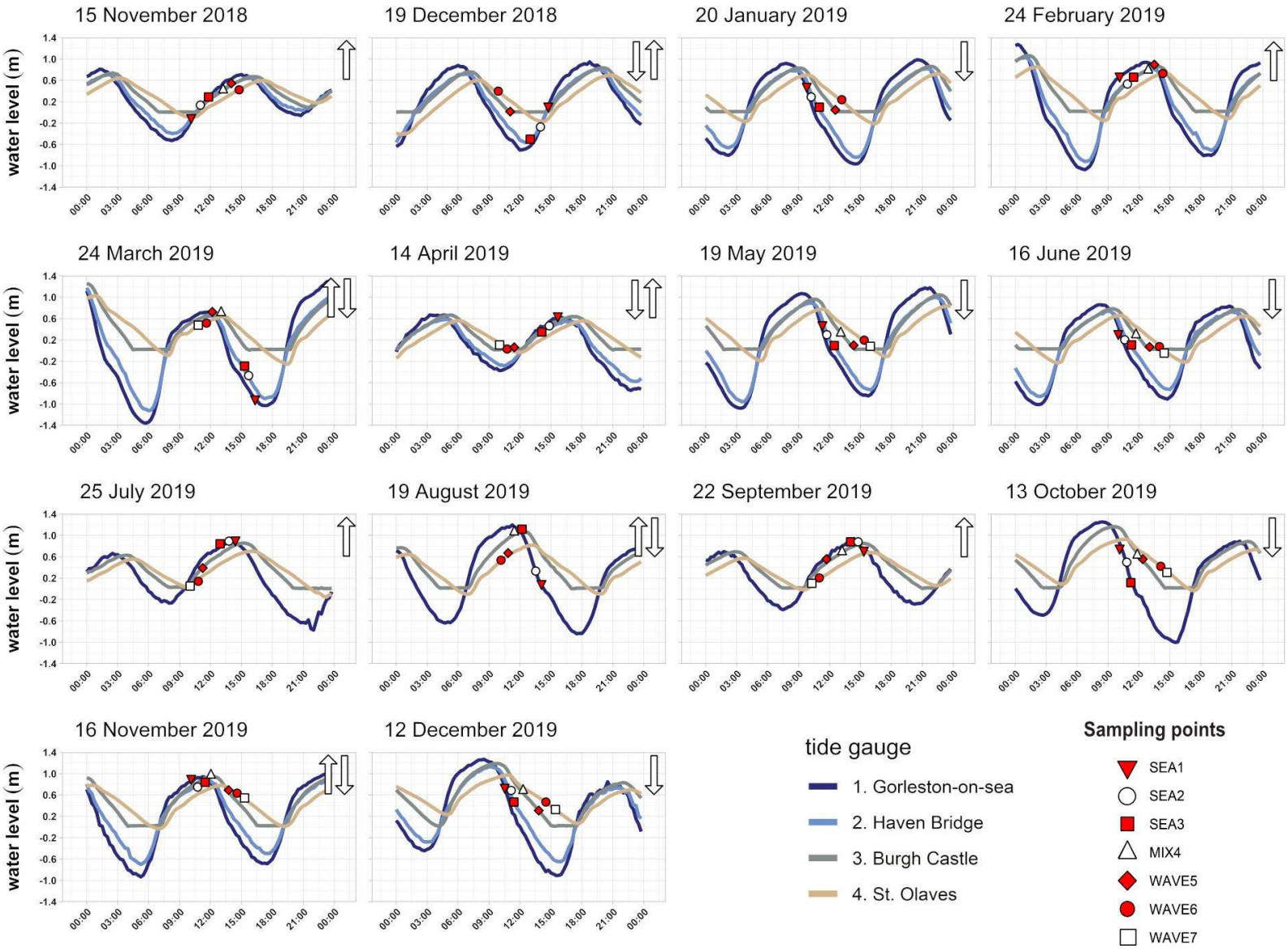
15 November 2018
19 December 2018
20 January 2019
24 February 2019
24 March 2019
14 April 2019
19 May 2019
16 June 2019
25 July 2019
19 August 2019
22 September 2019
13 October 2019
16 November 2019
12 December 2019
water level (m)
1.4
1.0
0.6
0.2
-0.2
-0.6
-1.0
-1.4
00:00
03:00
06:00
09:00
12:00
15:00
18:00
21:00
00:00
tide gauge
1. Gorleston-on-sea
2. Haven Bridge
3. Burgh Castle
4. St. Olaves
Sampling points
SEA1
SEA2
SEA3
MIX4
WAVE5
WAVE6
WAVE7

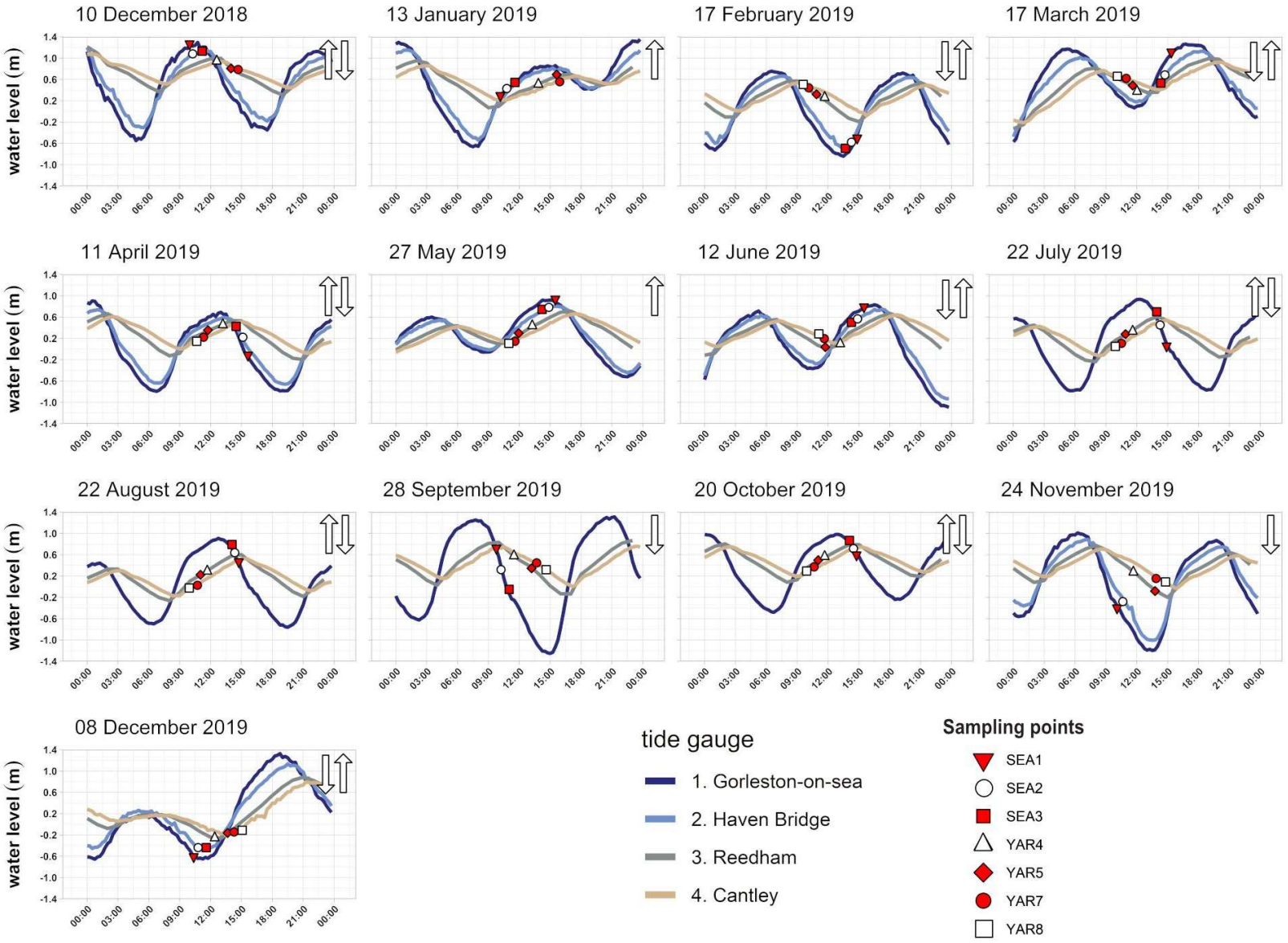
10 December 2018
13 January 2019
17 February 2019
17 March 2019
11 April 2019
27 May 2019
12 June 2019
22 July 2019
22 August 2019
28 September 2019
20 October 2019
24 November 2019
08 December 2019
water level (m)
1.4
1.0
0.6
0.2
-0.2
-0.6
-1.0
-1.4
00:00
03:00
06:00
09:00
12:00
15:00
18:00
21:00
00:00
tide gauge
1. Gorleston-on-sea
2. Haven Bridge
3. Reedham
4. Cantley
Sampling points
SEA1
SEA2
SEA3
YAR4
YAR5
YAR7
YAR8

Previous page: ***Figure 4.3.*** *Tidal cycles of the River Yare on the sampling days between December 2018 and December 2019. The white arrow pointing up reflects that the tide was rising when samples were collected whilst the arrow pointing down reflects that the tide was falling when samples were collected. The location of the tide gauges is shown in Figure 3.1 of Chapter 3.*

4.1.1 Calculation of riverine and estuarine effluxes

The fluxes of DOC, TDN, nitrate plus nitrite, TDP and DOP were calculated by using the concentrations sampled and river flow, in order to assess the amount of dissolved organic carbon and nutrients entering the shelf sea. The area used to calculate the flux entering the North Sea was estimated using the method described in Parmenter and Melcher (2012) with ArcMap 10.6.1 (ESRI, 2019). The sampling points used to calculate the riverine export were the freshwater end members (YAR6 and WAVE6) for the River Yare and the Waveney, whilst the sampling point used to calculate the estuarine export was the salinity end member (SEA1) at the last point before the shelf sea. As concentrations were sampled once per month per river, in these calculations it is assumed that concentrations for all the variables were the same for ~ 15 days before and after the sampling day. The results have been normalised to the rivers' catchment areas which for the River Waveney is its catchment, whilst for the River Yare also includes the River Wensum catchment. For the estuary, as this sampling point received water from all the catchments in the wider Broadland catchment (Figure 2.1 in Chapter 2), the flux was calculated taking into account the catchment areas of the Rivers Yare, Wensum, Waveney and the Bure (Figure 2.1 in Chapter2). All exports were estimated following the method described in Tipping et al. (1997), described below:

The flux in g d^{-1} was calculated using the following equation:

$$Flux\ (g\ d^{-1}) = (C\ \times Q) \times 60 \times 60 \times 24 \qquad Equation\ 4.1$$

where C is the concentration at the sampling point (freshwater end member or salinity end member) in g L^{-1}, whilst Q is the river discharge for the sampling point in L s^{-1}. The mean daily river discharges were extracted from the National River Flow Archive (2021) and normalised by the catchment area (including tributaries). As more than twelve months were sampled, the following equation was used to calculate the flux in g yr^{-1}:

$$\text{Flux}\ (\text{g}\ yr^{-1}) = \sum_{365}^{1} flux\ (g\ d^{-1}) \times \left(\frac{months\ sampled}{months\ per\ year}\right) \qquad Equation\ 4.2$$

Lastly, the flux in g m^{-2} yr^{-1} was estimated using the following equation:

$$Flux\ (g\ m^{-2}yr^{-1}) = \frac{flux\ (g\ yr^{-1})}{catchment\ area\ (m^2)} \qquad Equation\ 4.3$$

The uncertainty for the fluxes was calculated as the daily range in the concentrations of the variable during the tidal cycle (Chapter 3).

4.1.2 Calculation of the river discharge at the sampling points

The river discharge for the sampling points was calculated from the river discharge measured at the gauge closest to the sampling point (Figure 4.4). The daily river discharge data come from the National River Flow Archive (NRFA) of the UK Centre for Ecology and Hydrology (UK CEH). The river discharge of the tributaries of these rivers was also considered. For the river discharge of the two most upstream sampling points in the River Yare, YAR6 and YAR7 (Figure 2.6 of Chapter 2), the following tributaries were considered: the Rivers Wensum, Tud and Tas (Figure 4.4). Their river discharge was added to the river discharge of the Yare. The river discharge was also calculated for the two most upstream sampling points in the River Waveney, WAVE6 and WAVE7 (Figure 2.6 of Chapter 2). To calculate the river discharge at the sampling point, the data from the NRFA were divided by the catchment area of the rivers upstream of the gauges:

$$Q_T\ (m^3s^{-1}km^{-2}) = \frac{Q_{m_1}(m^3s^{-1}) + Q_{m_2}(m^3s^{-1}) + \cdots Q_{m_n}(m^3s^{-1})}{A_1(km^2) + A_2(km^2) + \cdots A_n(km^2)} \qquad Equation\ 4.4$$

where Q_T is the river discharge including the river discharge of the tributaries (if present), divided by the catchment area including that of the tributaries, Q_m is the river discharge measured at the gauge and A, is the catchment area of the river upstream of the gauge. The value Q_T is then multiplied by the drainage area A_C determined with the method described in Parmenter and Melcher (2012) with ArcMap 10.6.1 (ESRI, 2019) using the equation:

$$Q_C\ (m^3s^{-1}) = Q_T\ (m^3s^{-1}km^{-2}) \times A_C(km^2) \qquad Equation\ 4.5$$

where Q_C is the calculated river discharge for the sampling point.

Figure 4.4. *Gauges measuring the river discharge for the River Yare and its tributaries (Rivers Tud, Tas and Wensum) and for the River Waveney. Map modified from the NRFA of the UK CEH (2022).*

4.2 Results and discussion

4.2.1 PARAFAC components

172 samples were modelled with PARAFAC out of 178 total river samples collected. The six samples collected in July 2019 for the River Waveney were measured with a different fluorometer which was missing the correction factors for the fluorescence spectra.

The PARAFAC model identified and validated six components (Figure 4.5) which represent DOM composition in the water samples collected along the rivers. The fluorophores identified by the PARAFAC model were matched to components found in other research studies through the OpenFluor database as described in section 3.2.1 (Chapter 3). The studies matched with a Tucker Congruence Coefficient (TCC) > 0.95 (C1, C2, C3, C4 and C6) and TCC > 0.9 (C5) (Table C1 in Appendix C).

Component 1 (C1) had excitation maxima at wavelengths (λ) of 285 and 355 nm and an emission maximum at λ of 444 nm and is associated with terrestrially derived allochthonous humic-like substances and with degradation of lignin (Kothawala et al., 2012; Murphy et al., 2014; Chen et al., 2018). Component 2 (C2) with an excitation maximum at λ of 270 nm and an emission maximum at λ of 466 nm is also associated with terrestrially derived allochthonous humic-like compounds high in aromaticity, and has been suggested to be photorefractory and/or to be produced by photodegradation (Stedmon et al., 2007; Yamashita et al., 2010; Murphy et al., 2014; Dainard et al., 2015; Chen et al., 2017). Component 3 (C3) had an excitation maximum at λ of 310 nm and an emission maximum at λ of 392 nm and is representative of humic-like substances that are microbially produced, associated with anthropogenic activities and rivers impacted by wastewater and agricultural waste (Stedmon, 2003; Coble, 2007; Lapierre and del Giorgio, 2014; Wünsch et al., 2017).

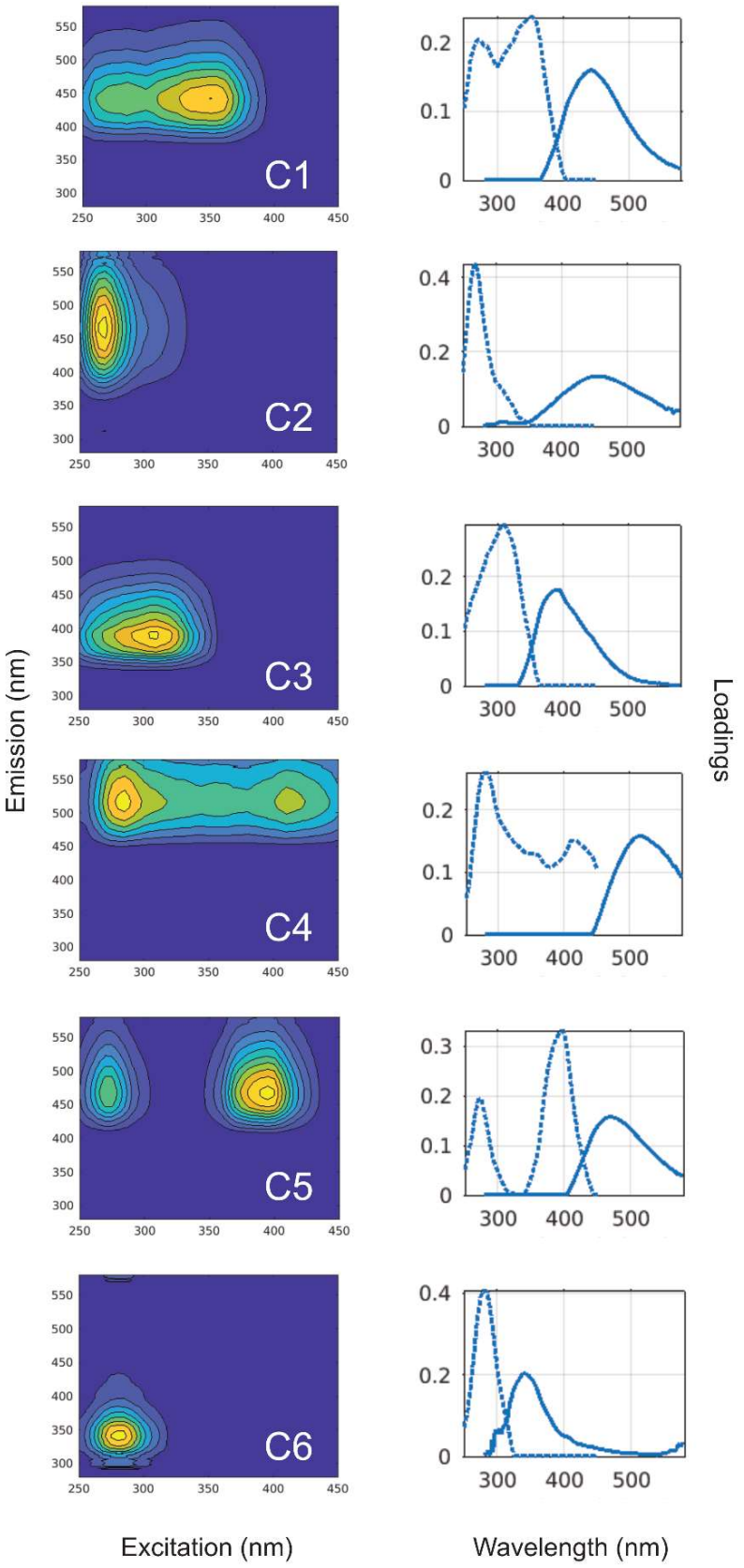

Figure 4.5. *The components validated by the PARAFAC model (C1 – C6) for the samples collected between November 2018 and December 2019 in the Rivers Yare and Waveney. On the left the fingerprint of the components and on the right the emission (line) and excitation (dashed line) spectra and relative loadings of the components.*

Component 4 (C4) had excitation maxima at λ of 285 and 410 nm and an emission maximum at λ of 518 nm and is reported to be a humic-like compound, produced by the photodegradation of terrestrially derived material (Murphy et al., 2014; Gullian-Klanian et al., 2021). Component 5 (C5) with excitation maxima at λ of 270 and 395 nm and an emission maximum at λ of 466 nm is representative of humic-like substances with a terrestrial origin, in particular, those derived from soils (Stedmon et al., 2011; Jutaporn et al., 2020). Component 6 (C6) with an excitation maximum at λ of 280 nm and an emission maximum at λ of 340 nm is indicative of protein-like substances (aminoacids free or bound in proteins), in particular, tryptophan-like compounds associated with high biological activity with low molecular weight. It has also been associated with rivers affected by wastewater (Murphy et al., 2008; Murphy et al., 2014; Peleato et al., 2016; Smith et al., 2021).

Table 4.1. *Description and spectral characterisation of the components identified and validated by the PARAFAC model for 172 of the samples collected between November 2018 and December 2019 in the River Waveney and in the River Yare.*

Component	Excitation/emission maxima λ (nm)	Description
C1	285, 385 / 444	Humic-like of terrestrial origin, photolabile
C2	270 / 466	Humic-like of terrestrial origin, photorefractory
C3	310 / 392	Humic-like microbially produced
C4	285, 410 / 518	Fulvic-like of terrestrial origin, associated with soils
C5	270, 385 / 466	Between humic- and fulvic-like of terrestrial origin
C6	280 / 340	Protein-like, particularly tryptophan-like produced *in-situ*

4.2.2 PCA to determine differences and similarities in the two rivers

A PCA was performed for all the samples collected following the procedure explained in section 3.2.2 (Chapter 3). Prior to the PCA an interpolation of the missing data across the dataset was performed using the missMDA package in R, already introduced in section 3.2.2 (Chapter 3) (Josse et al., 2011; Josse and Husson, 2016). This package allows the visualisation of the several replacements or imputations calculated for the missing values in order to verify how the uncertainty of the estimated data affects the PCA. Two principal components (PCs) were chosen, explaining most of the variability in the dataset (Figures 4.6 and 4.7). Consequently, the multiple data imputation was run 500 times with a Bayesian method (Audigier et al., 2015) and the uncertainty of the PCA was explored for the first two components which were the most important in explaining the variability of the dataset (Figure 4.7). Figure 4.7 shows the uncertainties of the interpolated missing values around the variables and components 1 and 2 of the PCA which were acceptable and did not affect the PCA. The data missing in this dataset represented 4.3% of the whole dataset which is smaller than the percentage of missing data reported by Josse et al. (2011) that did not affect the results of the PCA. As explained in section 3.2.2 (Chapter 3) the statistical significance of the PCA, the components and the loadings of the variables was also tested (Figures C1 and C2 in Appendix C). Two PCAs were run, as in section 3.2.2 (Chapter 3) with the first PCA investigating quantitative DOM data (CDOM, DOC, and fluorescent components) as primary variables, and nutrients, chlorophyll-*a,* TSS, salinity, and solar radiation as supplementary variables. The second PCA investigated qualitative DOM data (spectral slopes and ratio, $SUVA_{254}$, BIX, FI, peak T to peak C and HIX) as primary variables and the same variables mentioned above for the first PCA as supplementary.

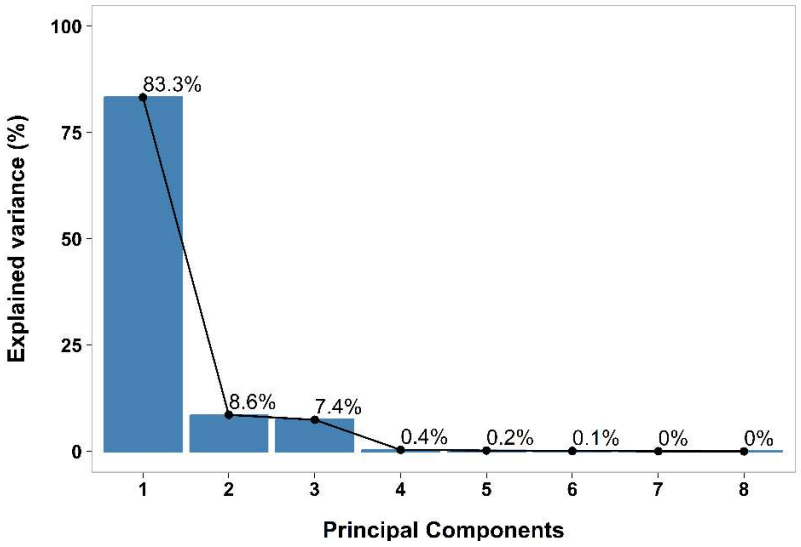

Figure 4.6. *Scree plot showing the contribution of every component of the PCA to the variance within the dataset for the samples collected in the River Yare and in the River Waveney between November 2018 and December 2019 for the PCA analysis of the quantitative data of DOM.*

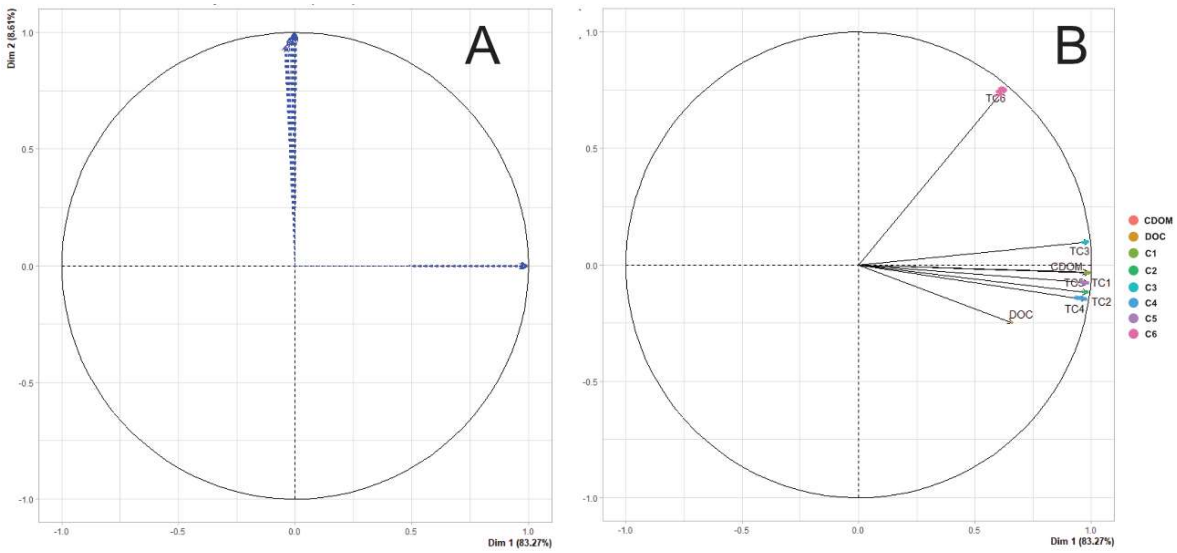

Figure 4.7. *Influence of the imputations on PC1 and PC2 (A) and coloured uncertainty for the variables with every coloured point representing an imputation (B) for the samples collected in the River Yare and in the River Waveney between November 2018 and December 2019 for the PCA analysis of the quantitative data of DOM.*

As shown in Figure 4.8, for the PCA of the quantitative DOM data, the variables with strong influence (R > 0.9) on component 1 were C1, C3, C5, $CDOM_{\alpha 254}$, C2 and C4, whilst only C6 had a high correlation (R ≥ 0.70) with component 2.

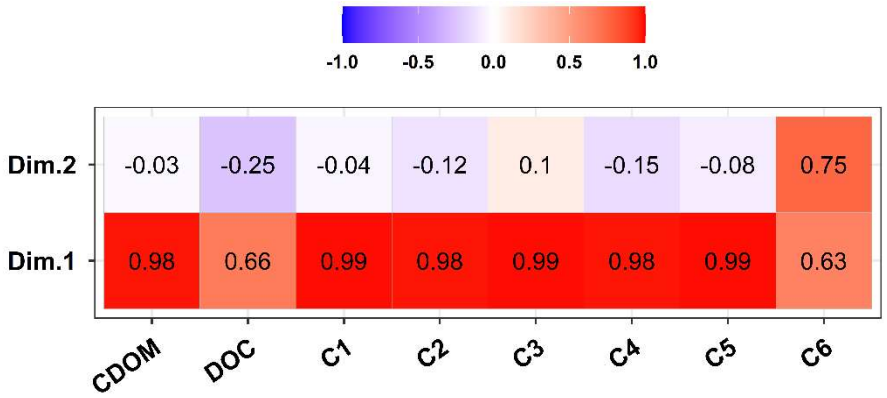

Figure 4.8. *Matrix showing the correlation between the variables analysed and the two components of the PCA for the samples collected in the River Yare and the River Waveney between November 2018 and December 2019 for the PCA analysis of the quantitative data of DOM.*

Figures 4.9A and 4.9B show the correlation between the primary and supplementary variables with PC1 and PC2, respectively, whilst figures 4.10A and 4.10B show the sampling points clustered by river and season, respectively. The samples collected in both rivers up to the estuary contained higher CDOM and the fluorescent components indicative of terrestrial DOM (PC1 from left to right), with the Yare also showing high values of C6, the fluorescent component indicative of *in-situ* produced DOM. As for the estuary, the samples

showed higher salinity and TSS, negatively correlated to the quantitative DOM variables, with the cluster markedly separated from the ones of the Yare and the Waveney.

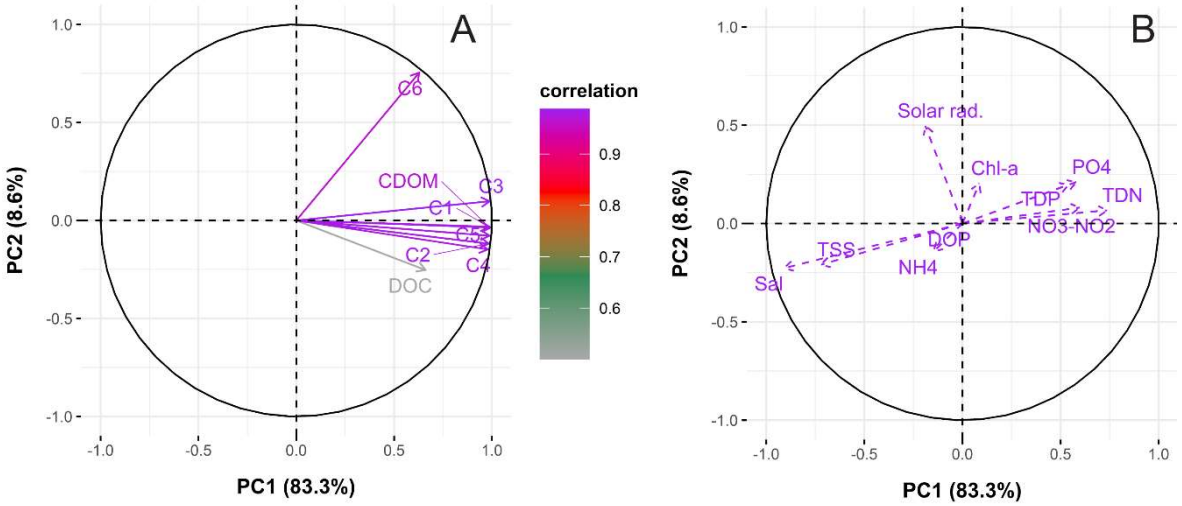

Figure 4.9. *Plot A represents the loadings of the primary variables analysed, coloured depending on how correlated they are to PC1 and PC2, whilst plot B represents the loadings of the supplementary variables analysed for the* samples collected between November 2018 and December 2019 in the River Yare and the River Waveney *the PCA analysis of the quantitative data of DOM*.

The grouping of the samples by season (Figure 4.10B) does not show any marked separation, as the clusters are overlapping. Nevertheless, a slight difference between the clusters of spring and summer is visible as they are tilted towards the first quadrant and the variables of C6 and to a lesser degree chlorophyll-*a,* which is somewhat expected as biological production is higher during these seasons.

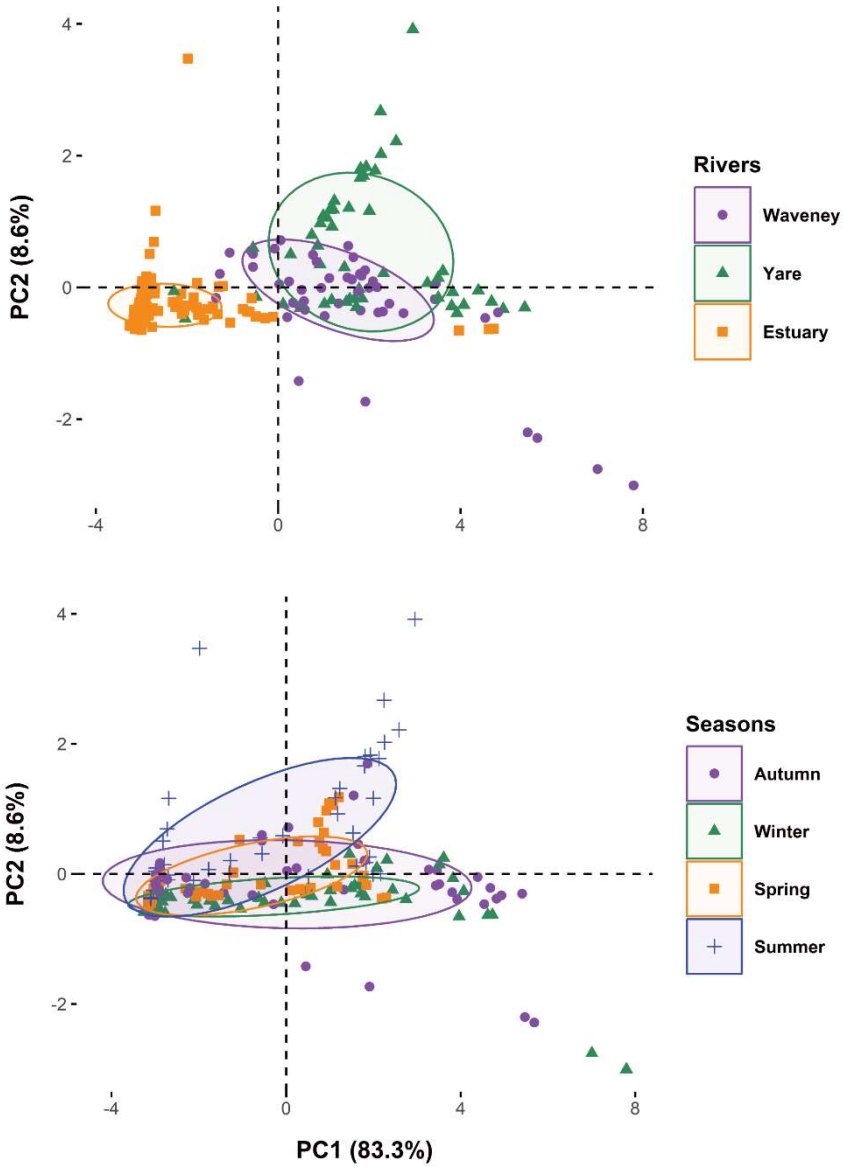

Figure 4.10. *Loadings of the samples collected between November 2018 and December 2019 in the River Yare and the River Waveney, clustered by location (top) and by season (bottom) with ellipses representing 66% confidence assuming the dataset as a multivariate t-distribution* for *the PCA analysis of the quantitative data of DOM.*

As mentioned previously, a second PCA was run with the qualitative data of DOM as primary variables and nutrients, chlorophyll-*a*, salinity, TSS and solar radiation. PC1 and PC2 explained most of the variance with 33.3% and 14.8%, respectively. As for the first PCA, the uncertainties of the interpolated missing values around the variables and components 1 and 2 of the PCA which were acceptable and did not affect the PCA. The variables with strong positive correlation with PC1 (> 0.7) were BIX and peak T to peak C, whilst HIX showed a strong negative correlation with PC1 (-0.82). For PC2, only $S_{350\text{-}400}$ presented a high positive correlation (0.75) (Figure 4.11).

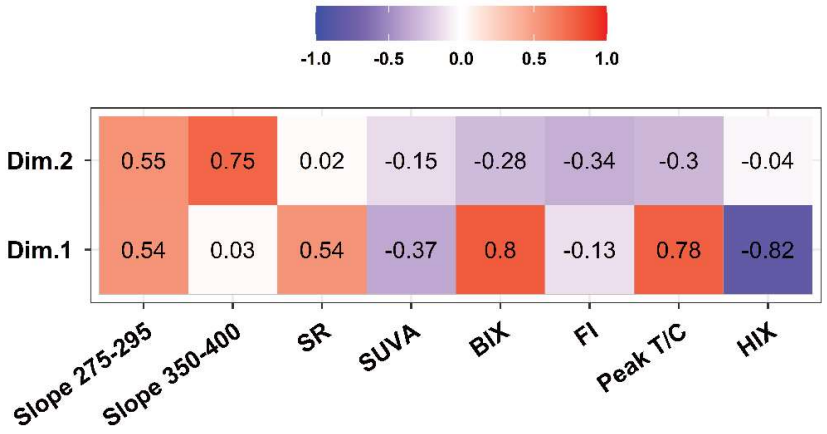

Figure 4.11. *Matrix showing the correlation between the variables analysed and the two components of the PCA for the samples collected in the River Yare and the River Waveney between November 2018 and December 2019 for the PCA analysis of the qualitative data of DOM.*

The correlation between both primary and supplementary values with PC1 and PC2 (Figures 4.12A and 4.12B) show that PC1 is highly correlated to HIX which in turn negatively correlated to BIX and peak T to peak C and $S_{275-295}$. Interestingly, figure 4.12B shows that TSS and salinity are negatively correlated to nutrients, which, with the results in figure 4.11A would indicate a separation between freshwater (higher HIX and nutrients) and more saline water (higher salinity, TSS and $S_{275-295}$).

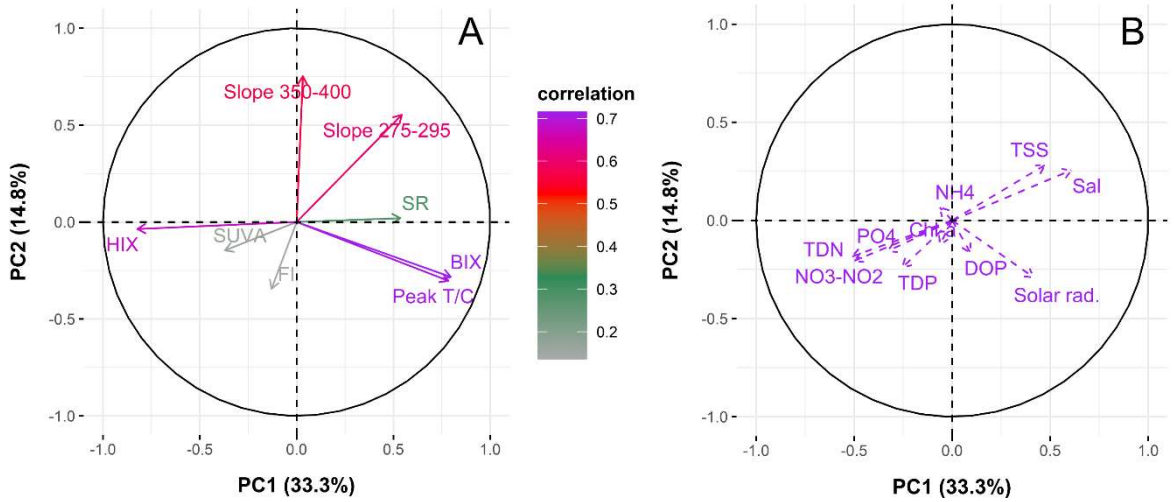

Figure 4.12. *Plot A represents the loadings of the primary variables analysed, coloured depending on how correlated they are to PC1 and PC2, whilst plot B represents the loadings of the supplementary variables analysed for the* samples collected between November 2018 and December 2019 in the River Yare and the River Waveney for *the PCA analysis of the qualitative data of DOM.*

The separation between freshwater and more saline water is confirmed by the top figure 4.13, whilst the clusters for the two rivers are heavily overlapped and suggest they are linked to DOM with a terrestrial origin due to the correlation to HIX and the negative

correlation to $S_{275-295}$. In addition, some of the estuarine samples are characterised by *in-situ* produced DOM (peak T to peak C and BIX) and correlated to solar radiation.

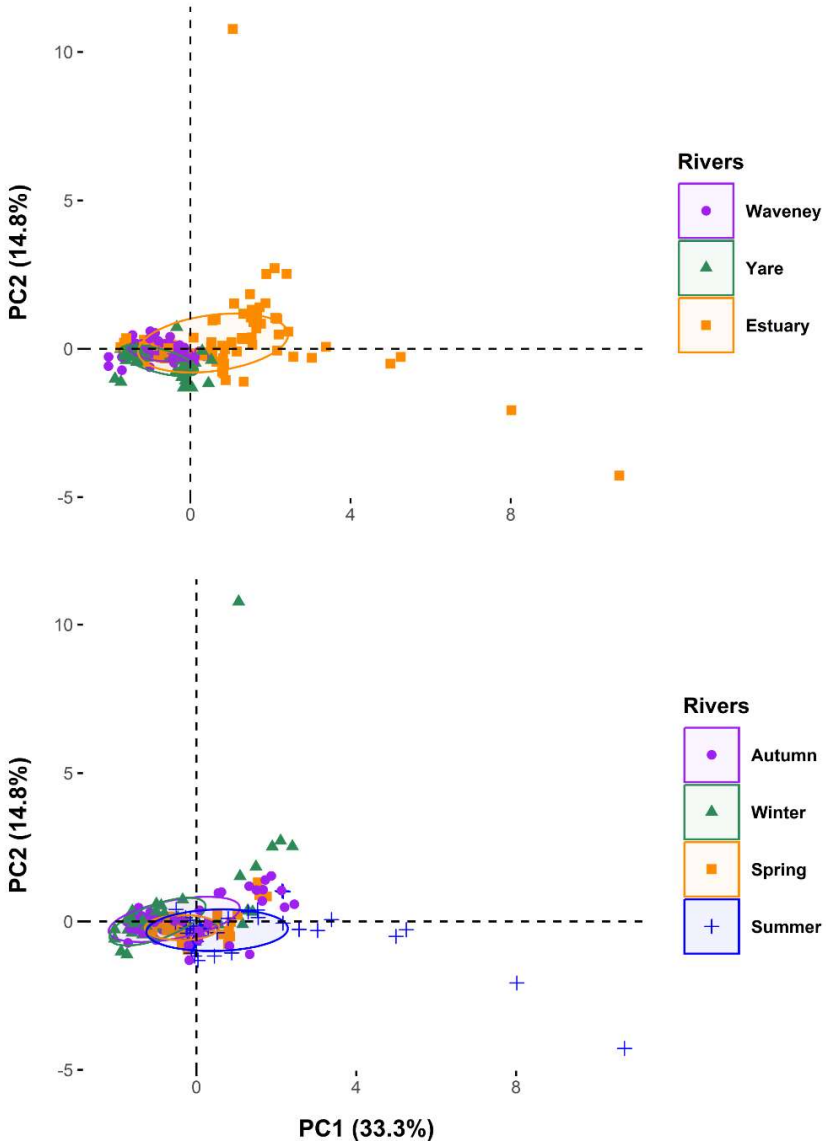

Figure 4.13. *Loadings of the samples collected between November 2018 and December 2019 in the River Yare and the River Waveney, clustered by location (top) and by season (bottom) with ellipses representing 66% confidence assuming the dataset as a multivariate t-distribution* for *the PCA analysis of the qualitative data of DOM.*

When the individual samples were clustered by season these are overlapping with no clear separation, except for some samples towards the first quadrant, showing higher $S_{275-295}$, TSS and salinity in autumn, winter and spring. There was a clear separation for the summer season with samples distributed in the second quadrant correlating with solar radiation, BIX and peak T to peak C, as expected for summer.

4.2.3 Hydrological conditions and temporal trends for precipitation, river discharge and solar radiation

Before analysing in more detail seasonality between the different variables, this section presents the timeseries of rainfall, solar radiation and the river discharge of the two rivers to give a meteorological and hydrological background. For the timeseries, only the two most upstream sampling points are presented for the two rivers, whilst for the estuary only the most downstream sampling point is plotted.

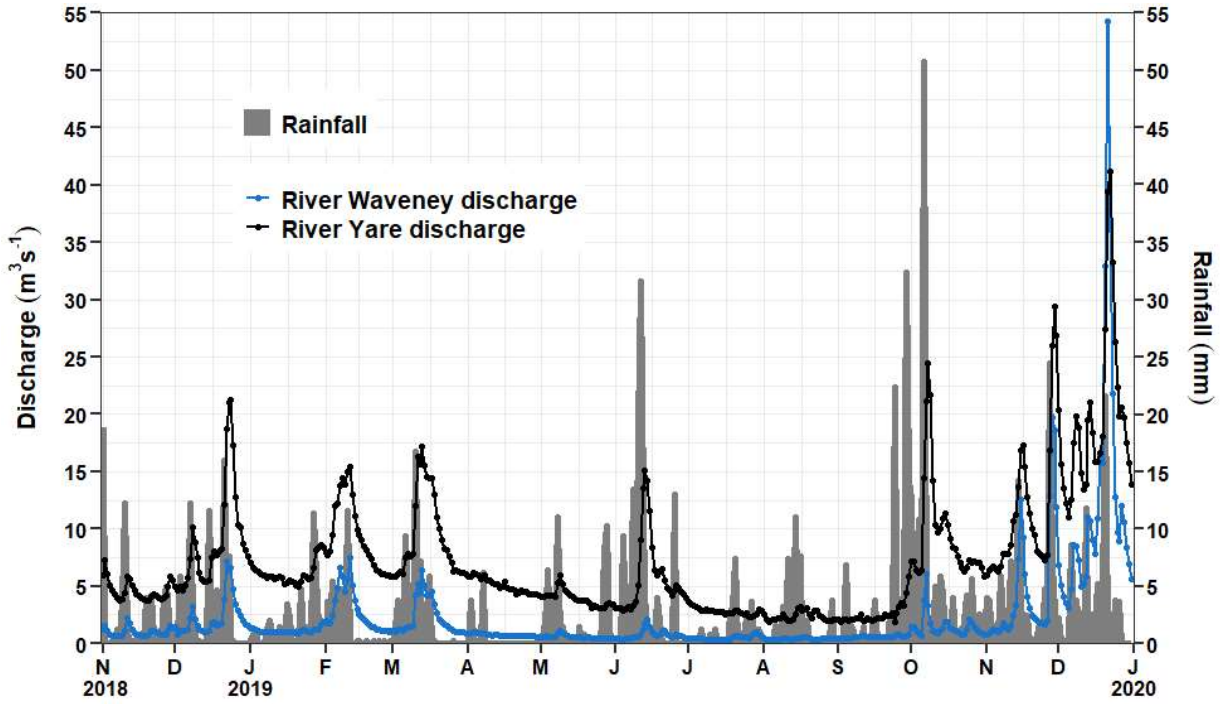

Figure 4.14. *Mean daily precipitation measured at Salle, Norfolk (UK) from the Wensum DTC project (Cooper* et al.*, 2018), mean daily discharge for the River Yare calculated for the sampling points YAR7 and YAR6 (December 2018 - January 2019) and mean daily discharge for the River Waveney calculated for the sampling points WAVE7 and WAVE6 (November 2018 – February 2019) between November 2018 and December 2019.*

The precipitation measured between November 2018 and December 2019 did not display a clear seasonal pattern with rainfall events occurring every month (Figure 4.14). The river discharge for both the River Yare and the River Waveney displayed a seasonal pattern with higher river flow in autumn and winter and lower river flow in spring and summer, although the river discharge of both rivers had a spike in June due to heavy rainfall. The seasonality in the river discharge is due to differences in evapotranspiration and groundwater levels. Values for river discharge in the UK are higher in autumn and winter, and lower in spring and summer as reported by Hannaford and Buys (2012) and by Cooper et al. (2020) for a catchment in East Anglia, due to increased evapotranspiration (influenced by rising temperatures from spring) and reduced groundwater levels in the summer months.

Figures 4.15A and 4.15B show timeseries for temperature and net solar radiation covering the sampling period. Both air temperature and net solar radiation show seasonal cycles in which both are lower in autumn and winter and higher in spring and summer.

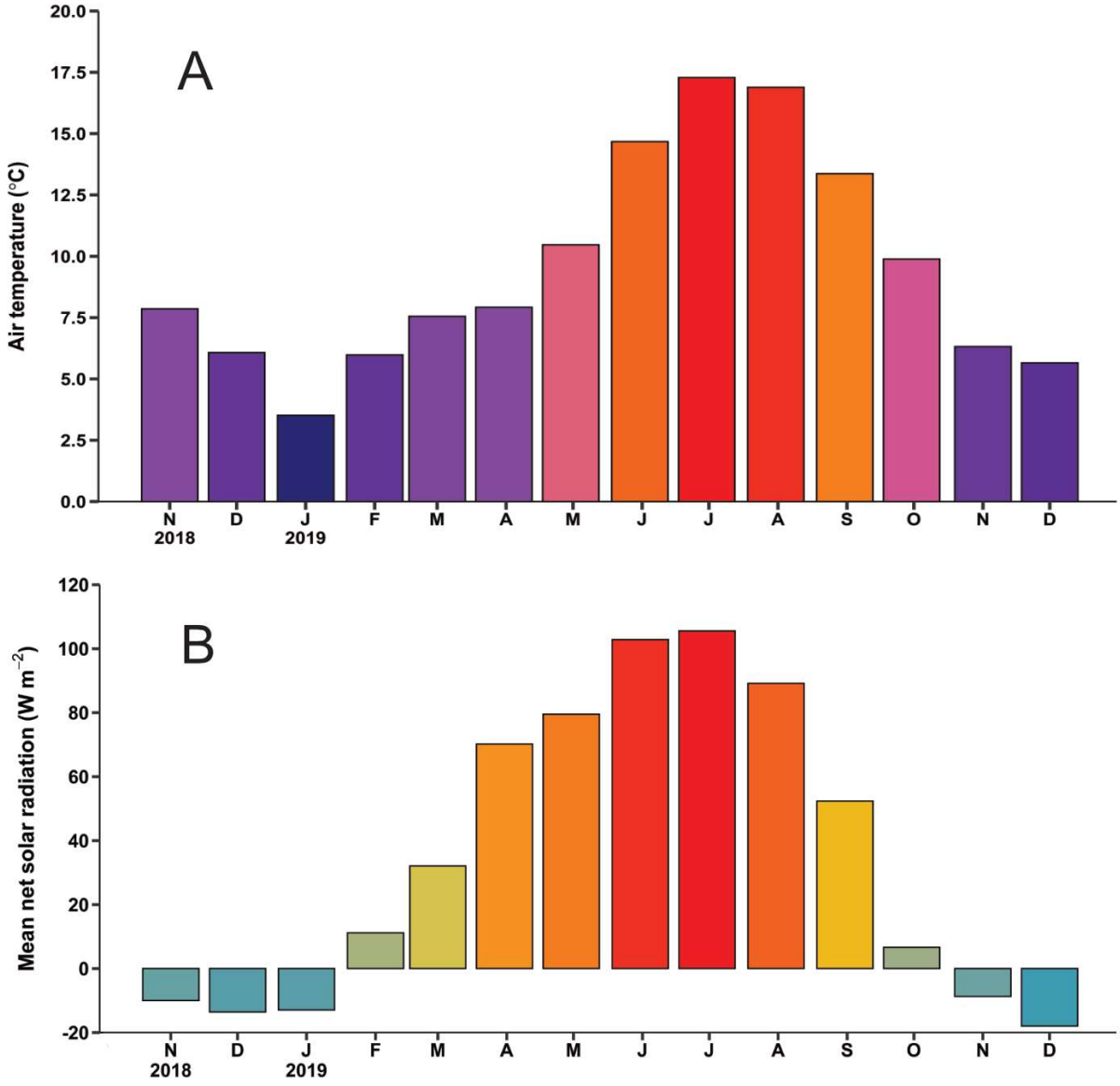

Figure 4.15. *Monthly timeseries of air temperature (A) and net solar radiation (difference between direct incoming solar radiation and outgoing radiation from Earth) (B) between November 2018 and December 2019 measured at Salle, Norfolk (UK) from the Wensum DTC project (Cooper* et al.*, 2018).*

As explained by Cooper et al. (2018, 2020) the relationship between precipitation and river discharge is affected by the river characteristics, in particular, by the amount of surface and groundwater interaction. Rivers that are groundwater-fed tend to be less responsive to precipitation, whilst river discharge for rivers that are not groundwater-fed, is more responsive to surface runoff and therefore to precipitation (Cooper et al., 2018). This

is usually inferred by the Baseflow Index (BFI) which was calculated for both rivers for the most upstream points sampled (Figure 4.16). First the baseflow was calculated by applying the Boughton two-parameter algorithm as described by Chapman (1999) and Cooper et al. (2018). Then the BFI was determined by dividing the baseflow by the total discharge. Daily discharge data integrated over a 5-day period were used for the calculation. For the River Yare the BFI calculated for the sampling period was 0.67, whilst for the River Waveney for the same period it was 0.41.

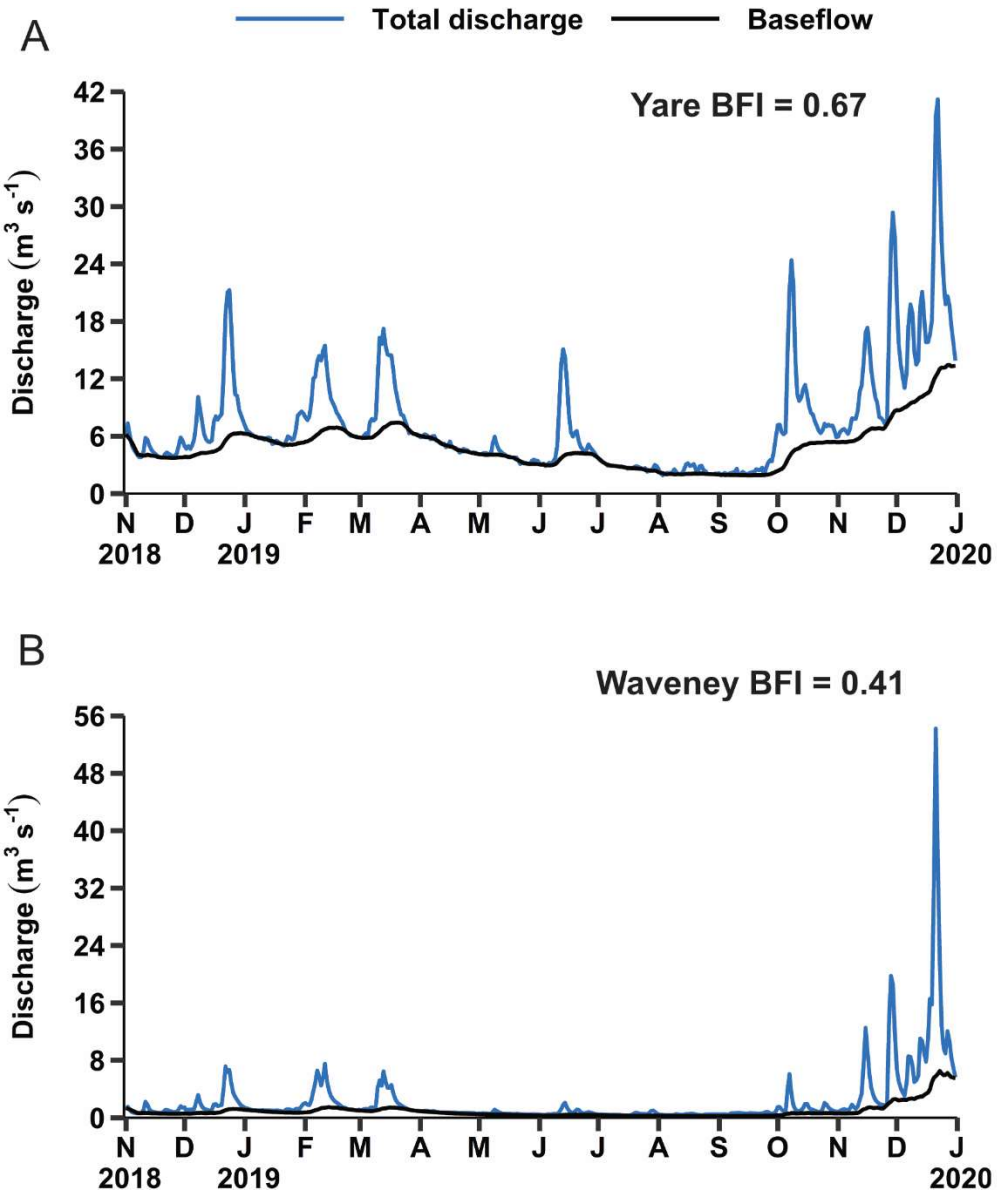

Figure 4.16. *Baseflow index and discharge between November 2018 and December 2019 for the River Yare (A) calculated for the sampling points YAR7 and YAR6 (December 2018 - January 2019) and baseflow index and discharge for the River Waveney (B) calculated for the sampling points WAVE7 and WAVE6 (November 2018 – February 2019).*

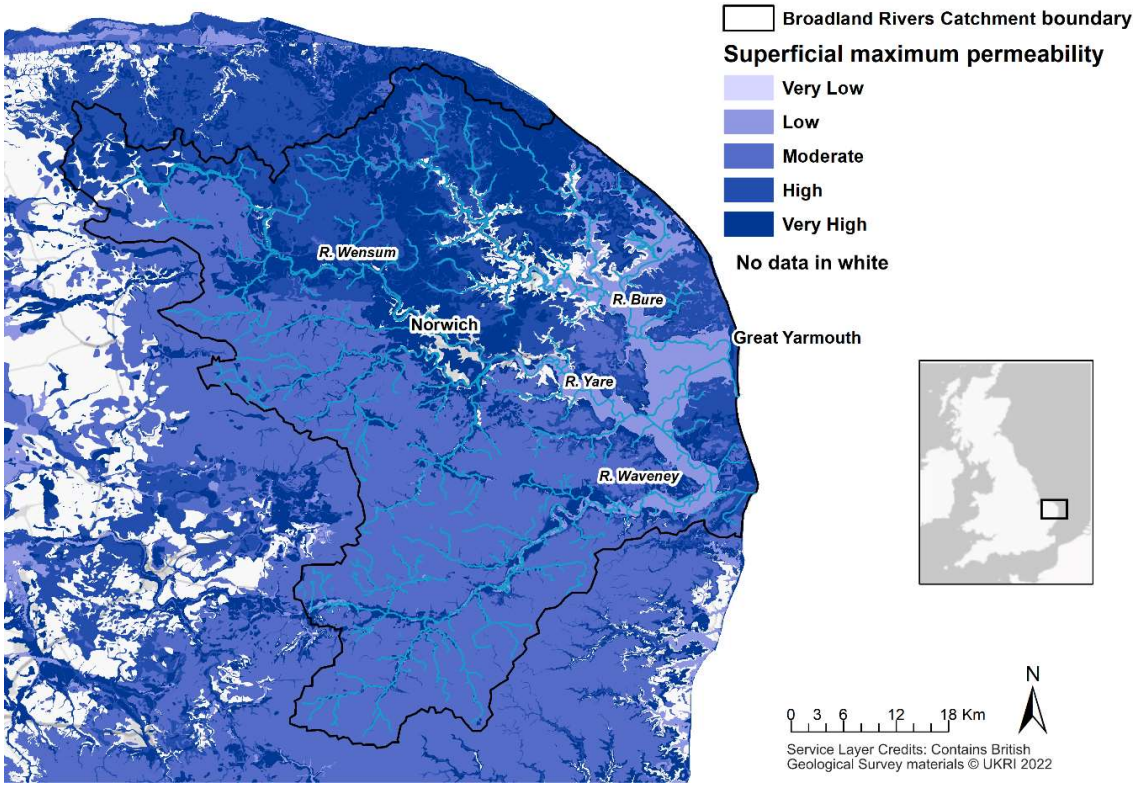

Figure 4.17. *Map of the superficial permeability of the Broadland Rivers Catchment in Norfolk (UK) from very low to very high. The maps contain data from the British Geological Society (BGS) (UKRI 2022).*

The difference in the BFI for the two rivers is reflected in the map of surface permeability (Figure 4.17) which highlights the greater permeability of the River Yare catchment compared to the permeability of the River Waveney catchment. Studies have shown that the BFI is influenced by the geology of the catchment (Longobardi and Villani, 2008; Bloomfield et al., 2009; Cooper et al., 2018, 2020). For the two rivers in this study the bedrock geology and their superficial geology is different (Figure 4.18). In particular, with reference to the bedrock geology, the western part of the catchment of the River Yare is characterised by chalk whilst the catchment of the River Waveney has proportionally less chalk and more undifferentiated gravel, sand, silt and clay. This difference is also reflected in Figure 4.18. All these features plus the catchment size and the climate regime control the spatial and temporal dynamics of nutrients, hence DOM (Cooper et al., 2018).

The correlation between river discharge and precipitation in Table 4.2, highlights differences between the estuary and the two rivers and between the two rivers themselves. The river discharge for the River Yare correlated to the precipitation 13 days after the rainfall event, whilst the river discharge calculated for the River Waveney correlated 2 days after the rainfall event. For the estuary, the higher correlation occurred after 2 days and after 11 days. The difference in response of the river discharge to rainfall of the two rivers could reflect the disparity in the BFI but could also be due to the difference in the drainage basin

size used for the correlations (1230 km^2 for YAR7 and 1242 km^2 for YAR6 for the Yare and 735 km^2 for WAVE7 and 824 km^2 for WAVE6 for the Waveney).

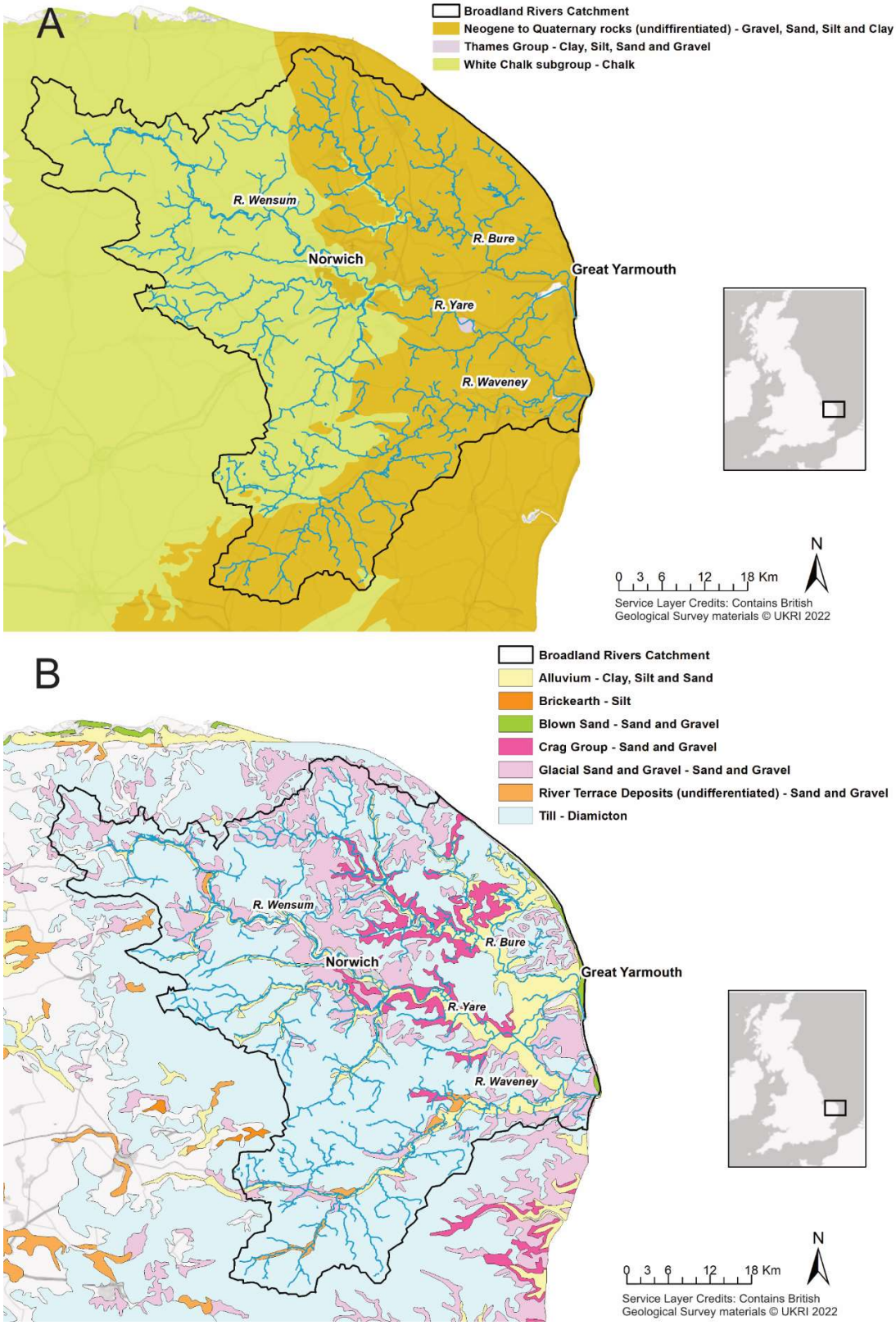

Figure 4.18. *Bedrock geology (A) and superficial geology (B) of the Broadland Rivers Catchment in Norfolk (UK). The maps contain data from the British Geological Society (BGS) (UKRI 2022).*

Table 4.2. *Correlation between rainfall events up to 14 days from the day of the sampling (t = 0) and river discharge for the sampling points YAR6 and YAR7 (December 2018 - January 2019), discharge for the River Waveney for the sampling points WAVE7 and WAVE6 (November 2018 – February 2019) and discharge for the estuary for sampling point SEA1 between November 2018 and December 2019. The p-value for the highlighted values is < 0.05.*

Rainfall events	Yare R^2 and equation	Waveney R^2 and equation	Estuary R^2 and equation
t = 0	**0.07** y = 0.227 x + 1.474	**0.09** y = 0.227 x + 1.474	**0.11** y = 2.641 x + 44.325
t -1	**0.12** y = 0.154 x + 7.002	**0.24** y = 0.361 x + 0.894	**0.14** y = 1.260 x + 44.517
t -2	**0.18** y = 0.132 x + 6.632	**0.70** y = 0.365 x + 0.245	**0.26** y = 1.187 x + 41.620
t -3	**0.16** y = 0.125 x + 6.439	**0.57** y = 0.313 x + 0.400	**0.23** y = 1.118 x + 40.167
t -4	**0.07** y = 0.069 x + 6.814	**0.37** y = 0.190 x + 0.307	**0.16** y = 0.729 x + 41.234
t -5	**0.09** y = 0.074 x + 6.632	**0.11** y = 0.060 x + 1.083	**0.13** y = 0.583 x + 40.980
t -6	**0.07** y = 0.068 x + 6.643	**0.07** y = 0.037 x + 1.283	**0.10** y = 0.475 x + 41.547
t -7	**0.15** y = 0.096 x + 5.816	**0.02** y = 0.017 x + 1.549	**0.13** y = 0.496 x + 39.189
t -8	**0.12** y = 0.079 x + 6.013	**0.01** y = 0.012 x + 1.610	**0.11** y = 0.411 x + 40.165
t -9	**0.15** y = 0.091 x + 5.578	**0.02** y = 0.014 x + 1.551	**0.13** y = 0.435 x + 38.819
t -10	**0.22** y = 0.114 x + 4.695	**0.02** y = 0.013 x + 1.551	**0.16** y = 0.481 x + 36.847
t -11	**0.44** y = 0.154 x + 3.010	**0.02** y = 0.014 x + 1.523	**0.24** y = 0.589 x + 32.378
t -12	**0.44** y = 0.153 x + 2.876	**0.10** y = 0.009 x + 1.623	**0.22** y = 0.525 x + 33.018
t -13	**0.47** y = 0.156 x + 2.445	**0.01** y = 0.007 x + 1.659	**0.22** y = 0.495 x + 33.084
t -14	**0.39** y = 0.126 x + 2.875	**0.01** y = 0.005 x + 1.698	**0.18** y = 0.395 x + 34.120

Although the correlations between precipitation and river discharge for the estuary in Table 4.2 were significant, they were not strong. The highest correlation was found 2 days and 11 days after the rainfall event. This could be due to the interaction the estuary

has with both the rivers and the sea. The lack of a high correlation could be related to the tidal influence and the seawater entering the estuary, disrupting the “normal” flow regime of the river flowing out to sea as reported in a study by Camenen et al. (2021). As investigated in Chapter 3, tidal cycles can impact DOM dynamics and processes by affecting the river discharge.

In order to see if the difference in the BFI of the two rivers has an effect on DOM dynamics, correlation matrices between all the variables are presented, followed by timeseries of DOC, DON, DOP plus inorganic nutrients, the six components identified through the PARAFAC model and the absorption and fluorescence indices for the sampling period.

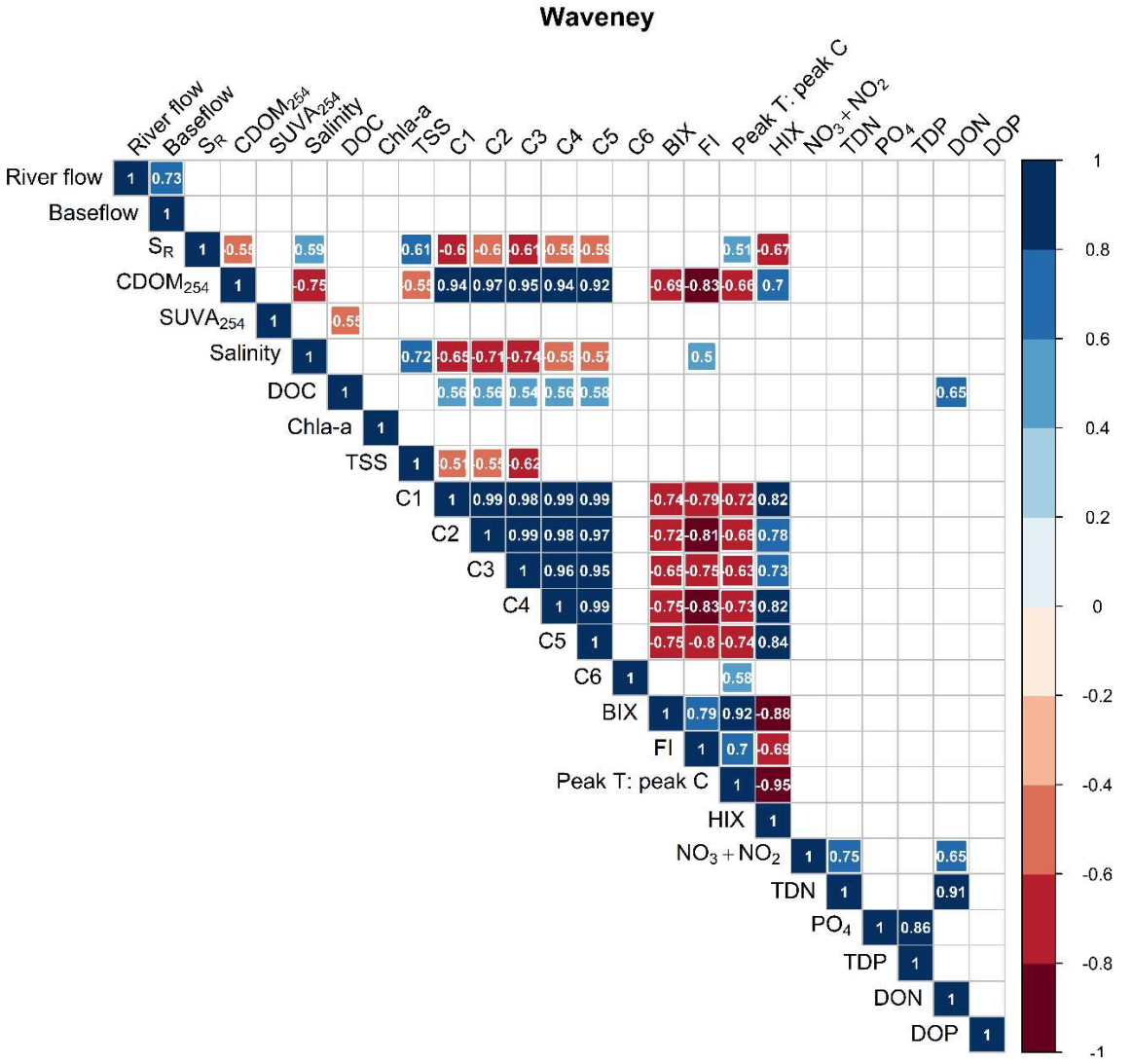

Figure 4.19. *Pearson’s correlation matrix of all the values from all the sampling points for the River Waveney between November 2018 and December 2019. The R^2 is reported within the squares in white, whilst where p-values were greater than 0.05 the squares are blank.*

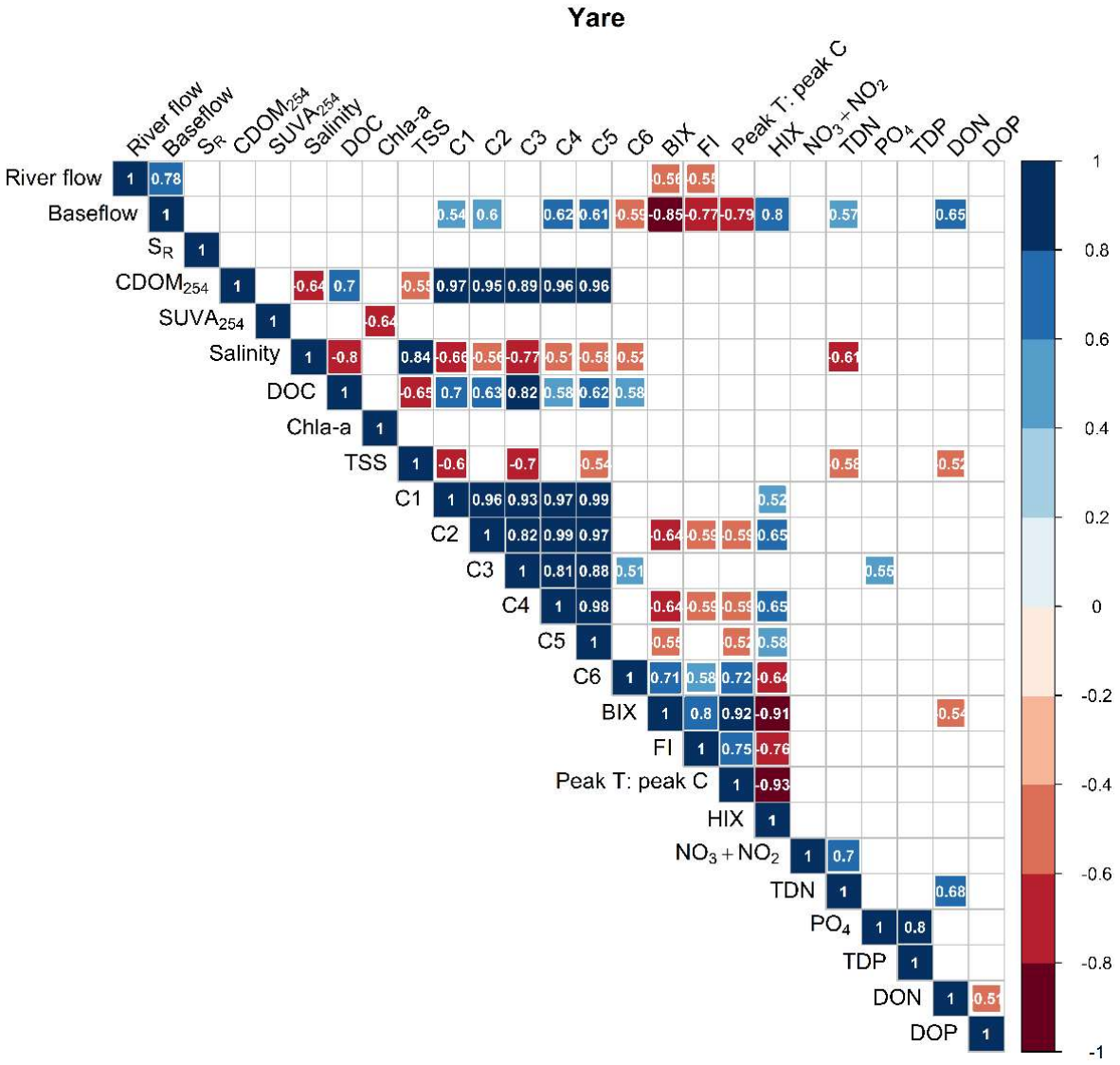

Figure 4.20. *Pearson's correlation matrix of all the values from all the sampling points for the River Yare between December 2018 and December 2019. The R^2 is reported within the squares in white, whilst where p-values were greater than 0.05 the squares are blank.*

In the correlation matrices of the River Waveney (Figure 4.19) and the estuary (Figure 4.21), the river flow and the baseflow did not show a correlation with any other variable. Inevitably, the correlation between the river flow and the baseflow was positive as the baseflow is part of the river discharge. For the River Yare (Figure 4.20), in addition to the positive correlation between the river discharge and the baseflow, the baseflow also had a significant relationship with other variables. This difference between the two rivers could reflect the difference in surface and groundwater connection previously discussed. Interestingly, a significant positive correlation was found between the baseflow of the River Yare and variables linked to terrestrial DOM (C1, C2, C4, C5 and HIX), as well as with TDN and DON. In addition, a significant negative correlation was found between the baseflow

and variables linked to biologically produced or altered DOM (C6, BIX, FI, peak T to peak C), with BIX and FI also negatively correlated to the baseflow of the River Yare. Several studies have investigated the hydrological connectivity between aquifer and surface water in catchments, with some of these confirming terrestrially derived DOM in groundwater as evidence of such connectivity (Chen et al., 2010; Longnecker and Kujawinski, 2011; Lloyd et al., 2016; Shen et al., 2015; Outram et al., 2016; Cooper et al., 2020). The positive relationship between baseflow and terrestrially derived DOM reported for the Yare would confirm the permeability of the Yare catchment, whilst the correlation with TDN and DON suggest downward transport of nitrogen through soil leaching (Shen et al., 2015; Outram et al., 2016).

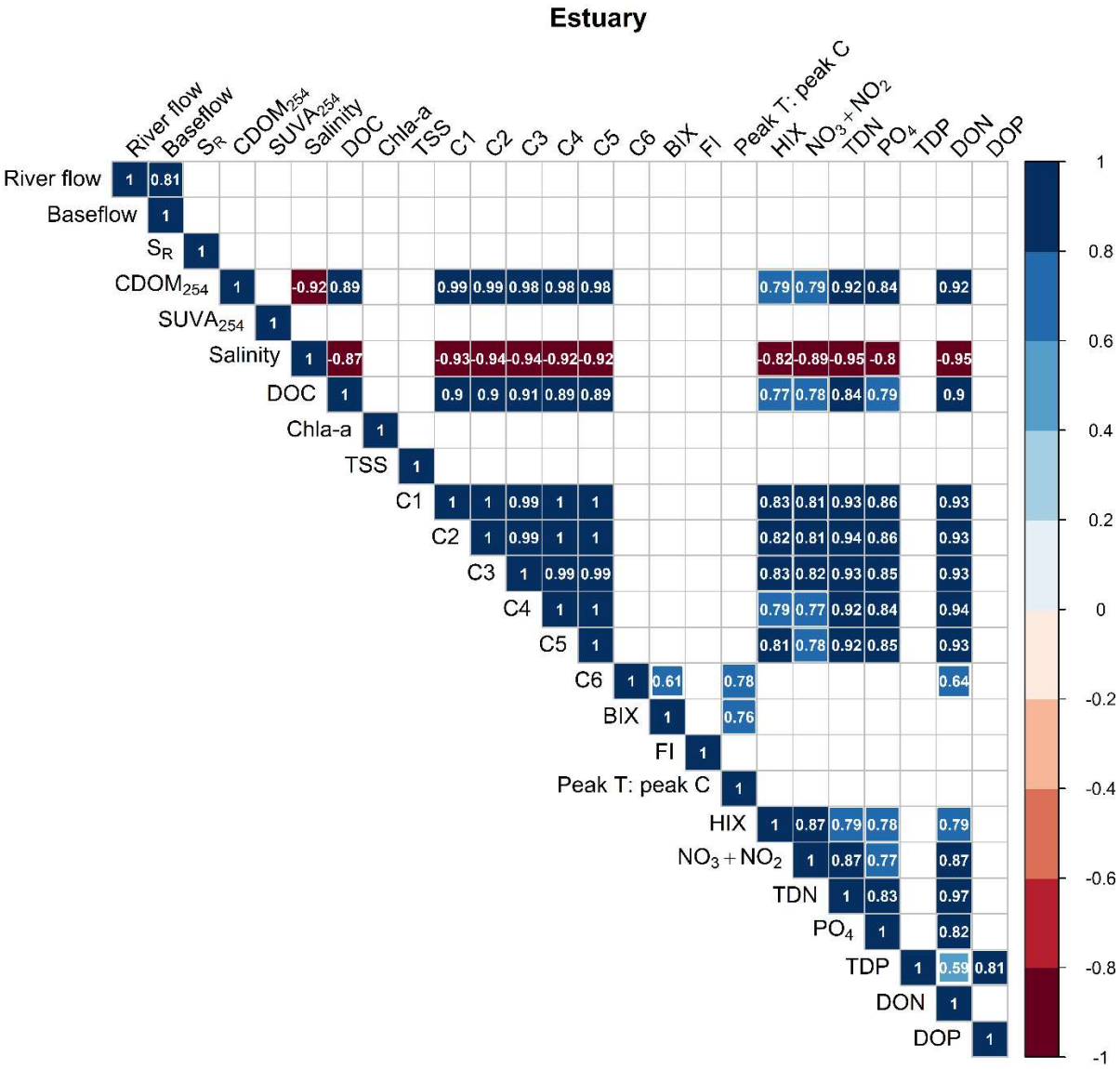

Figure 4.21. *Pearson's correlation matrix of all the values from all the sampling points for the estuary between November 2018 and December 2019. The R^2 is reported within the squares in white, whilst where p-values were greater than 0.05 the squares are blank.*

In particular, the presence of DON in groundwater could be due to decreased microbial processing to inorganic nitrogen compared to surface water, as also reported by Longnecker and Kujawinski (2011). The negative correlations of the baseflow with the previously mentioned variables indicating DOM from biotic processes, could suggest marine influence with fresh or microbially processed DOM affected by seawater coming in with tidal cycles as reported by Chen et al. (2010) in coastal wetlands, also confirmed by the negative correlation between BIX, FI and the river discharge. All the sampling points in both rivers (except YAR7, YAR6, WAVE7 and WAVE6) had salinities above 3 with maximum salinities between 20.8 and 27.7.

The lack of significant correlations between baseflow, river flow and DOM for the River Waveney and the estuary could reflect the complexity of hydrological processes within a catchment which are influenced by channel morphology, conditions before and after storm events, seasonality, channel erosion propensity, etc. (Outram et al., 2016; Cooper et al., 2018, 2020).

4.2.4 Temporal trends of DOM

Figure 4.22 shows timeseries for organic and inorganic nutrient concentrations. Some of the data points for TDP, nitrate plus nitrite and phosphate are missing due to instrument problems and missing samples. For the same reason, the timeseries for DON and DOP for the most upstream points sampled in the two rivers are not shown. For all the variables in Figure 4.22, the estuary had lower concentrations than the two rivers. The two rivers follow the same pattern throughout the year, although with some differences in concentrations. For DOC, the Waveney showed somewhat higher concentrations compared to the Yare and the estuary with a maximum of 4.5 mmol L^{-1} in December 2019, while in the same month the estuary also recorded its maximum concentration (0.63 mmol L^{-1}). This could be due to the high precipitation during this month (Figure 4.14 in section 4.2.3). TDN and nitrate plus nitrite showed higher concentrations for the River Yare than for the River Waveney throughout the year, with particularly low concentrations for the estuary (average of 0.05 mmol L^{-1}).

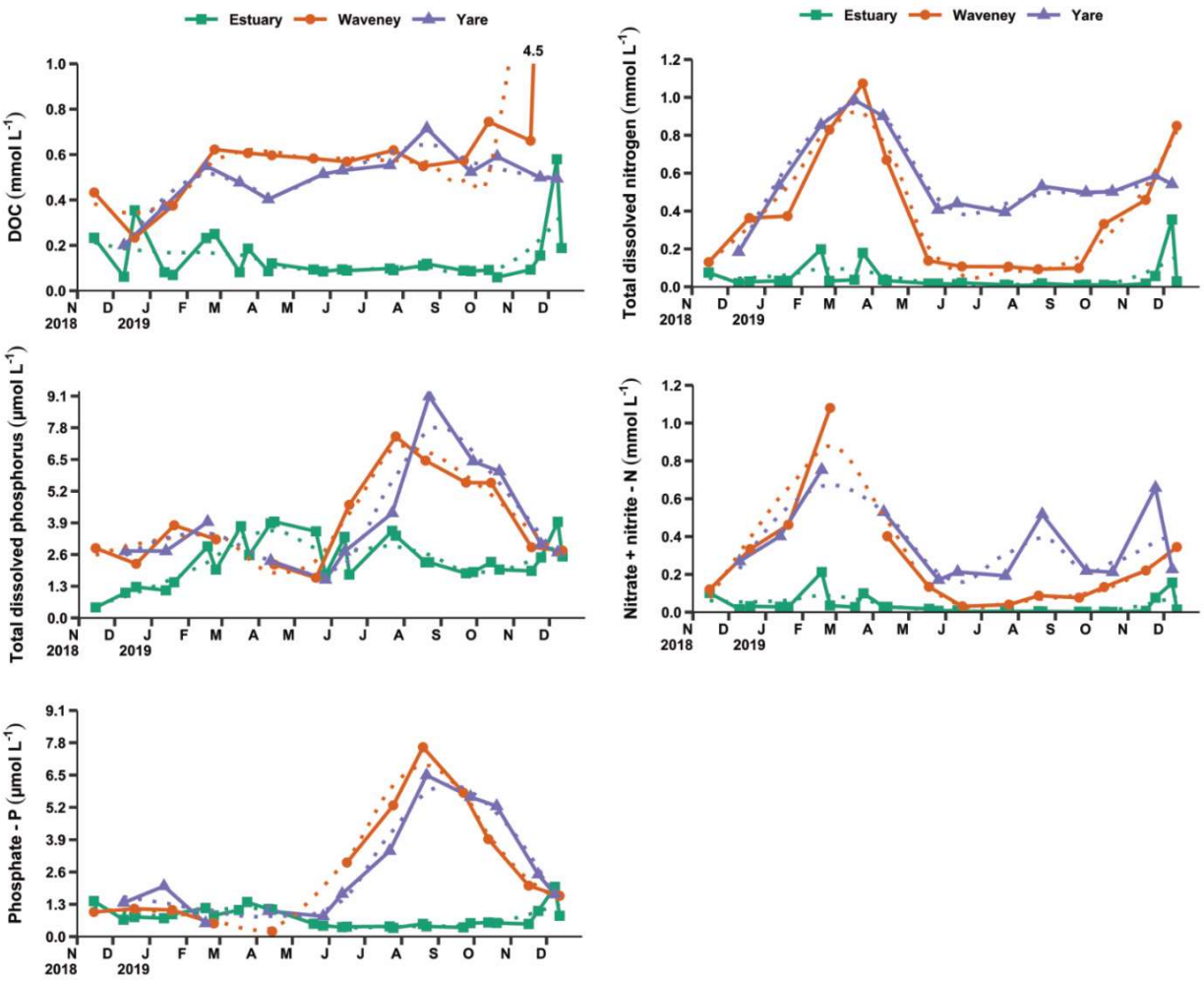

Figure 4.22. *Timeseries of DOC, TDN, TDP, nitrate plus nitrite and phosphate for the most upstream points sampled in the River Yare, YAR7 and YAR6 (December 2018 - January 2019), in the River Waveney, WAVE7 and WAVE6 (November 2018 – February 2019), and for the most downstream sampled point for both rivers (Estuary, SEA1) for November 2018 to December 2019. The dotted line represents a Locally Estimated Scatterplot Smoothing (LOESS) line.*

For all the sampling points plotted in Figure 4.22, nitrate plus nitrite represented most of TDN with ~60% for the Waveney, ~59% for the Yare and ~73% for the estuary. Timeseries for TDP and phosphate are less clear for the two rivers because of missing data, although for TDP the estuary showed higher concentrations than the two rivers between April and July 2019, and in December 2019 than the Yare. TDP and phosphate concentrations in the Yare and in the Waveney started to increase in June and reached a maximum in August 2019 with 6.49 and 7.62 µmol L^{-1} for phosphate in the Yare and in the Waveney, respectively, and 9.09 and 7.44 µmol L^{-1} for TDP in the Yare and in the Waveney, respectively. The composition of TDP was different between the estuary and the two rivers with phosphate comprising ~65% of TDP in the Waveney, ~68% of TDP in the Yare and ~32% of TDP in the estuary with the remainder present as DOP. This could be due to the high productivity at the interface with the coastal zone and/or the tide bringing productive

coastal seawater (Chaichana et al., 2019) into the estuary. The resuspension of sediments can also be a source of P that can be taken up by the microbial community as explained in section 3.2.4 (Chapter 3).

Figure 4.23 shows the timeseries for the DOM components identified through the PARAFAC model. Values for July 2019 for the River Waveney are missing due to the inability to use the spectra analysed with a different instrument. For all components the fluorescence intensities are higher for the two rivers than the estuary, whilst the River Waveney showed the highest fluorescence intensity average compared to the Yare, except for C6 where the Yare displayed the highest average. However, the difference in the average fluorescence intensity between the River Waveney and the Yare for C3 and C5 was only 0.01. Although these values reflect only the most upstream and downstream sampling points in this dataset, it is interesting to highlight the slightly more terrestrial DOM nature of the Waveney (C1, C2, C4 and C5) and the more *in-situ* produced DOM characteristic of the Yare (C6). Although C3 is also linked to microbially produced humic-like DOM, it might retain a terrestrial signature as it results from remineralisation of terrestrial DOM.

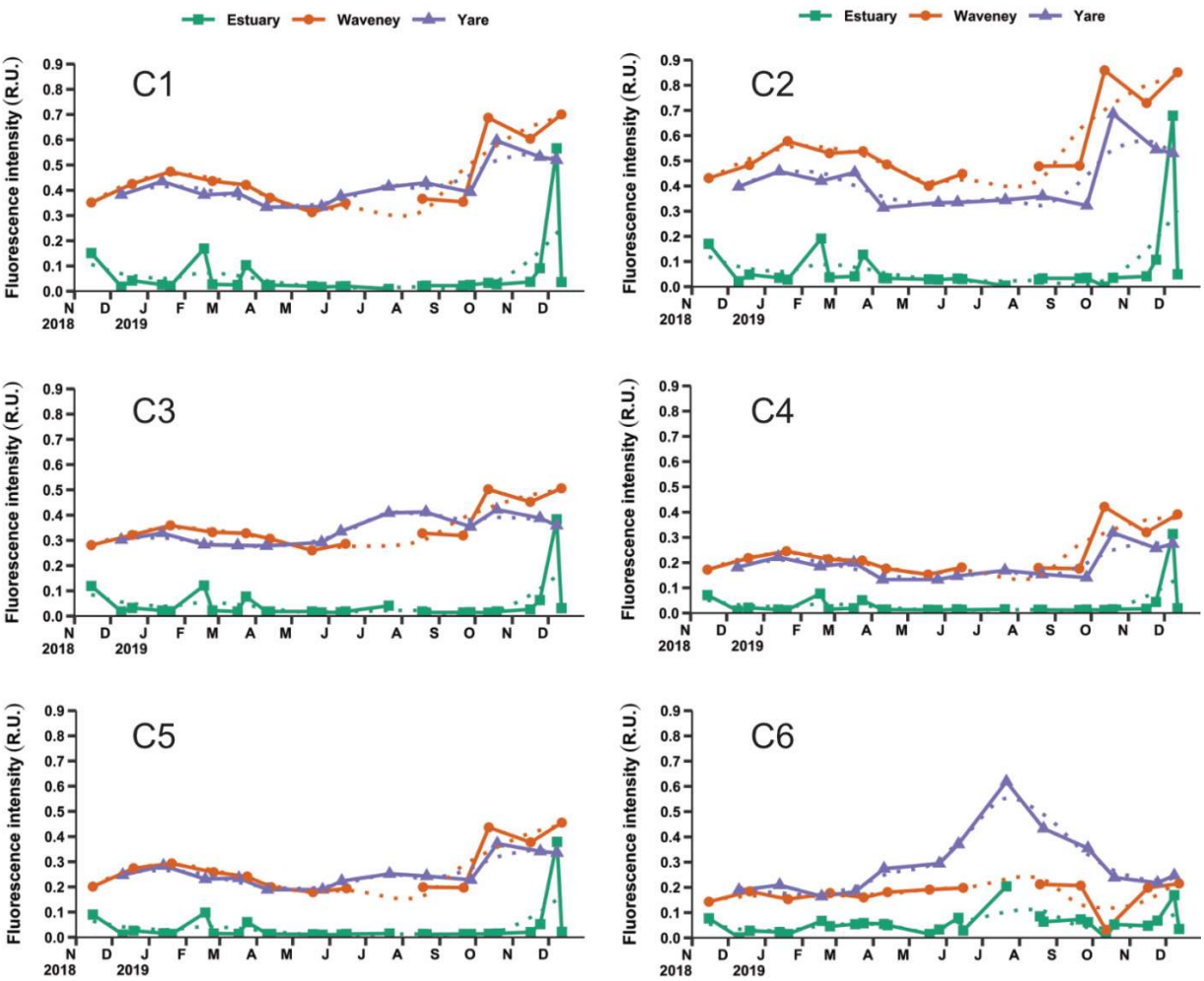

Figure 4.23. *Timeseries of the six components identified through PARAFAC for the most upstream points sampled in the River Yare, YAR7 and YAR6 (December 2018 - January 2019), in the River Waveney, WAVE7 and WAVE6 (November 2018 – February 2019) and for the most downstream sampled point for both rivers (Estuary, SEA1) for November 2018 to December 2019. The dotted line represents a Locally Estimated Scatterplot Smoothing (LOESS) line.*

Figure 4.24 shows the timeseries for the spectral fluorescence indices, $CDOM_{\alpha 254}$ and S_R which give insights about the processes involving DOM. For most of the sampling year S_R (Figure 4.24F) values for the estuary were twofold those for the rivers as also reported by Helms et al (2008). This indicates a difference in the molecular weight of DOM between the estuary and the rivers and the effect of DOM photodegradation as DOM travels downstream. Figure 4.24F shows no temporal change in the low S_R for the two rivers, suggesting no photodegradation and DOM with high molecular weight, whilst there was a peak in S_R for the estuary in June which coincides with high solar radiation in summer (Figure 4.15B) (Stubbins et al., 2012). Whilst S_R values in the estuary were lower between November 2018 and April 2019, with some variability, after the peak in June, there were higher values alternating with lower values. This could be a result of the mixing of the more photodegraded seawater DOM (Helms et al., 2008; Stedmon and Nelson, 2015) with the

freshwater coming from the rivers due to the tidal cycle. As previously discussed, the river flow is lower in summer and autumn and this could affect the amount of water coming in from the sea. The values of S_R are reflected in $CDOM_{\alpha 254}$ (Figure 4.24A) albeit in opposite directions. Higher absorption is linked to more terrestrial and higher molecular weight DOM (Bricaud et al.,1981) as shown in Figure 4.24A, where the $CDOM_{\alpha 254}$ of the two rivers was always higher than that of the estuary, suggesting a transformation of CDOM as it travels downstream. The inverse relationship between S_R and CDOM has been reported by several studies such as Helms et al. (2008), Stubbins et al. (2012) and Catalá et al. (2015).

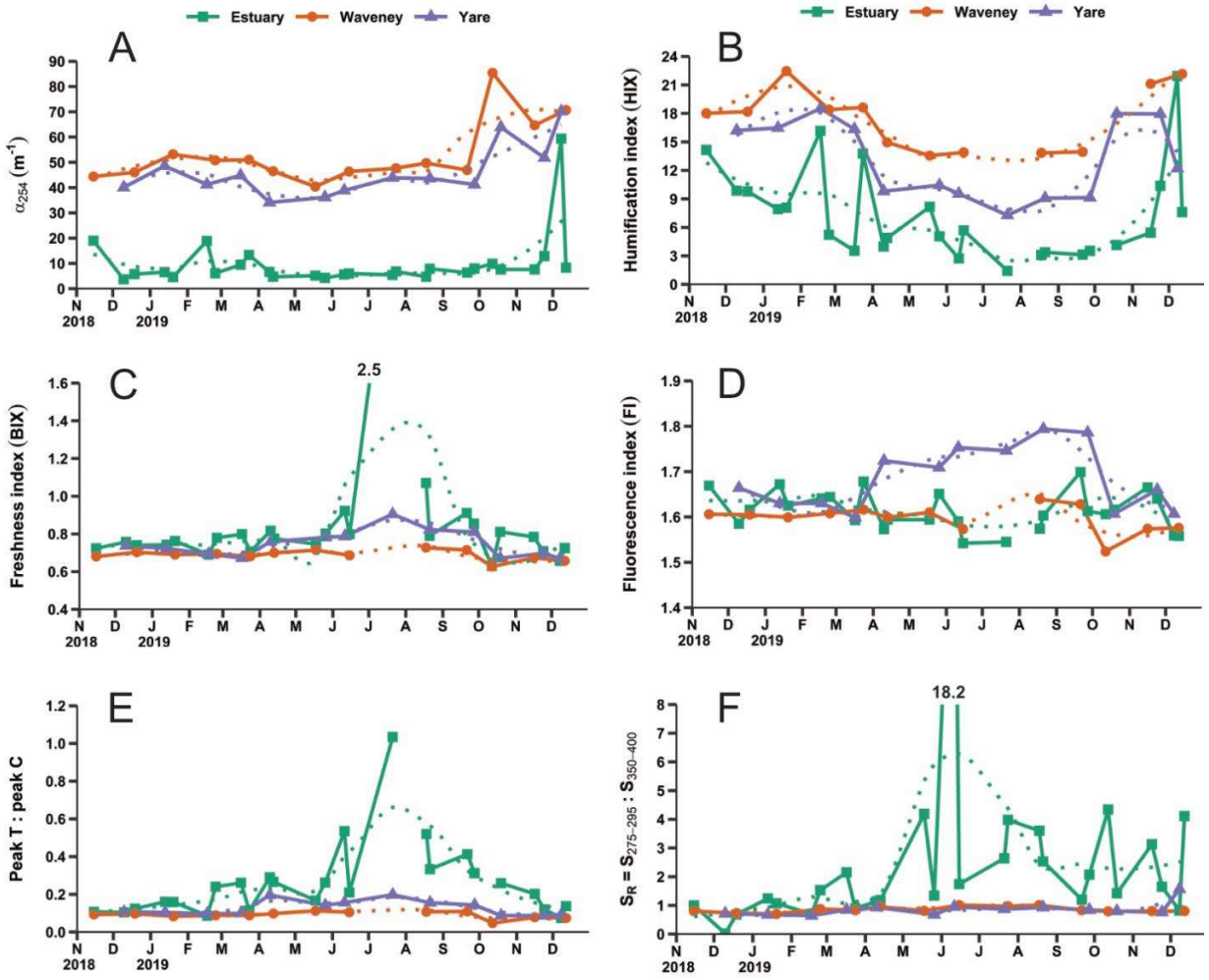

Figure 4.24. *Timeseries of $CDOM_{\alpha 254}$, HIX, BIX, FI, peak T to peak C and S_R for the most upstream points sampled in the River Yare, YAR7 and YAR6 (December 2018 - January 2019), in the River Waveney, WAVE7 and WAVE6 (November 2018 – February 2019) and for the most downstream sampling point for both rivers (Estuary, SEA1) for November 2018 to December 2019. The dotted line represents a Locally Estimated Scatterplot Smoothing (LOESS) line.*

In addition, HIX confirmed the differences in DOM between the rivers and the estuary but also possibly the influence of the tidal cycle and the river flow. Figure 4.24B shows higher HIX values in winter and lower in summer for all sampling sites. The Waveney

displayed the highest HIX average, followed by the Yare and the estuary with the lowest average (17.4, 13.1, 7.3, respectively). The HIX indicate a higher aromatic content for the two rivers with an average over 10, whilst the average for the estuary indicates a mixed content of humified and *in-situ* produced DOM. The decrease in HIX values in summer could reflect the lower river flow (high in humified DOM) and the larger contribution of seawater (low in humified DOM) entering through the tidal cycle as discussed for S_R. It could also indicate a shift from allochthonous DOM to autochthonous DOM given the increase in biological production in summer, highlighted by the protein-like C6 in Figure 4.23. Moreover, photodegradation could decrease HIX because of its effect on aromatic DOM as indicated by high S_R values at the same time (Cory et al., 2010; Para et al., 2010; Chen et al., 2011). The variability in the HIX between January and March 2019 in the estuary, could be due to the increased river flow which would increase the transport of highly humified DOM into the estuary.

With regard to biological processes, BIX, FI and peak T to peak C in Figure 4.24 C, D and E, respectively, agree with the other variables in Figure 4.24. Overall, both BIX and peak T to peak C displayed higher values for the estuary than the rivers, although the River Yare showed similar BIX values to the estuary for most months with an average of 0.69 for the Waveney, 0.75 for the Yare and 0.85 for the estuary. As indicated by BIX, there was a clear increase in freshly produced DOM between April and October 2019 in the Yare, and a slight increase in the same period for the Waveney. Note that BIX values > 0.7 indicate the dominance of fresh DOM, whilst values > 1 correspond to only fresh DOM. The increase in DOM production was also observed for the estuary, in particular the peak in BIX in July. Peak T to peak C displayed the same increase between April and October for the estuary. Overall, the trend for this peak T to peak C ratio is consistent with the BIX, showing higher values for the estuary, followed by the Yare and the Waveney (averages 0.26, 0.13 and 0.09, respectively). As discussed in section 3.2.4 (Chapter 3), low values of this peak T to peak C ratio indicate more aromatic DOM, whilst values over 0.3 indicate fresher DOM, so whilst both upstream values showed a prevalence of terrestrial DOM, the estuary showed a mix of terrestrial and fresh DOM.

Figure 4.24D shows higher FI values for the Yare and lower values for the estuary and the Waveney. The average FI value for the Yare was 1.68, followed by 1.61 for the estuary and 1.60 for the Waveney. This index reflects the C : N ratio in DOM (see section 3.1.2 of Chapter 3) and the high values reported for the River Yare between April and October agreed with the timeseries of TDN in Figure 4.22. The FI values for all the sampling points suggest a mix of terrestrial and *in-situ* produced DOM, although the higher FI values for the River Yare highlight the prevalence of the freshly produced DOM between April and October for the most upstream sampling point. Note that the low FI values for the estuary

could be an effect of photodegradation since exposure to solar radiation has been found to reduce FI (Hansen et al., 2016). This is confirmed by the S_R values previously discussed.

4.2.5 Seasonal changes in DOM in the River Waveney, the River Yare and the estuary

This section discusses differences in DOM composition and processes during the meteorological seasons autumn, winter, spring and summer as defined by Trenberth (1983), where autumn goes from September to November, winter from December to February, spring from March to May and summer from June to August.

- Seasonality of DOC, nitrate plus nitrite, DON, phosphate and DOP

As expected, DOC represented the largest proportion of DOM compared to DON and DOP (Hao et al., 2017) (Figures 4.25, 4.26 and 4.27). In Figure 4.26, DON in the estuary displayed concentrations almost as high as DOC during winter for the upper interquartile range, although the median was much lower than that of DOC. The two rivers had a similar median for DOC in all seasons (Figure 4.25). DOC is mostly influenced by surface runoff transporting DOM rich in carbon into the river and/or by *in-situ* production (Markager et al., 2011; Graeber et al., 2012; Bittar et al., 2016), therefore DOC increases would be expected during autumn and winter because of the increase in river discharge and during spring and summer because of the rise in biological production, resulting in the lack of seasonality in DOC both in the River Waveney and the River Yare. Conversely, DOC concentrations in the estuary showed some differences with lower concentrations in autumn and summer and higher concentrations in spring, although the median was the same. During winter there was an increase in DOC concentration in the estuary with a higher median (Figure 4.25). Whilst the increase in winter could be linked to the higher surface runoff, the lower concentrations in spring and summer could be a result of *in-situ* photo- or biodegradation (Opsahl and Benner, 1998; Stedmon and Cory, 2014; Bittar et al., 2015).

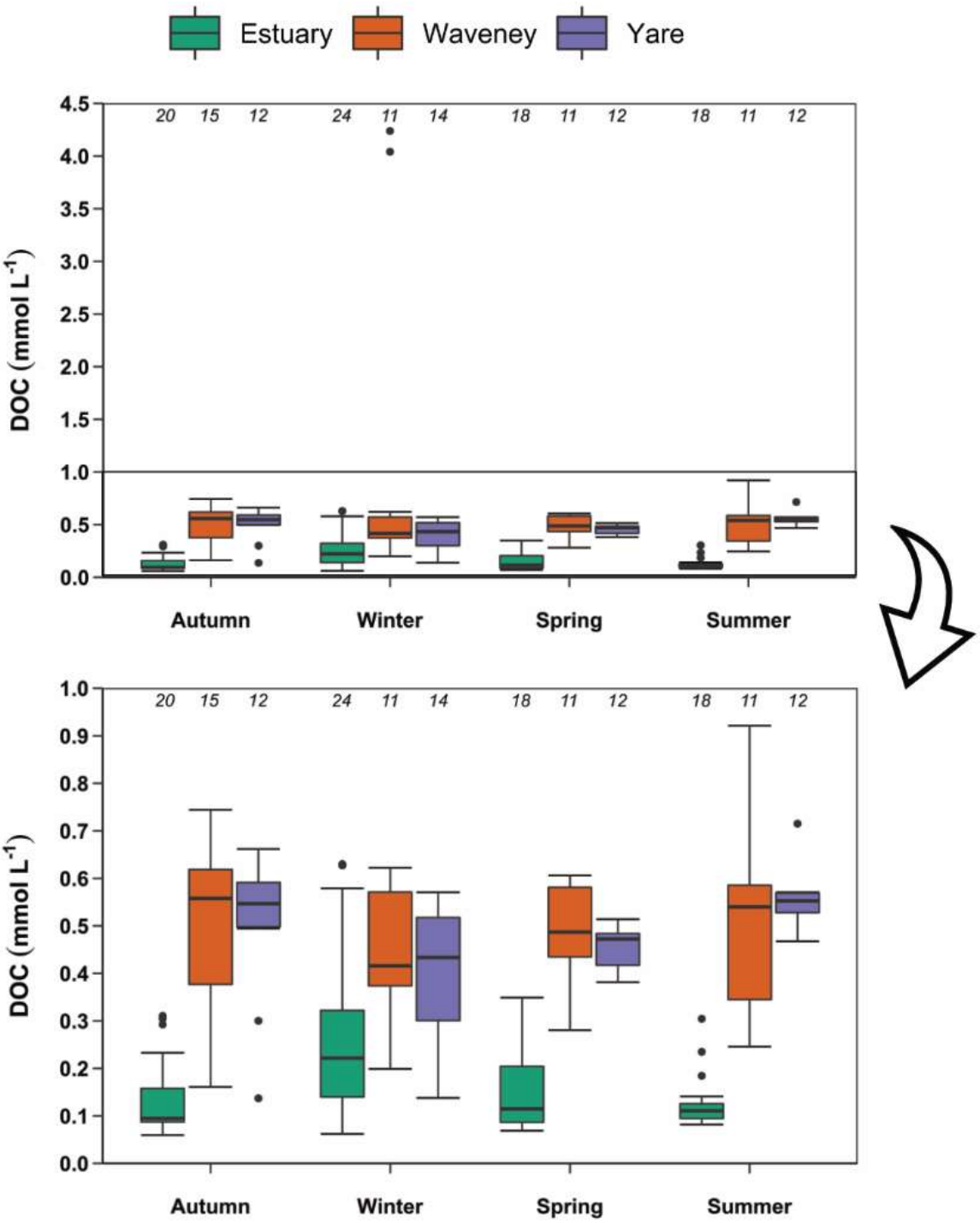

Figure 4.25. *Boxplot of DOC for the River Waveney, the River Yare and the estuary separated into seasons (autumn, winter, spring and summer) for the sampling period between November 2018 and December 2019 for all the sampling stations in the Yare and in the Waveney and the three stations in the estuary (top plot contains all data, whilst bottom is a zoom of the top plot). The bars represent the interquartile range with the horizontal line being the median (50th percentile). Below the median is the 25th percentile and above is the 75th percentile. The error bars on top represent the largest value within 1.5 times the range above the 75th percentile, whist the ones below represent the smallest value within 1.5 times the range below the 25th percentile. The black dots represent values that are > 1.5 times and < 3 times the interquartile range beyond either end of the bars. The numbers at the top of the plot are the number of samples used to create the boxplot.*

Nitrate plus nitrite displayed strong changes in seasons for both rivers and the estuary with similar median concentrations for nitrate plus nitrite between the two rivers in winter and spring. The River Yare showed higher DON median concentrations than the River Waveney and the estuary, with the latter displaying concentrations between 0.001 and 0.295 mmol L^{-1} for nitrate plus nitrite and between 0.001 and 0.356 mmol L^{-1} for DON with great variability in winter (Figure 4.26). Whilst nitrate plus nitrite made up most of TDN (as reported in the previous section) which is typical of agricultural and urban catchments (Rothwell et al., 2010; Jickells et al., 2014; Yates et al., 2019; Panton et al., 2020), concentrations of DON had averages of 0.21, 0.14 and 0.04 mmol L^{-1} for the River Yare, the River Waveney and the estuary, respectively. In general, both nitrate plus nitrite and DON showed the same trends with respect to seasons for the rivers and the estuary. Concentrations were higher in winter and spring and lower in autumn and summer, except for DON in the Waveney in winter where the median was similar to the autumn, although the variability was greater. As inorganic and organic nitrogen concentrations in rivers are determined by both biotic and abiotic processes, the seasonal trends reported here could be a product of both. Nitrate plus nitrite concentrations in autumn and winter could be due to increased concentrations of inorganic nitrogen leaching through the soil (Jickells et al., 2000; 2014; Cooper et al., 2020). In addition, the higher concentrations in winter are a result of nitrate plus nitrite and DON transported into the rivers and the estuary through overland flows which are greater in this season due to lower evapotranspiration (section 4.2.3 of this Chapter) (Dixon et al., 2014; Yates et al., 2019). DON is also produced and consumed by autotrophs and heterotrophic bacteria, contributing to the decrease in spring and summer (Bronk et al., 1998; Sipler and Bronk, 2015), although its relatively high concentrations could be due to inputs from water treatment plants and septic tanks (Yates et al., 2016; 2019).

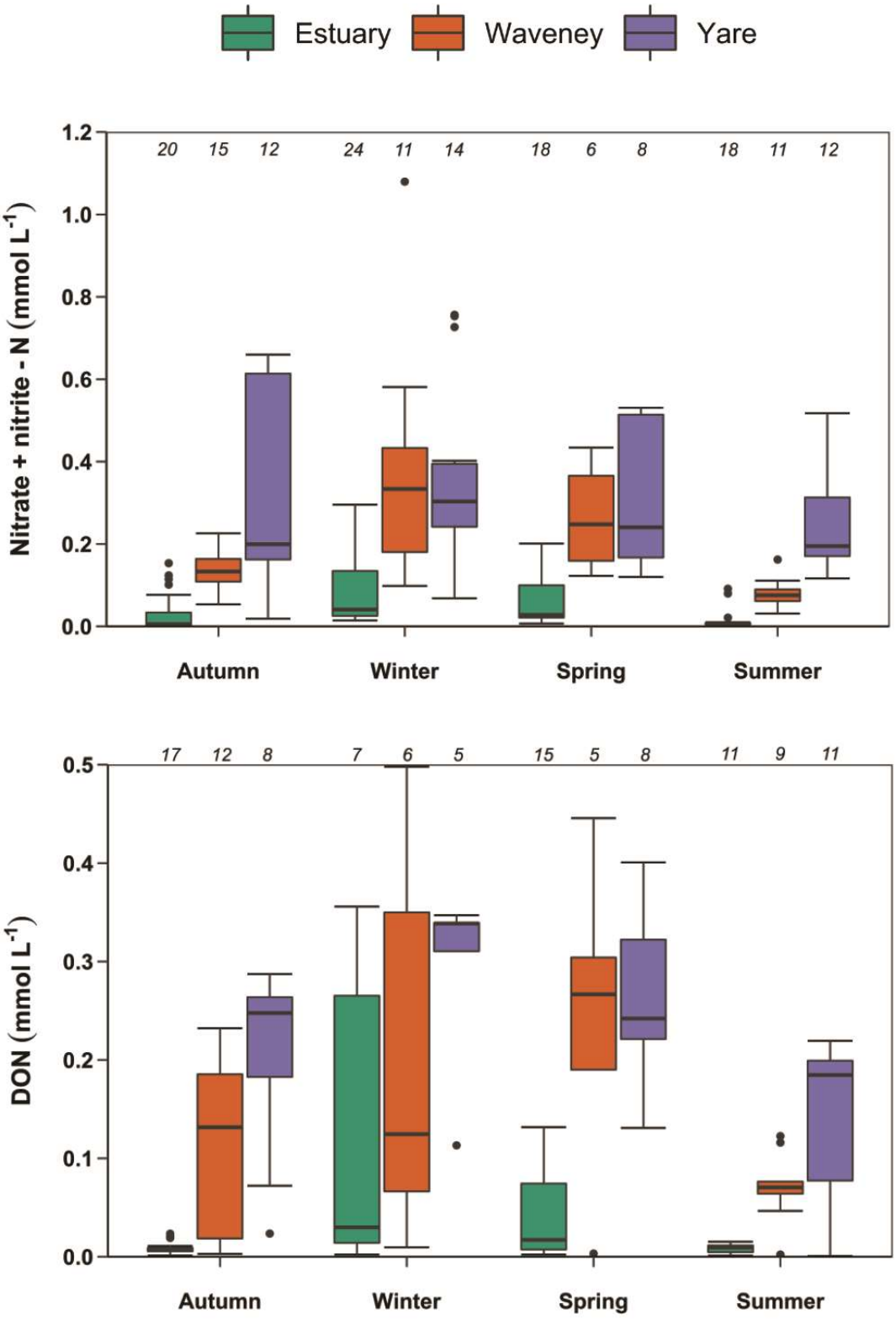

Figure 4.26. *Boxplot of nitrate plus nitrite and DON for the River Waveney, the River Yare and the estuary separated into seasons (autumn, winter, spring and summer) for the sampling period between November 2018 and December 2019 for all the sampling stations in the Yare and in the Waveney and the three stations in the estuary. See Figure 4.21 for an explanation of the boxplots.*

Phosphate had higher concentrations in the two rivers during autumn and summer and lower during winter and spring, whilst the concentrations in the estuary varied little between the seasons with slightly lower values in autumn and summer (Figure 4.27). This pattern in the two rivers has been reported also by Cooper et al. (2020) for the River Wensum (a tributary of the River Yare) where it was linked to the remineralisation of DOP by the microbial community and to the release of phosphate from septic tanks especially when the river flow is low in the summer months, although for these two rivers input from water treatment plants would be more important (see Figure 2.2 in Chapter 2). The lower concentrations in the rivers in winter could indicate phosphate sorption to sediments which has been reported to be a sink for phosphorus in rivers and estuaries by Statham (2012) and Withers and Jarvie (2008), whilst the lower concentrations in spring could be linked to the use of phosphate by primary producers and bacteria (Withers and Jarvie, 2008). For the estuary, phosphate concentrations did not show any marked seasonality, but the median displayed slightly lower concentrations in summer and autumn, probably linked to its uptake by microbes as well as absorption to the sediments.

DOP did not show any clear seasonality except for the estuary which displayed the highest DOP concentrations in spring and summer (Figure 4.27). DOP formed 68% of TDP in the estuary and the high concentrations would suggest DOP produced by primary producers and bacteria (which would explain the lower concentrations of phosphate) but also from water treatment plants (Monbet et al., 2009). The River Waveney had the highest median concentration throughout the year compared to the Yare, except for winter, where the median of the Yare was higher than the Waveney (2.77 and 1.65 µmol L^{-1}, respectively). DOP formed 32% of TDP in the Yare and 35% of TDP in the Waveney and the lack of clear seasonality could indicate continuous input of DOP from wastewater, overland flow, sediment resuspension and biological production throughout the year (Withers and Jarvie, 2008; Monbet et al., 2009; Statham, 2012; Cooper et al., 2020).

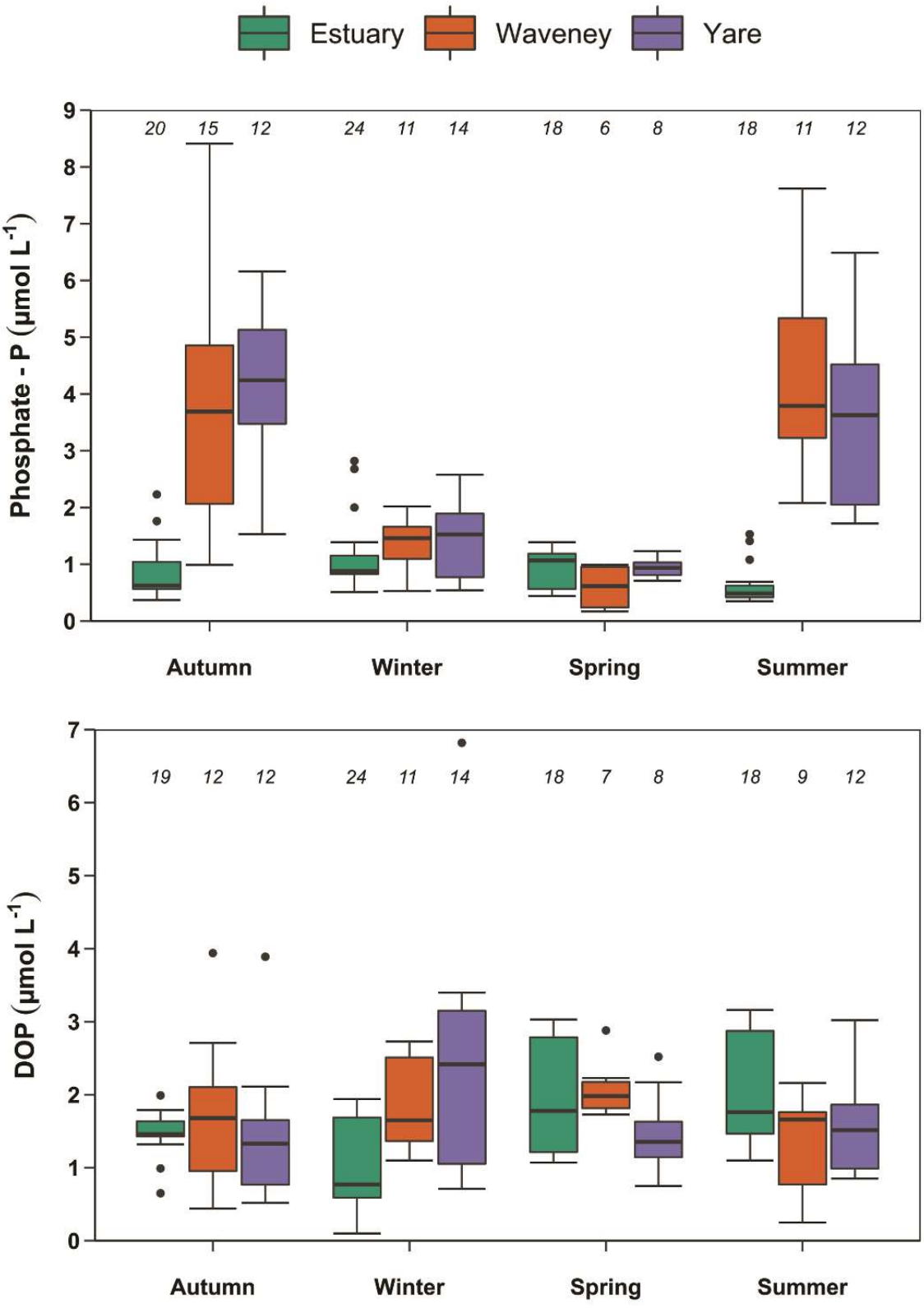

Figure 4.27. *Boxplot of phosphate and DOP for the River Waveney, the River Yare and the estuary separated into seasons (autumn, winter, spring and summer) for the sampling period between November 2018 and December 2019 for all the sampling stations in the Yare and in the Waveney and the three stations in the estuary. See Figure 4.21 for an explanation of the boxplots.*

- Seasonality of the fluorescent components identified through the PARAFAC model

In regard to the composition of DOM during the seasons, the relative contribution of each of the six components identified through the PARAFAC analysis gives an insight into the importance of various processes in any season. Focussing first on the components indicative of *in-situ* biological processes, C3 and more importantly C6, Figure 4.28 and Figure 4.29 show that the fraction of C3 did not show much change throughout the seasons, increasing slightly during spring and summer. As C3 is linked to microbial processing of DOM, these results could indicate that remineralisation of DOM by the microbial community in rivers and estuaries, was not greatly affected by the change in river flow, water temperature or solar radiation and that bacterial activity was not impacted by seasonal changes, as reported in a review by del Giorgio and Cole (1998).

Conversely, C6 displayed seasonal changes, with low values in autumn and winter and high values in spring and summer. The River Yare showed the highest contributions of C6 throughout the year, except for autumn where the estuary had the highest contribution. The River Waveney had the lowest percentages for C6. The contribution of C6 in winter showed similar low values across all locations, whilst in general, higher values were found in spring and summer. These results suggest an increase in primary production in spring and summer which is partly reflected in the concentrations of chlorophyll-*a* shown in Figure 4.30. The results for chlorophyll-*a* display elevated concentrations in spring (especially for the River Waveney) and slightly elevated values in summer. Concentrations were highest in the River Waveney in all the seasons, followed by the River Yare and lastly the estuary. Although C6 is indicative of biological production of DOM, it does not indicate solely production by autotrophs, hence it is perhaps not surprising that chlorophyll-*a* only partially reflected the seasonality observed in Figures 4.27 and 4.28. As reported in Fox et al. (2017, 2021) C6 is also a product of heterotrophic bacteria, found predominantly inside bacterial cells and it is strongly linked to microbial metabolism. The seasonality of C6 in all sampling locations is therefore associated with increased activity of both autotrophic and heterotrophic organisms.

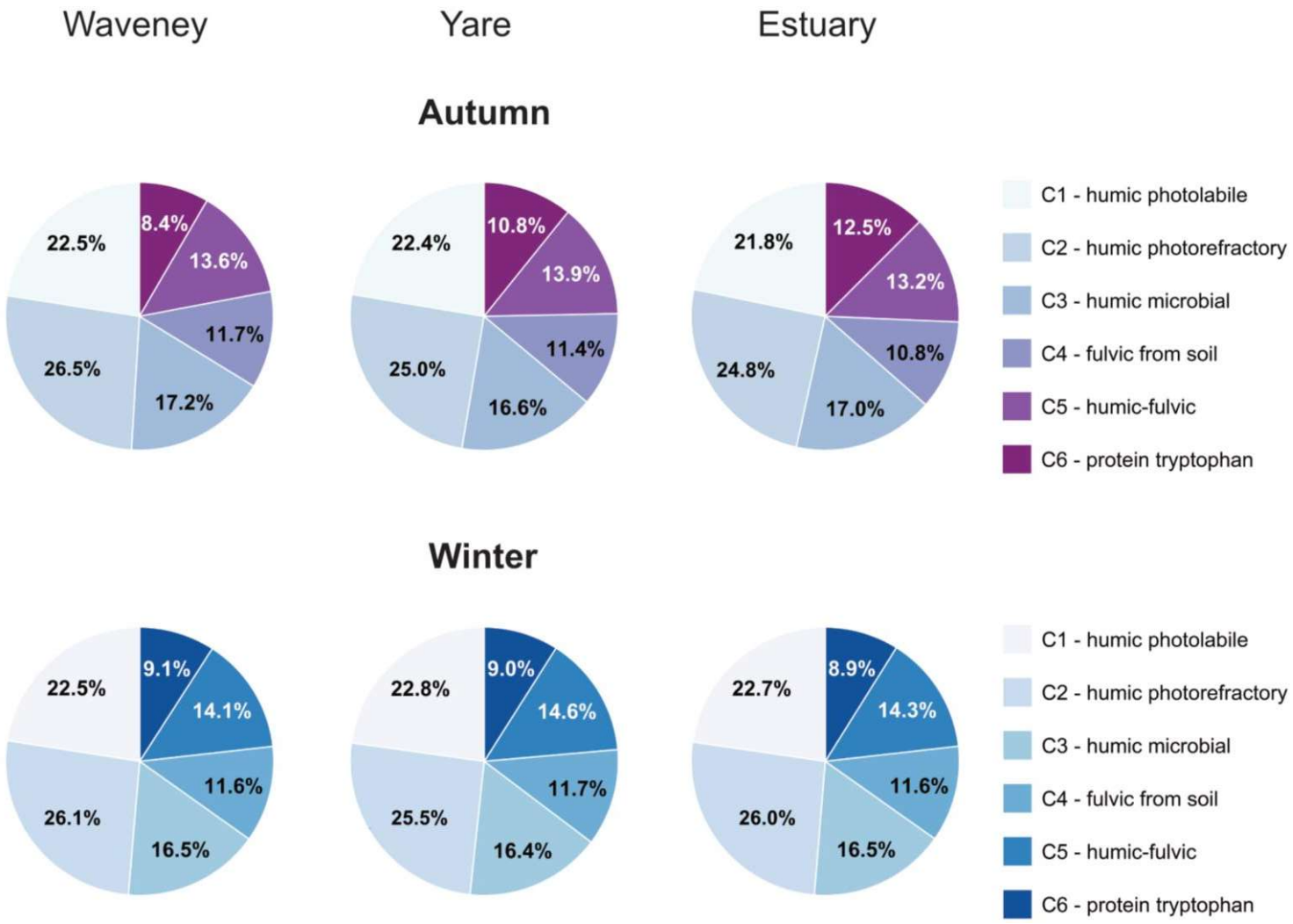

Figure 4.28. *Pie charts of the relative contribution of the six components identified through the PARAFAC analysis for the River Waveney, the River Yare and the estuary divided by autumn and winter for the sampling period between November 2018 and December 2019.*

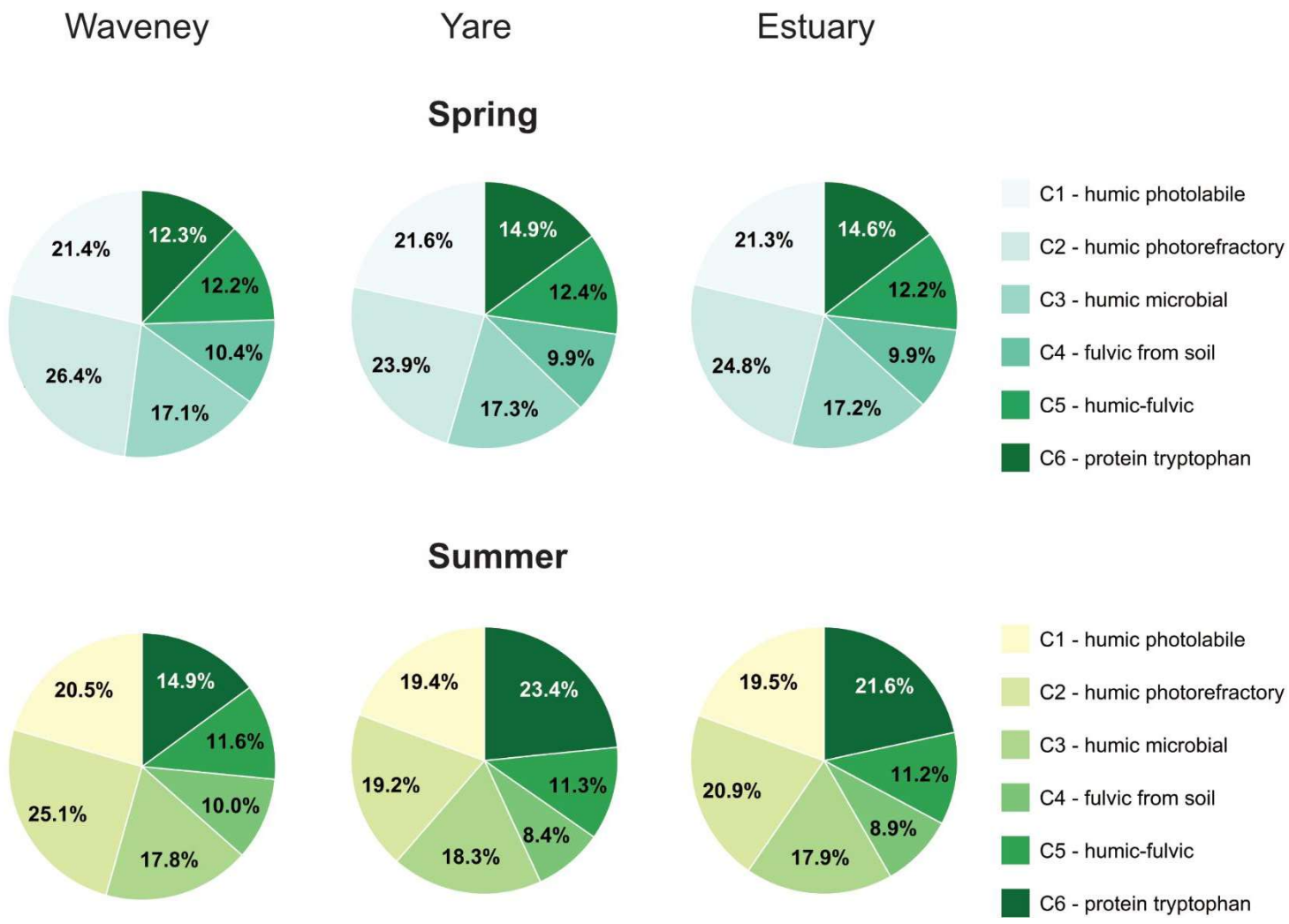

Figure 4.29. *Pie charts of the relative contribution of the six components identified through the PARAFAC analysis for the River Waveney, the River Yare and the estuary divided by spring and summer for the sampling period between November 2018 and December 2019.*

With regards to the other components C1, C2, C4 and C5, considered linked to terrestrial DOM, there were no clear seasonal changes, apart from a slight decrease of the proportion of C5 in spring and summer for the River Yare and the estuary. As this component was linked to fulvic acids originating from soils it is possible that the combination of low river flow and less precipitation in spring and summer decreased the contribution of fulvic acids to DOM. The lack of seasonal changes for the other terrestrial components reflects the large proportion of DOM originating from terrestrial sources in these rivers throughout the year, which is also evident in the estuary.

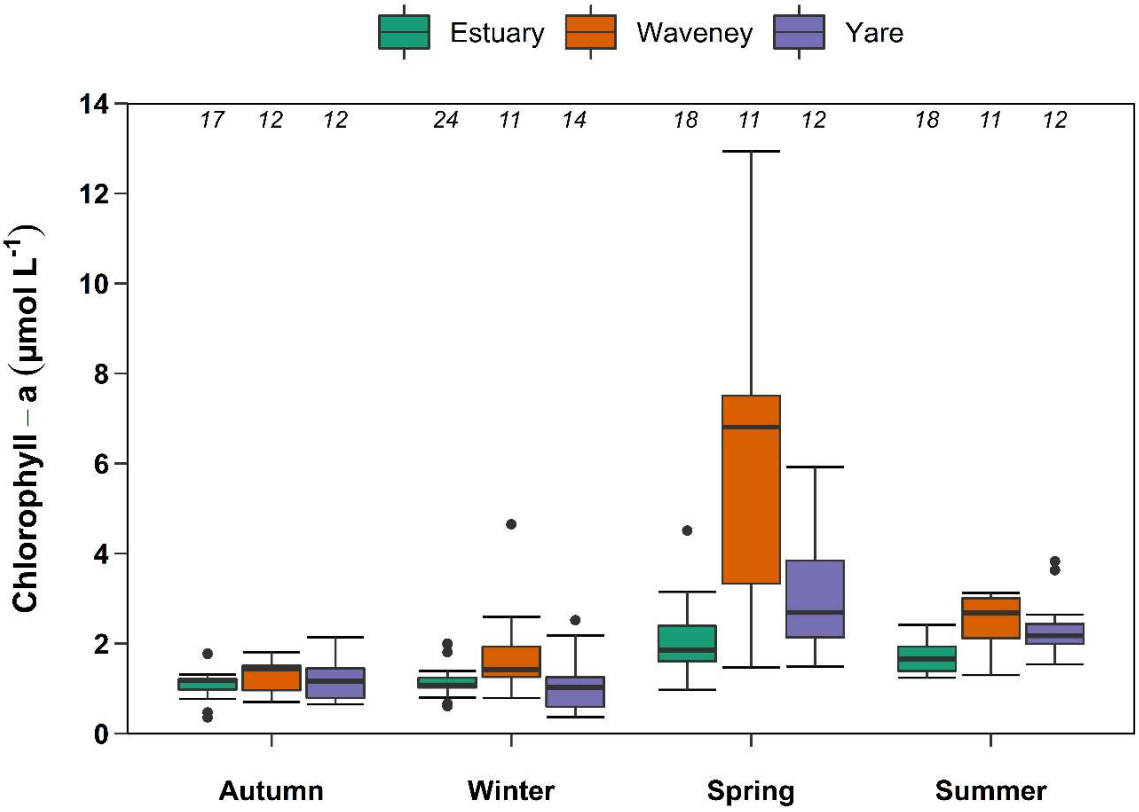

Figure 4.30. *Boxplot of chlorophyll-a for the River Waveney, the River Yare and the estuary separated into seasons (autumn, winter, spring and summer) for the sampling period between November 2018 and December 2019 for all the sampling stations in the Yare and in the Waveney and the three stations in the estuary. See Figure 4.21 for an explanation of the boxplots.*

- Seasonality of $CDOM_{\alpha 254}$, HIX, BIX, peak T to peak C, FI and S_R

Seasonal changes were also studied for $CDOM_{\alpha 254}$, fluorescence indices and S_R (Figures 4.31 and 4.32). Boxplots for $CDOM_{\alpha 254}$ and HIX (Figure 4.31) reflected both the variation reported for DOC (Figure 4.25) and for the humic-like components (Figure 4.28 and Figure 4.29). Both DOC and $CDOM_{\alpha 254}$ values for the estuary were lower than in the rivers, reflecting a decrease by mixing with seawater as well as possibly by photodegradation or biodegradation as DOM was transported downstream. The seasonal

changes in humic acids in DOM are reflected in the HIX (Figure 4.31), with higher values in the rivers during the months characterised by high river flows (autumn and winter) and lower values during the months with low river flows (spring and summer) (Figure 4.14), although HIX values in spring were not as low as in summer (Figure 4.31).

BIX and peak T to peak C in Figure 4.32 did not display strong seasonality except for an increase for the estuary in summer. As reported for the relative contribution of the six components identified through PARAFAC, these rivers and the estuary are characterised by terrestrial DOM throughout the year with an increase in percentages for the *in-situ* biologically produced DOM in spring and especially in summer. These two indices were also in agreement with the $CDOM_{\alpha 254}$ and HIX in Figure 4.31, where lower values for BIX and peak T : C indicated less *in-situ* biologically produced DOM.

FI (Figure 4.32) did not display strong seasonality with only slight increases in spring and summer for the River Waveney, a summertime increase in FI values for the River Yare and a summertime decrease for the estuary. This is compatible with *in-situ* microbial activity throughout the year as shown in Figures 4.32 and 4.29 for C3. As shown for C3 but also for C6, the River Yare and the estuary displayed an important increase in biological activity in spring and especially in summer. The low FI values for the estuary in summer in Figure 4.32 could reflect the effect of photodegradation on FI as explained in section 4.2.3 and confirmed by the high S_R (Figure 4.32). S_R values were high for the estuary suggesting a reduction in DOM molecular weight by photodegradation. The estuary in this study area is a tidal flat where water has a relatively long residence time compared to the rivers which enhances photodegradation of DOM. The S_R values were low in both rivers throughout the seasons, evidence of little photodegradation of DOM in the rivers between November 2018 and December 2019.

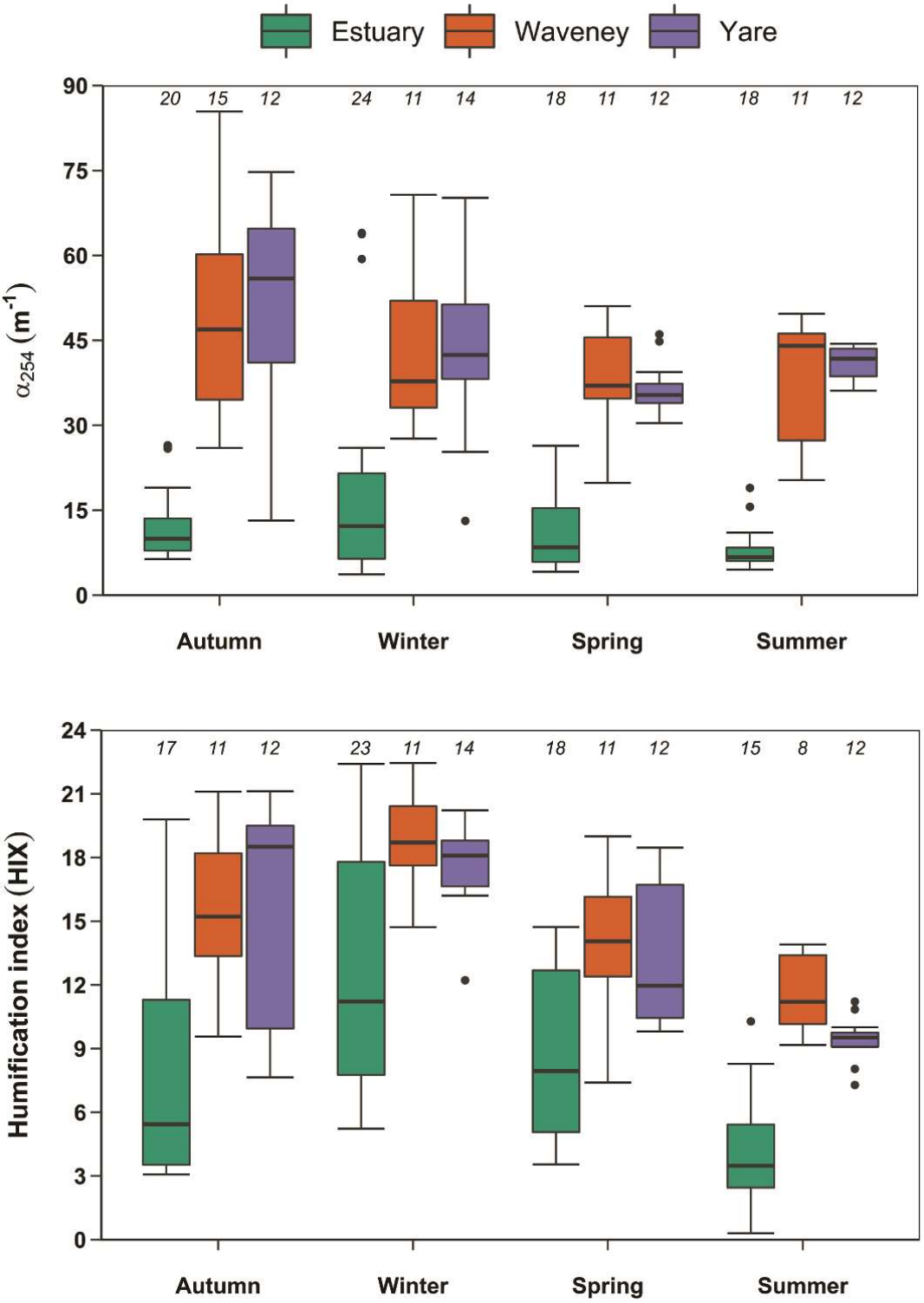

Figure 4.31. *Boxplot of $CDOM_{\alpha 254}$ and HIX for the River Waveney, the River Yare and the estuary separated into seasons (autumn, winter, spring and summer) for the sampling period between November 2018 and December 2019 for all the sampling stations in the Yare and in the Waveney and the three stations in the estuary. See Figure 4.21 for an explanation of the boxplots.*

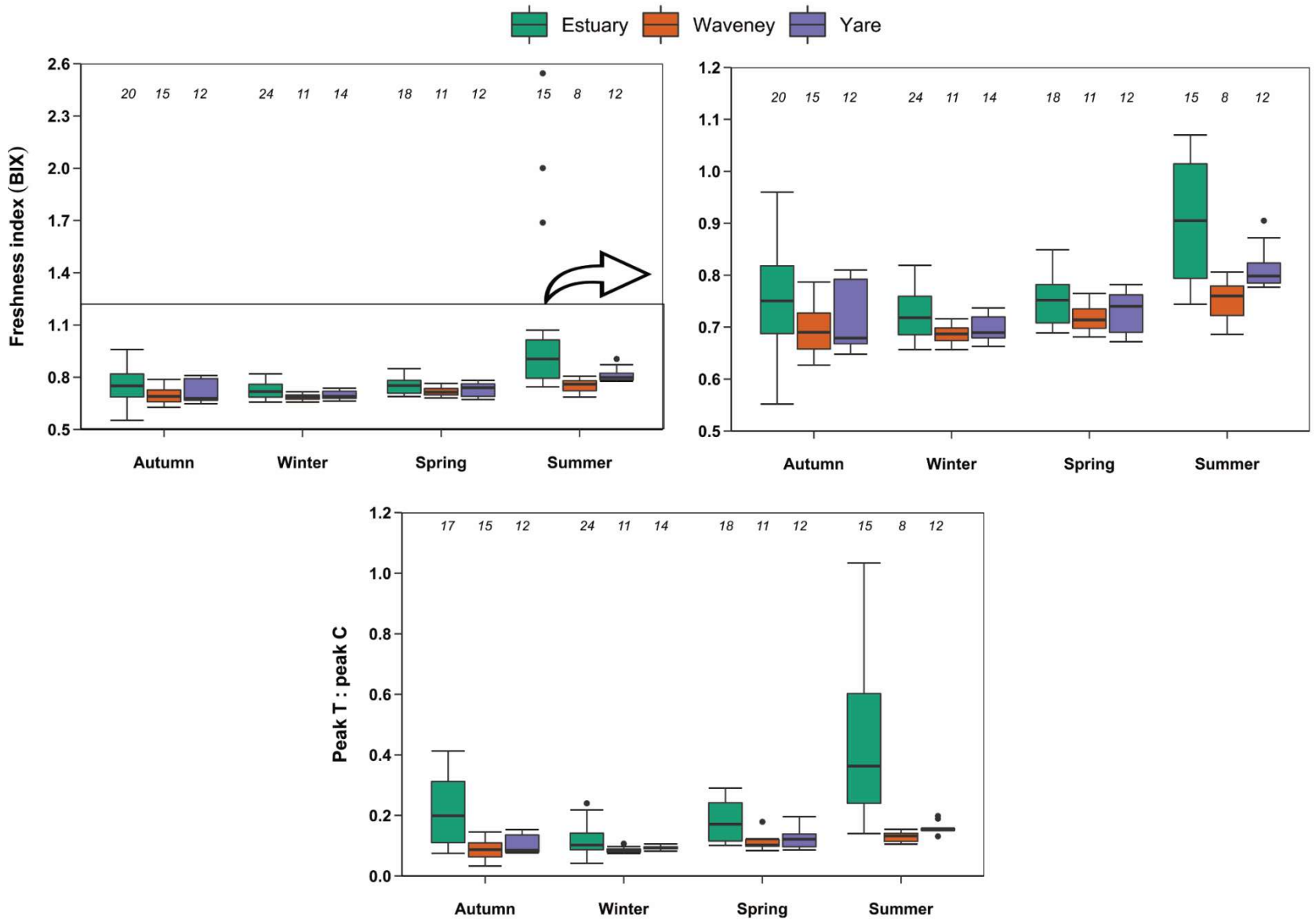
Estuary
Waveney
Yare
Freshness index (BIX)
2.6
2.3
2.0
1.7
1.4
1.1
0.8
0.5
20 15 12 24 11 14 18 11 12 15 8 12
Autumn
Winter
Spring
Summer
1.2
1.1
1.0
0.9
0.8
0.7
0.6
0.5
20 15 12 24 11 14 18 11 12 15 8 12
Autumn
Winter
Spring
Summer
Peak T : peak C
1.2
1.0
0.8
0.6
0.4
0.2
0.0
17 15 12 24 11 14 18 11 12 15 8 12
Autumn
Winter
Spring
Summer

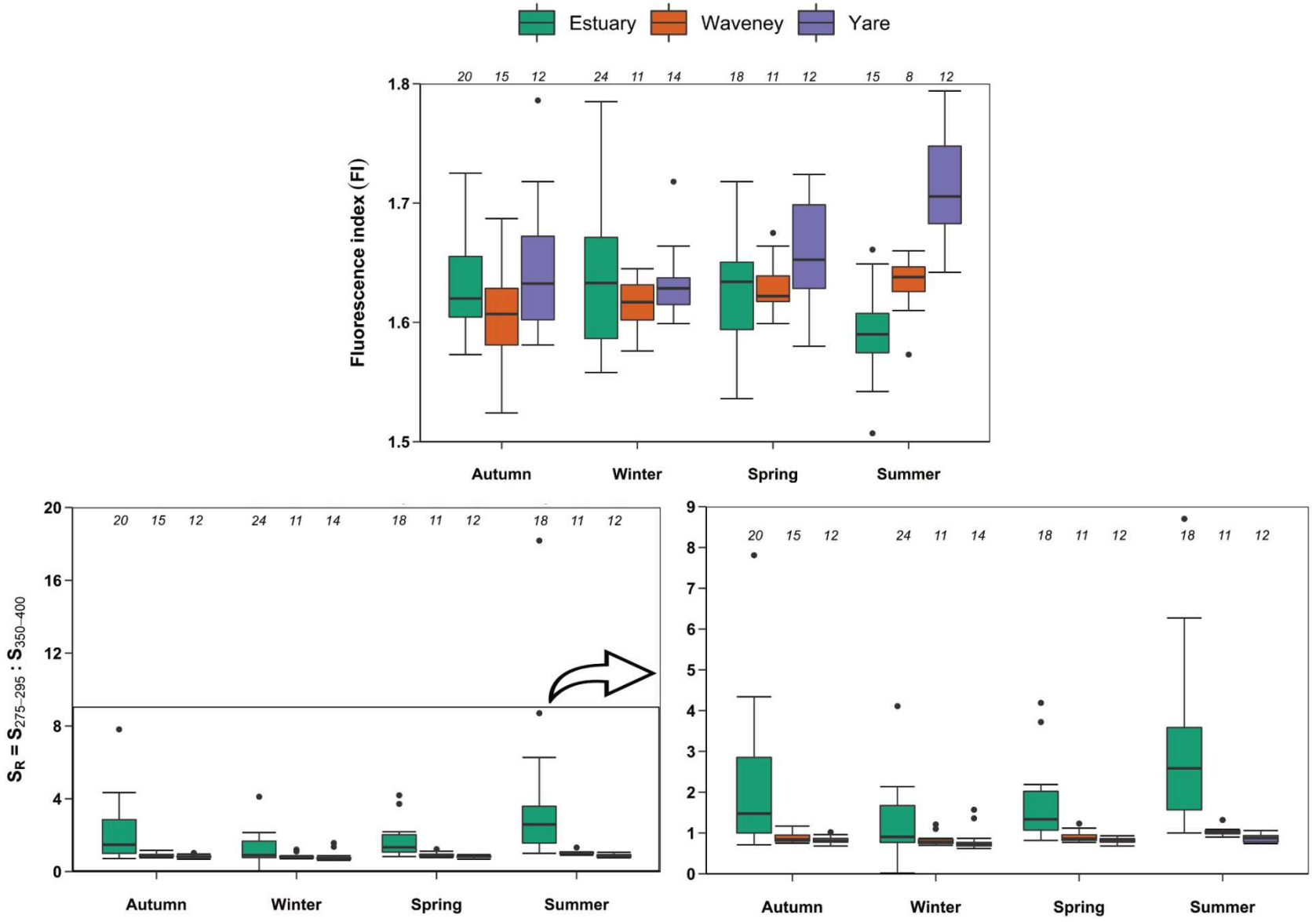
Estuary
Waveney
Yare
Fluorescence index (FI)
1.8
1.7
1.6
1.5
20 15 12 24 11 14 18 11 12 15 8 12
Autumn
Winter
Spring
Summer
$S_R = S_{275-295} : S_{350-400}$
20
16
12
8
4
0
20 15 12 24 11 14 18 11 12 18 11 12
Autumn
Winter
Spring
Summer
9
8
7
6
5
4
3
2
1
0
20 15 12 24 11 14 18 11 12 18 11 12
Autumn
Winter
Spring
Summer

Figure 4.32. *Boxplot of BIX and peak T to peak C, FI and S_R for the River Waveney, the River Yare and the estuary separated into seasons (autumn, winter, spring and summer) for the sampling period between November 2018 and December 2019 for all the sampling stations in the Yare and in the Waveney and the three stations in the estuary. See Figure 4.21 for an explanation of the boxplots.*

4.2.6 DOC dynamics and fluxes across salinity gradients

In order to understand DOC cycling in the River Yare and River Waveney, a calculation of the internal flux of DOC from the most upstream sampling point to the mouth of the rivers is presented. The internal flux is the difference between the flux exported from the estuary and the riverine flux calculated at the most upstream sampling point. The calculation of the DOC internal flux in these two rivers gives insight into the rivers' characteristics and processes and the amount of carbon lost or produced when DOC displays non-conservative behaviour. Figure 4.33 shows the different DOC behaviours when travelling downstream across salinity gradients as also reported by García-Martín et al. (2021).

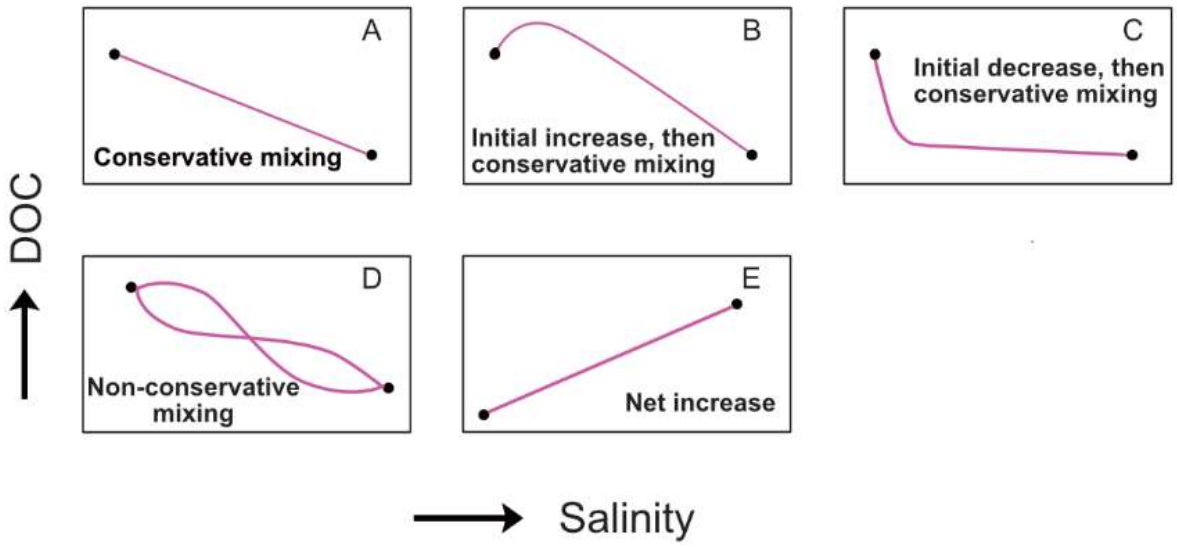

Figure 4.33. *Representation of different DOC distributions as a function of salinity in estuaries after García-Martín et al. (2021).*

When there is conservative mixing (Figure 4.33A), DOC is diluted and no process other than mixing is occurring. In Figure 4.33B DOC is initially produced, but then mixes conservatively as it travels downstream. In Figure 4.33C DOC is initially removed and afterwards behaves conservatively. In Figure 4.33D DOC is both produced and lost, in addition to mixing, resulting in a net decrease when reaching the sea. Lastly, in Figure 4.33E DOC is mixing linearly, and its concentration is higher downstream than upstream. This is only possible when DOC concentration at the estuary is higher than at the freshwater end

member in the river. The distribution of DOC concentration against salinity for my dataset is shown in Figure 4.34 for the River Waveney and in Figure 4.35 for the River Yare, respectively, as a deviation from the theoretical dilution line. This line was derived as the line connecting the DOC concentrations of the most upstream sampling point (freshwater end member) and of the most downstream sampling point (marine end member), as reported in Guo et al. (2007). The DOC distributions versus salinity were calculated by fitting different type of curves through the *Curve Fitting Toolbox*™ in MATLAB (The MathWorks, 2020) for every monthly sampling. The best fits were chosen by examining the statistics for the goodness-of-fit within the same MATLAB toolbox, consisting of a combination of the highest R^2, lowest SSE (Sum of Squares Errors), highest Adjusted R^2, lowest RMSE (Root Mean Squared Error) and the highest degrees of freedom (DF). Curves fitted with a linear regression were indicative of conservative mixing, whilst the other curves indicated other distributions where DOC behaved non conservatively.

Amongst the distributions reported in Figure 4.33, the River Waveney displayed conservative mixing (January, March, May, July, September and October 2019), an initial increase and then conservative mixing in August 2019, a decrease and then conservative mixing (April and November 2019), non-conservative mixing (November 2018, February, June and December 2019) and a net increase in December 2018. The River Yare showed conservative mixing (May and September 2019), an initial decrease and then conservative mixing (August and February 2019), non-conservative mixing (December 2018, January, March, April, June, July, October and November 2019) and a slight net increase in December 2019 (although the salinity range was only 0.4 – 8.7).

In order to verify these results and quantify the loss or gain of DOC in the rivers between the most upstream and downstream sampling location, DOC internal fluxes were calculated following the equation below, developed by Kaul and Froelich (1984) and also reported by Raymond and Bauer (2001).

$$Internal\ flux = Q(C_s - C_0) \qquad \text{equation 4.6}$$

where Q is the river flow in $m^3\ s^{-1}$ calculated for the freshwater sampling point from the value recorded by the nearest gauge upstream of the sampling point, on the sampling day, C_s is the DOC concentration in $\mu mol\ L^{-1}$ when the tangent line of the fitted curve at salinity 32 intercepts the y axis (Kaul and Froelich, 1984), and C_0 is the DOC concentration in $\mu mol\ L^{-1}$ when the fitted curve intercepts the y-axis at salinity 0. For C_s a salinity of 32 was chosen as it was recorded for all sampling days except for the sampling in November (maximum salinity of 29.4) and December 2019 (maximum salinity of 8.7) for the Yare. For these two

sampling days the value was extrapolated from the equation of the fitted curve as reported in García-Martín et al. (2021) for some of the samples in their dataset. The calculated internal flux is zero in case of conservative mixing. The uncertainty of the fluxes for my dataset was calculated from the DOC concentrations analysed during the tidal cycles discussed in Chapter 3 where DOC was determined at one point (per river) over 12 hours sampling during July 2020. The uncertainty was calculated as the range in DOC concentration analysed during the tidal cycles. Only curves with an R^2 above 0.50 were used to determine the input fluxes.

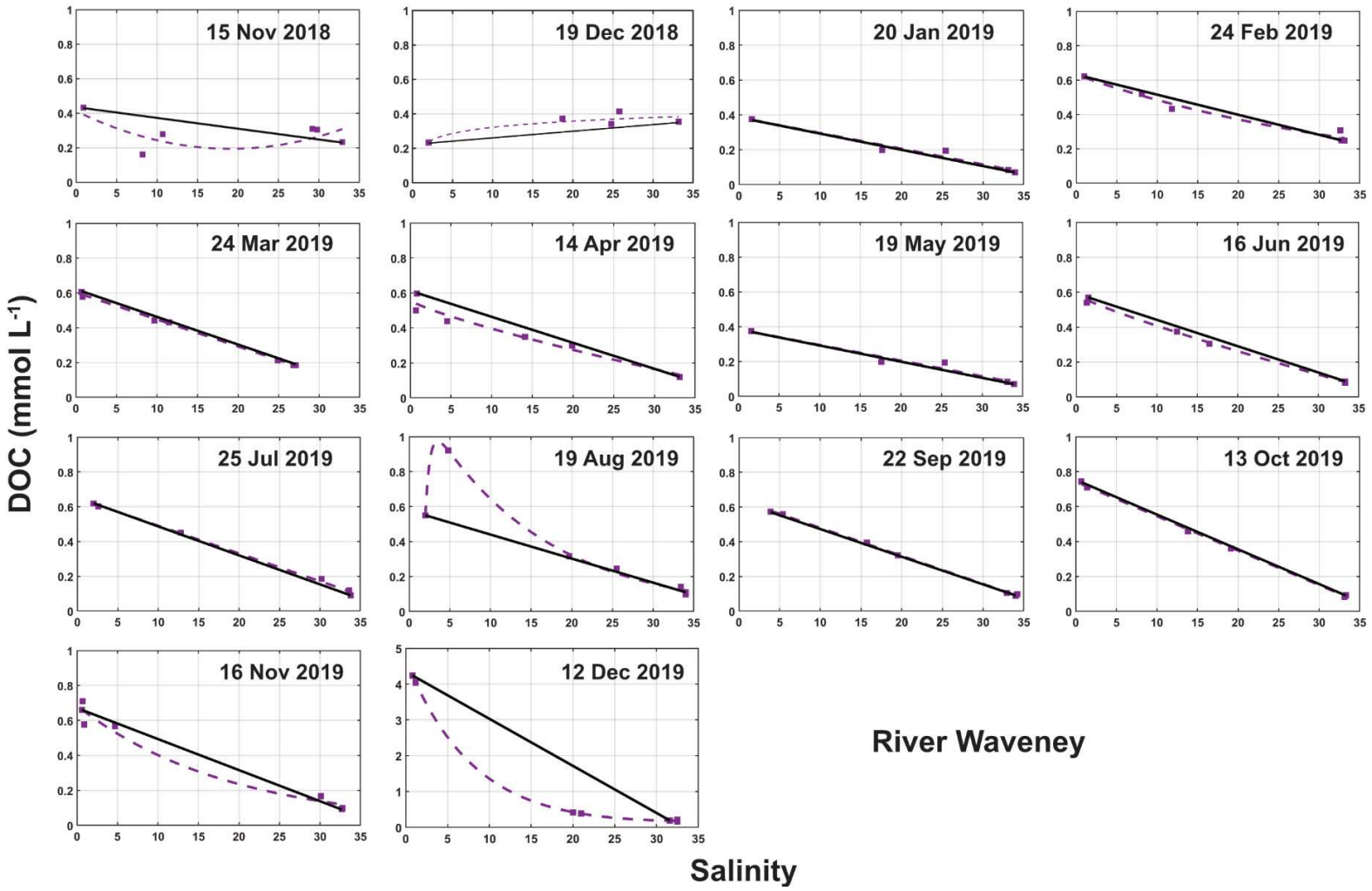

Figure 4.34. *DOC as a function of salinity for the River Waveney between November 2018 and December 2019. Samples are shown as purple squares. The black solid line is the theoretical dilution line between DOC values at the lowest and highest salinity, whilst the dashed line is the polynomial fit between DOC and salinity for all samples.*

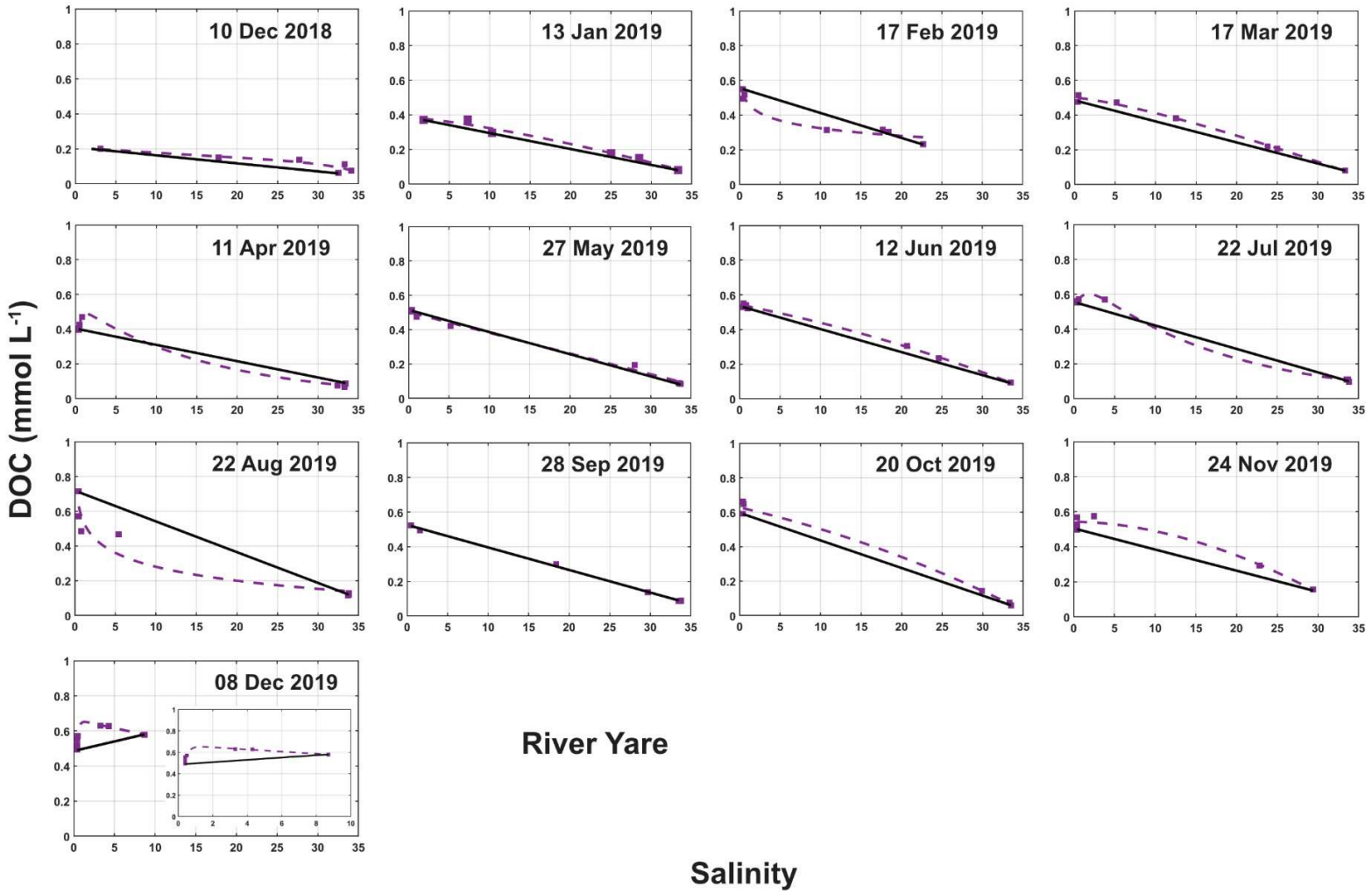

Figure 4.35. *DOC as a function of salinity for the River Yare between November 2018 and December 2019. Samples are shown as purple squares. The black solid line is the theoretical dilution line between DOC values at the lowest and highest salinity, whilst the dashed line is the polynomial fit between DOC and salinity for all samples.*

Table 4.3. *River flow, DOC concentrations and internal net fluxes with their uncertainty for the River Waveney between November 2018 and December 2019. SD is the standard deviation.*

RIVER WAVENEY							
Date	River discharge Q (m^3 s^{-1})	Upstream point DOC (µM)	River mouth DOC (µM)	C_0 (µM)	C_s (µM)	$C_s - C_0$ (µM)	Internal flux (10^3 mol d^{-1})
15 Nov 2018*							
19 Dec 2018	1.9	234.0	354.1	203.1	330.3	127.2	20.9 ± 41.9
20 Jan 2019	1.0	374.9	69.9	385.1	385.1	0	0 ± 22.0
24 Feb 2019	1.3	622.2	249.6	631.2	499.5	-131.7	-14.8 ± 28.6
24 Mar 2019	1.4	606.2	185.8	602.8	602.8	0	0 ± 30.8
14 Apr 2019	0.7	596.5	120.1	558.7	477.9	-80.8	-4.9 ± 15.4
19 May 2019	0.5	582.8	93.2	559.8	559.8	0	0 ± 11.0
16 Jun 2019	1.0	568.5	89.1	587.9	515.6	-72.2	-6.2 ± 22.0
25 Jul 2019	0.5	618.6	90.6	649.8	649.8	0	0 ± 11.0
19 Aug 2019	0.5	548.3	110.6	280.5	4.4e-10	-280.5	-12.1 ± 11.0
22 Sep 2019	0.6	573.4	88.8	641.4	641.4	0	0 ± 13.2
13 Oct 2019	1.1	744.2	91.3	742.7	742.7	0	0 ± 24.2
16 Nov 2019	9.3	660.9	92.6	684.0	336.3	-347.7	-279.4 ± 204.9
12 Dec 2019	5.9	4238.9	188.0	4688.1	287.7	-4400.4	-2243.1 ±130.0
Median	1.0	596.5	93.2	602.8	499.5	0	0 ± 22.0
Average	2.0	843.8	140.3	862.7	463.8	-397.2	-195.3 ± 43.5
SD	2.5	987.7	79.8	114.8	188.7	1162.4	595.8 ± 55.5

*R^2 = 0.39, so it was not included in the influx calculations

Table 4.4. *River flow, DOC concentrations and internal net fluxes with their uncertainty for the River Yare between December 2018 and December 2019. SD is the standard deviation.*

RIVER YARE							
Date	River discharge Q (m^3 s^{-1})	Upstream point DOC (µM)	River mouth DOC (µM)	C_0 (µM)	C_s (µM)	$C_s - C_0$ (µM)	Internal flux (10^3 mol d^{-1})
10 Dec 2018	7.6	200.4	62.0	209.0	359.0	150.0	98.5 ± 85.4
13 Jan 2019	5.9	370.8	81.5	383.9	474.2	90.3	46.1 ± 66.3
17 Feb 2019*	8.4	549.4	232.1	470.9	314.0	-156.9	-113.9 ± 94.3
17 Mar 2019	14.4	476.6	81.6	500.6	616.2	115.6	143.8 ± 161.7
11 Apr 2019	5.3	402.9	86.2	167.7	236.6	68.8	31.5 ± 59.5
27 May 2019	3.1	513.9	85.1	502.0	502.0	0	0 ± 34.8
12 Jun 2019	13.5	529.8	93.8	542.3	676.0	133.7	156.0 ± 151.6
22 Jul 2019	2.8	553.1	98.1	516.7	328.5	-188.2	-45.5 ± 31.4
22 Aug 2019	2.9	715.0	118.7	547.7	261.7	-286.1	-71.7 ± 32.6
28 Sep 2019	3.4	523.5	86.4	525.7	525.7	0	0 ± 38.2
20 Oct 2019	7.6	591.0	59.5	627.7	812.0	184.3	121.0 ± 85.4
24 Nov 2019	7.6	499.0	155.1	542.4	928.6	386.2	253.6 ± 85.4
08 Dec 2019*	19.8	494.4	579.1	640.8	327.9	-312.9	-535.3 ± 222.4
Median	7.6	513.9	86.4	516.7	474.2	68.8	31.5 ± 85.4
Average	7.9	493.8	139.9	475.2	489.4	14.2	6.5 ± 88.4
SD	5.0	116.8	134.2	137.1	208.5	193.5	184.6 ± 55.8

*Values were extrapolated as maximum salinity was < 32

There was a net loss of DOC in the River Waveney with an average loss of 195.3 ± 43.5 x 10^3 mol per day, whilst more DOC was produced in the River Yare with an average increase of 6.5 ± 88.4 x 10^3 mol per day. Note that the Waveney average is influenced by the influx calculated for December 2019 since this was much lower on the other sampling days. If the median flux is considered, then overall DOC mixed conservatively between the freshwater and the marine end members with a value of 0 ± 22.0 x 10^3 mol per day. For the River Yare, if the median is considered DOC was produced with a value of 31.5 ± 85.4 x 10^3 mol per day. These results are interesting, considering that both the average and the median DOC concentration at the most upstream point both sampled and calculated was higher in the Waveney than in the Yare (Tables 4.3 and 4.4). These results agree with the difference in DOM characteristics in the two rivers. As discussed in Chapter 3 and in the previous sections, the River Waveney showed more terrestrial DOM than the River Yare, whilst the latter showed more *in-situ* biological DOM production. This would confirm the production of DOC exceeding the losses of DOC in the Yare. The losses of DOC in the River Waveney could be linked to adsorption to suspended solids and precipitation through flocculation (Raymond and Bauer, 2001) since mean TSS concentrations were significantly higher in the River Waveney than in the River Yare (averages of 63.66 and 25.86 mg L^{-1}, respectively). Another process contributing to losses of DOC in the River Waveney could be photodegradation (Raymond and Bauer, 2001). As previously described, a proxy for photodegradation is S_R which was higher for the River Waveney compared to the River Yare (averages of 0.92 and 0.84, respectively), and for comparison terrestrial values are ~0.7 and estuarine values are ~1.1 (Helms et al., 2008).

Land use in river catchments has been found to affect dissolved organic carbon concentrations and distributions in rivers (García-Martín et al., 2021 and references therein). The land use is similar between the two river catchments (Table 4.5) and therefore it does not appear to explain the differences in the internal fluxes discussed above. In a study on two contrasting lowland catchments, Yates et al. (2016) found that the DOM from a chalk stream (groundwater dominated) had a lower aromatic content and lower molecular weight due to microbial processing both remineralising DOM and producing novel DOM compounds, compared to a surface water dominated stream. In addition, the authors reported that DOM from groundwater could have a less terrestrial signature, therefore affecting the DOM composition in surface water. Although the difference in baseflow index between the River Yare and the River Waveney was not as large as in the study by Yates et al. (2016), nonetheless, the differences in the characteristics of DOM could be a result of the same drivers and could explain the differences between the rivers in my study.

Wastewater discharges could be another source of more reactive DOM in the River Yare. Wastewater DOM rich in nitrogen and phosphorus is readily usable by autotrophs and

heterotrophs and contributes to the production as well as processing of DOM. The River Yare has ~ 0.47 per km^2 of wastewater discharges from water companies, private and industrial sources, whilst the River Waveney has ~ 0.32 per km^2 (Rivers Trust, 2021).

Table 4.5. *Land use in percentages of the catchment areas of the River Yare, the River Waveney and the estuary Breydon Water where the two rivers mix. The land use data are from the Copernicus Land Monitoring Service 2018 (European Environment Agency, EEA).*

Land use	River Yare	River Waveney	Yare + Waveney Estuary
Urban (%)	9.83	7.58	8.94
Quarry (%)	0.23	0.17	0.21
Arable (%)	69.31	75.14	71.62
Pasture (%)	15.70	14.80	15.34
Natural grassland (%)	0.13	0.05	0.10
Woodland (%)	3.66	1.49	2.80
Heathland (%)	0	0.07	0.03
Marshes (%)	0.81	0.40	0.65
Beach (%)	0	0	0
Water (%)	0.33	0.27	0.31
Catchment area (km^2)	1386	912	2298 (1386 + 912)

4.2.7 Riverine and estuarine DOC, TDN, nitrate plus nitrite, TDP and DOP fluxes

The fluxes estimated in Table 4.6 normalised for the area of the catchments were derived as explained in section 4.1.1. They show a loss for DOC, TDN and nitrate plus nitrite from the riverine fluxes of both the River Yare and the River Waveney in the estuary. Only TDP and DOP increased as they travelled through the estuary. As discussed in section 4.2.4, phosphate formed the majority of TDP in both rivers, whilst DOP formed the majority of TDP in the estuary. This could explain the net gain of TDP and in particular DOP, along the estuary. As shown in the correlation matrices in Figures 4.15 – 4.17, DOP and phosphate did not show any correlation for the rivers and for the estuary, which might suggest different processes for these variables. Interestingly, TDN always correlated with nitrate plus nitrite and DON (although some values were not available), possibly implying similar processes or sources. The fluxes calculated for TDN (Table 4.6) were within the estimates by Nedwell et al. (2002) for the same estuary as in my research (Breydon Water), although their values were higher, with 1.0 x 10^5 moles N km^{-2} yr^{-1} compared to 0.27 10^5 moles N km^{-2} yr^{-1} in this study. This was the same for TDP, although they estimated phosphate instead of TDP with values slightly above 1.0 x 10^3 moles P km^{-2} yr^{-1} of phosphate for Breydon Water, compared to 0.27 x 10^3 moles P km^{-2} yr^{-1} of TDP for this study. Note, these values are converted from kg km^{-2} yr^{-1} in Table 4.6.

As discussed previously for the influxes, the area normalised riverine export of DOC is greater for the River Waveney (2.18 ± 0.96 g m^2 yr^{-1}) than for the River Yare (1.00 ± 0.40 g m^2 yr^{-1}) (Table 4.6). This could reflect the difference in DOM composition of the two rivers discussed previously, with DOM in the chalk catchment being less aromatic and river water less rich in carbon (Yates et al., 2016). The fluxes shown in Table 4.6 for DOC were in agreement with other studies for rivers in the UK. Hope et al. (1997) reported values between 0.82 and 1.53 g m^{-2} yr^{-1} for the eastern area of the Anglian region between 1990 and 1993, whilst Tipping et al. (1997) calculated a flux of 3.0 g m^{-2} yr^{-1} for the Ouse catchment, which is close to the 2.18 ± 0.96 g m^{-2} yr^{-1} of the Waveney catchment and well within the 1-10 g m^{-2} yr^{-1} of DOC stated for lowland rivers. The Ouse catchment is also characterised by ~ 95% agricultural land use, somewhat higher than for the rivers in this project (Environment Agency, 2010). A study from Mantoura and Woodward (1983) calculated the DOC flux of the River Severn between 1.7 and 2.8 g m^{-2} yr^{-1}, with a similar land use to the Broadland Catchment with ~ 90% used for agriculture (Environment Agency, 2009). A recent study modelled the DOC yields for the whole of Great Britain (GB) from sampling 36% of its catchments at the freshwater end member (Williamson et al., 2021). Their samples did not include the eastern region of East Anglia, and the riverine export calculated for the River Yare and the River Waveney are well below the average DOC yield

calculated for the rivers in their study which was 5.04 g m^{-2} yr^{-1}. Note the study by Williamson et al. (2021) include catchments with land cover dissimilar to that of the River Yare and the River Waveney and their average might reflect some rivers flowing through peat and forest (high in DOC). Nevertheless, the DOC fluxes calculated for the rivers in my study were in agreement with the DOC yield of their model estimate for the eastern region of East Anglia between 1.0 and 7.5 g m^{-2} yr^{-1}.

Table 4.6. *Annual transport in g m^{-2} yr-1 of carbon for DOC, of nitrogen for TDN and nitrate plus nitrite and of phosphorus for TDP and DOP, calculated for the River Yare, the River Waveney, the River Yare + the River Waveney and the estuary (SEA1) between December 2018 and December 2019.*

	Waveney Riverine export (g m^{-2} yr^{-1})	Yare Riverine export (g m^{-2} yr^{-1})	Waveney + Yare Riverine export (g m^{-2} yr^{-1})	Waveney + Yare + Bure Estuarine export (g m^{-2} yr^{-1})
DOC	2.176 ± 0.957	0.995 ± 0.405	1.464 ± 0.830	0.988 ± 0.560
TDN	0.743 ± 0.166	1.346 ± 0.490	1.107 ± 0.779	0.389 ± 0.274
NO_3 + NO_2	0.479 ± 0.073	0.940 ± 0.380	0.757 ± 0.591	0.285 ± 0.222
TDP	0.010 ± 0.001	0.020 ± 0.005	0.016 ± 0.007	0.039 ± 0.017
DOP	0.005 ± 0.001	0.007 ± 0.003	0.006 ± 0.005	0.025 ± 0.020

In regards to the fluxes entering the shelf sea (estuarine export in Table 4.6), García-Martín et al. (2021) calculated the estuarine DOC export in g m^{-2} yr^{-1} using data from 13 estuaries across GB sampled five times between April 2017 and April 2018. These estuaries did not include any catchment in the East Anglia region, thus the riverine and estuarine DOC exports provided by this study of the River Yare and the River Waveney add value to the dataset of García-Martín et al. (2021) and also to that of Williamson et al. (2021) which included the Great Ouse catchment. The fluxes for DOC reported by García-Martín et al. (2021) were of the same order of magnitude as the fluxes calculated in this study with similar land use both for the riverine and estuarine end member. The Rivers Avon, Clwyd, and Test with comparable land use to the Rivers Waveney and Yare, had estuarine fluxes between 0.88 and 4.29 Gg yr^{-1} whilst the estuarine export calculated from this dataset was 3.20 ± 1.81 Gg yr^{-1} (not area normalised). When comparing the area-specific estuarine DOC export, the flux of 1.0 ± 0.6 g m^{-2} yr^{-1} was in accordance with estimates from the Thames and the Test estuaries (1.1 and 0.9 g m^{-2} yr^{-1}, respectively) which are located in southeast England.

When the export was not normalised by the whole Broadland catchment area, the difference between the DOC fluxes from the River Yare (1.38 ± 0.56 Gg yr^{-1}) and the River Waveney (1.98 ± 0.87 Gg yr^{-1}) and the estuarine export (3.2 ± 1.81 Gg yr^{-1}) was - 0.16 ± 0.38 Gg yr^{-1} of DOC, indicative of a removal from the water column, burial within the river or the estuary, the transformation of DOC to CO_2 through bio- or photodegradation, or all processes combined (Kitidis et al., 2019). Although there is a loss of DOC within the estuary, the estuarine export : riverine export ratio was 0.95, indicating that the DOC distribution in these rivers is mostly conservative, which was in agreement with a study from Abril et al. (2002) that found that DOC in nine rivers across Europe decreased linearly with the increase in salinity most of the time. This is usually explained as conservative mixing, even though it might be a result of opposite processes (sinks and sources) occurring at the same time (Abril et al., 2002).

The fluxes calculated in this project contain large uncertainties, as well as lacking the riverine export from the River Bure which is the other river contributing to the estuarine flux of the study area. Whilst the catchment area of the River Bure has been taken into account for the estimate of the estuarine flux, the difference between the combined riverine export and the estuarine export does not include the riverine flux from this river, adding uncertainty to the estimates. In addition, samples were collected once a month and it was assumed that the concentrations were the same for 30 days. More importantly, these are tidal rivers receiving seawater intrusion twice a day, affecting DOM behaviour as it travels downstream but also the estuarine efflux. In these estimates the contributing seawater flow was not included.

Nevertheless, if the export from the rivers in this study is compared to the net organic carbon budget of the English Channel estimated by Thomas et al. (2005) which is 0.02 x 10^{12} mol C yr^{-1}, it represents 1.33%, although their calculation comprises POC in addition to DOC. Alternatively, the estuarine export from these rivers is 0.30% of the DOC plus POC riverine input of the North Sea (Thomas et al., 2005), and 0.01% of the DOC plus POC riverine input range of the northwest European shelf calculated by Legge et al. (2020). Furthermore, the estuarine export calculated for these two East Anglian rivers represents 0.12% of the estimated post-estuary DOC flux of 2.6 Tg yr^{-1} for the northwest European shelf by Kitidis et al. (2019).

In terms of processes, as previously mentioned, DOC could be produced and remineralised at the same time, especially with high nutrient inputs, a characteristic of catchments that have land use similar to the catchments in this study. The smaller flux of both TDN and nitrate plus nitrite in the estuary compared to the rivers could be due to remineralisation or photodegradation, whilst the increases in TDP and DOP between the rivers and the estuary, could be due to input from wastewater discharges which usually

have a lower N : P ratio, whilst the N : P ratio is usually higher when derived from agriculture (Nedwell et al., 2002; Cooper et al., 2022). Furthermore, Nedwell et al. (2002) state that freshwaters are limited in phosphorus, therefore any additional input would fuel both the autotrophic and heterotrophic communities. As phosphorus tends to be adsorbed to suspended solids (as explained in Chapter 3 section 3.2.3), an increase in TDP by resuspension of solids in the estuarine zone, would also contribute to decrease the P limitation and could further explain the increase in DOP in the estuarine zone.

4.2.8 Fluorescence-based estimate of fluxes of terrestrial DOM and of DOM produced *in-situ*

This section presents the estuarine fluxes differentiated into the six components identified by the PARAFAC analysis to quantify the composition of DOM entering into the North Sea from the rivers in this study. For this purpose, it was assumed that fluorescent DOM reflects the entire DOM pool. Fluorescent DOM is only a fraction of CDOM, and CDOM itself is a fraction of DOM (Stedmon and Cory, 2014), hence the assumption for the calculations. The fluxes of each fluorescent component were determined by assuming that the fluorescence intensities for all the variables were the same for ~ 15 days before and after the sampling day, as discussed in section 4.1.1 for the calculation of the other fluxes. The uncertainty was determined as the range of DOC, TDN and TDP concentration analysed during the tidal cycles discussed in Chapter 3.

DOM entering the shelf sea is mostly terrestrial as four of the six fluorescent components identified through the PARAFAC analysis were of terrestrial origin (C1, C2, C4 and C5), with C4 associated with soils and C5 linked to soils to some extent. C3 in this study was produced microbially, and it is often a product of bacterial degradation of DOM, whilst C6 is a clear indication of elevated biological activity (Stedmon and Cory, 2014). The percentage of all the terrestrial components was higher in autumn and winter when the river flow is higher than spring and summer (Table 4.7). Components C4 and C5 (linked to soils) had a minor contribution to the estuarine flux in comparison to the rest of the components with 0.15 ± 0.09 g m^2 yr^{-1} and 0.17 ± 0.10 g m^2 yr^{-1}, respectively. The component indicative of microbial degradation of DOM was slightly higher in winter, with similar percentages for spring, summer and autumn (Table 4.7), suggesting bacterial activity throughout the year as discussed in section 4.2.4. Not surprisingly, C6 which is produced *in-situ*, had the highest percentage in summer, representing 44.6% of the DOM pool, whilst it had the lowest percentage in winter with 12.7%. Overall, DOM exported into the shelf sea from the Broadland catchment consists of 67.5% of material of terrestrial origin and 32.5% of material

produced and processed *in-situ*, with 3.09 ± 1.87 Gg yr^{-1} and 1.49 ± 0.90 Gg yr^{-1}, respectively.

Table 4.7. *Relative seasonal contribution of the six fluorescent components identified through the PARAFAC analysis for the estuary, and the total estuarine export in g m^{-2} yr^{-1} for each component between December 2018 and December 2019.*

Components	Winter %	Spring %	Summer %	Autumn %	Whole year g m^2 yr^{-1}	Whole year Gg yr^{-1}
C1	21.13	18.16	11.05	23.59	0.29 ± 0.17	0.93 ± 0.56
C2	26.23	24.71	15.85	19.69	0.34 ± 0.20	1.11 ± 0.67
C3	15.95	13.93	12.53	14.00	0.22 ± 0.13	0.70 ± 0.42
C4	10.98	10.39	8.20	10.71	0.15 ± 0.09	0.49 ± 0.30
C5	12.99	10.37	7.77	12.24	0.17 ± 0.10	0.56 ± 0.34
C6	12.72	22.43	44.59	19.77	0.25 ± 0.15	0.79 ± 0.48
Catchment area 3237 km^2 (River Waveney + River Yare + River Bure)						

4.3 Conclusions

This section summarises the results discussed in the previous sections, addressing the questions posed at the beginning of the chapter.

a) Is there a difference in DOM composition between the two rivers?

The PCA results highlighted a difference in DOM composition between the two rivers, with the River Waveney showing a more terrestrial signature, whilst the River Yare is more characterised by DOM produced *in-situ*. This difference was also found in Chapter 3. This difference is not attributable to dissimilarity in land use as the two rivers have both a high proportion of arable land and pasture (69.3% and 15.7% for the Yare and 75.1% and 14.8% for the Waveney, respectively). Alternatively, the two rivers have different bedrock geology, affecting the surface permeability and the hydrological connectivity between groundwater and surface water. The higher permeability of the River Yare, compared to the River Waveney more influenced by surface runoff, could be the reason for their difference in DOM composition. In addition, the higher number of wastewater discharges in the River Yare could be another contributing factor.

b) Is there a seasonal change in DOM composition and concentration?

c) How does DOM change with salinity, between the rivers and the estuary?

The PCA suggested a seasonality in DOM composition and as expected more DOM produced *in-situ* in spring and summer (correlated to high solar radiation in these months) and less in autumn and winter. Concentrations of DOC, TDN, TDP, nitrate plus nitrite and phosphate, as well as fluorescence intensity of the six components (identified through PARAFAC), were lower in the estuary than in the rivers throughout the year. The River Waveney had higher DOC concentrations than the River Yare, whilst the latter displayed higher TDN than the River Waveney. As expected in river catchments with mostly agriculture land use, the inorganic nutrients, nitrate plus nitrite and phosphate formed most of TDN and TDP in both rivers, respectively. Nitrate plus nitrite was the majority of TDN in the estuary as well, whilst DOP was the dominant form of TDP. The fluorescence intensity of the terrestrial components (C1, C2, C4 and C5) plus that of the microbially produced component C3, were higher in the River Waveney than in the Yare, except for C6 (freshly produced *in-situ* DOM) which was higher in the River Yare.

DOC concentrations did not display a clear seasonality in the rivers, whilst the estuary showed a clear increase in winter and some variability in autumn and summer. Concentrations in both rivers and the estuary were higher in winter and spring than in

autumn and summer for DON and nitrate plus nitrite. Phosphate showed opposite seasonality, with higher concentrations in autumn and summer than in winter and spring in the rivers, whilst the estuary had no clear seasonality. DOP did not display any change throughout the year in the rivers, but it had the highest concentrations in the estuary during spring and summer. The fraction of terrestrial DOM fluorescent components (C1, C2, C4 and C5) and component C3 did not change much throughout the year, whereas the fraction of C6 was highest in spring and summer.

d) What processes DOM is exposed to along the salinity gradient?

DOM in the two rivers and the estuary is both subject to biological processes like biodegradation and biological *in*-situ production, and to non-biological processes like conservative mixing, photodegradation and possibly resuspension from and adsorption to sediments. The fluorescence index HIX indicated the influence of the tidal cycle and the mixing of freshwater and seawater in these rivers. As freshwater travels downstream and as seawater travels upstream, the more humified DOM of freshwater mixes with the less humified DOM of seawater. These findings confirm the results of Chapter 3 where the tidal cycle had different effects on the DOM of both rivers. In addition, the spectral slope ratio S_R, also showed values in agreement with changes in the molecular weight of DOM between freshwater and seawater, either due to the presence of seawater with lower molecular weight DOM or because of the effect of photodegradation as DOM travelled downstream into the estuary, especially in summer. As $CDOM_{\alpha 254}$ in the rivers had a higher molecular weight than in the estuary, the high S_R in the estuary would indicate lower molecular weight than in the rivers. Compatible with processes such as desorption from sediments and sorption to sediments are the lower concentrations of phosphate in winter than in the other seasons, and the higher DOP concentration compared to that of phosphate in the estuary.

Biological processes such as biodegradation occurred throughout the year as suggested by lack of seasonality in the fluorescent component C3 and in the fluorescence index FI. Conversely, the fluorescent component C6 and the fluorescence indices BIX and peak T to peak C indicative of biological activity, microbial growth and DOM produced *in-situ*, showed an increase in both spring and summer for the estuary and the River Yare. The River Waveney also showed an increase, albeit small, in BIX in spring and summer.

e) What are the riverine and estuarine fluxes of DOM?

The fluxes calculated for the River Waveney and the estuary indicated DOC was subject to mainly conservative mixing for six of the thirteen months between December

2018 and December 2019 with most of the remaining months indicating DOC removal as well as mixing, whilst DOC was produced in addition to mixing during December 2018. In contrast, the fluxes calculated for the River Yare and the estuary indicated that DOC was produced in addition to mixing most of the months between December 2018 and December 2019, with DOC removal as well as mixing during three of the thirteen months and the remainder subject mainly to conservative mixing. These results agree with the variables analysed throughout the sampling period highlighting a difference in DOM composition and behaviour in the two rivers as discussed at the beginning of this section.

The riverine fluxes agree with previous studies for rivers across the UK. The estuarine fluxes are also in agreement with values found in the literature, although some of the conclusions from García-Martín et al. (2021) differ from the results of my study. Their research found that estuaries with agricultural and (sub)urban land uses showed non-conservative mixing for DOC, and that these types of estuaries produced double the DOC compared to the freshwater end of the rivers, which is then transported into the sea. Furthermore, DOC in estuaries not characterised by anthropogenic activities (with more peatland and woodland) displayed a conservative behaviour. On the contrary, the estuarine fluxes estimated for the River Waveney and the River Yare showed a removal of the riverine DOC of only 4.8%, indicating that the majority of freshwater DOC is mixing with seawater and is transferred into the shelf sea. This is in agreement with a study by Kitidis et al. (2019) where it is stated that whilst DOC in larger estuaries tends to be degraded and converted into CO_2, DOC in smaller estuaries (with smaller residence times in comparison) tends to be transported to the shelf sea with little transformation. This could mean that catchments draining into smaller estuaries are an important source of DOC to the sea. Based on the estimates from the estuarine fluxes of these two East Anglian rivers, their DOC export represents 0.12% of the post-estuary flux calculated by Kitidis et al. (2019) for the north west European shelf. These results highlight the importance of investigating the riverine carbon fluxes as well as the estuarine fluxes (García-Martín et al., 2021).

f) What are the sources of DOM to the shelf sea? Are they linked to the land use of the catchments?

The sources of DOM from the rivers for the North Sea investigated in this study are both of terrestrial origin and produced or remineralised *in-situ*. As expected, the majority of DOM entering the shelf sea is terrestrial DOM (67.5%). Moreover, in a review of global DOM distribution, Massicotte et al. (2017) stated that most DOM in rivers is of terrestrial origin from surface runoff, soil erosion and groundwater inputs. The percentage of DOM that is produced and biodegraded within these two East Anglian rivers and exported through the

estuary, is 32.5% which is considerable, given that only two of the six components identified by the PARAFAC analysis indicated DOM produced and remineralised *in-situ*. These findings are in agreement with García-Martín et al. (2021) where DOM of estuaries with a similar land use to the Rivers Yare and Waveney, was composed of 33% of components indicative of biological activity *in-situ* and 67% was of terrestrial origin. Thus, DOM exported from these rivers reflects the land use of the catchments.

In terms of fluxes, a total of 3.09 ± 1.87 Gg yr^{-1} of terrestrial DOM enters the shelf sea every year from the Broadland catchment, whilst a total of 1.49 ± 0.90 Gg yr^{-1} of microbially produced DOM is exported annually to the shelf sea, where it can be further transformed through photodegradation, microbial remineralisation and sedimentation or mixed conservatively with seawater.

Chapter 5

Fate of riverine DOM in the southern North Sea

This chapter discusses the results of six cruises carried out onboard the research vessel (RV) *Cefas Endeavour* in the southern North Sea between November 2018 and July 2020. This chapter aims to understand the composition and the changes in DOM throughout the year in the shelf sea. The aim is achieved through the following objectives:

i. Determine the spatial and temporal variability in optical (absorption and fluorescence) and biogeochemical (carbon, nitrogen and phosphorus (properties of DOM in the southern North Sea;
ii. Determine the processing of DOM in the southern North Sea;

The chapter will test the following hypotheses:

H1) The composition of DOM in the southern North Sea reflects that of the rivers flowing into it, here exemplified by the rivers Yare and Waveney;

H2) The southern North Sea shows a stronger signal for autochthonous DOM than for terrestrial-derived DOM, as evident from the fluorescence intensity and the fluorescent indexes;

H3) DOM components originating from land should display an inverse relationship with salinity, therefore DOC, CDOM and nutrient concentrations should be higher near the coast and decrease further out as near-shore water mixes with the shelf seawater;

H4) DOM of riverine origin in the southern North Sea is photo-oxidised and subject to microbial remineralisation depending on the season;

5.1 Additional methodology

A total of 114 samples was collected during six cruises carried out by Cefas in the southern North Sea. Table 5.1 lists the cruises and the variables analysed for each cruise. All the samples were collected at a depth of a maximum of 6 m from the underway supply and the CTD rosette, except for 8 samples which were collected at a depth more than 12 m and are not considered in this study. Furthermore, one more sample is excluded due to missing coordinates. A total of 105 samples is discussed in this chapter. The samples were collected during cruises in November 2018, May 2019, August 2019, November 2019, February 2020 and July 2020. The methods used to analyse the samples are described in Chapters 2 and 3 (sections 3.1.1 and 3.1.2). Note that CDOM in this chapter has been investigated using the absorption coefficient at λ of 300 nm instead of λ of 254 nm. This was decided after some values analysed for $SUVA_{254}$ exceeded 5 L mg-C^{-1} m^{-1} which indicates a possible effect of dissolved iron (Stedmon and Nelson, 2015). As a result, $SUVA_{254}$ is not discussed for these data. In addition, for the spectral slopes and the ratio, only $S_{275-295}$ will be discussed as the limit of quantification (LOQ) resulted below 400 nm for the majority of the samples (Helms et al., 2008). Figure 5.1 shows the sites sampled during the cruises (see Chapter 2 section 2.2.2 for subplots with the sites per cruise). Note that I only participated in cruise CEND 16-19 in November 2019. The samples for the other cruises were collected by staff at Cefas following a Standard Operating Procedure (SOP) which I provided.

Table 5.1. *Names, dates and variables analysed for the 105 samples collected on the cruises carried out onboard the RV Cefas Endeavour.*

Cruise	Dates	Number of samples	DOC	CDOM	FDOM	Inorganic nutrients	Organic nutrients	Chlorophyll-*a*	TSS
CEND* 18-18	12 – 16 November 2018	21	✗	✓	✓	✗	✗	✓	✓
CEND* 06-19	14 – 16 May 2019	17	✓	✓	✓	✓	✓	✓	✓
CEND* 11A-19	02 – 04 August 2019	10	✓	✓	✗	✓	✓	✓	✓
CEND* 16-19	05 – 06 November 2019	17	✓	✓	✓	✓	✓	✓	✓
CEND* 02-20	03 – 08 February 2020	32	✓	✓	✓	✓	✓	✓	✓
CEND* 09-20	02 – 10 July 2020	8	✓	✓	✗	✓	✓	✓	✓

*CEND = Cefas Endeavour

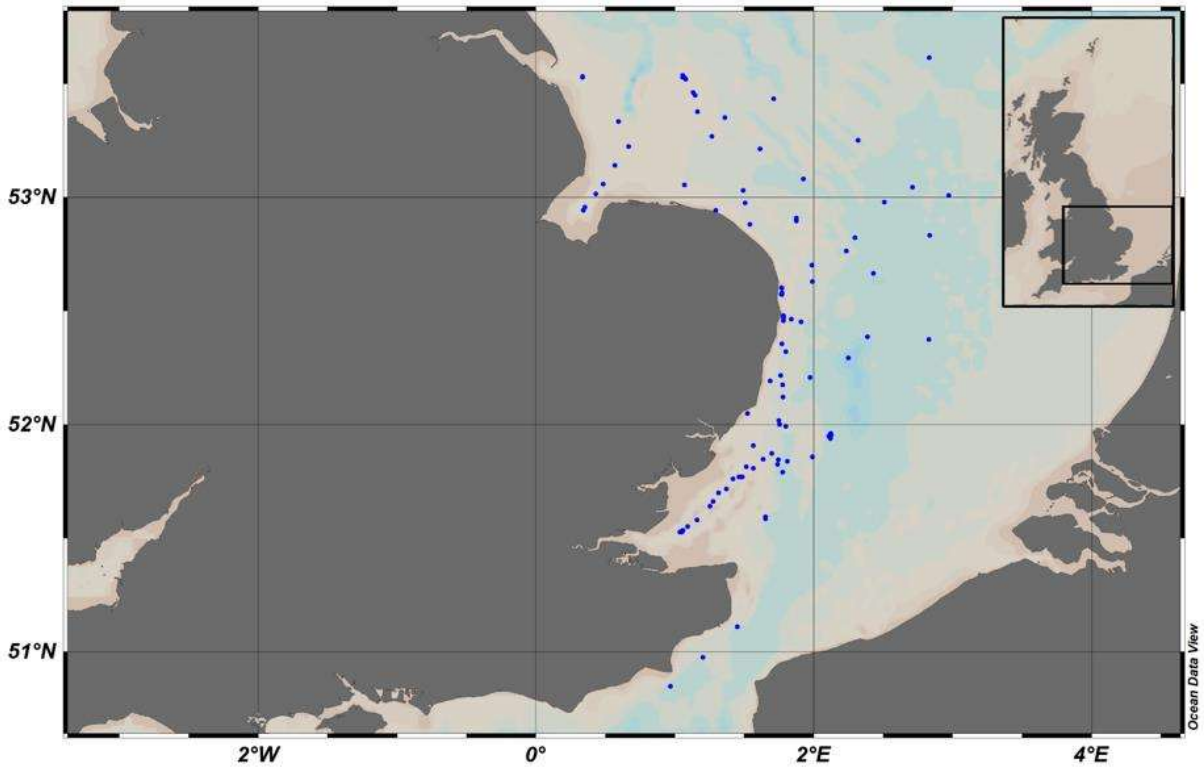

Figure 5.1. *Map of the sites where the 105 samples were collected during the cruises carried out by Cefas in the southern North Sea between November 2018 and July 2020.*

5.2 Results and discussion

5.2.1 PARAFAC components

Five components were identified and validated through the PARAFAC model (Figure 5.2, and Table 5.2). As described in Chapter 3 section 3.2.1 the results of the PARAFAC model were compared to published studies through the OpenFluor database developed by Murphy et al. (2014). Those studies which matched with the components in this chapter with a TCC > 0.9 (Tucker Congruence Coefficient) are listed in Table D1 in Appendix D. The first fluorophore SC1 (Sea Component 1) has excitation maxima at λ of 270 and 360 nm and an emission maximum at λ of 460 nm. SC1 is indicative of humic-like compounds associated with terrestrial and coastal environments but it has also been linked to microbial degradation (Stedmon, 2003; Yamashita et al., 2010; Sharma et al., 2017). SC2 has excitation maxima at λ of 275 and 310 nm and an emission maximum at λ of 406 nm. This component is generally assumed to be prevalent in marine environments, especially in areas affected by riverine discharge and it is considered to be new humic-like material due to biological remineralisation of organic matter in coastal waters (Coble, 1996; Amaral et al., 2020). Several studies have identified this component in other environments and it is now considered ubiquitous (Shutova et al., 2014; Lambert et al., 2016; Gao and Guéguen,

2017; Sharma et al., 2017b; Catalán et al., 2018). SC3 has excitation maxima at λ of 275 and 400 nm and an emission maximum at λ of 506 nm and it is considered a humic-like or fulvic-like component of terrestrial origin, linked to soil and sediments in different environments, from riverine to marine (Yamashita et al., 2010; Osburn et al., 2011; Eder et al., 2022). Yamashita et al. (2010) also suggested that it could be a reduced quinone-like component resulting from the breakdown of lignin and therefore of terrestrial origin. In addition, other studies have reported components with an emission maximum at wavelengths longer than 500 nm (like SC3) to be subject equally to bio- and photodegradation and similarly to be a product of photodegraded terrestrial organic matter (Stedmon et al., 2007; Murphy et al., 2014). The SC4 excitation maximum is at λ of 285 nm with an emission maximum at λ of 350 nm. This component is indicative of recent biological production and it is deemed to be protein-like, specifically tryptophan-like (Stedmon and Markager, 2005; Murphy et al., 2011; Cawley et al., 2012; Murphy et al., 2014). SC5 has an excitation maximum at λ of 275 nm and an emission maximum at λ of 312 nm and is considered to be another protein-like component but tyrosine-like, linked to freshly produced as well as degraded DOM (Murphy et al., 2011; D'Andrilli et al., 2019; Derrien et al., 2019; Pucher et al., 2021).

Table 5.2 shows the components and their description. The five components identified in these samples have components in common with the dataset in Chapters 3 and 4. SC1, SC2, SC3 and SC4 were also found in the River Yare and the River Waveney (Chapters 3 and 4). Only SC5, the tyrosine-like component was solely found in this dataset for the southern North Sea.

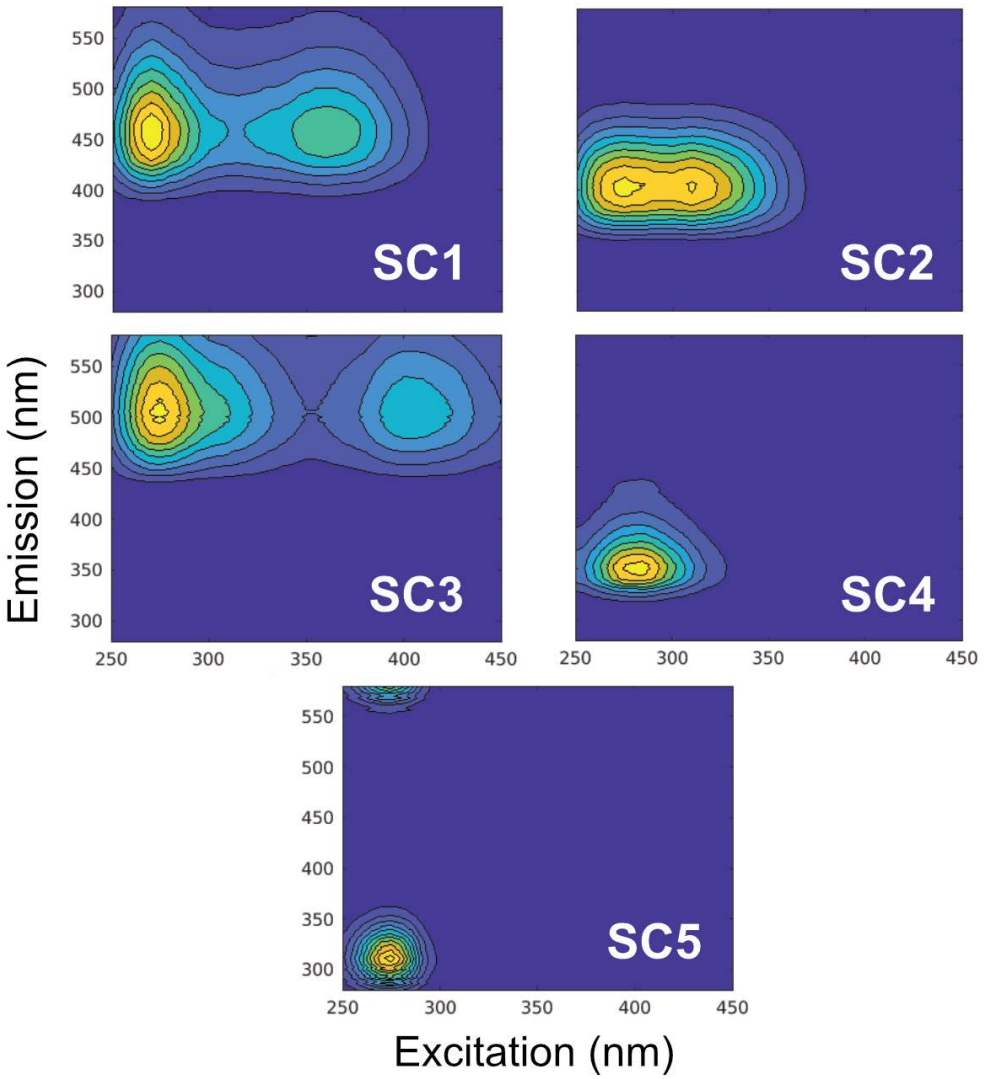

Figure 5.2. *Plots of the five components (SC1 – SC5) identified through the PARAFAC model for 105 samples collected during the cruises onboard the RV Cefas Endeavour between November 2018 and July 2020 in the southern North Sea.*

Table 5.2. *Description and spectral characteristics of the five components identified and validated by the PARAFAC model for 105 samples collected during the cruises onboard the RV Cefas Endeavour between November 2018 and July 2020 in the southern North Sea.*

Component	Excitation/emission maxima λ (nm)	Description
SC1	270, 360 / 460	Humic-like of terrestrial origin with high aromaticity and molecular weight
SC2	275, 310 / 406	Humic-like from microbial processing of organic matter of terrestrial origin
SC3	275, 400 / 506	Humic-like or fulvic-like of terrestrial origin, linked to soil and sediments but reported also as a product of photodegradation
SC4	285 / 350	Protein-like, particularly tryptophan-like from recent *in-situ* biological activity
SC5	275 / 312	Protein-like, particularly tyrosine-like from recent *in-situ* biological activity and degraded proteinaceous material

5.2.2 PCA results for the North Sea cruises

In this section are discussed two PCAs run for the samples collected in the Southern North Sea. As in Chapter 3 and 4 the two PCAs were run first with the quantitative data of DOM (CDOM, DOC and the fluorescent components) and secondly with the qualitative data of DOM ($S_{275-295}$, BIX, FI and HIX) as primary variables and in both PCAs, nutrients, chlorophyll-*a*, TSS and salinity were input as supplementary variables. Prior to the PCA an interpolation of the missing data across the datasets for the North Sea was performed using the missMDA package in R, introduced in section 3.2.2 (Chapter 3) and explored in detail in section 4.2.2 (Chapter 4) (Josse et al., 2011; Josse and Husson, 2016). The statistical significance of the PCA, analysed through PCAtest (see section 3.2.2 of Chapter 3) is shown in Figures D5 and D6 in Appendix D).

Two principal components (PCs) were chosen for both PCAs, explaining most of the variability in the dataset (Figure 5.3 for the first PCA).

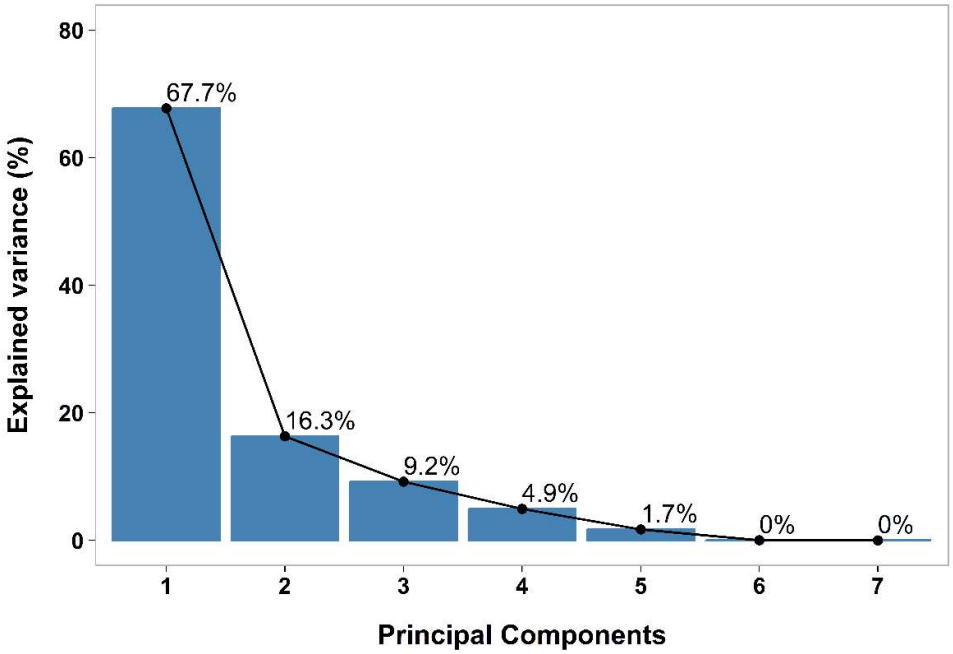

Figure 5.3. *Scree plot of the principal components and their variance in percentage for the samples collected during the cruises onboard the RV Cefas Endeavour between November 2018 and July 2020 in the southern North Sea.*

PCA was run using the R packages mentioned in section 3.2.2 (Chapter 3). The variables that were most influential in the first PCA were SC2, SC3, SC1 and DOC (Dim.1 in Figure 5.4) for R > 0.80, and CDOM PC2 (Dim.2 in Figure 5.4) for R > 0.70.

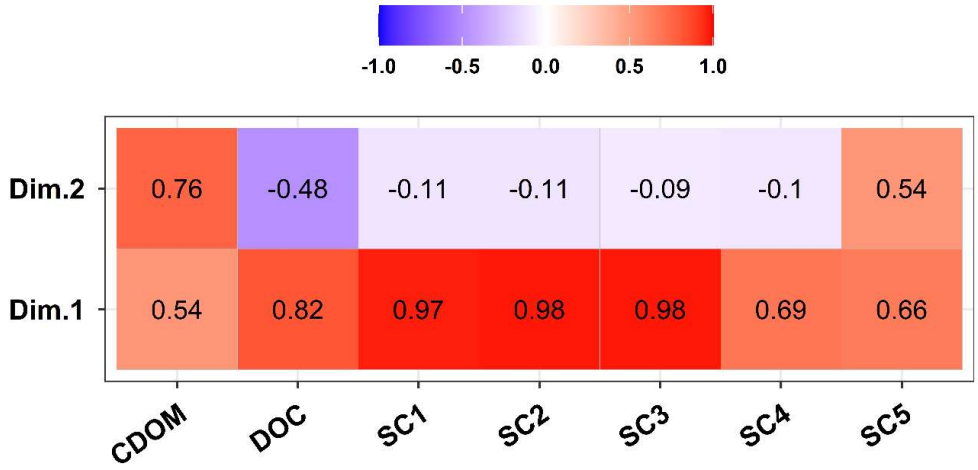

Figure 5.4. *Correlation between the variables of the quantities of DOM analysed in this study and the first two principal components chosen for the PCA. The numbers within the squares represent the correlation coefficients.*

Figure 5.5 shows the correlation between both primary (Figure 5.5C) and supplementary variables (5.5D) with the components, whilst Figures 5.5A and B show the samples clustered by cruise and season, respectively. All the primary variables were negatively correlated to salinity, together with TDP and DOP, indicating higher concentration of these towards the marine endmember, whilst nitrate plus nitrite, TDN, phosphate and TSS were correlated to CDOM and SC5 (the tyrosine-like fluorescent component), indicating a possible association with freshwater, or coastal waters influenced by freshwater.

Interestingly, CDOM and SC5 (although weakly correlated with PC2) are separated by other variables associated with terrestrial DOM (SC1, SC2 and SC3). This could indicate a different source between these variables. The samples clustered by cruise (Figure 5.5A) show that the cruises are overlapping and mostly correlating negatively with all the primary variables, with some samples from the cruise in February 2020 distributed on the first quadrant indicating high concentration of CDOM. Only the cruise in July 2020 is completely separated by the others, showing high concentration for DOC and chlorophyll-*a*, although still influenced by the fluorescent components indicating DOM with terrestrial origin. The lack of a clear seasonality for the quantitative data of DOM could indicate the occurrence of some of the processes to which DOM is subject (microbial degradation, dilution, photodegradation, etc.) throughout the year albeit with some seasonal differences.

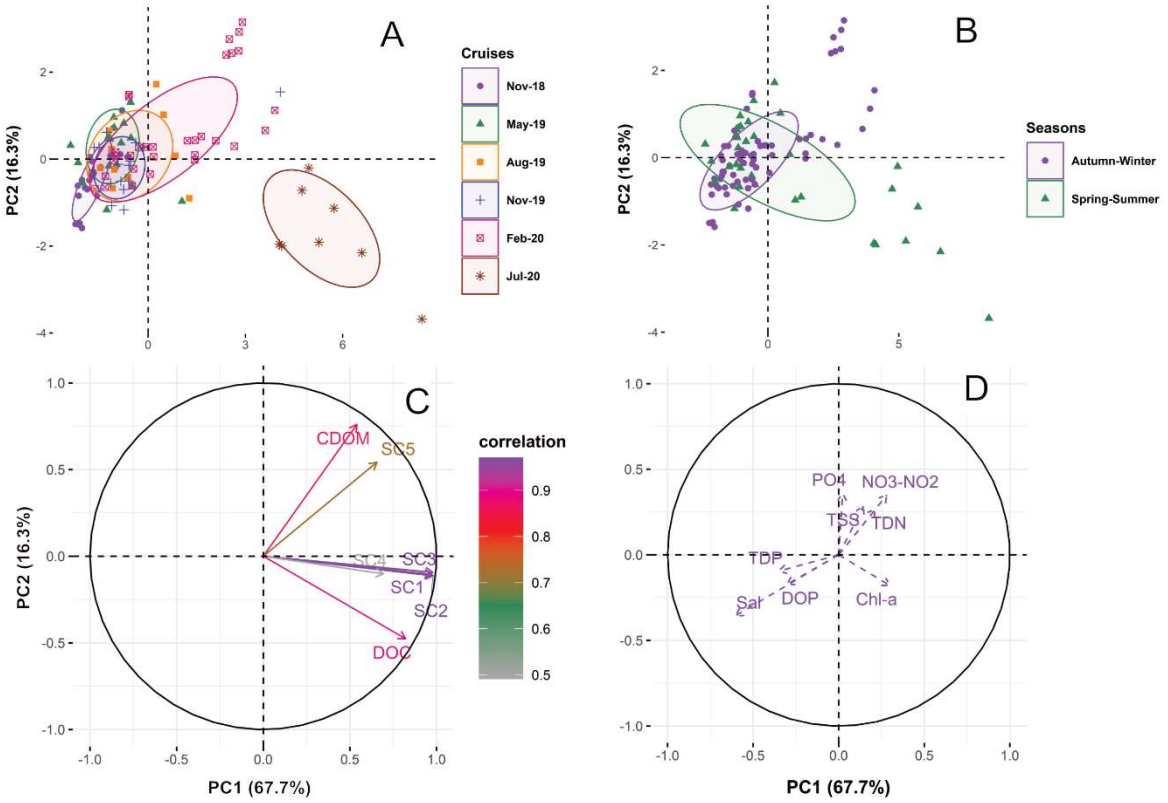

Figure 5.5. *Scores of the individual samples during the cruises onboard the RV Cefas Endeavour between November 2018 and July 2020 in the southern North Sea for the PCA of the quantitative data of DOM, clustered by cruise (A) and by season (B) with ellipses representing 60% confidence assuming the dataset as a multivariate t-distribution. Plots C and D represent the visualisation of the loadings of the primary and supplementary variables of the quantitative DOM data in this dataset.*

For the second PCA, analysing the qualitative data of DOM, the correlation between the primary variables and the first two dimensions (Figure 5.6) showed that BIX (R = 0.83) and HIX (R = -0.85) were highly correlated to PC1, whilst $S_{275\text{-}295}$ was highly negatively correlated to PC2 (r = -0.78) and PC2 was positively correlated, albeit moderately, to FI (R = 0.63).

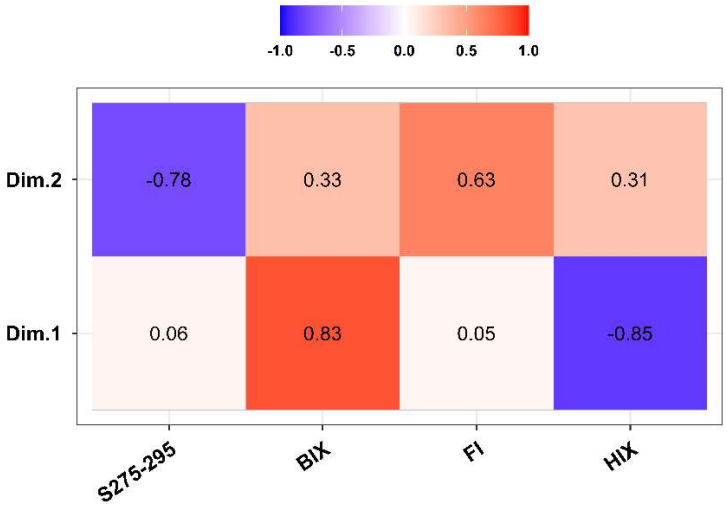

Figure 5.6. *Correlation between the variables of the qualities of DOM analysed in this study and the first two principal components chosen for the PCA. The numbers within the squares represent the correlation coefficients.*

Figure 5.7C show a negative correlation between the primary variables, as expected, given BIX is indicative of DOM produced *in-situ*, whilst HIX is associated with terrestrial DOM. For the negative correlation between FI and $S_{275-295}$, higher values of FI are associated with DOM of microbial origin which tend to be smaller in molecular size, hence higher values of $S_{275-295}$. Interestingly, the supplementary variables (Figure 5.7D) are distributed only along the PC1, with variables associated with the freshwater endmember positively correlated with HIX and the variables with a higher concentration in the marine endmember correlating with BIX.

The samples clustered by cruise (Figure 5.7A) showed an overlap, although the cruises in November 2019 and February 2020 were correlated with HIX, indicating a terrestrial influence, whilst the cruise in May 2019 showed samples correlated with BIX, possibly due to increase of *in-situ* production at this time of the year. To note that some samples from the cruise in November 2018 showed higher values for $S_{275-295}$. The differentiation between seasons (Figure 5.7B), also showed that samples for spring-summer were correlated with BIX, whilst samples for autumn-winter were more correlated with HIX, noting again some values with high $S_{275-295}$.

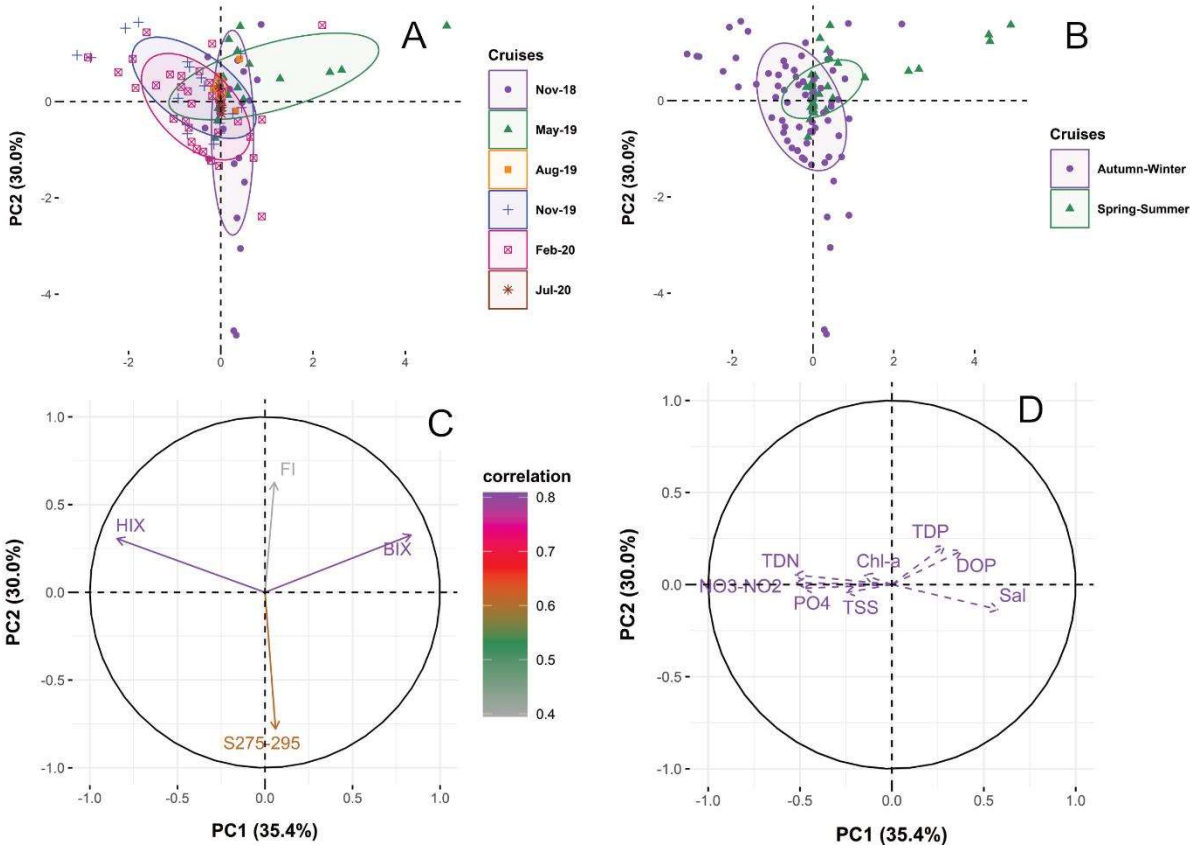

Figure 5.7. *Scores of the individual samples during the cruises onboard the RV Cefas Endeavour between November 2018 and July 2020 in the southern North Sea for the PCA of the qualitative data of DOM, clustered by cruise (A) and by season (B) with ellipses representing 60% confidence assuming the dataset as a multivariate t-distribution. Plots C and D represent the visualisation of the loadings of the primary and supplementary variables of the qualitative DOM data in this dataset.*

5.2.3 Spatial distribution of FDOM, $CDOM_{\alpha 300}$, DOC and $S_{275-295}$

This section discusses fluorescence and absorbance spectra for all the cruises, as well as DOC and the spectral slope $S_{275-295}$. Note that FDOM values are not available for the cruises of August 2019 and July 2020, whilst DOC concentrations are not available for the cruise of July 2020. Figure 5.8 shows the salinity of all the samples collected between November 2018 and July 2020. Salinity ranged between 31.4 and 35.3 with lower values near the coast (between 31.4 and 33.8), a result of the rivers flowing out to the sea.

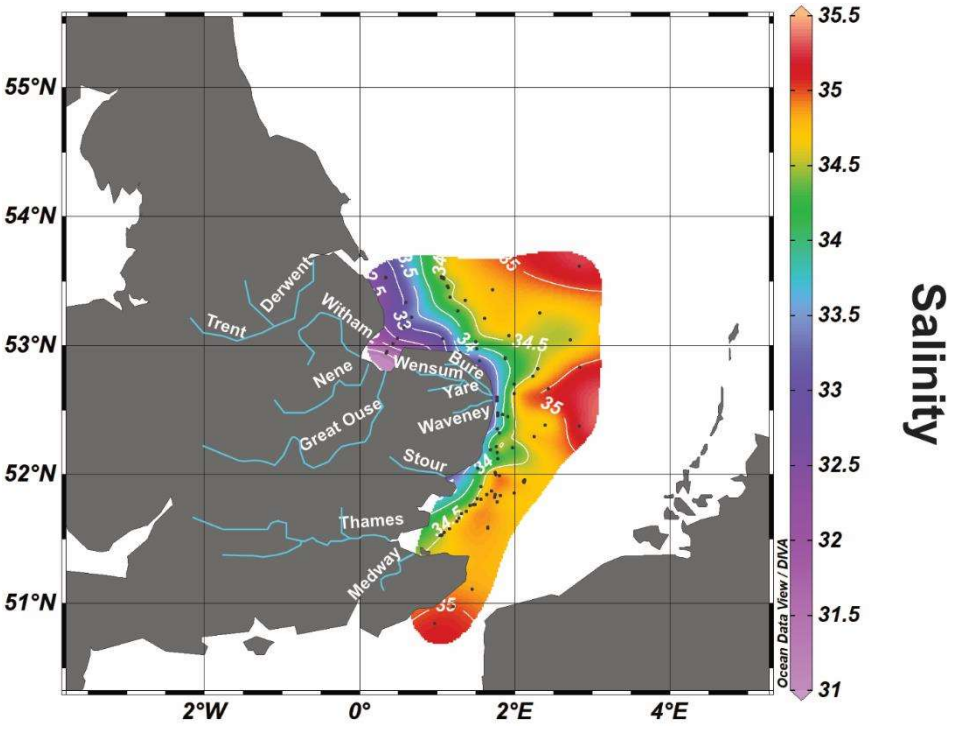

Figure 5.8. *Distribution of salinity for 105 of the samples between November 2018 and July 2020 in the southern North Sea. The black dots represent the sampling positions.*

Table 5.3 reports the range, average and the equations and significance of the linear correlation with salinity of the five components identified through the PARAFAC model, CDOM absorption coefficient at λ 300 nm, DOC concentration and the non-linear correlation between salinity and $S_{275-295}$, whilst Figure 5.9 shows the distribution of those variables. The fluorescence intensities of SC1, SC2 and SC3 show high values closer to the coast, with lower values as the distance from the land increases. In addition, they have a negative correlation with salinity with an R^2 of 0.90, 0.88 and 0.89 for SC1, SC2 and SC3, respectively (Figure 5.9). The protein-like components SC4 and SC5 do not show any correlation with salinity, in agreement with these two components being produced *in-situ* and not originating from the land. Nonetheless, both components show high fluorescent intensities near the coast indicating high microbial activity, a possible effect of the riverine transport of organic

matter rich waters into the coast. Note that SC5 shows a high fluorescence intensity offshore at a latitude of 53.5° N and at a longitude of 3° E. This sample could indicate DOM production as well as biodegradation of proteinaceous material and the $S_{275-295}$ values for the area at latitude between 53° and 53.5° N and at longitude between 2° and 3° E indicate low molecular weight typical of ocean waters or very photodegraded DOM. Generally, low values of $S_{275-295}$ are indicative of high molecular weight and terrestrial DOM, whilst higher values indicate DOM with a lower molecular weight associated with photodegradation or very clear waters (Stedmon and Nelson, 2015), which is not the case for the southern North Sea (Wilson and Heath, 2019). In this case, the smaller molecular weight of DOM could be a product of photobleaching or biological production of CDOM as reported by Astoreca et al. (2009) and Dias et al. (2020).

Table 5.3. *Range, average and equation describing the relationship with salinity of the fluorescence intensity of the five components identified by the PARAFAC model, $CDOM_{\alpha 300}$, DOC concentration and $S_{275-295}$ for the samples collected during the cruises onboard the RV Cefas Endeavour between November 2018 and July 2020 in the southern North Sea. The R^2 and the p value of the correlations are also listed.*

Variable	Range	Average	Relationship with salinity	R^2	*p* value
SC1 (R.U.)	0.009 – 0.118	0.031	y = - 0.024 x + 0.845	0.90	< 0.001
SC2 (R.U.)	0.009 – 0.086	0.025	y = - 0.017 x + 0.606	0.88	< 0.001
SC3 (R.U.)	0.007 – 0.070	0.019	y = - 0.014 x + 0.500	0.89	< 0.001
SC4 (R.U.)	0.004 – 0.174	0.028	y = - 0.009 x + 0.354	0.11	< 0.01
SC5 (R.U.)	0.000 – 0.103	0.024	y = - 0.011 x + 0.404	0.19	< 0.001
$CDOM_{\alpha 300}$ (m^{-1})	0.000 – 4.660	1.895	y = - 0.804 x + 29.478	0.46	< 0.001
DOC (µmol L^{-1})	25.307 – 335.519	101.779	y = - 11.556 x + 496.576	0.04	> 0.05
$S_{275-295}$	0.006 – 0.184	0.030	y = - 0.0003 x^2 + 0.021 x – 0.359	0.01	> 0.05

Near the coast $S_{275-295}$ showed also higher values where the rivers described in Chapter 4 flow out at sea, in agreement with the results from Chapter 4 (Figure 4.30 and Figure 4.37) that show photodegraded DOM in the estuary that is transported eventually into the southern North Sea. As explained before, higher $S_{275-295}$ values could also indicate possible biological production given that coastal waters are generally very productive (Chaichana et al., 2019). The range of values for $S_{275-295}$ in this study compares well with other studies in coastal and shelf waters that showed ranges between 1.3 and 12.86 (Helms et al., 2008; Helms et al., 2013; Painter et al., 2018), although some values in this study are higher (Table 5.3). Overall, $CDOM_{\alpha 300}$ showed higher values near the coast and lower values offshore, with some variability offshore. It has a negative correlation with salinity (R^2 = 0.46) which is not as strong as reported in other studies (Stedmon et al., 2010; Osburn and Stedmon, 2011), possibly because the sites sampled in those studies were closer to the coast. Values for $CDOM_{\alpha 300}$ agree with those from other studies in the transition zone between the Baltic and the North Sea, between the Skagerrak and the Kattegat (Stedmon et al., 2010; Osburn and Stedmon, 2011). As for $S_{275-295}$ and for SC5, the variability in the correlation between salinity and $CDOM_{\alpha 300}$ could be due to higher values north of 53° N east of 2° E, where CDOM is biologically produced.

DOC concentrations show higher values along the coast, but also offshore with the highest values north of 52° N and at longitude 2° E. This is a possible indication of DOC produced *in-situ*, as shown also by the corresponding $S_{275-295}$ values. DOC concentrations did not correlate with salinity, indicating other sources of organic carbon apart from the rivers. This is supported by the lack of a relationship between $CDOM_{\alpha 300}$ and DOC (R^2 = 0.0005 and *p* value > 0.05). This has been also reported by Stedmon and Nelson (2015) for offshore waters, where the influence of the surface runoff from rivers becomes negligible and production and photodegradation of DOC (which affects the composition of both DOC and CDOM) contribute to the decoupling of DOC and CDOM. Usually rivers show a high correlation between DOC and CDOM (Spencer et al., 2012), so as the riverine input decreases and DOC and CDOM are characterised by other sources (DOC production) and sinks (CDOM degradation), their correlation decreases (Massicotte et al., 2017). The range of values for DOC in this chapter compares well with other studies in the North Sea (Van Engeland et al., 2010; Chaichana, 2017; Painter et al., 2018; Chaichana et al., 2019).

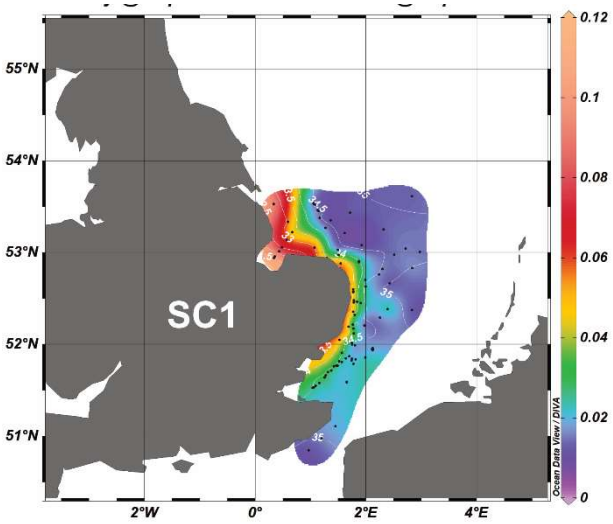
SC1
55°N
54°N
53°N
52°N
51°N
2°W
0°
2°E
4°E
0.12
0.1
0.08
0.06
0.04
0.02
0
Ocean Data View / DIVA

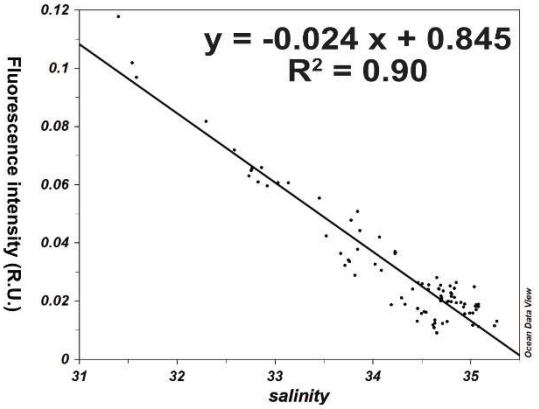
y = -0.024 x + 0.845
R² = 0.90
Fluorescence intensity (R.U.)
salinity
0.12
0.1
0.08
0.06
0.04
0.02
0
31
32
33
34
35
Ocean Data View

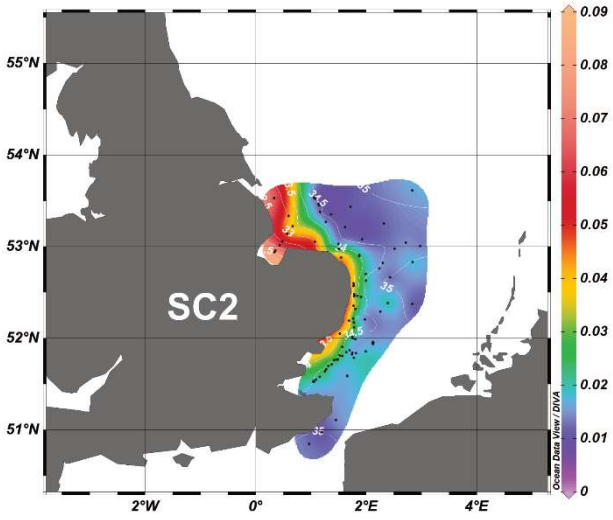
SC2
55°N
54°N
53°N
52°N
51°N
2°W
0°
2°E
4°E
0.09
0.08
0.07
0.06
0.05
0.04
0.03
0.02
0.01
0
Ocean Data View / DIVA

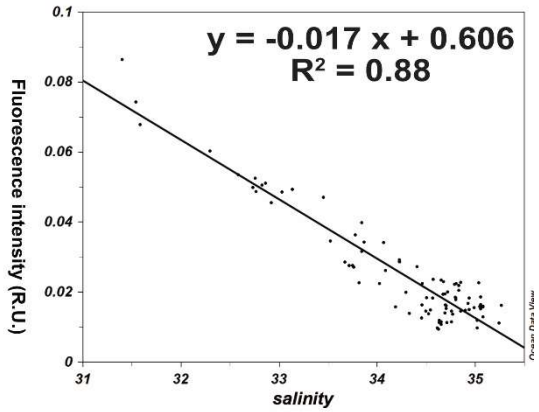
y = -0.017 x + 0.606
R² = 0.88
Fluorescence intensity (R.U.)
salinity
0.1
0.08
0.06
0.04
0.02
0
31
32
33
34
35

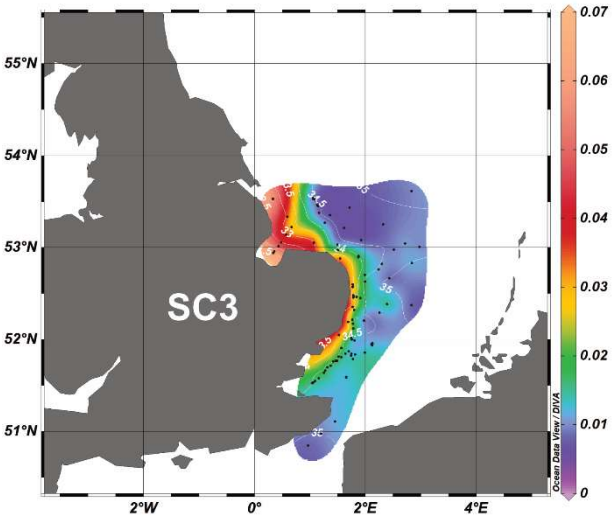
SC3
55°N
54°N
53°N
52°N
51°N
2°W
0°
2°E
4°E
0.07
0.06
0.05
0.04
0.03
0.02
0.01
0
Ocean Data View / DIVA

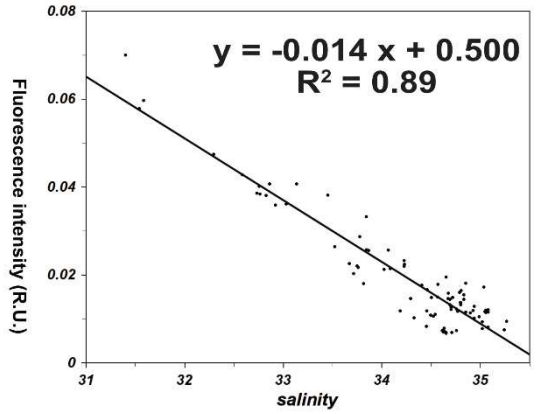
y = -0.014 x + 0.500
R² = 0.89
Fluorescence intensity (R.U.)
salinity
0.08
0.06
0.04
0.02
0
31
32
33
34
35

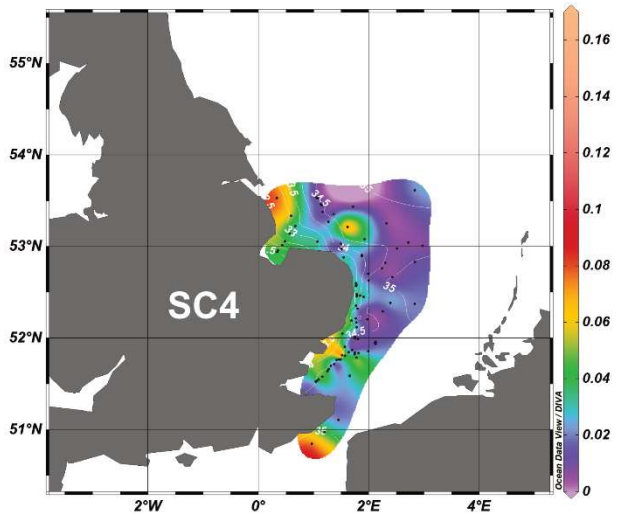
SC4
55°N
54°N
53°N
52°N
51°N
2°W
0°
2°E
4°E
Ocean Data View / DIVA

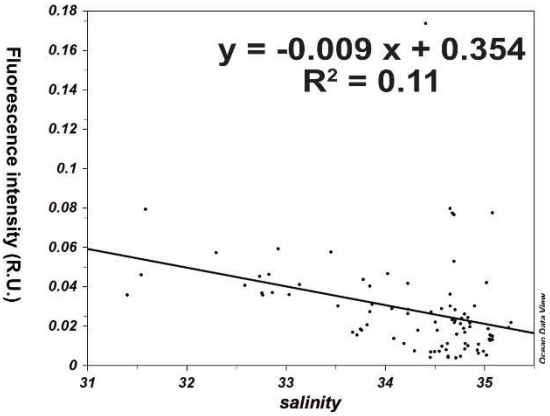
y = -0.009 x + 0.354
R² = 0.11
Fluorescence intensity (R.U.)
salinity
Ocean Data View

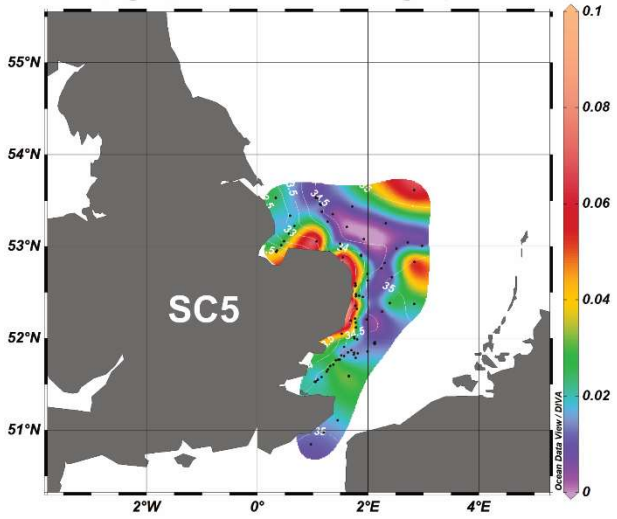
SC5
55°N
54°N
53°N
52°N
51°N
2°W
0°
2°E
4°E
Ocean Data View / DIVA

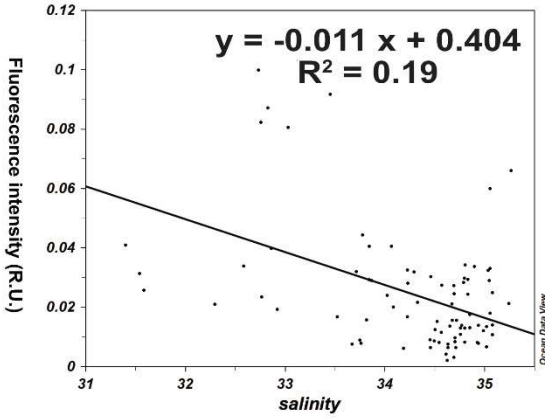
y = -0.011 x + 0.404
R² = 0.19
Fluorescence intensity (R.U.)
salinity
Ocean Data View

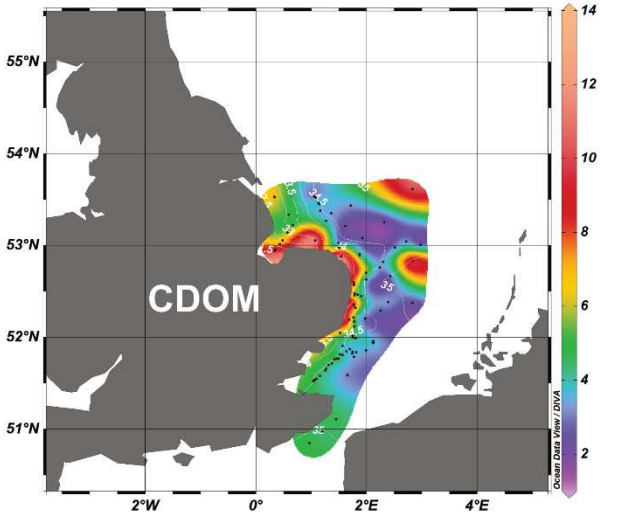
CDOM
55°N
54°N
53°N
52°N
51°N
2°W
0°
2°E
4°E
Ocean Data View / DIVA

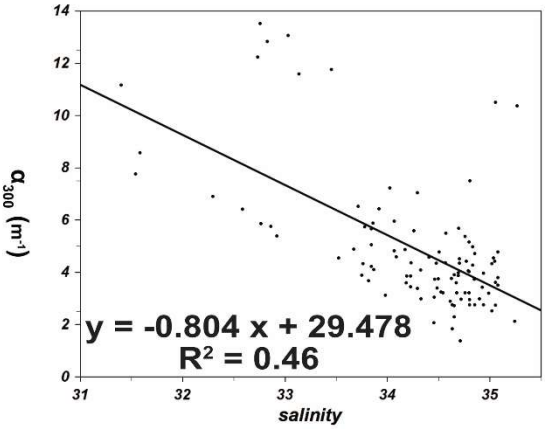
y = -0.804 x + 29.478
R² = 0.46
α300 (m-1)
salinity

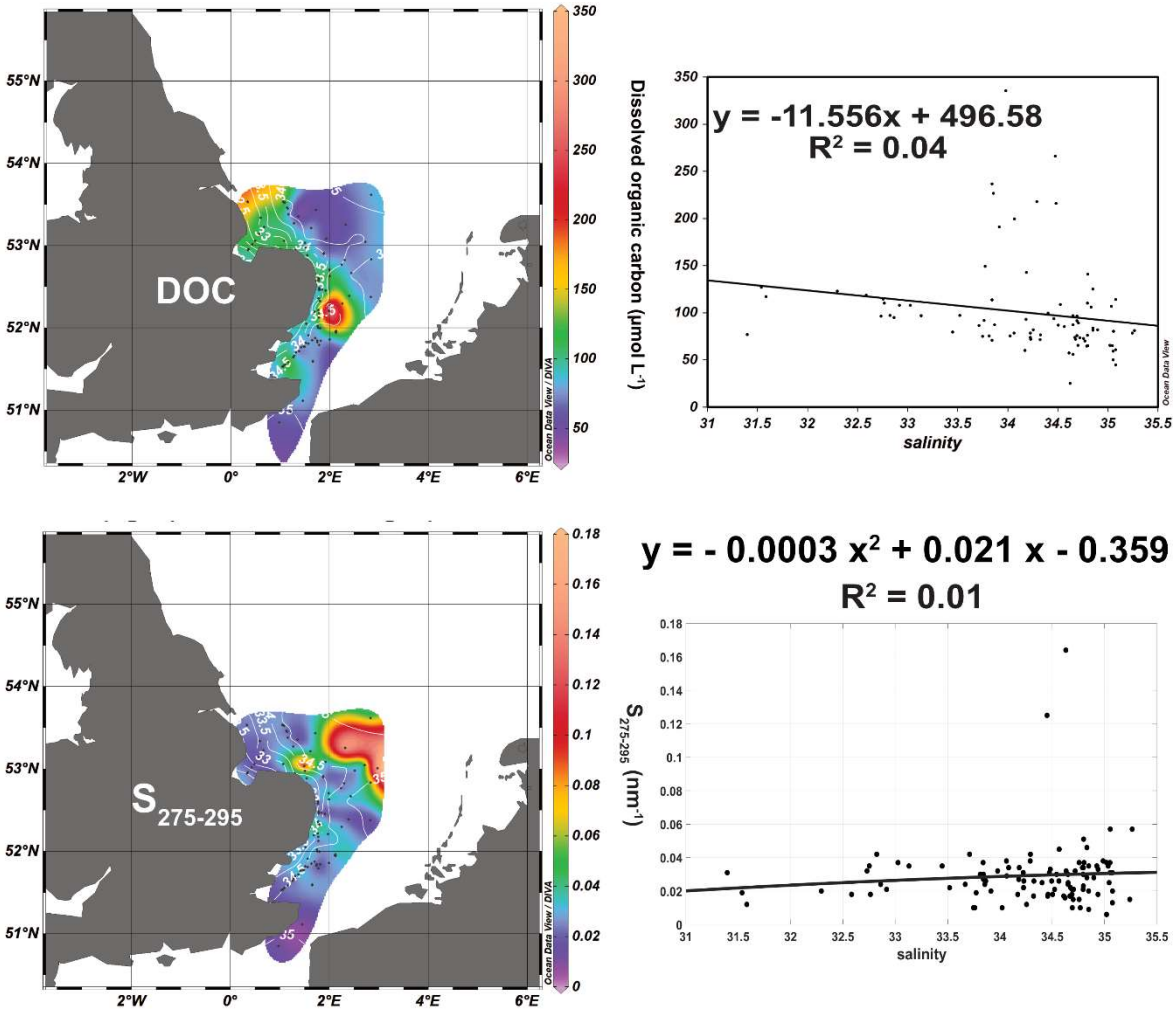

Figure 5.9. *On the left the distribution of the maximum fluorescence intensities of the five components identified through the PARAFAC model, of* $CDOM_{\alpha 300}$ *and DOC concentrations and* $S_{275-295}$ *values for the samples collected during the cruises onboard the RV Cefas Endeavour between November 2018 and July 2020 in the southern North Sea (DOC concentrations are missing for November 2018). The dots represent the stations sampled. On the right the correlation of the variables against salinity.*

5.2.4 Spatial distribution of inorganic nutrients and DOP

Inorganic and organic nutrient concentrations are available for 84 of the 105 samples. The cruise in November 2018 (CEND 18-18) did not sample for inorganic and organic nutrients. Figure 5.10 shows the spatial distribution of the nutrients, chlorophyll-*a* and TSS. The range, average and equations for the correlations between the variables and salinity are in Table 5.4. The nutrient concentrations in this study compared well with other studies in the North Sea (Brockmann et al., 1990; Laane et al., 1993; Prandle et al., 1997; Grunwald et al., 2010; Van Engeland et al., 2010; Johnson et al., 2013; Painter et al., 2018; Chaichana et al., 2019).

TDN and nitrate plus nitrite show higher concentrations near the coast where the riverine influence is stronger, with lower concentrations as the distance from the land

increases. On average, nitrate plus nitrite for all the data represented 82.6% of TDN, leaving the remaining 17.4% formed by ammonium and DON. The distribution of the data shows some variability for TDN and nitrate, also confirmed by their relationship with salinity showing an R^2 of 0.34 and 0.53 for TDN and nitrate plus nitrite, respectively. This variability is visible between 51° N and 52° N and between 1° E and 2° E. The decoupling of salinity and the variables could be an indication of biological processes with either phytoplankton using nitrate or bacteria remineralising DOM. This variability could also be a result of the circulation pattern which follows a southward pattern south of 52° N degrees north with a subsequent northward movement of the water off the coast (Figure 2.5 in Chapter 2) (Hydes et al., 2004).

In contrast to TDN, DOP was the major contributor to TDP (average 76%), with phosphate making up the remaining 24%. TDP and DOP show a similar distribution, which is expected given that DOP formed most of the TDP in this study. Figure 5.10 does not show higher concentrations near the coast for TDP and DOP, but there are patches of high concentrations at between 52.5° N and 53.8° N, corresponding to the mouth of the River Thames (51.5° N and 1° E), the English Channel and the Strait of Dover, the latter possibly because of runoff of the River Seine, also confirmed by Laane et al. (1993). TDP and DOP have a weak correlation with salinity indicating a non-conservative behaviour, especially at salinities between 34 and 35 (see Table 5.4 for the equations). This could be explained by offshore production of DOP. Interestingly, phosphate shows a mixing behaviour between salinity 31 and ~33.5, and a non-conservative behaviour at salinities above 34, indicating a loss of inorganic phosphorus by phytoplankton uptake. This is in agreement with the biological production of DOP as reported by Monaghan and Ruttenberg (1999) for the Eel River shelf. To see whether the nutrient distribution was related to the chlorophyll-*a* distribution, correlations between the nutrients and chlorophyll-*a* concentrations have been calculated. There was no significant correlation between the nutrients and chlorophyll-a apart for nitrate plus nitrite (see Table D2 in Appendix D). Other studies have reported coupling between nutrients and primary production (Brockmann et al., 1990; Peeters et al., 1991; Grunwald et al., 2010) (of which chlorophyll-*a* is an indirect indicator). The lack of significant correlation in this study could be a result of the inclusion of all the data, which masks any interannual or seasonal variability. Nevertheless, a long-term study by McQuatters-Gollop et al. (2007) found that chlorophyll-*a* was not linked to nutrient concentrations. This is further explored in the next section where the seasonal distribution of the data is presented.

Chlorophyll-*a* concentrations for this chapter were in agreement with other studies in the North Sea (Brockmann et al., 1990; Tiedje et al., 2010; Van Engeland et al., 2010; Johnson et al., 2013; Chaichana, 2017; Painter et al., 2018). The distribution of chlorophyll-

a does not show a clear pattern (Figure 5.10), although the highest concentrations are close to the coast. In particular, there are clusters of high concentrations corresponding to The Wash (approximately 52.8° N and 0.2° E), Gorleston on Sea (approximately 52.6° N and 1.7° E), the mouth of the River Yare and the River Waveney, and further south where the Rivers Deben, Orwell, Stour and Thames flow out to sea (approximately between 51.5° and 51.7° N and 1.3° and 1.5° E). However, there were very low concentrations closest to the coast, where the rivers discharge to the sea. The TSS distribution in Figure 5.10, has very high concentrations from Gorleston on Sea going south corresponding to the mouth of the Rivers Deben, Orwell and Stour that could have resulted in poor light penetration and thus limitation to or inability of algal growth (McQuatters-Gollop et al., 2007; Capuzzo et al., 2015). Chlorophyll-*a* was also high further offshore where the salinity was higher, which is visible in Figure 5.10 where chlorophyll-*a* is shown as a function of salinity. There is no relationship between chlorophyll-a and salinity, but chlorophyll-*a* increased steeply at salinities over 33.7, although with some variability. There was also no relationship between TSS and salinity and concentrations were very high from Gorleston on Sea to approximately Clacton on Sea (51.8° N and 1.2° E). These high concentrations near the East Anglian coast are in agreement with Capuzzo et al. (2015) and Wilson and Heath (2019) describing it as the East Anglia Plume (EAP). These studies indicate that the probable cause of this plume are sediment resuspension riverine discharge and bottom and coastal erosion (Capuzzo et al., 2015; Wilson and Heath, 2019). The variability of chlorophyll-*a* and TSS concentrations is investigated further in the next section to see if the spatial distribution is affected by seasonal changes.

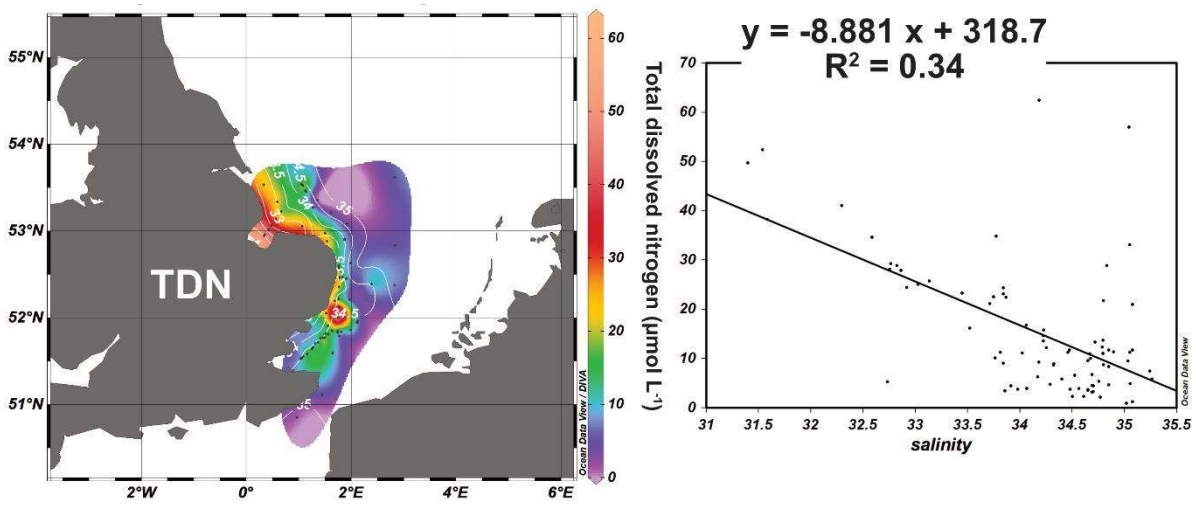
TDN
y = -8.881 x + 318.7
R² = 0.34
Total dissolved nitrogen (µmol L⁻¹)
salinity
55°N
54°N
53°N
52°N
51°N
2°W
0°
2°E
4°E
6°E
Ocean Data View / DIVA
Ocean Data View

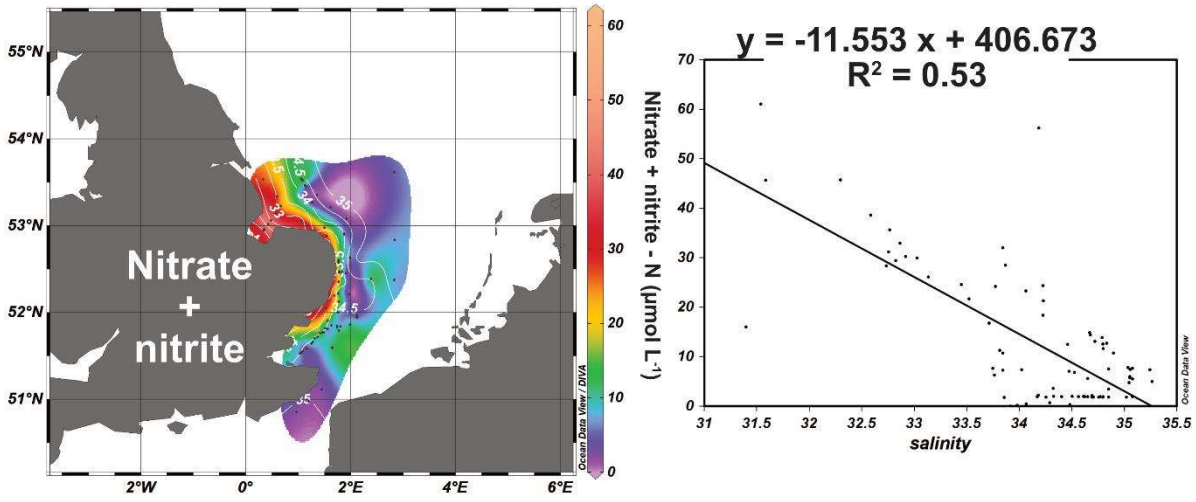
Nitrate
+
nitrite
y = -11.553 x + 406.673
R² = 0.53
Nitrate + nitrite - N (µmol L⁻¹)
salinity
55°N
54°N
53°N
52°N
51°N
2°W
0°
2°E
4°E
6°E
Ocean Data View / DIVA
Ocean Data View

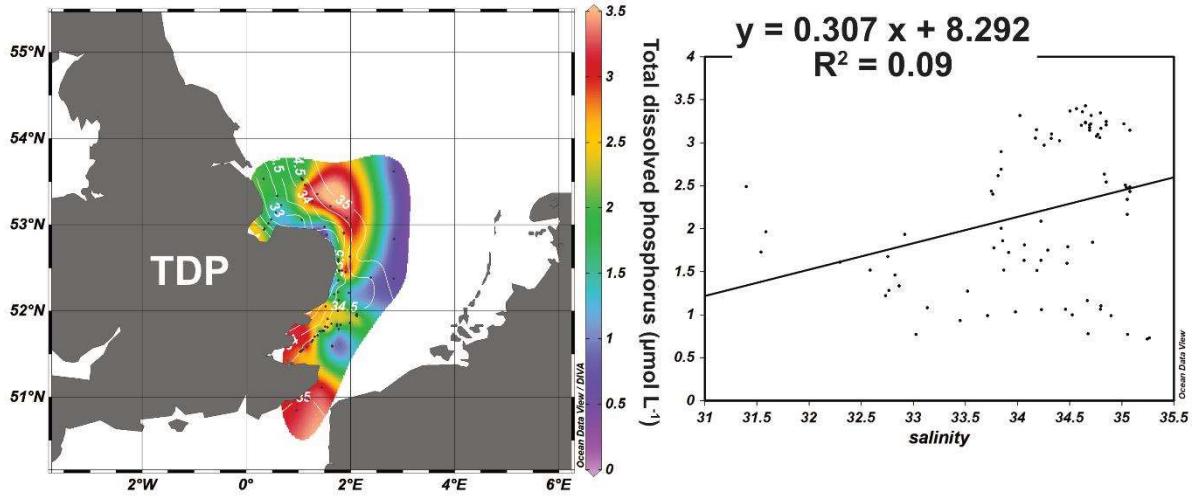
TDP
y = 0.307 x + 8.292
R² = 0.09
Total dissolved phosphorus (µmol L⁻¹)
salinity
55°N
54°N
53°N
52°N
51°N
2°W
0°
2°E
4°E
6°E
Ocean Data View / DIVA
Ocean Data View

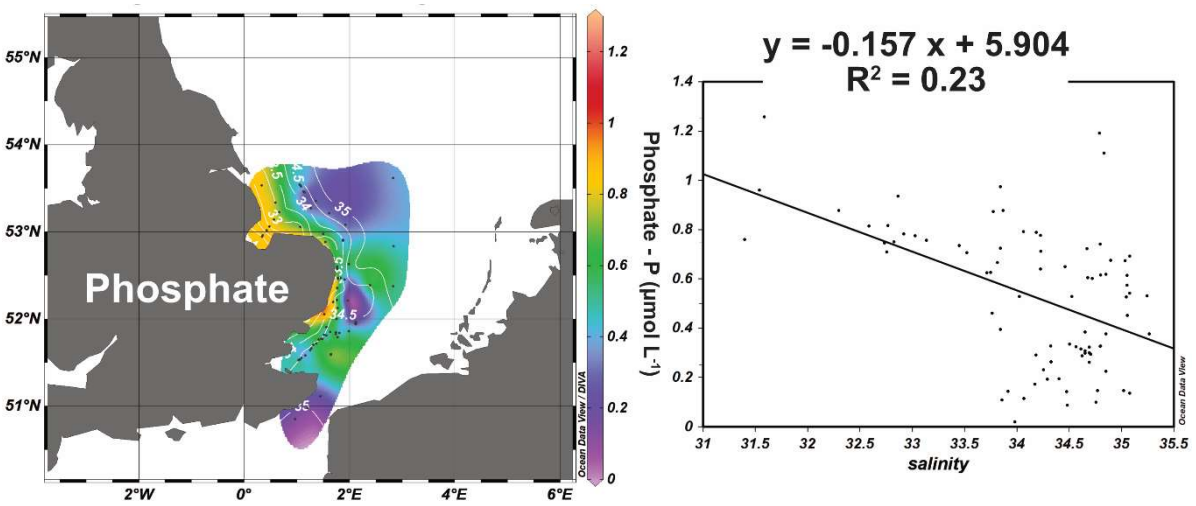
Phosphate
55°N
54°N
53°N
52°N
51°N
2°W
0°
2°E
4°E
6°E
Ocean Data View / DIVA
Phosphate - P (µmol L-1)
y = -0.157 x + 5.904
R2 = 0.23
salinity
Ocean Data View

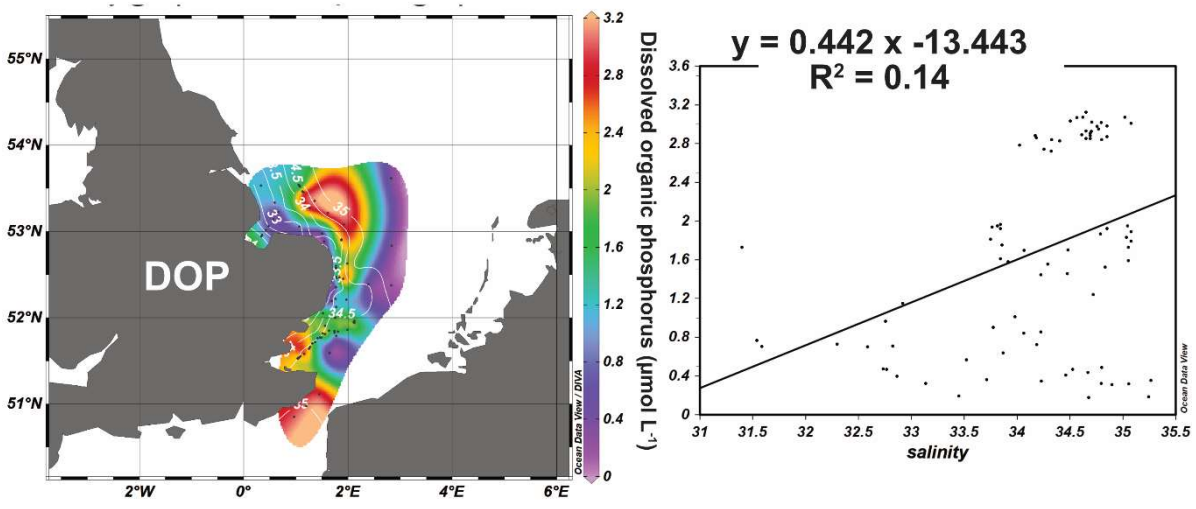
DOP
55°N
54°N
53°N
52°N
51°N
2°W
0°
2°E
4°E
6°E
Ocean Data View / DIVA
Dissolved organic phosphorus (µmol L-1)
y = 0.442 x -13.443
R2 = 0.14
salinity
Ocean Data View

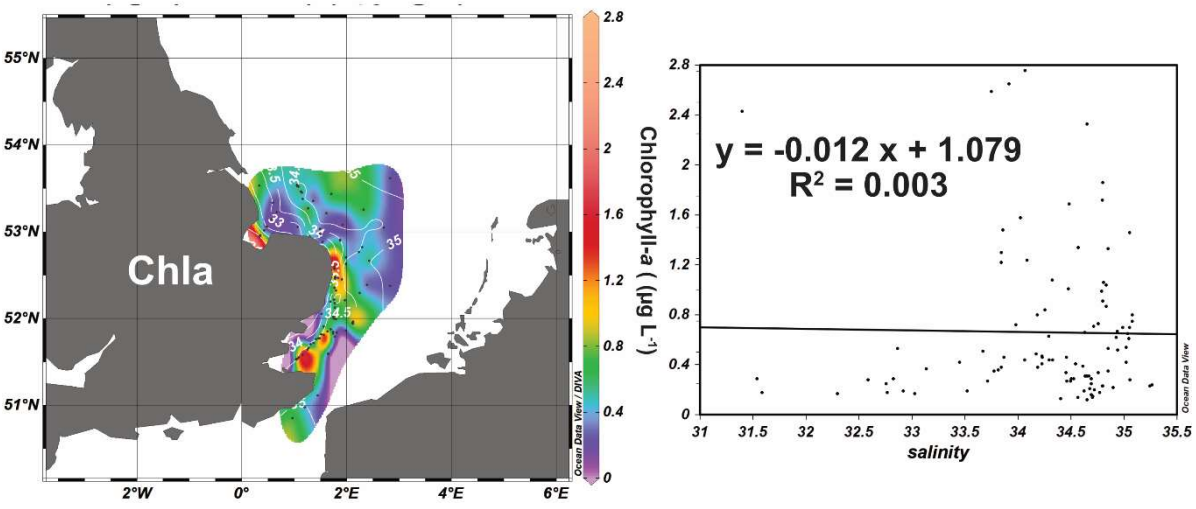
Chla
55°N
54°N
53°N
52°N
51°N
2°W
0°
2°E
4°E
6°E
Ocean Data View / DIVA
Chlorophyll-a ((µg L-1)
y = -0.012 x + 1.079
R2 = 0.003
salinity
Ocean Data View

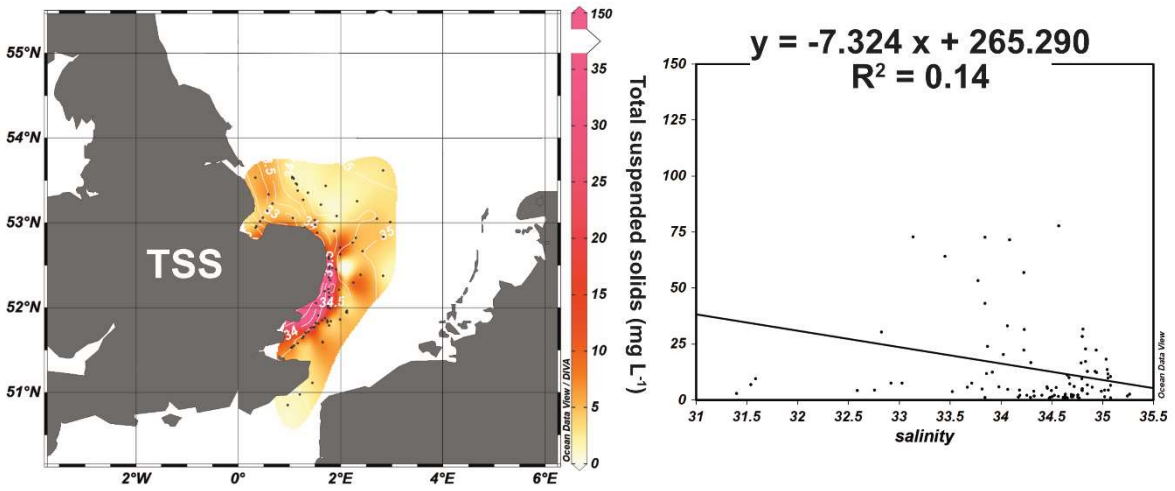

Figure 5.10. *Distribution of the concentrations of TDN, nitrate plus nitrite, TDP, phosphate, DOP, chlorophyll-a and TSS for the samples collected during the cruises onboard the RV Cefas Endeavour between May 2019 and July 2020 in the southern North Sea. The distribution of chlorophyll-a and TSS concentrations includes also samples collected in November 2018. The dots represent the sites sampled. On the right the linear correlation with the variables against salinity.*

Table 5.4. *Range, average and equation describing the relationship with salinity of the concentrations of TDN, nitrate plus nitrite, TDP, phosphate, DOP, chlorophyll-a and TSS for the samples collected during the cruises onboard the RV Cefas Endeavour between November 2018 and July 2020 in the southern North Sea. The R^2 and the p value of the correlations are also listed.*

Variable	Range	Average	Relationship with salinity	R^2	*p* value
TDN ($\mu mol\ L^{-1}$)	0.93 – 62.49	15.32	y = - 8.88 x + 318.70	0.34	< 0.001
$NO_3 + NO_2$ ($\mu mol\ L^{-1}$)	0.06 – 61.10	12.66	y = - 11.53 x + 406.67	0.53	< 0.001
TDP ($\mu mol\ L^{-1}$)	0.72 – 3.43	2.19	y = 0.31 x – 8.29	0.09	< 0.01
PO_4 ($\mu mol\ L^{-1}$)	0.02 – 1.26	0.53	y = - 0.16 x + 5.90	0.23	< 0.001
DOP ($\mu mol\ L^{-1}$)	0.18 – 3.13	1.68	y = 0.44 x – 13.44	0.14	< 0.001
Chla-*a* ($\mu g\ L^{-1}$)	0.12 – 2.76	0.66	y = - 0.01 x + 1.08	0.003	> 0.05
TSS ($mg\ L^{-1}$)	0.89 - 145.59	13.88	y = -7.32 x + 265.29	0.07	< 0.05

5.2.5 Spatial distribution of fluorescence indices

Fluorescence indices are shown in Figure 5.11 whilst Table 5.5 reports the range, averages and the equations for the correlation of the indices with salinity. HIX is an index informing on the level of humification of DOM and its negative correlation with salinity aligns with the relationship between salinity and the terrestrial fluorescent components identified through the PARAFAC model (SC1, SC2 and SC3) in this study. DOM was less humified and therefore less aromatic further away from the coast towards the shelf, although with some variability which could be due to the TSS containing more aromatic DOM, given that the SC3 in this study is linked to soils. The highest HIX values (between 6 and 10), were found near the coast where the riverine influence is higher, whilst intermediate values (between 4 and 6), could be seen further offshore indicating mostly less humified DOM and DOM of autochthonous origin, with values lower than 4 indicating high microbial activity.

The relationships between salinity and BIX and FI, respectively, were not indicative of any spatial gradient but pointed to high microbial activity within these waters as shown by the relatively high fluorescence intensities of SC4 and SC5. The range for BIX values indicates high biological activity and freshly produced DOM (Liu et al., 2021) with more values greater than 1 some distance offshore. BIX values below 0.6 have been reported for rivers (Gonçalves-Araujo et al., 2015) and in this study most of the lowest values are clustered around the coast. The FI index distribution confirmed that DOM in this study had a microbial signature (FI > 1.4) (Cory et al., 2010) with the highest values some distance offshore as seen for BIX. This is interesting given that the fluorescent components identified with the PARAFAC model indicated DOM of terrestrial origin around the coast. It is possible that as DOM and nutrients from the rivers are discharged into the sea, microbial activity increases.

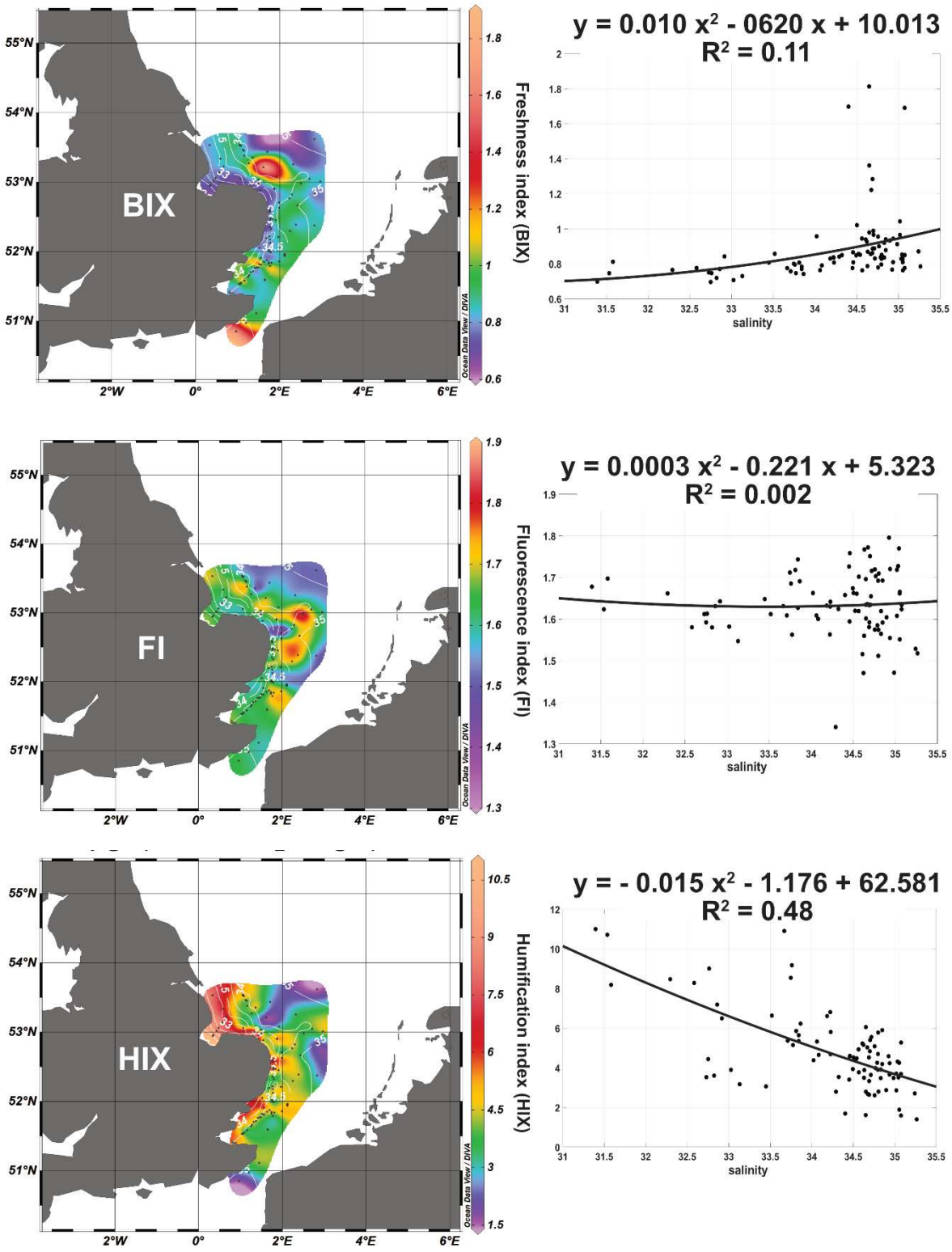

Figure 5.11. *Distribution of the indices BIX, FI and HIX for the samples collected during the cruises onboard the RV Cefas Endeavour between November 2018 and August 2019 in the southern North Sea. The dots represent the stations sampled. On the right the non-linear correlation with the variables against salinity.*

Table 5.5. *Range, average and equation describing the relationship with salinity of the indices BIX, FI and HIX for the samples collected during the cruises onboard the RV Cefas Endeavour between November 2018 and August 2019 in the southern North Sea. The R^2 and the p value of the correlations are also listed.*

Variable	Range	Average	Relationship with salinity	R^2	*p* value
BIX	0.70 – 1.81	0.88	$y = 0.010 x^2 – 0.620 x + 10.0.13$	0.11	< 0.05
FI	1.34 – 1.84	1.64	$y = 0.0003 x^2 – 0.221 x + 5.323$	0.00	> 0.05
HIX	1.40 – 11.00	4.75	$y = - 0.015 x^2 – 1.176 x + 62.581$	0.48	< 0.05

5.2.6 Seasonal variation of DOM

This section discusses the differences of some of the variables considered in the previous section between the meteorological seasons of autumn-winter and spring-summer as explained in section 4.2.4 (Chapter 4). Boxplots for the seasonal differences of all variables and linear correlations of TDN, nitrate plus nitrite, TDP phosphate and DOP with salinity are in Appendix D Figures D1 – D4 and Table D1.

- Seasonal changes in the salinity distribution

Figure 5.12 shows the salinity distribution during autumn and winter and in spring and summer. The number of samples differs between the figures (70 in autumn and winter and 35 in spring and summer). The salinity near the coast is lower in autumn-winter than in spring-summer. The minimum salinity value for autumn-winter was 31.4 whilst for spring-summer it was 33.8. This difference is almost certainly due to seasonality in the riverine influences on the shelf sea. River discharge in the UK is higher in autumn and winter, then in spring and summer as reported by Hannaford and Buys (2012) and by Cooper et al. (2020), the latter for a catchment in East Anglia, due to increased rainfall in winter months and increased evapotranspiration and reduced groundwater levels in the summer months. The autumn-winter cruises had a strong salinity gradient from the coast to the open sea. A salinity gradient is also present in spring-summer (Figure 5.12).

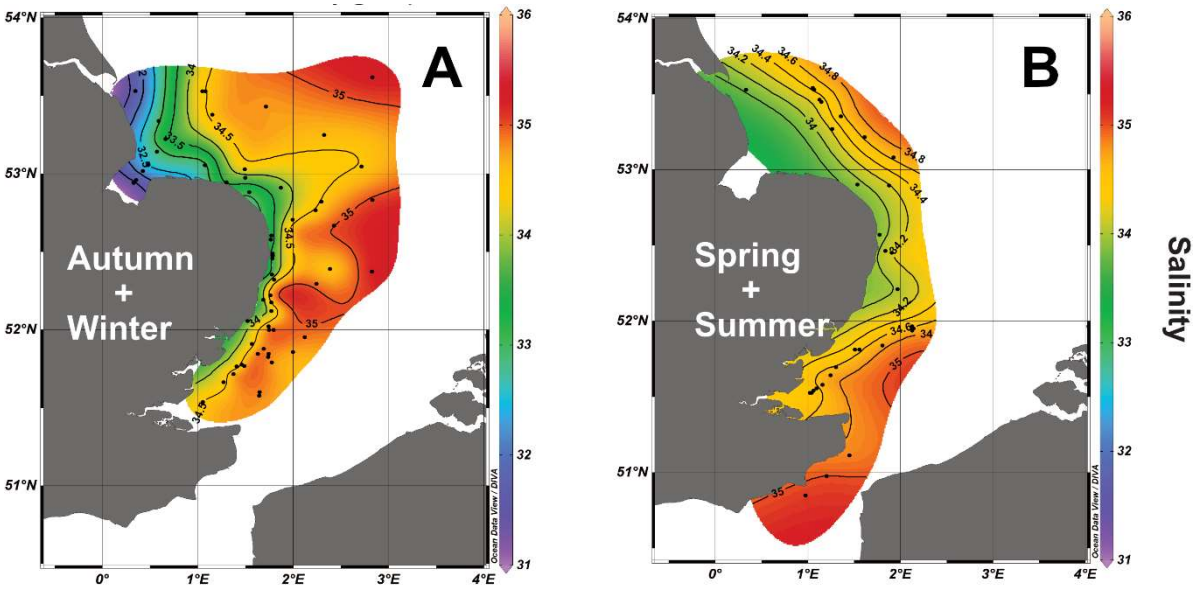

Figure 5.12. *Salinity distribution for the samples collected during the cruises onboard the RV Cefas Endeavour in the southern North Sea in November 2018, November 2019 and February 2020 (A) and May 2019, August 2019 and July 2020 (B). The dots represent the sites sampled.*

- Seasonal changes in the distribution of FDOM

The pie charts in Figure 5.13 show the relative contribution of fluorescence intensity of the PARAFAC components by season, whilst Figure 5.15 shows the FDOM components in autumn-winter and spring-summer. The spatial distribution of the humic-like components is shown only for SC1 because the pattern was similar for SC1, SC2 and SC3, albeit with different intensity maxima. The range of the variables discussed in this section divided by season and the equations of the regressions are shown in Table 5.6.

The three terrestrial FDOM components (SC1, SC2 and SC3) had higher intensities during the autumn and winter seasons, with very low intensity in spring and summer. These components formed the majority of the FDOM for autumn and winter (Figure 5.13), and together they contributed 46.9% to FDOM in spring and summer. SC4, the tryptophan-like component contributed 41.7% of FDOM in spring and summer. In autumn and winter the contribution of the tyrosine-like component SC5 was higher than of SC4, with 20.8% and 17.6%, respectively.

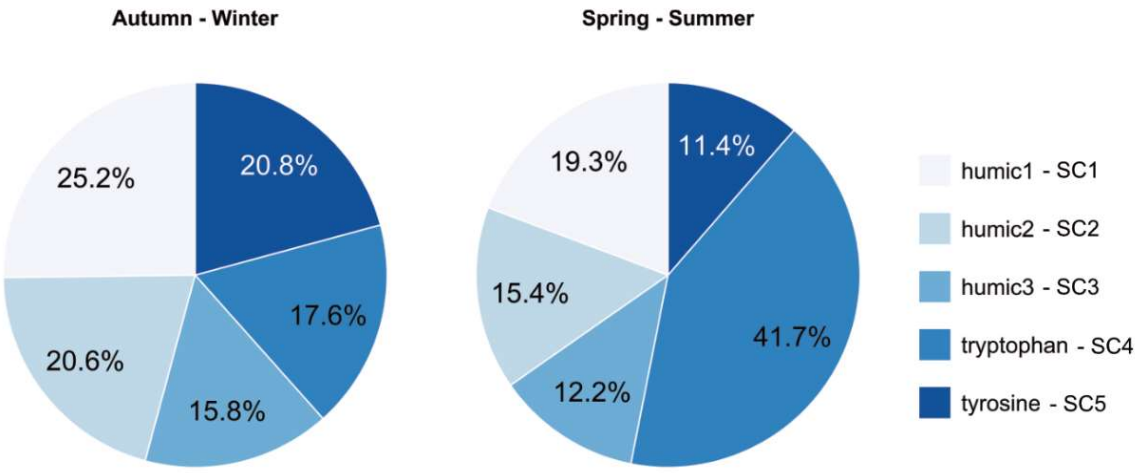

Figure 5.13. *Pie charts with relative contribution in percentage of the five fluorescent components identified through the PARAFAC model for the samples collected on the cruises onboard the RV Cefas Endeavour between November 2018 and August 2019 in the southern North Sea for autumn-winter and spring-summer.*

The intensities of the terrestrial components (SC1 to SC3) were higher around the coast during the autumn-winter months and decreased offshore as the salinity increased (Figure 5.15). Although the fluorescence intensity of the terrestrial components was not high during the spring-summer months, a higher intensity is still visible near the coast, especially at Great Yarmouth (52.5° N and 1.5° E), which is confirmed by the moderate anticorrelation with salinity (Table 5.6) for the three humic-like components. The seasonality of the three allochthonous components is a confirmation of the greater riverine influence during the winter months (as discussed previously for salinity) which decreases during spring and summer. In addition, the very low fluorescence intensity displayed by these three terrestrial components could indicate photodegraded DOM, as the intensity of solar radiation becomes strong but also lasts longer due to long days during the spring and summer months. Most of the southern North Sea is well mixed all year round and only temporarily stratified in summer due to salinity (Otto et al., 1990), causing DOM to be more susceptible to photodegradation due to its shallow depth between 25 – 35 m (Van Ledden et al., 2014). Furthermore, TSS concentrations in spring and summer were lower, increasing light penetration into the water column (Figure 5.14). This was described in Otto et al. (1990) who divided the Southern North Sea into a period with higher TSS (June to November) and a period with lower TSS (December to May), following a study by Visser (1970).

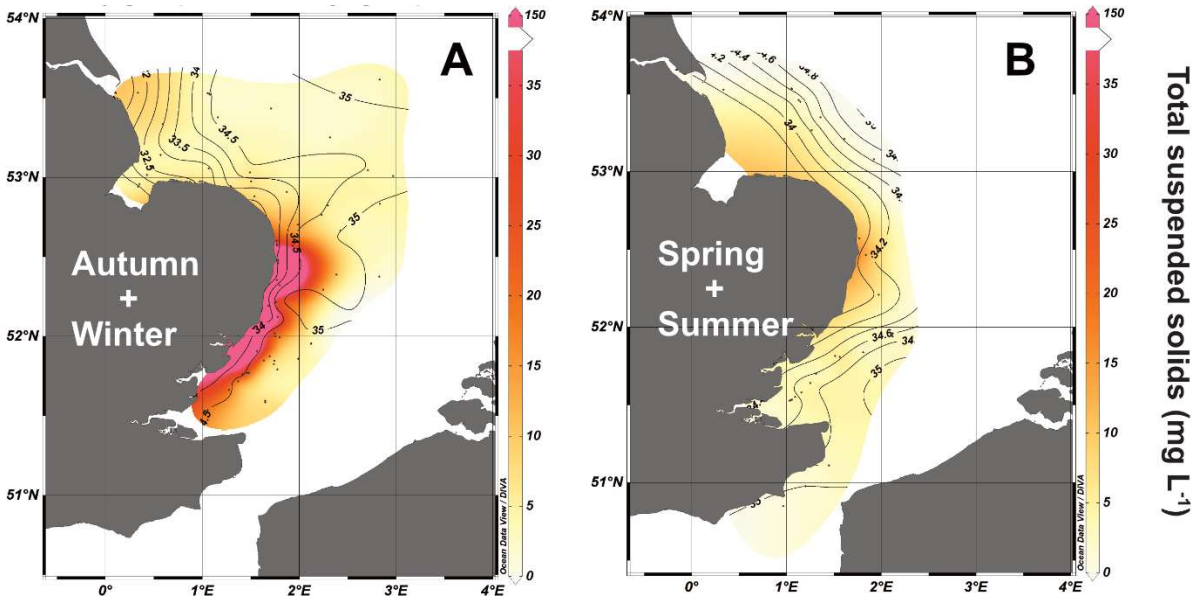

Figure 5.14. *TSS distribution for the samples collected during the cruises onboard the RV Cefas Endeavour in the southern North Sea in November 2018, November 2019 and February 2020 (A) and May 2019, August 2019 and July 2020 (B). The dots represent the sites sampled.*

Interestingly, SC4 and SC5 show different patterns depending on the seasons with SC4 displaying higher intensities in spring-summer and SC5 the opposite. Given that both components are linked to *in-situ* microbial DOM production, it is unexpected that SC5 or the tyrosine-like fluorescence intensity was higher in autumn-winter than in spring-summer. Several studies have shown that the type of molecular structure containing amino acids like tryptophan and tyrosine has an influence on their fluorescence properties. When tryptophan and tyrosine are together in a protein or polypeptide structure instead of the less complex peptide form or as free amino acids, there is an energy emission transfer from tyrosine to tryptophan which causes only the latter to fluoresce (Creighton, 1993; Yamashita and Tanoue, 2003; Lakowicz, 2008; Yamashita et al., 2015). Yamashita and Tanoue (2003) found that when only tryptophan fluorescence was recorded, chlorophyll-*a* concentration was also higher indicating freshly produced DOM from microorganisms, inferring that most of their amino acids are in a protein structure. This could be an explanation for the different patterns of SC4 and SC5 in Figure 5.15. SC4 fluorescence was high in spring-summer whilst SC5 in the same seasons was very low. Note that the chlorophyll-*a* concentration was higher in spring-summer than in autumn-winter (Table 5.6), although the fluorescence of SC5 was probably not solely attributable to phytoplankton. As tyrosine fluoresces when not bound in a protein or polypeptide molecule, it is probable that the high fluorescence of SC5 in autumn-winter in this study is attributable to less freshly produced DOM, perhaps a product of degraded autochthonous DOM after the spring and summer bloom.

Furthermore, high fluorescence intensity values for both SC4 and SC5 were recorded in autumn-winter but they were not spatially overlapping. This could result from their different molecular structure influencing the fluorescence with the lack of tyrosine (SC5) fluorescence indicating DOM in a more complex structure (polypeptide or protein). This difference in their composition and their source (freshly produced versus more degraded autochthonous DOM) can be also supported by the correlations with salinity. While SC4 showed a moderate correlation with salinity (R^2 = 0.47), indicating some DOM coming from terrestrial ecosystems in autumn-winter (Carr et al., 2018), the SC5 relationship with salinity was very weak (R^2 = 0.16), confirming a mostly marine source (Table 5.6).

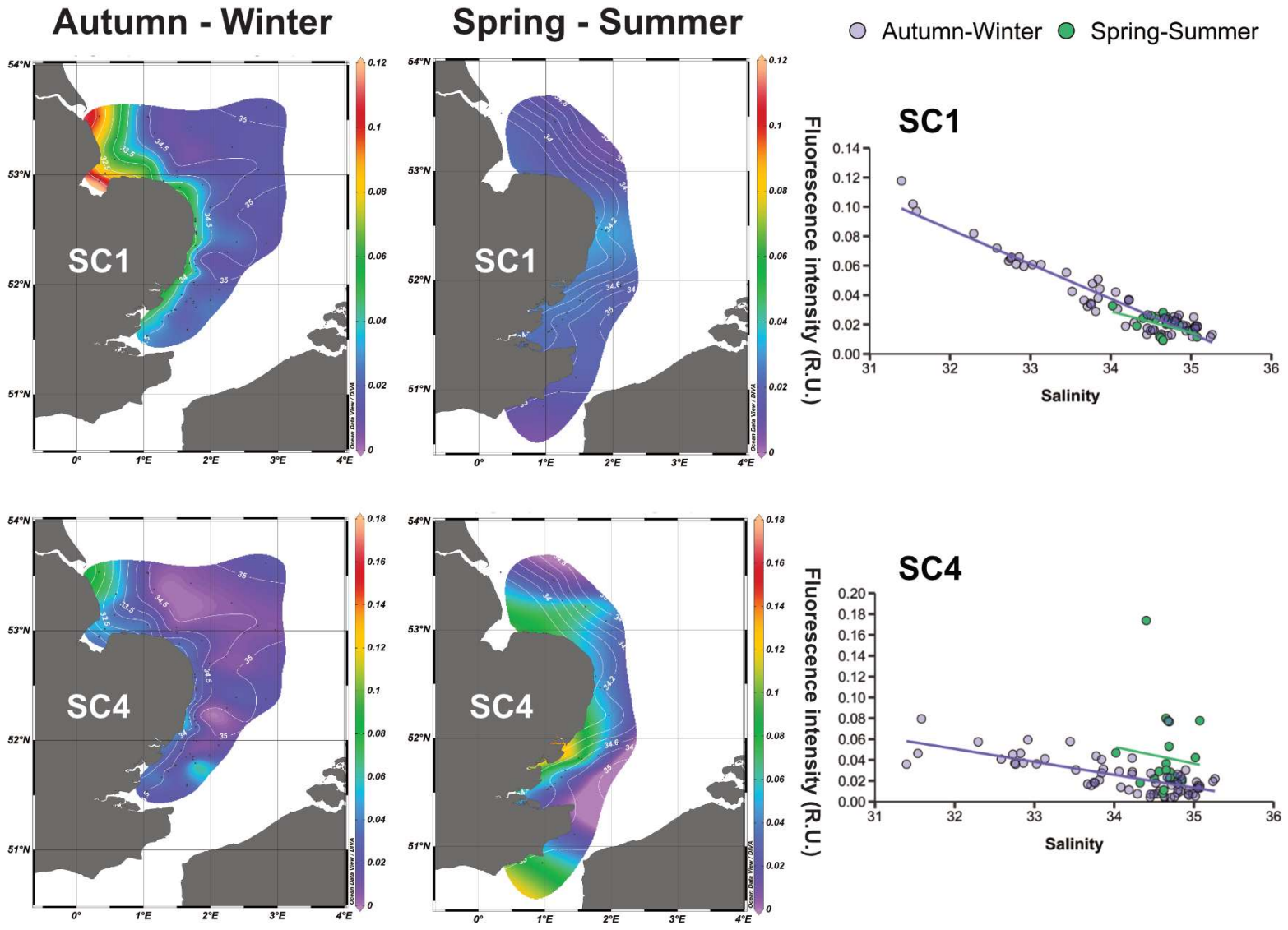
Autumn - Winter
Spring - Summer
Autumn-Winter
Spring-Summer
SC1
SC4
Fluorescence intensity (R.U.)
Salinity
54°N
53°N
52°N
51°N
0°
1°E
2°E
3°E
4°E

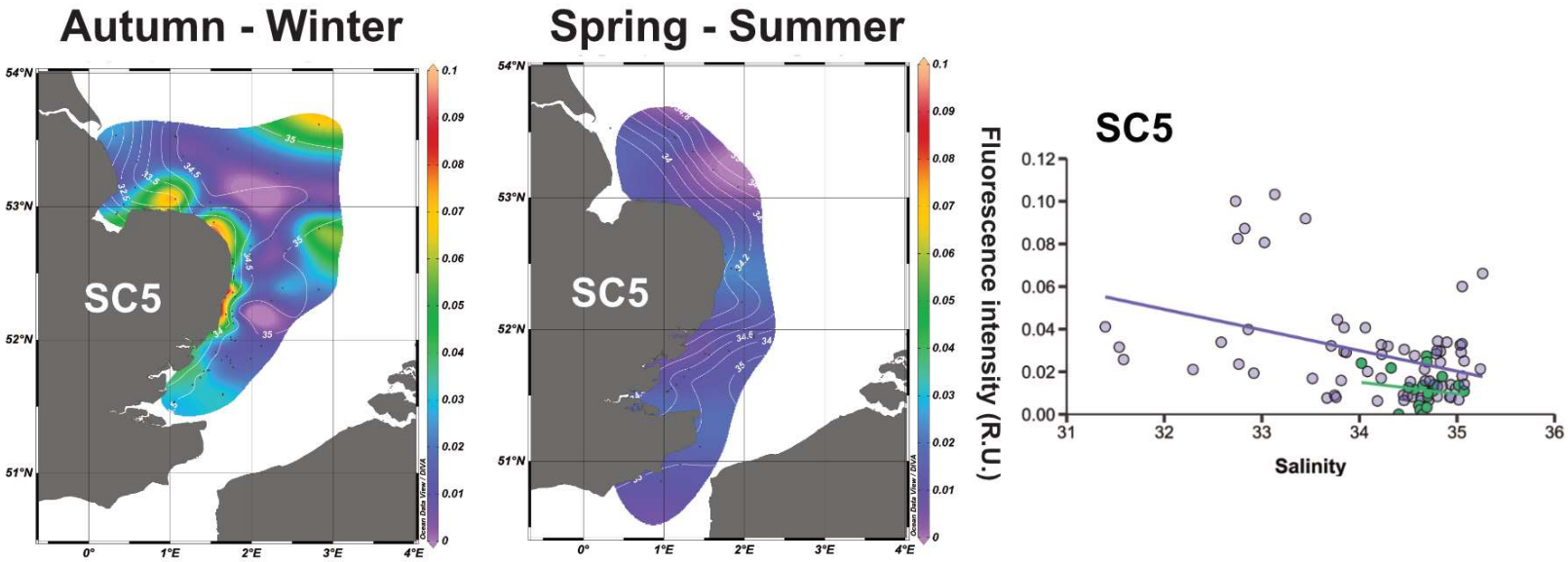

Figure 5.15. *Fluorescence intensity of three of the five components identified through the PARAFAC model for the samples collected during the cruises onboard the RV Cefas Endeavour between November 2018 and August 2019 in the southern North Sea divided by autumn-winter and spring-summer seasons. In addition, on the right the correlations between the fluorescence intensity of the same three components with salinity.*

- Seasonal changes in the distribution of $CDOM_{\alpha 300}$, DOC, $S_{275\text{-}295}$, BIX and HIX

$CDOM_{\alpha 300}$ and DOC displayed dissimilar seasonal patterns suggesting different sources and sinks (Figure 5.16). Overall $CDOM_{\alpha 300}$ values did not vary much between the seasons with an average of 1.82 in autumn-winter and 2.04 for spring-summer, although there were higher values around the coast in autumn-winter. The correlation with salinity is fairly high during autumn-winter ($R^2 = 0.67$), whilst no significant relationship is found during spring-summer. This is somewhat similar to the pattern of the three terrestrial fluorescent components (SC1, SC2 and SC3), although $CDOM_{\alpha 300}$ also displayed some relatively high values offshore corresponding to the high values shown by SC5 in spring-summer. DOC concentration was higher in spring-summer with an average of 115.83 µmol L^{-1} compared to an average of 91.54 µmol L^{-1} in autumn-winter. The DOC relationship with salinity was very different between autumn-winter and spring-summer, even though the correlations with salinity were moderate in both season divisions with $R^2 = 0.21$ in autumn-winter and $R^2 = 0.33$ in spring-summer. These results indicate that CDOM and DOC had different sources depending on the seasons. Whilst the majority of CDOM during autumn-winter could be originating from the land through riverine discharge, in summer CDOM could be more of a microbial product (Helms et al., 2013). As for DOC, the correlations with salinity suggest a minimal influence from the land both in autumn-winter and spring-summer. This could be related to the amount of nutrients coming from terrestrial ecosystems fuelling the growth of phytoplankton and other microbes which in turn affects DOC. Whilst nutrient concentrations around the coast are relatively high all year round (Figure 5.10) fuelling microbial production, in spring-summer algal blooms contribute further to the production of DOC increasing its concentration. $CDOM_{\alpha 300}$ and DOC were very weakly correlated in autumn-winter and did not have a significant correlation in spring-summer (Figure 5.17), a confimation of the decoupling of DOC and CDOM in marine waters where *in-situ* production and photodegradation of DOM are the dominant processes (Stedmon and Nelson, 2015).

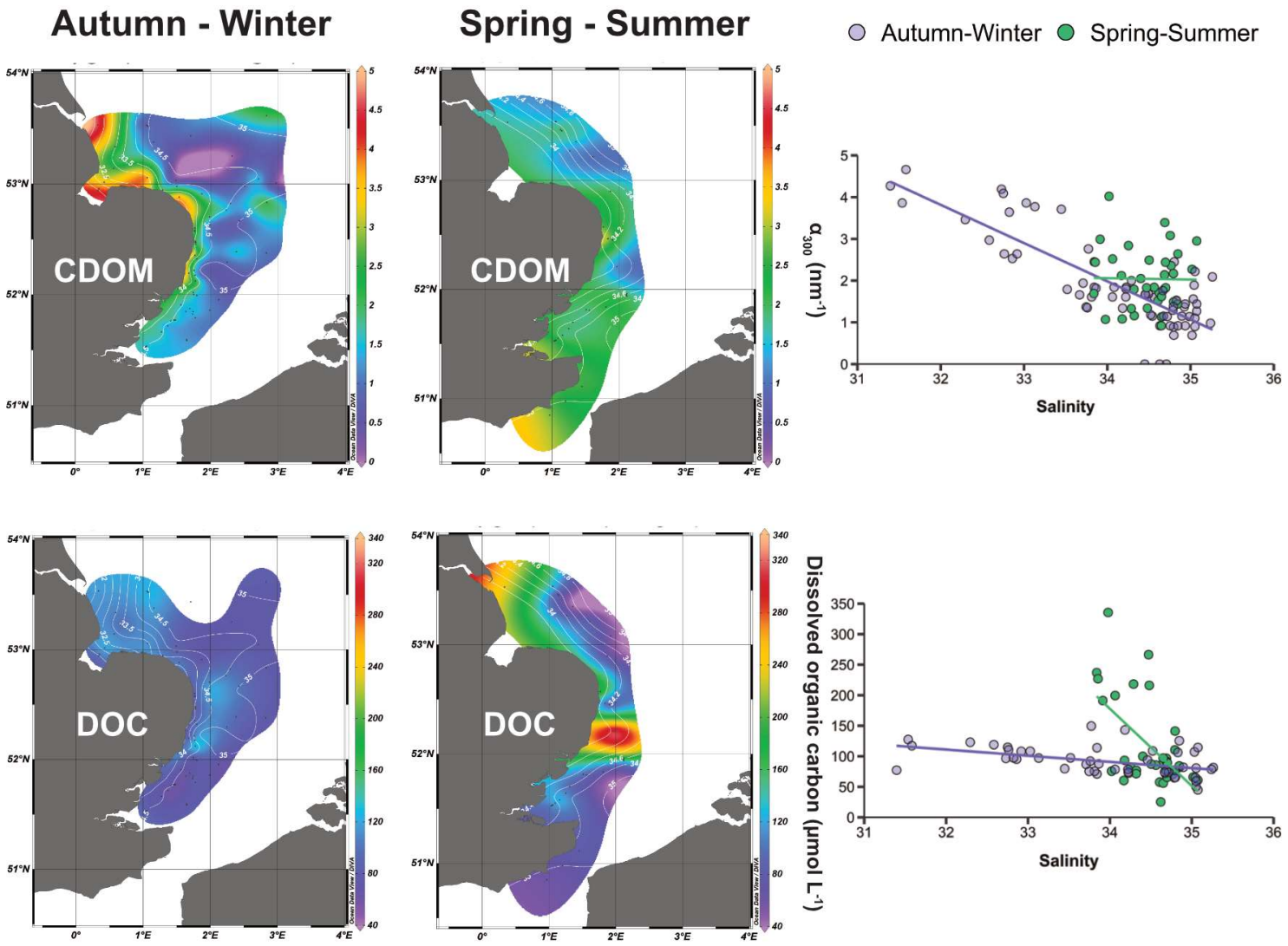
Autumn - Winter
Spring - Summer
Autumn-Winter
Spring-Summer
CDOM
CDOM
DOC
DOC
54°N
53°N
52°N
51°N
0°
1°E
2°E
3°E
4°E
a_{300} (nm^{-1})
Salinity
Dissolved organic carbon (µmol L^{-1})
Salinity

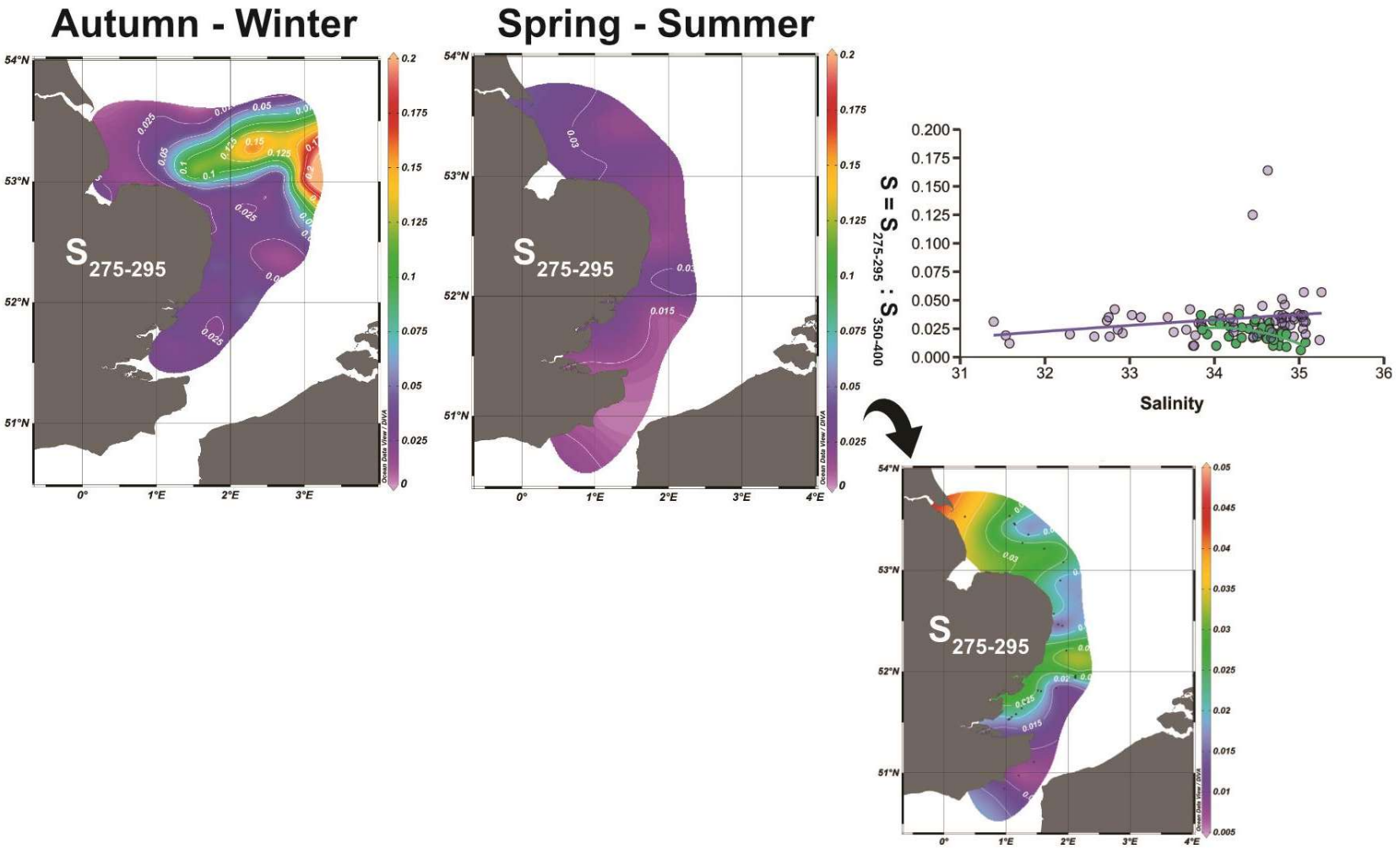

Figure 5.16. *$CDOM_{a300}$, DOC concentrations, and $S_{275-295}$ values (plus rescaled plot of $S_{275-295}$ in spring-summer) for the samples collected during the cruises onboard the RV Cefas Endeavour between November 2018 and August 2019 in the southern North Sea divided by autumn-winter and spring-summer seasons (DOC concentrations are missing for November 2018). In addition, on the right the correlations between the $CDOM_{a300}$, DOC and $S_{275-295}$ with salinity.*

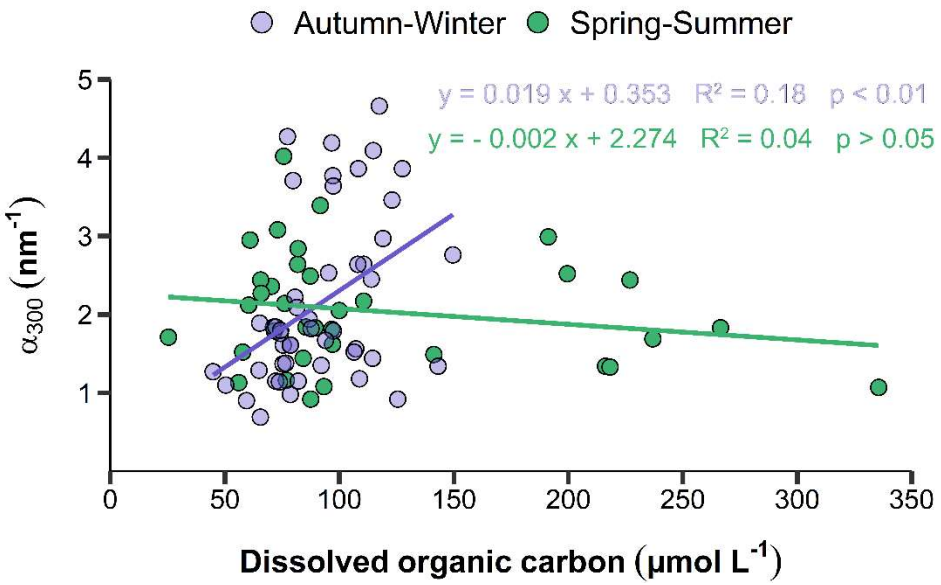

Figure 5.17. *Linear correlation between $CDOM_{\alpha 300}$ and DOC for the samples collected during the cruises onboard the RV Cefas Endeavour between May 2019 and August 2019 in the southern North Sea divided by autumn-winter and spring-summer seasons.*

The effect of photodegradation on DOM is investigated by the $S_{275\text{-}295}$ which shows relatively high values (Figure 5.16). As higher values indicate marine and/or photodegraded DOM, most of the DOM analysed in this study was oceanic or transformed by photoexposure. A cluster of high values is visible in autumn-winter at ~ 53° N and between 1.2° and 3.0° E, that could indicate photobleached DOM possibly progressively moved offshore by the circulation (Figure 2.5 in Chapter 2). High values of $S_{275\text{-}295}$ are also affected by the time that DOM is exposed to solar radiation (Fichot and Benner, 2012) which could be substantial even in autumn given the shallow depth of the southern North Sea. Although it was previously thought that terrestrial DOM was more affected by photobleaching than DOM produced *in-situ*, several studies have shown that *in-situ* produced DOM can also be photolabile (Helms et al., 2013; Stedmon and Cory, 2014). This could explain the elevated $S_{275\text{-}295}$ values during the spring-summer months around the coast. In addition, Helms et al. (2008) also reported the oppsite effect on spectral slopes values depending if DOM was photodegraded or microbially transformed. In that study, S_R values increased when DOM was being photodegraded and they decreased when DOM was microbially processed. Therefore, in this study $S_{275\text{-}295}$ values could indicate a combination of processes (both photodegradation and microbial processing), that could explain the lack of correlation between $S_{275\text{-}295}$ and salinity for autumn-winter and the weak correlation between $_{S275\text{-}}295$ and salinity for spring-summer (Table 5.6). Microbial degradation could result in an increase of the molecular weight of DOM (linked to lower values of $S_{275\text{-}295}$) as microbes could

selectively degrade DOM leaving behind compounds that absorb at long wavelengths (Helms et al., 2008).

Figure 5.18 shows BIX and HIX for autumn-winter and spring-summer. Freshness index (BIX) values were higher in spring-summer with an average of 1.10, indicative of freshly produced DOM, whilst in autumn-winter the average was 0.82 indicating more degraded and older DOM, in line with the findings from FDOM and DOC. In addition, BIX had a weak positive correlation with salinity only in autumn-winter (R^2 = 0.24) suggesting a slight riverine influence of more degraded DOM and an increase of fresh DOM further offshore. Humification index (HIX) values were in agreement with these findings with no significant correlation with salinity in spring-summer and an average value indicating a mixture of autochthonous and allochthonous DOM. A significant negative correlation with salinity in autumn-winter (R^2 = 0.45) indicated more terrestrial DOM near the coast and less terrestrial and more autochthonous DOM offshore.

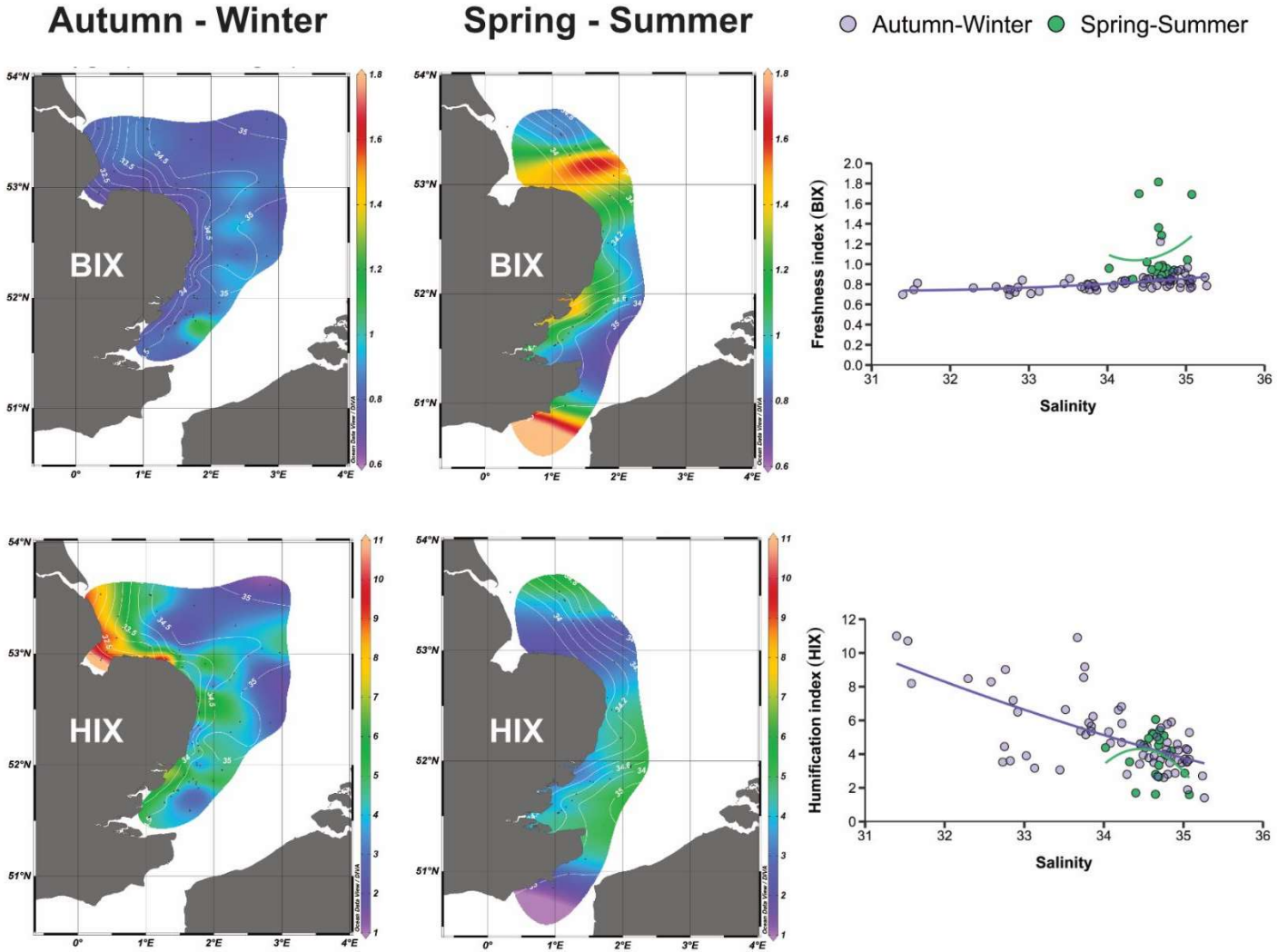

Figure 5.18. *BIX and HIX values for the samples collected during the cruises onboard the RV Cefas Endeavour between November 2018 and August 2019 in the southern North Sea divided by autumn-winter and spring-summer seasons. In addition, on the right the correlations between the BIX and HIX with salinity.*

Table 5.6. *Range, mean and equation describing the relationship with salinity of the fluorescent intensity of the five components identified by the PARAFAC model, $CDOM_{\alpha 300}$, DOC concentration, S_R, BIX, HIX, chlorophyll-a and TSS divided by season for the samples collected during the cruises onboard the RV Cefas Endeavour between November 2018 and July 2020 in the southern North Sea. The R^2 and the p value of the correlations are also listed.*

Season	Variable	Range	Mean	Relationship with salinity	R^2	*p* value
Autumn-winter	Salinity	31.39 – 35.26	34.13			
Spring-summer	Salinity	33.84 – 35.07	34.49			
Autumn-winter	SC1 (R.U.)	0.01 – 0.12	0.03	y = - 0.024 x + 0.839	0.91	< 0.001
Spring-summer	SC1 (R.U.)	0.01 – 0.03	0.02	y = - 0.014 x + 0.523	0.26	< 0.05
Autumn-winter	SC2 (R.U.)	0.01 – 0.09	0.03	y = - 0.016 x + 0.593	0.90	< 0.001
Spring-summer	SC2 (R.U.)	0.01 – 0.03	0.01	y = - 0.011 x + 0.386	0.26	< 0.05
Autumn-winter	SC3 (R.U.)	0.01 – 0.07	0.02	y = - 0.014 x + 0.494	0.90	< 0.001
Spring-summer	SC3 (R.U.)	0.01 – 0.02	0.01	y = - 0.009 x + 0.344	0.28	< 0.05
Autumn-winter	SC4 (R.U.)	0.00 – 0.08	0.02	y = - 0.012 x + 0.447	0.47	< 0.001
Spring-summer	SC4 (R.U.)	0.01 – 0.17	0.04	y = - 0.016 x + 0.594	0.01	> 0.05
Autumn-winter	SC5 (R.U.)	0.01 – 0.10	0.03	y = - 0.010 x + 0.359	0.16	< 0.001
Spring-summer	SC5 (R.U.)	0.00 – 0.03	0.01	y = - 0.006 x + 0.202	0.02	> 0.05
Autumn-winter	$CDOM_{\alpha 300}$ (m^{-1})	0.00 – 4.66	1.82	y = - 0.916 x + 33.123	0.67	< 0.001
Spring-summer	$CDOM_{\alpha 300}$ (m^{-1})	0.92 – 4.02	2.04	y = - 0.032 x + 3.133	0.00	> 0.05
Autumn-winter	DOC (µmol L^{-1})	44.85 – 149.60	91.54	y = - 10.105 x + 434.370	0.21	< 0.01
Spring-summer	DOC (µmol L^{-1})	25.31 – 335.52	115.82	y = - 126.350 x + 4473.750	0.33	< 0.001
Autumn-winter	$S_{275-295}$	0.01 – 0.18	0.03	y = - 0.0002 x^2 + 0.015 x – 0.304	0.04	> 0.05
Spring-summer	$S_{275-295}$	0.06 – 0.04	0.02	y = - 0.015 x^2 + 1.043 x – 17.729	0.26	< 0.05
Autumn-winter	BIX	0.70 – 1.22	0.82	y = 0.007 x^2 – 0.453 x + 7.735	0.25	< 0.001
Spring-summer	BIX	0.85 – 1.81	1.10	y = 0.462 x^2 – 31.75 x + 546.39	0.04	> 0.05
Autumn-winter	HIX	1.40 – 11.00	4.98	y = 0.076 x^2 – 6.609 + 141.79	0.45	< 0.001
Spring-summer	HIX	1.47 – 1.75	1.63	y = -4.463 x^2 + 307.52 x – 5293.3	0.12	> 0.05

Season	Variable	Range	Mean	Relationship with salinity	R^2	*p* value
Autumn-winter	Chla	0.17 – 2.59	0.56	y = 0.01x + 0.229	0.00	> 0.05
Spring-summer	Chla	0.11 – 1.91	0.61	y = -0.924x + 32.717	0.16	< 0.05
Autumn-winter	TSS	1.81 – 145.59	19.53	y = - 5.779x + 217.527	0.04	> 0.05
Spring-summer	TSS	0.89 – 20.44	3.69	y = - 5.722x + 201.064	0.20	< 0.01

5.3 Conclusions

This section draws on the key points from the results discussed in the previous sections with a link to the hypotheses introduced at the beginning of the Chapter.

H1) The composition of DOM in the southern North Sea reflects that of the rivers flowing into it, here exemplified by the rivers Yare and Waveney

H3) DOM components originating from land should display an inverse relationship with salinity, therefore DOC, $CDOM_{\alpha 300}$ and nutrient concentrations should be higher near the coast and decrease further out as near-shore water mixes with the shelf seawater

The hypotheses H1 and H3 posed at the beginning of this Chapter are accepted. The PARAFAC model identified five components. Four of these were also found in the River Yare and the River Waveney (SC1, SC2, SC3 and SC4), three components indicating a terrestrial origin (SC1-SC3) and one protein-like component indicative of *in-situ* DOM production (SC4). The three allochthonous components identified for this dataset were highly negatively correlated to salinity indicating an influence from terrestrial ecosystems, carried as DOM into the shelf sea through riverine discharge. An inverse relationship between the fluorescence of terrestrial components and salinity was also reported by Yamashita et al. (2010) in the eastern Irish Sea, by Carr et al. (2018) in the Celtic Sea and by Painter et al. (2018) in the North Sea. For the protein-like component identified in this dataset, which it has also been found for the River Yare and the River Waveney (SC4), its moderate correlation with salinity in autumn-winter suggests an origin from both riverine discharge and the shelf sea.

In addition to the allochthonous fluorescent components confirming a riverine influence to the shelf sea, also CDOM, nitrate plus nitrite and to a lesser extent

phosphate showed higher concentrations near the coast decreasing further offshore, a result of mixing of river water with seawater (as confirmed by the inverse relationship with salinity). DOC instead, showed a moderate negative correlation with salinity both in autumn-winter and spring-summer. Its highest concentration in spring-summer in combination with an elevated chlorophyll-*a* concentration was an indication of *in-situ* DOC production (probably linked to the higher nutrient concentrations near the coast).

H2) The southern North Sea should show a stronger signal for autochthonous DOM compared to terrestrial DOM as shown by the fluorescence intensity and the fluorescent indexes

This study showed that the southern North Sea was not only is influenced by DOM transported from terrestrial ecosystems, but also by DOM produced *in-situ*. The fluorescence of the protein-like component SC4, was much higher in spring-summer than in autumn-winter. The lower contribution to the fluorescence intensity by the terrestrial components in spring-summer and the values of $S_{275-295}$ indicated photodegradation and/or biodegradation of DOM. This could suggest the utilisation of the inorganic nutrients released through DOM degradation by phytoplankton and other organisms which resulted in the production of DOM. The southern North Sea was characterised by a strong terrestrial signal in autumn-winter and by a strong autochthonous DOM signal in spring-summer. Therefore, hypothesis H2 is accepted.

H4) DOM of riverine origin in the southern North Sea is photo-oxidised and subject to microbial remineralisation depending on the season

This study confirms the findings from Painter et al. (2018) and Dai et al. (2012). They both reported a significant terrestrial signal in the southern North Sea off East Anglia, but could not confirm the origin of this signal as the study from Dai et al. (2012) did not include rivers in East Anglia, whilst the analysis from Painter et al. (2018) did not have sampling points close to the East Anglian coast. This chapter however confirms the terrestrial signature inferred by these earlier investigations. Furthermore, this study also confirms the suggestion from Painter et al. (2018) of removal of terrestrial DOM at increasing salinities by photodegradation indicated by the $S_{275-295}$ values. High $S_{275-295}$ values in some sampling points off the coast could suggest a progressive increase of photodegradation of DOM from the coast to the open sea and/or an increase in $S_{275-295}$ with the time of DOM photoexposure (Fichot and Benner, 2014; Painter et al., 2018). The fluorescence intensity of the tyrosine-like component (SC5) confirmed the presence of biodegraded DOM especially in autumn-

winter, whilst BIX confirmed production of DOM in spring-summer and HIX indicated microbial processing in both autumn-winter and spring-summer. Through the analysis of these variables, it is possible to confirm that both photodegradation and microbial remineralisation occur throughout the year in the southern North Sea. H4 is accepted as photodegradation and biodegradation affects DOM in the study area.

This study helps understanding the fate of the DOM flux transported from the rivers into the southern North Sea through samples taken throughout the year. This study confirms that the DOM in the sampling area in the southern North Sea partially has the same composition as the DOM coming from the rivers of the East Anglia region. This research also confirms the riverine origin of DOM in the southern North Sea suggested by Painter et al. (2018). These findings also shed a light into the seasonality of DOM characteristics and the processes DOM is subject to.

Chapter 6

Conclusions, limitations, and future work

This chapter brings together the main findings and discussions of this research. In addition, the limitations and the uncertainties of the sampling and calculations of this study will be addressed. Finally, there will be an outline of possible future directions for this research.

6.1 Key findings

All the outcomes from the previous chapters helped in addressing the main aim of the thesis, namely: *What happens to DOM within rivers affected by tidal cycles as it travels downstream and enters the shelf sea?* All three studies were conceived with the aim of having a better understanding of DOM within the land-ocean aquatic continuum. Until recently, terrestrial ecosystems and marine ecosystems were studied separately. Moreover, within terrestrial ecosystems, rivers and estuaries have been analysed independently. Only in the last decade has the interconnection of terrestrial and marine ecosystems been recognised (Xenopoulos et al., 2017; Regnier et al., 2022), although even many studies from land-to-sea do not go further than the estuary as in García-Martín et al. (2021).

This research helped understanding fluxes, composition and molecular changes of DOM as it travels from rivers to the sea with relatively high resolution and systematic sampling which has not been done previously in the study area of interest, although the North Sea is one of most studied shelf seas (Thomas et al., 2005). This research provided an insight into the effects of tidal cycles on DOM dynamics that is lacking when researching DOM processes through the LOAC (Indivero et al., 2021). It also highlighted that the assumption that similar sources of DOM will undergo similar processes is not always true, stressing the importance of the local environmental context (Lapierre and del Giorgio, 2014), such as the differences in hydrological connectivity between surface and groundwater, which has been only investigated by (Yates et al., 2016). As an example of the importance of the local environmental context, the two rivers investigated in this research showed lower TSS concentrations upstream than in the estuary and coastal waters, probably due to coastal erosion or resuspension of solids from tidal mixing. This is in opposition to coastal waters which are generally clear (Wilson and Heath, 2019).

In terms of DOM composition, the fluorescent components found in the rivers studied and in the sea were consistent, as DOM was identified to have a terrestrial origin,

produced by microbial remineralisation and freshly produced *in-situ*. Only one component was found only in the North Sea, associated with degraded DOM produced *in-situ*. This confirmed the results from the fluxes calculated for the two rivers investigated, which showed that DOM was subject to several processes as it was transported within the rivers to the sea (including microbial processing, photodegradation, biological production, resuspension, flocculation and tidal mixing), with nitrate and nitrite decreasing traveling downstream, whilst phosphate and DOP increasing in the estuary (possibly due to wastewater inputs and solids resuspension), and DOC behaving conservatively. This is another example of how important is to study the local environmental context previously mentioned, particularly, as a recent study by García-Martín et al. (2021) concluded that estuaries with agricultural and (sub)urban land uses showed non-conservative behaviour for DOC. In addition, the study concluded that these types of estuaries produce double the DOC compared to freshwater endmember. Whilst this might be true for some estuaries, it is not always the case, as demonstrated by the results in this study, where the estuarine flux estimated for the River Yare and the River Waveney showed that the majority of freshwater DOC had a conservative behaviour, transporting DOC into the shelf sea.

The spectral slopes and fluorescent indices also showed that as DOM travelled through the rivers and into the shelf sea, its molecular size varied depending on the processes, resulting in a change in reactivity as it was transported (Helms et al., 2008; Helms et al., 2013; Stubbins, 2013). These results, in addition with the fluxes showing a conservative behaviour of DOC reiterate the complexity of investigating DOM dynamics from a LOAC perspective, demonstrating that no matter all the processing DOM undergo from the freshwater to the marine endmember, they can counterbalance themselves, resulting in an unexpected result (Abril et al., 2002). This is even more important if taken into account that the aquatic systems investigated in this research are small compared to catchments such as the Thames or the Humber. The small size of the catchments investigated in this study, does not mean a less important contribution to the carbon cycle, as they are an important source of DOC to the sea as also reported by Kitidis et al. (2019), stating that smaller estuaries have shorter residence times and therefore contribute more to the shelf sea air-sea flux. Furthermore, based on the estimates from the estuarine fluxes of the two East Anglian rivers studied in this research, their DOC export represents 0.12% of the post-estuary flux based on Kitidis et al. (2019) for the north west European shelf. As DOM was exported into the shelf sea, results showed a terrestrial signature that decreased moving offshore and with increase in salinity continuing to behave conservatively confirming the suggested results from Painter et al. (2018) in the Southern North Sea. Together with mixing, the terrestrial signature was found to be lost further offshore as a result of photodegradation and microbial processing, whilst both the fluorescent components and

spectral slopes indicated that DOM was being produced mostly in spring and summer. As river discharge is higher in autumn and winter, the terrestrial signal was also higher during these seasons, which it could lead to a major increase in terrestrial DOM export to the shelf sea, due to river discharge increase following climate change. Following Traving et al. (2017) the increase in river loads (and consequently DOM and inorganic nutrients) due to climate change, will affect the microbial community composition and function, with changes to the nutrient biogeochemistry as well. Furthermore, considering the research from Jiao et al. (2014) where DOM reactivity can change depending on the biogeochemical setting, or its bioavailability can differ depending on the microbial community present, a shift in DOM biogeochemistry and microbial composition and function could significantly affect the DOM dynamics as it travels through the LOAC.

These results highlighted the importance not only of the lateral DOM dynamics from rivers to the sea and the differences in DOM composition and dynamics between two river catchments with same land uses, but also the risk of generalisation. Because the LOAC is characterised by many components and processes, it would be incorrect to assume that it is the same for every catchment, as shown in this study with the differences with the study by García-Martín et al. (2021). In addition, this study has shown that even small estuaries are an important source of DOC to the sea, therefore not only is important to include LOAC processes into IPCC estimates and regional models, but it would be accurate if the LOAC data would also take into account the differences between catchments and of the environmental context. Those factors can play an important part in variations in DOM composition, size and reactivity, stressing the need to study DOM at regional scales, with a high spatial and temporal resolution, to enable greater understanding of the effects of climate change on DOC fluxes, processes and on the atmospheric CO_2 uptake capacity of marine ecosystems. (Stedmon and Cory, 2014; Worrall et al., 2018; Regnier et al., 2022).

6.1.1 Influence of tidal cycles on DOM dynamics in rivers

During two sampling days in July 2020, two points along the River Waveney and the River Yare were sampled hourly for 12 hours. DOM was investigated during the tidal cycle to understand the effect of seawater cyclically entering the rivers. The main hypothesis stated that DOM would mix conservatively as seawater was transported upstream by the tidal cycles. Interestingly, the tidal cycle affected DOM differently in the two rivers for those sampling days. They key findings are:

1. Most of the variables analysed for DOM in the River Yare mixed conservatively as freshwater and seawater mixed as a result of the tidal cycle. These include DOC, CDOM, FDOM, TDN, nitrate plus nitrite and TDP.
2. In the River Waveney, a salt wedge developed as seawater entered the river through the tidal cycle. The seawater pushed the less dense freshwater upwards, resulting in water column stratification.
3. The salt wedge in the Waveney affected the microbial community resulting in an increase of both DOM production and remineralisation due to the longer residence time of the freshwater on top of the seawater layer. This was found in DOC, FDOM and the fluorescence indices. There was also an effect on TDN, nitrate plus nitrite, TDP and DOP.
4. All the variables were subject to conservative mixing as the water column stratification dissipated in the Waveney.
5. In the River Yare the correlation between DOC and CDOM was high, whilst it was lower in the River Waveney, possibly due to production of colourless DOC during the salt wedge.
6. In both rivers, phosphate and ammonium were affected by sediment resuspension that released them back into the water column. In addition, concentrations of ammonium in the River Yare increased by salinity mediated release, whilst ammonium and phosphate in the River Waveney were also affected by biodegradation of DOM by the microbial community due to the water column stratification.
7. TSS in both rivers was correlated to salinity and its concentrations were higher at the seawater end member than at the freshwater end member. As the southern North Sea is very shallow, this suggests TSS enters the rivers through the tidal cycle. High TSS concentrations in seawater may be produced by coastal erosion or tidal mixing.
8. The PARAFAC analysis identified six components, four of which indicate DOM of terrestrial origin, one suggests plant degradation and the last one is linked to DOM produced *in-situ*. One of the components indicative of terrestrial DOM has been previously found in rivers with waters affected by wastewater and agriculture.
9. A principal component analysis identified pronounced differences in the DOM biogeochemistry of the two rivers, with the River Waveney having more prominent components indicating DOM of terrestrial origin and produced by biodegradation.

Conversely, the River Yare was found to have more prominent components indicative of *in-situ* produced DOM.

This research emphasises the need to incorporate the influence of tidal cycles on DOM dynamics from rivers to the sea in future studies, especially for those systems highly influenced by tidal changes as also highlighted by Indivero et al. (2021) and in García-Martín et al. (2021) in the discussion of the limitations of their work.

6.1.2 DOM dynamics and fluxes from land to sea over a year sampling

Between November 2018 and December 2019, the River Yare and the River Waveney were sampled monthly. The aim of this study was to investigate DOM composition and the processes is subject to as it travels downstream. In addition, temporal changes of DOM were studied and both riverine and estuarine fluxes were calculated to see whether DOM is produced, removed or mixed between freshwater and seawater and how much DOC is exported into the southern North Sea. Estuarine fluxes of FDOM were also calculated to quantify how much DOM of terrestrial and produced or degraded *in-situ* enters the southern North Sea. The key findings are:

1. DOM in these rivers is composed of terrestrial material, DOM biodegradation products and DOM produced *in-situ*. Six components were identified through PARAFAC, as in Chapter 3, four of which were linked to terrestrial DOM and the other two indicative of microbial processing and *in-situ* production of DOM.
2. The results from the PCA confirmed the difference in DOM composition between the rivers, as found in Chapter 3, and confirmed by the fluorescence intensity of the components identified through PARAFAC. The two rivers are quite similar in terms of land use, but because of their different bedrock geology, the River Yare is fed more by groundwater, whilst the River Waveney is more affected by surface runoff. This impacts on how DOM is transformed and reaches the rivers and is the cause of their differences in DOM composition.
3. Inorganic nutrients, nitrate plus nitrite and phosphate, formed the majority of TDN and TDP, respectively, in rivers. In the estuary, nitrate plus nitrite formed most of TDN, whilst DOP formed most of TDP.
4. The increase in DOC concentration in spring and summer and the increase in DOC concentration in winter due to high river flow resulted in a lack of seasonality in the

freshwater end member, whilst DOC concentration was higher in winter in the estuary than in summer.

5. Nitrate plus nitrite and DON concentrations were higher in winter and spring than in summer and autumn at the freshwater end member and in the estuary. This is due to their transport through surface runoff and overland flows, increasing their concentrations in winter, and the higher biological activity in spring and summer, resulting in a decrease in their concentrations.

6. Phosphate showed opposite seasonality to nitrate plus nitrite and DON in the freshwater end member with higher concentrations in autumn and summer due to increased remineralisation of DOP and a stronger influence of release from wastewater. The lower phosphate concentration in winter is linked to sediment adsorption of phosphate, whilst in spring phosphate is used by the microbial community. DOP did not show any seasonality in the freshwater end member, but it had high concentrations in the estuary during spring and summer, a result of DOP production by autotrophs and heterotrophs.

7. The absorption and fluorescence indices indicated that DOM in the rivers and the estuary is transformed by biodegradation, *in-situ* biological production, photodegradation, suspended solids resuspension and adsorption to sediments. Another important process affecting DOM from land to sea was conservative mixing.

8. Biodegradation of DOM occurred steadily throughout the year, whilst DOM production was high in spring and summer. Photodegradation was found only in the estuary and was strongest in summer. Conservative mixing of DOM occurred in both rivers throughout the year. Other processes adding or removing DOM were stronger in the Yare than in the Waveney.

9. DOC fluxes between the freshwater and the seawater end members showed that most of DOC mixes conservatively in the River Waveney, whilst there is additional production in the River Yare. Moreover, the distribution of DOC within the rivers changed during the year and did not show the same behaviour from month to month.

10. Estuarine fluxes indicated that overall, during 2019, DOC was mixing conservatively from land to sea, whilst there was a removal of TDN and nitrate plus nitrite and a production of TDP, and particularly of DOP between the freshwater and seawater end members.

11. The Broadland Rivers Catchment in East Anglia exported a total of 3.2 ± 1.81 Gg yr^{-1} of DOC, 1.26 ± 0.89 Gg yr^{-1} of TDN and 0.13 ± 0.06 Gg yr^{-1} of TDP to the shelf

sea. In addition, 67.5% of those amounts represents DOM of terrestrial origin (3.09 ± 1.87 Gg yr^{-1}) and 32.5% represents DOM produced and remineralised *in-situ* (1.49 ± 0.90 Gg yr^{-1}).

12. DOC transported within small estuaries tends to undergo little transformation due to shorter residence times than in larger estuaries. Thus, small estuaries represent a source of DOC to the sea.

This study showed that rivers which have similar land use and location, can have different DOM composition and distribution throughout the year due to differences in hydrological connectivity between surface water and groundwater. This has been seldom studied and to my knowledge, only the study by Yates et al. (2016) has investigated this topic.

In addition, this research highlighted the need of high-resolution sampling within rivers, including estuaries, because of the different processes happening at the freshwater and the seawater end members. Generally, investigations on this subject cover only few months across the year or a couple of seasons, as stated also in a review of global studies of DOM distribution along the aquatic continuum by Massicotte et al. (2017), stating that usually samples are collected between the summer months (June to August). As a confirmation of this, in a recent study of DOM in 13 estuaries around Great Britain by García-Martín et al. (2021), samples were collected during five sampling campaigns covering five months over two years (April, July and October 2017, and January and April 2018).

Moreover, out of the over 12,000 studies reviewed across rivers, lakes and oceans by Massicotte et al. (2017), whilst 38.2% were carried out in rivers, only 10.7% investigated DOM in estuaries.

6.1.3 DOM composition and spatial-temporal changes in the southern North Sea

This section reports the key conclusions on DOM dynamics in the southern North Sea from six cruises on board of the RV *Cefas Endeavour* between November 2018 and July 2020. The aim of this study was to understand what happens to DOM and what changes and processes it is subject to when it gets exported from the estuary. The key findings are:

1. The PARAFAC analysis identified five components in the shelf sea. DOM mainly had the same components found in the rivers (SC1 to SC4) except for one

component which was found only in the shelf sea (SC5). Of the components also found in the rivers (SC1, SC2, SC3 and SC4), three were of terrestrial origin (SC1 to SC3), while SC4 indicated DOM produced *in-situ*. In addition, another component indicative of DOM produced *in-situ* was identified only in the southern North Sea (SC5).

2. As the terrestrial components (SC1 to SC3) reached the shelf sea, they showed a decrease with increase in salinity, an effect of freshwater and seawater mixing. SC4 and SC5 showed higher values near the coast but were not correlated to salinity, indicating their *in-situ* origin.
3. As a result of riverine DOM transported into the shelf sea, CDOM, nitrate plus nitrite and phosphate concentrations showed a decrease with increasing salinity. In addition, TSS was not correlated to salinity, but high concentrations were found near the coast. This could indicate the contribution of coastal erosion and sediment resuspension near the coast (e.g., by tidal mixing).
4. DOC and CDOM did not correlate as a result of different processes affecting the two variables. This puts into question the common practice of inferring DOC concentrations from CDOM values (as reported in section 6.1.1).
5. Most of the terrestrial organic matter coming from rivers is delivered to the southern North Sea during autumn and winter.
6. The processes affecting DOM in the southern North Sea are mixing between riverine freshwater and seawater (especially in autumn and winter), production in spring and summer, photodegradation of DOM of terrestrial origin and biodegradation throughout the year.
7. DOM coming from the Rivers Waveney and Yare is therefore mixed and processed to the point that the terrestrial signal is lost further offshore. The production of DOM in response to the riverine input of nutrients, is also limited to the coast and a few areas further offshore. This is due to the light-limitation in the southern North Sea as a result of high TSS concentrations. This suggests that off the coast of the southern North Sea more degradation than *in-situ* production of DOM occurs.

This study highlights the need of high resolution of near shore sampling in order to understand the temporal dynamics and the fate of DOM entering the sea from terrestrial ecosystems. Although the North Sea is one of the most studied shelf seas (Thomas et al.,

2005), Painter et al. (2018) highlighted a gap in the understanding of the processes affecting terrestrial DOM in shelf seas.

Another important finding from this study is the seasonal variability of the riverine input of DOM and of the processes DOM is subject to when it enters the shelf sea, which is also mentioned by Painter et al. (2018). Only few studies of DOM in the North Sea used fluorescence to understand DOM composition and, to my knowledge, none of those covered all four seasons to investigate the intra-annual variability of DOM sources and sinks in the southern North Sea (Laane and Kramer, 1990; Obernosterer and Herndl, 2000; Osburn and Stedmon, 2011; Miranda et al., 2018; Painter et al., 2018).

6.2 Limitations

The themes investigated in this thesis were not without limitations, due to the methods used for collecting, storing, and analysing the variables, but also due to some calculations which implied several assumptions. A list is provided below with a brief discussion:

1. River water samples were collected from the water surface near the riverbank using a bucket on a throwline. Ideally, water samples should be collected from the centre of the river channel at ~ 50% depth where the water is likely to be well-mixed and thus more representative of the overall composition. Moreover, surface samples only do not reflect possible changes throughout the water column (e.g., salt wedge) both in rivers and in the sea.
2. Water samples were collected with a HDPE bucket from the rivers, and all water samples were filtered in the field and on the ship using a syringe and a syringe filter. These methods could lead to contamination, so to avoid this, the utmost care has been taken. Measures included the rinsing of the bucket at every sampling point before the sample was collected. When using the syringe and the syringe filter, nitrile gloves were used and changed at every sampling point in the rivers. To verify that the contamination was kept at a minimum, a field blank was also filtered in the field, using ultrapure water carried from the lab. All the containers used were cleaned and treated before the sampling following widely accepted methods (Yoro et al., 1999; Wurl, 2009). These steps were necessary to minimise contamination of the samples.
3. The storage of the water samples immediately after collection could contribute to uncertainty in the variables analysed for DOM. To minimise this, ice was used to refrigerate the samples before reaching the laboratory where they were frozen, whilst they were frozen immediately after filtering on the ship. Methods commonly

employed were used (Dore et al., 1996; Wurl, 2009; Kotlash and Chessman, 1998; Peacock et al., 2015).

4. The monthly river samples were collected far apart in time, albeit with smaller intervals than most similar studies. Whilst this allowed to have data for every month for 14 months, it does not consider changes happening at short timescales. An example was the study of the tidal effects on DOM in Chapter 3.
5. The calculation of the DOC fluxes between the freshwater and the seawater endmember, of the DOM riverine and estuarine fluxes, and the fluorescent DOM estuarine fluxes required several assumptions (as explained in Chapter 4). Although the uncertainty of these estimates has been calculated, this was also based on an assumption, therefore allowing for bias in these fluxes.

6.3 Future work

In view of the findings and the limitations from this project, below are given some directions to develop this research further.

1. In addition to the sampling of the River Yare and the River Waveney, the sampling of the River Bure should be included if the study is continued, so to capture the full picture of the DOM composition and variability in the Broadland Catchment. Moreover, the sampling should be carried out at higher resolution than once per month, with at least weekly sampling and ideally continuous monitoring. Such a continuous monitoring system could be set up with probes measuring the river discharge, chlorophyll-*a*, fluorescent DOM, turbidity and coloured DOM (Coble, 2013; Cooper et al., 2018; Carstea et al., 2020; Cooper et al., 2020), as well as automated collection of water samples (Martin et al., 2004; von Freyberg et al., 2020) to capture the full tidal cycle and any variations in DOM at a small scale. Moreover, the need for higher resolution sampling is of concern also for the marine end member. If possible, it would be beneficial to have monthly samples from the southern North Sea, to allow the study of DOM within the land-ocean aquatic continuum to allow for intra- and inter-annual comparisons.
2. The continuous monitoring of DOM within the rivers and the estuary of the Broadland Catchment, and within the southern North Sea, would allow more accurate estimates of DOC, DON, DOP and inorganic nutrients fluxes. It would be beneficial for biogeochemical marine models to understand and accurately quantify the

estuarine export and the composition of DOM into the sea. Smaller estuaries with short residence times compared to larger rivers tend to be a source of DOC to the sea (as found in this study). The study of DOM at high spatial and temporal resolution would enable greater understanding of the effects of climate change on DOC fluxes, processes, and on the atmospheric CO_2 uptake capacity of marine ecosystems (Stedmon and Cory, 2014; Worral et al., 2018; Regnier et al., 2022).

3. The data collected could be used for the establishment of a land-ocean aquatic continuum data network collecting and exchanging DOM data from different institutions not only across the UK, like the UK Environmental Change Network supervised by the UK Centre for Ecology and Hydrology (Rennie et al., 2017), but also throughout Europe via the ICOS (Integrated Carbon Observation System) network for carbon measurements across terrestrial and marine ecosystems.

Reference List

Abdellatif, M., Atherton, W. and Alkhaddar, R. (2014) 'Assessing combined sewer overflows with long lead time for better surface water management', *Environmental Technology*, 35(5), pp. 568–580. Available at: https://doi.org/10.1080/09593330.2013.837938.

Abdi, H. and Williams, L.J. (2010) 'Principal component analysis: Principal component analysis', *Wiley Interdisciplinary Reviews: Computational Statistics*, 2(4), pp. 433–459. Available at: https://doi.org/10.1002/wics.101.

Abril, G. *et al.* (2002) 'Behaviour of Organic Carbon in Nine Contrasting European Estuaries', *Estuarine, Coastal and Shelf Science*, 54(2), pp. 241–262. Available at: https://doi.org/10.1006/ecss.2001.0844.

Alam, M.M. *et al.* (2021) 'Status and advances in technologies for phosphorus species detection and characterization in natural environment- A comprehensive review', *Talanta*, 233, p. 122458. Available at: https://doi.org/10.1016/j.talanta.2021.122458.

Álvarez-Salgado, X.A. and Miller, A.E.J. (1999) 'Dissolved Organic Carbon in a Large Macrotidal Estuary (the Humber, UK): Behaviour During Estuarine Mixing', *Marine Pollution Bulletin*, 37(3), pp. 216–224. Available at: https://doi.org/10.1016/S0025-326X(98)00156-8.

Amaral, V. *et al.* (2016) 'Strong linkages between DOM optical properties and main clades of aquatic bacteria', *Limnology and Oceanography*, 61(3), pp. 906–918. Available at: https://doi.org/10.1002/lno.10258.

Amaral, V. *et al.* (2020) 'Distribution of dissolved organic matter in estuaries of the southern Iberian Atlantic Basin: Sources, behavior and export to the coastal zone', *Marine Chemistry*, p. 103857. Available at: https://doi.org/10.1016/j.marchem.2020.103857.

Amaral, V. *et al.* (2021) 'Linkages between greenhouse gases (CO2, CH4, and N2O) and dissolved organic matter composition in a shallow estuary', *Science of The Total Environment*, 788, p. 147863. Available at: https://doi.org/10.1016/j.scitotenv.2021.147863.

Amaral, V., Romera-Castillo, C. and Forja, J. (2020) 'Dissolved Organic Matter in the Gulf of Cádiz: Distribution and Drivers of Chromophoric and Fluorescent Properties',

Frontiers in Marine Science, 7, p. 126. Available at: https://doi.org/10.3389/fmars.2020.00126.

Andersen, C.M. and Bro, R. (2003) 'Practical aspects of PARAFAC modeling of fluorescence excitation-emission data', *Journal of Chemometrics*, 17(4), pp. 200–215. Available at: https://doi.org/10.1002/cem.790.

Andersson, C.A. and Bro, R. (2000) 'The N-way Toolbox for MATLAB', *Chemometrics and Intelligent Laboratory Systems*, 52(1), pp. 1–4. Available at: https://doi.org/10.1016/S0169-7439(00)00071-X.

Anne-Sophie, M.-H. *et al.* (2015) 'Temporal analysis of E. coli, TSS and wastewater micropollutant loads from combined sewer overflows: implications for management', *Environmental Science: Processes & Impacts*, 17(5), pp. 965–974. Available at: https://doi.org/10.1039/C5EM00093A.

APHA (1999a) '2540 SOLIDS (1999)', in *Standard Methods For the Examination of Water and Wastewater*. American Public Health Association (Standard Methods for the Examination of Water and Wastewater). Available at: https://doi.org/10.2105/SMWW.2882.030.

APHA (1999b) '10200 PLANKTON (1999)', in *Standard Methods For the Examination of Water and Wastewater*. American Public Health Association (Standard Methods for the Examination of Water and Wastewater). Available at: https://doi.org/10.2105/SMWW.2882.207.

Arar, E.J. (1997) 'In Vitro Determination of Chlorophyll a and Pheophytin a in Marine and Freshwater Algae by Fluorescence', p. 22.

Asmala, E. *et al.* (2013) 'Bioavailability of riverine dissolved organic matter in three Baltic Sea estuaries and the effect of catchment land use', *Biogeosciences*, 10(11), pp. 6969–6986. Available at: https://doi.org/10.5194/bg-10-6969-2013.

Asmala, E. *et al.* (2014) 'Qualitative changes of riverine dissolved organic matter at low salinities due to flocculation', *Journal of Geophysical Research: Biogeosciences*, 119(10), pp. 1919–1933. Available at: https://doi.org/10.1002/2014JG002722.

Asmala, E., Massicotte, P. and Carstensen, J. (2021) 'Identification of dissolved organic matter size components in freshwater and marine environments', *Limnology and Oceanography*, 66(4), pp. 1381–1393. Available at: https://doi.org/10.1002/lno.11692.

Astoreca, R., Rousseau, V. and Lancelot, C. (2009) 'Coloured dissolved organic matter (CDOM) in Southern North Sea waters: Optical characterization and possible origin', *Estuarine, Coastal and Shelf Science*, 85(4), pp. 633–640. Available at: https://doi.org/10.1016/j.ecss.2009.10.010.

Audigier, V., Husson, F. and Josse, J. (2015) 'Multiple imputation for continuous variables using a Bayesian principal component analysis', *arXiv:1401.5747 [stat]* [Preprint]. Available at: http://arxiv.org/abs/1401.5747 (Accessed: 9 March 2022).

Bahram, M. *et al.* (2006) 'Handling of Rayleigh and Raman scatter for PARAFAC modeling of fluorescence data using interpolation', *Journal of Chemometrics*, 20(3–4), pp. 99–105. Available at: https://doi.org/10.1002/cem.978.

Baker, A. (2001) 'Fluorescence Excitation−Emission Matrix Characterization of Some Sewage-Impacted Rivers', *Environmental Science & Technology*, 35(5), pp. 948–953. Available at: https://doi.org/10.1021/es000177t.

Baker, A. *et al.* (2003) 'Detecting river pollution using fluorescence spectrophotometry: case studies from the Ouseburn, NE England', *Environmental Pollution*, 124(1), pp. 57–70. Available at: https://doi.org/10.1016/S0269-7491(02)00408-6.

Baker, A. and Inverarity, R. (2004) 'Protein-like fluorescence intensity as a possible tool for determining river water quality', *Hydrological Processes*, 18(15), pp. 2927–2945. Available at: https://doi.org/10.1002/hyp.5597.

Baker, A. and Spencer, R.G. (2004) 'Characterization of dissolved organic matter from source to sea using fluorescence and absorbance spectroscopy', *Sci Total Environ*, 333(1–3), pp. 217–32. Available at: https://doi.org/10.1016/j.scitotenv.2004.04.013.

Bakker, D. *et al.* (2014) 'Air-Sea Interactions of Natural Long-Lived Greenhouse Gases (CO2, N2O, CH4) in a Changing Climate', in *Ocean-Atmosphere Interactions of Gases and Particles*, pp. 113–170. Available at: https://doi.org/10.1007/978-3-642-25643-1_3.

Barrón, C. and Duarte, C.M. (2015) 'Dissolved organic carbon pools and export from the coastal ocean', *Global Biogeochemical Cycles*, 29(10), pp. 1725–1738. Available at: https://doi.org/10.1002/2014gb005056.

Bauer, J.E. and Bianchi, T.S. (2011) 'Dissolved Organic Carbon Cycling and Transformation', in *Treatise on Estuarine and Coastal Science*. Elsevier, pp. 7–67. Available at: https://doi.org/10.1016/B978-0-12-374711-2.00502-7.

Benner, R. (2002) ‘Chapter 3 - Chemical Composition and Reactivity’, in D.A. Hansell and C.A. Carlson (eds) *Biogeochemistry of Marine Dissolved Organic Matter*. San Diego: Academic Press, pp. 59–90. Available at: https://doi.org/10.1016/B978-012323841-2/50005-1.

Benner, R. (2003) ‘5 - Molecular Indicators of the Bioavailability of Dissolved Organic Matter’, in S.E.G. Findlay and R.L. Sinsabaugh (eds) *Aquatic Ecosystems*. Burlington: Academic Press, pp. 121–137. Available at: https://doi.org/10.1016/B978-012256371-3/50006-8.

Benner, R. and Amon, R.M.W. (2015) ‘The Size-Reactivity Continuum of Major Bioelements in the Ocean’, *Annual Review of Marine Science*, 7(1), pp. 185–205. Available at: https://doi.org/10.1146/annurev-marine-010213-135126.

Bertilsson, S. and Jones, J.B. (2003) ‘1 - Supply of Dissolved Organic Matter to Aquatic Ecosystems: Autochthonous Sources’, in S.E.G. Findlay and R.L. Sinsabaugh (eds) *Aquatic Ecosystems*. Burlington: Academic Press, pp. 3–24. Available at: https://doi.org/10.1016/B978-012256371-3/50002-0.

Beusen, A.H.W. *et al.* (2016) ‘Global riverine N and P transport to ocean increased during the 20th century despite increased retention along the aquatic continuum’, *Biogeosciences*, 13(8), pp. 2441–2451. Available at: https://doi.org/10.5194/bg-13-2441-2016.

Bittar, T.B. *et al.* (2015) ‘Competition between photochemical and biological degradation of dissolved organic matter from the cyanobacteria Microcystis aeruginosa’, *Limnology and Oceanography*, 60(4), pp. 1172–1194. Available at: https://doi.org/10.1002/lno.10090.

Bittar, T.B. *et al.* (2016) ‘Seasonal dynamics of dissolved, particulate and microbial components of a tidal saltmarsh-dominated estuary under contrasting levels of freshwater discharge’, *Estuarine, Coastal and Shelf Science*, 182, pp. 72–85. Available at: https://doi.org/10.1016/j.ecss.2016.08.046.

Bjørrisen, P.K. (1988) ‘Phytoplankton exudation of organic matter: Why do healthy cells do it?1’, *Limnology and Oceanography*, 33(1), pp. 151–154. Available at: https://doi.org/10.4319/lo.1988.33.1.0151.

Bloomfield, J.P., Allen, D.J. and Griffiths, K.J. (2009) ‘Examining geological controls on baseflow index (BFI) using regression analysis: An illustration from the Thames Basin, UK’, *Journal of Hydrology*, 373(1–2), pp. 164–176. Available at: https://doi.org/10.1016/j.jhydrol.2009.04.025.

Bozec, Y. *et al.* (2005) 'The continental shelf pump for CO2 in the North Sea—evidence from summer observation', *Marine Chemistry*, 93(2), pp. 131–147. Available at: https://doi.org/10.1016/j.marchem.2004.07.006.

Bricaud, A., Morel, A. and Prieur, L. (1981) 'Absorption by dissolved organic matter of the sea (yellow substance) in the UV and visible domains', *Limnology and Oceanography*, 26(1), pp. 43–53. Available at: https://doi.org/10.4319/lo.1981.26.1.0043.

British Geological Society (2020) 'East Anglia and adjoining areas region'. Internal report, pp. 10.

British Geological Survey (2022) 'Bedrock geology and superficial geology maps'. British Geological Survey (BGS), UK, Using: EDINA Geology Digimap Service

British Oceanographic Data Centre (2021) 'Sea Level Data File Format'. Internal report, pp. 3.

Bro, R. (1997) 'PARAFAC. Tutorial and applications', *Chemometrics and Intelligent Laboratory Systems*, 38(2), pp. 149–171. Available at: https://doi.org/10.1016/S0169-7439(97)00032-4.

Broadland Catchment Partnership (2014) 'Broadland Rivers Catchment Plan'. Internal report, pp. 32.

Broadland Catchment Partnership (2022a) *The River Waveney and Waveney catchment*, *Broadland Catchment Partnership*. Available at: https://broadlandcatchmentpartnership.org.uk/our-catchment/river-waveney/ (Accessed: 22 June 2022).

Broadland Catchment Partnership (2022b) *The River Yare and Yare catchment*, *Broadland Catchment Partnership*. Available at: https://broadlandcatchmentpartnership.org.uk/our-catchment/river-yare/ (Accessed: 22 June 2022).

Broads Authority (2017) 'Broads Plan 2017'. Available at: https://www.broads-authority.gov.uk/__data/assets/pdf_file/0023/240665/Broads-Plan-2017.pdf (Accessed: 4 August 2021).

Broads Authority (2019) 'Local Plan for the Broads'. Available at: https://www.broads-authority.gov.uk/__data/assets/pdf_file/0036/259596/Local-Plan-for-the-Broads.pdf (Accessed: 4 August 2021).

Brockmann, U.H., Laane, R.W.P.M. and Postma, J. (1990) 'Cycling of nutrient elements in the North Sea', *Netherlands Journal of Sea Research*, 26(2), pp. 239–264. Available at: https://doi.org/10.1016/0077-7579(90)90092-U.

Bronk, D. *et al.* (1998) 'Inorganic and organic nitrogen cycling in Chesapeake Bay: autotrophic versus heterotrophic processes and relationships to carbon flux', *Aquatic Microbial Ecology*, 15, pp. 177–189. Available at: https://doi.org/10.3354/ame015177.

Bronk, D.A. *et al.* (2010) 'Effluent Organic Nitrogen (EON): Bioavailability and Photochemical and Salinity-Mediated Release', *Environmental Science & Technology*, 44(15), pp. 5830–5835. Available at: https://doi.org/10.1021/es101115g.

Brym, A. *et al.* (2014) 'Optical and chemical characterization of base-extracted particulate organic matter in coastal marine environments', *Marine Chemistry*, 162, pp. 96–113. Available at: https://doi.org/10.1016/j.marchem.2014.03.006.

Camargo, A. (2022) PCAtest: testing the statistical significance of Principal Component Analysis in R. *PeerJ*. [Online] 10e12967. Available from: doi:10.7717/peerj.12967.

Camenen, B. *et al.* (2021) 'Monitoring discharge in a tidal river using water level observations: Application to the Saigon River, Vietnam', *Science of The Total Environment*, 761, p. 143195. Available at: https://doi.org/10.1016/j.scitotenv.2020.143195.

Canadell *et al.* (2022) 'Chapter 5: Global Carbon and Other Biogeochemical Cycles and Feedbacks', p. 144. Available at: https://doi.org/ 10.1017/9781009157896.007

Capuzzo, E. *et al.* (2015) 'Decrease in water clarity of the southern and central North Sea during the 20th century', *Global Change Biology*, 21(6), pp. 2206–2214. Available at: https://doi.org/10.1111/gcb.12854.

Carder, K.L. *et al.* (1989) 'Marine humic and fulvic acids: Their effects on remote sensing of ocean chlorophyll', *Limnology and Oceanography*, 34(1), pp. 68–81. Available at: https://doi.org/10.4319/lo.1989.34.1.0068.

Carlson, C.A. and Hansell, D.A. (2015) 'DOM Sources, Sinks, Reactivity, and Budgets', in *Biogeochemistry of Marine Dissolved Organic Matter*. Elsevier, pp. 65–126. Available at: https://doi.org/10.1016/B978-0-12-405940-5.00003-0.

Carr, N. *et al.* (2018) 'Seasonal and spatial variability in the optical characteristics of DOM in a temperate shelf sea', *Progress in Oceanography* [Preprint]. Available at: https://doi.org/10.1016/j.pocean.2018.02.025.

Carstea, E.M. *et al.* (2020) 'In situ fluorescence measurements of dissolved organic matter: A review', *Science of The Total Environment*, 699, p. 134361. Available at: https://doi.org/10.1016/j.scitotenv.2019.134361.

Catalá, T.S. *et al.* (2015) 'Turnover time of fluorescent dissolved organic matter in the dark global ocean', *Nature Communications*, 6, p. 5986.

Catalán, N. *et al.* (2018) 'Behind the Scenes: Mechanisms Regulating Climatic Patterns of Dissolved Organic Carbon Uptake in Headwater Streams', *Global Biogeochemical Cycles*, 32(10), pp. 1528–1541. Available at: https://doi.org/10.1029/2018GB005919.

Catalán, N. *et al.* (2021) 'The relevance of environment vs. composition on dissolved organic matter degradation in freshwaters', *Limnology and Oceanography*, 66(2), pp. 306–320. Available at: https://doi.org/10.1002/lno.11606.

Cauwet, G. (2002) 'Chapter 12 - DOM in the Coastal Zone', in D.A. Hansell and C.A. Carlson (eds) *Biogeochemistry of Marine Dissolved Organic Matter*. San Diego: Academic Press, pp. 579–609. Available at: https://doi.org/10.1016/B978-012323841-2/50014-2.

Cawley, K.M. *et al.* (2012) 'Characterising the sources and fate of dissolved organic matter in Shark Bay, Australia: a preliminary study using optical properties and stable carbon isotopes', *Marine and Freshwater Research*, 63(11), p. 1098. Available at: https://doi.org/10.1071/MF12028.

Chaichana, S. (2017) 'DISSOLVED ORGANIC CARBON AND NITROGEN IN COASTAL WATERS'. PhD thesis, p. 366.

Chaichana, S., Jickells, T. and Johnson, M. (2019) 'Interannual variability in the summer dissolved organic matter inventory of the North Sea: implications for the continental shelf pump', *Biogeosciences*, 16(5), pp. 1073–1096. Available at: https://doi.org/10.5194/bg-16-1073-2019.

Chapman, T. (1999) 'A comparison of algorithms for stream flow recession and baseflow separation', *Hydrological Processes*, 13(5), pp. 701–714. Available at: https://doi.org/10.1002/(SICI)1099-1085(19990415)13:5<701::AID-HYP774>3.0.CO;2-2.

Chen, B. *et al.* (2018) 'Characterization of Chromophoric Dissolved Organic Matter in the Littoral Zones of Eutrophic Lakes Taihu and Hongze during the Algal Bloom Season', *Water*, 10(7), p. 861. Available at: https://doi.org/10.3390/w10070861.

Chen, H. *et al.* (2011) 'Correlation between molecular absorption spectral slope ratios and fluorescence humification indices in characterizing CDOM', *Aquatic Sciences*, 73(1), pp. 103–112. Available at: https://doi.org/10.1007/s00027-010-0164-5.

Chen, M. *et al.* (2010) 'Comparative study of dissolved organic matter from groundwater and surface water in the Florida coastal Everglades using multi-dimensional spectrofluorometry combined with multivariate statistics', *Applied Geochemistry*, 25(6), pp. 872–880. Available at: https://doi.org/10.1016/j.apgeochem.2010.03.005.

Chen, M. *et al.* (2017) 'Dynamics of dissolved organic matter in riverine sediments affected by weir impoundments: Production, benthic flux, and environmental implications', *Water Research*, 121, pp. 150–161. Available at: https://doi.org/10.1016/j.watres.2017.05.022.

Chen, M. *et al.* (2018) 'Surface accumulation of low molecular weight dissolved organic matter in surface waters and horizontal off-shelf spreading of nutrients and humic-like fluorescence in the Chukchi Sea of the Arctic Ocean', *Science of The Total Environment*, 639, pp. 624–632. Available at: https://doi.org/10.1016/j.scitotenv.2018.05.205.

Ciais *et al.* (2014) *Carbon and Other Biogeochemical Cycles*.

Clark, J.B. *et al.* (2019) 'A mechanistic model of photochemical transformation and degradation of colored dissolved organic matter', *Marine Chemistry*, 214, p. 103666. Available at: https://doi.org/10.1016/j.marchem.2019.103666.

Coble, P.G. (1990) 'Characterization of dissolved organic matter in the Black Sea by fluorescence spectroscopy', *Nature*, 348(6300), p. 432.

Coble, P.G. (1996) 'Characterization of marine and terrestrial DOM in seawater using excitation-emission matrix spectroscopy', *Marine chemistry*, 51(4), pp. 325–346.

Coble, P.G. (2007) 'Marine Optical Biogeochemistry: The Chemistry of Ocean Color', p. 17.

Coble, P.G. (2013) '5 - Colored dissolved organic matter in seawater', in J. Watson and O. Zielinski (eds) *Subsea Optics and Imaging*. Woodhead Publishing, pp. 98–118. Available at: https://doi.org/10.1533/9780857093523.2.98.

Coble, P.G. (2014) *Aquatic organic matter fluorescence*. New York : Cambridge University Press, 2014. (Cambridge environmental chemistry series). Available at:

http://search.ebscohost.com/login.aspx?direct=true&db=cat01883a&AN=uea.003885191&authtype=sso&custid=s8993828&site=eds-live&scope=site.

Colin A. Stedmon, author and Stiig Markager, author (2005) 'Resolving the Variability in Dissolved Organic Matter Fluorescence in a Temperate Estuary and Its Catchment Using PARAFAC Analysis', *Limnology and Oceanography*, (2), p. 686.

Cooper, R.J. *et al.* (2018) 'Application of high-resolution telemetered sensor technology to develop conceptual models of catchment hydrogeological processes', *Journal of Hydrology X*, 1, p. 100007. Available at: https://doi.org/10.1016/j.hydroa.2018.100007.

Cooper, R.J. *et al.* (2020) 'Temporal hydrochemical dynamics of the River Wensum, UK: Observations from long-term high-resolution monitoring (2011–2018)', *Science of The Total Environment*, 724, p. 138253. Available at: https://doi.org/10.1016/j.scitotenv.2020.138253.

Cooper, R.J. *et al.* (2022) 'Evaluating the impacts of contrasting sewage treatment methods on nutrient dynamics across the River Wensum catchment, UK', *Science of The Total Environment*, 804, p. 150146. Available at: https://doi.org/10.1016/j.scitotenv.2021.150146.

European Environment Agency (EEA) (2018) 'Corine Land Cover 2018 (CLC)'. Copernicus Land Monitoring Service 2018, Using: EDINA Geology Digimap Service

Corbett, C.A. (2007) 'Colored Dissolved Organic Matter (CDOM) Workshop summary', p. 91.

Cory, R.M., Miller, M.P., *et al.* (2010) 'Effect of instrument-specific response on the analysis of fulvic acid fluorescence spectra', *Limnology and Oceanography: Methods*, 8(2), pp. 67–78. Available at: https://doi.org/10.4319/lom.2010.8.67.

Cory, R.M., McNeill, K., *et al.* (2010) 'Singlet Oxygen in the Coupled Photochemical and Biochemical Oxidation of Dissolved Organic Matter', *Environmental Science & Technology*, 44(10), pp. 3683–3689. Available at: https://doi.org/10.1021/es902989y.

Creighton, T.E. 1940- (1993) *Proteins : structures and molecular properties* (1 online resource (xiii, 507 pages) : illustrations vol). 2nd ed. New York: W.H. Freeman. Available at: http://catalog.hathitrust.org/api/volumes/oclc/25373213.html.

Dai, M. *et al.* (2012) 'Spatial distribution of riverine DOC inputs to the ocean: an updated global synthesis', *Carbon and nitrogen cycles*, 4(2), pp. 170–178. Available at: https://doi.org/10.1016/j.cosust.2012.03.003.

Dainard, P.G. *et al.* (2015) 'Photobleaching of fluorescent dissolved organic matter in Beaufort Sea and North Atlantic Subtropical Gyre', *Marine Chemistry*, 177, pp. 630–637. Available at: https://doi.org/10.1016/j.marchem.2015.10.004.

Dainard, P.G. *et al.* (2019) 'Interannual Variability in the Absorption and Fluorescence Characteristics of Dissolved Organic Matter in the Canada Basin Polar Mixed Waters', *Journal of Geophysical Research: Oceans*, 124(7), pp. 5258–5269. Available at: https://doi.org/10.1029/2018JC014896.

D'Andrilli, J. *et al.* (2019) 'DOM composition alters ecosystem function during microbial processing of isolated sources', *Biogeochemistry*, 142(2), pp. 281–298. Available at: https://doi.org/10.1007/s10533-018-00534-5.

DeFrancesco, C. and Guéguen, C. (2021) 'Long-term Trends in Dissolved Organic Matter Composition and Its Relation to Sea Ice in the Canada Basin, Arctic Ocean (2007–2017)', *Journal of Geophysical Research: Oceans*, 126(2), p. e2020JC016578. Available at: https://doi.org/10.1029/2020JC016578.

Derrien, M., Shin, K.-H. and Hur, J. (2019) 'Biodegradation-induced signatures in sediment pore water dissolved organic matter: Implications from artificial sediments composed of two contrasting sources', *Science of The Total Environment*, 694, p. 133714. Available at: https://doi.org/10.1016/j.scitotenv.2019.133714.

Dias, A., Kurian, S. and Thayapurath, S. (2020) 'Optical characteristics of colored dissolved organic matter during blooms of Trichodesmium in the coastal waters off Goa', *Environmental Monitoring and Assessment*, 192(8), p. 526. Available at: https://doi.org/10.1007/s10661-020-08494-w.

Dittmar, T. and Stubbins, A. (2014) '12.6 - Dissolved Organic Matter in Aquatic Systems', in H.D. Holland and K.K. Turekian (eds) *Treatise on Geochemistry (Second Edition)*. Oxford: Elsevier, pp. 125–156. Available at: https://doi.org/10.1016/B978-0-08-095975-7.01010-X.

Dixon, J.L. *et al.* (2014) 'Seasonal changes in estuarine dissolved organic matter due to variable flushing time and wind-driven mixing events', *Estuarine, Coastal and Shelf Science*, 151, pp. 210–220. Available at: https://doi.org/10.1016/j.ecss.2014.10.013.

Dore, J.E. *et al.* (1996) 'Freezing as a method of sample preservation for the analysis of dissolved inorganic nutrients in seawater', *Marine Chemistry*, 53(3), pp. 173–185. Available at: https://doi.org/10.1016/0304-4203(96)00004-7.

Du, Y. *et al.* (2021) 'Direct versus indirect effects of human activities on dissolved organic matter in highly impacted lakes', *Science of The Total Environment*, 752, p. 141839. Available at: https://doi.org/10.1016/j.scitotenv.2020.141839.

Duan, S.-W. and Kaushal, S.S. (2012) 'Warming increases carbon-nutrient fluxes from sediments in streams across land use', *Biogeosciences Discussions*, 9(8), pp. 11293–11330. Available at: https://doi.org/10.5194/bgd-9-11293-2012.

Ducrotoy, J.-P. and Elliott, M. (2008) 'The science and management of the North Sea and the Baltic Sea: Natural history, present threats and future challenges', *EMECS 7/ECSA 40, Caen (France), May 2006*, 57(1), pp. 8–21. Available at: https://doi.org/10.1016/j.marpolbul.2008.04.030.

Eder, A. *et al.* (2022) 'Pathways and composition of dissolved organic carbon in a small agricultural catchment during base flow conditions', *Ecohydrology & Hydrobiology*, 22(1), pp. 96–112. Available at: https://doi.org/10.1016/j.ecohyd.2021.07.012.

Eisma, D. (1986) 'Flocculation and de-flocculation of suspended matter in estuaries', *Netherlands Journal of Sea Research*, 20(2–3), pp. 183–199. Available at: https://doi.org/10.1016/0077-7579(86)90041-4.

Emeis, K.-C. *et al.* (2015) 'The North Sea — A shelf sea in the Anthropocene', *Journal of Marine Systems*, 141, pp. 18–33. Available at: https://doi.org/10.1016/j.jmarsys.2014.03.012.

Emerson, S. and Hedges, J. (2008) *Chemical Oceanography and the Marine Carbon Cycle*. Cambridge: Cambridge University Press. Available at: https://search.ebscohost.com/login.aspx?direct=true&AuthType=sso&db=nlebk&AN=304646&authtype=sso&custid=s8993828&site=eds-live&scope=site.

Environment Agency (1999) 'BFAS Environmental Monitoring: Strategic River Surveys 1998'. Internal report, pp. 163.

Environment Agency (2009) 'River Severn Catchment Flood Management Plan'. Internal report, pp. 68.

Environment Agency (2010) 'River Ouse Catchment Flood Management Plan'. Internal report, pp. 32.

Environment Agency (2014) 'Broadland Rivers Catchment summary'. Internal report, pp. 58.

Environment Agency (2015) 'Anglian_RBD_Part_1_river_basin_management_plan.pdf'. Available at: https://assets.publishing.service.gov.uk/government/uploads/system/uploads/attachment_data/file/718327/Anglian_RBD_Part_1_river_basin_management_plan.pdf (Accessed: 5 April 2019).

Environment Agency (2020) *Combined Sewer Overflows Explained - Creating a better place*. Available at: https://environmentagency.blog.gov.uk/2020/07/02/combined-sewer-overflows-explained/ (Accessed: 5 August 2021).

Environment Agency (2021) 'Permitted wastewater discharges map'. Accessed in 2021: https://environment.data.gov.uk/portalstg/home/item.html?id=5e618f2b5c7f47cca44eb468aa2e43f0.

ESRI (2019) *ArrcMap*.

Falco et al. (2006) 'Chlorophyll a and Phytoplankton Maximum at the Halocline of Ebro River Estuary', *Journal of Coastal Research*, (39), p. 6.

Fanela, M.A.P., Takarina, N.D., and Supriatna (2019) 'Distribution of total suspended solids (TSS) and chlorophyll-a in Kendari Bay, Southeast Sulawesi', *Journal of Physics: Conference Series*, 1217(1), p. 012150. Available at: https://doi.org/10.1088/1742-6596/1217/1/012150.

Fanning, K.A., Carder, K.L. and Betzer, P.R. (1982) 'Sediment resuspension by coastal waters: a potential mechanism for nutrient re-cycling on the ocean's margins', *Deep Sea Research Part A. Oceanographic Research Papers*, 29(8), pp. 953–965. Available at: https://doi.org/10.1016/0198-0149(82)90020-6.

Fargion, G.S. and Mueller, J.L. (2000) 'Ocean Optics Protocols For Satellite Ocean Color Sensor Validation, Revision 2', p. 9.

Fasching, C. *et al.* (2015) 'Microbial degradation of terrigenous dissolved organic matter and potential consequences for carbon cycling in brown-water streams', *Scientific Reports*, 4(1), p. 4981. Available at: https://doi.org/10.1038/srep04981.

Fellman, J.B., Hood, E., D'Amore, D.V., Edwards, R.T., et al. (2009) Seasonal changes in the chemical quality and biodegradability of dissolved organic matter exported from soils to streams in coastal temperate rainforest watersheds. *Biogeochemistry*. [Online] 95 (2), 277–293. Available from: doi:10.1007/s10533-009-9336-6.

Fellman, J.B., Hood, E. and Spencer, R.G.M. (2010) 'Fluorescence spectroscopy opens new windows into dissolved organic matter dynamics in freshwater ecosystems: A review', *Limnology and Oceanography*, 55(6), pp. 2452–2462. Available at: https://doi.org/10.4319/lo.2010.55.6.2452.

Fichot, C.G. and Benner, R. (2012) 'The spectral slope coefficient of chromophoric dissolved organic matter (S275–295) as a tracer of terrigenous dissolved organic carbon in river-influenced ocean margins', *Limnology and Oceanography*, 57(5), pp. 1453–1466. Available at: https://doi.org/10.4319/lo.2012.57.5.1453.

Fichot, C.G. and Benner, R. (2014) 'The fate of terrigenous dissolved organic carbon in a river-influenced ocean margin', *Global Biogeochemical Cycles*, 28(3), pp. 300–318. Available at: https://doi.org/10.1002/2013GB004670.

Fitzsimons, M.F. *et al.* (2006) 'Desorption kinetics of ammonium and methylamines from estuarine sediments: Consequences for the cycling of nitrogen', *Marine Chemistry*, 101(1), pp. 12–26. Available at: https://doi.org/10.1016/j.marchem.2005.12.006.

Foden, J. *et al.* (2008) 'Spatial and temporal distribution of chromophoric dissolved organic matter (CDOM) fluorescence and its contribution to light attenuation in UK waterbodies', *Estuarine, Coastal and Shelf Science*, 79(4), pp. 707–717. Available at: https://doi.org/10.1016/j.ecss.2008.06.015.

Fox, B.G. *et al.* (2017) 'The in situ bacterial production of fluorescent organic matter; an investigation at a species level', *Water Research*, 125, pp. 350–359. Available at: https://doi.org/10.1016/j.watres.2017.08.040.

Fox, B.G., Thorn, R.M.S. and Reynolds, D.M. (2021) 'Laboratory In-Situ Production of Autochthonous and Allochthonous Fluorescent Organic Matter by Freshwater Bacteria', *Microorganisms*, 9(8), p. 1623. Available at: https://doi.org/10.3390/microorganisms9081623.

von Freyberg, J. *et al.* (2020) 'Technical note: Evaluation of a low-cost evaporation protection method for portable water samplers', *Hydrology and Earth System Sciences*, 24(12), pp. 5821–5834. Available at: https://doi.org/10.5194/hess-24-5821-2020.

Friedlingstein, P. *et al.* (2022) 'Global Carbon Budget 2021', *Earth System Science Data*, 14(4), pp. 1917–2005. Available at: https://doi.org/10.5194/essd-14-1917-2022.

Gabor, R. *et al.* (2014) 'Fluorescence indices and their interpretation', in, p. 303.

Gao, Z. and Guéguen, C. (2017) 'Size distribution of absorbing and fluorescing DOM in Beaufort Sea, Canada Basin', *Deep Sea Research Part I: Oceanographic Research Papers*, 121, pp. 30–37. Available at: https://doi.org/10.1016/j.dsr.2016.12.014.

García-Martín, E.E. *et al.* (2021) 'Contrasting Estuarine Processing of Dissolved Organic Matter Derived From Natural and Human-Impacted Landscapes', *Global Biogeochemical Cycles*, 35(10), p. e2021GB007023. Available at: https://doi.org/10.1029/2021GB007023.

del Giorgio, P.A. and Cole, J.J. (1998) 'BACTERIAL GROWTH EFFICIENCY IN NATURAL AQUATIC SYSTEMS', *Annual Review of Ecology and Systematics*, 29(1), pp. 503–541. Available at: https://doi.org/10.1146/annurev.ecolsys.29.1.503.

Global Carbon Project (2022) 'Global Carbon Budget of the Land to Ocean Aquatic Continuum'. Accessed in 2021 at: http://globalcarbonatlas.org/en/LOAC-emissions.

Gonçalves-Araujo, R. *et al.* (2015) 'From Fresh to Marine Waters: Characterization and Fate of Dissolved Organic Matter in the Lena River Delta Region, Siberia', *Frontiers in Marine Science*, 2, p. 108. Available at: https://doi.org/10.3389/fmars.2015.00108.

Graeber, Daniel *et al.* (2012a) 'Agriculture has changed the amount and composition of dissolved organic matter in Central European headwater streams', *Science of The Total Environment*, 438, pp. 435–446. Available at: https://doi.org/10.1016/j.scitotenv.2012.08.087.

Graeber, D. *et al.* (2012b) 'Technical Note: Comparison between a direct and the standard, indirect method for dissolved organic nitrogen determination in freshwater environments with high dissolved inorganic nitrogen concentrations', *Biogeosciences*, 9(11), pp. 4873–4884. Available at: https://doi.org/10.5194/bg-9-4873-2012.

Green, S.A. and Blough, N.V. (1994) 'Optical absorption and fluorescence properties of chromophoric dissolved organic matter in natural waters', *Limnology and Oceanography*, 39(8), pp. 1903–1916. Available at: https://doi.org/10.4319/lo.1994.39.8.1903.

Grunwald, M. *et al.* (2010) 'Nutrient dynamics in a back barrier tidal basin of the Southern North Sea: Time-series, model simulations, and budget estimates', *Journal of Sea Research*, 64(3), pp. 199–212. Available at: https://doi.org/10.1016/j.seares.2010.02.008.

Guéguen, C. *et al.* (2016) 'Mixing and photoreactivity of dissolved organic matter in the Nelson/Hayes estuarine system (Hudson Bay, Canada)', *Journal of Marine*

Systems, 161, pp. 42–48. Available at: https://doi.org/10.1016/j.jmarsys.2016.05.005.

Gullian-Klanian, M. *et al.* (2021) 'Effect of the use of Bacillus spp. on the characteristics of dissolved fluorescent organic matter and the phytochemical quality of Stevia rebaudiana grown in a recirculating aquaponic system', *Environmental Science and Pollution Research*, 28(27), pp. 36326–36343. Available at: https://doi.org/10.1007/s11356-021-13148-6.

Guo, L. and Santschi, P.H. (2000) 'Sedimentary sources of old high molecular weight dissolved organic carbon from the ocean margin benthic nepheloid layer', *Geochimica et Cosmochimica Acta*, 64(4), pp. 651–660. Available at: https://doi.org/10.1016/S0016-7037(99)00335-X.

Guo, W. *et al.* (2007) 'The conservative and non-conservative behavior of chromophoric dissolved organic matter in Chinese estuarine waters', *Marine Chemistry*, 107(3), pp. 357–366. Available at: https://doi.org/10.1016/j.marchem.2007.03.006.

Hambly, A.C. *et al.* (2015) 'Characterising organic matter in recirculating aquaculture systems with fluorescence EEM spectroscopy', *Water Research*, 83, pp. 112–120. Available at: https://doi.org/10.1016/j.watres.2015.06.037.

Hannaford, J. and Buys, G. (2012) 'Trends in seasonal river flow regimes in the UK', *Journal of Hydrology*, 475, pp. 158–174. Available at: https://doi.org/10.1016/j.jhydrol.2012.09.044.

Hansell, D.A. (2005) 'Dissolved Organic Carbon Reference Material Program', *Eos, Transactions American Geophysical Union*, 86(35), pp. 318–318. Available at: https://doi.org/10.1029/2005EO350003.

Hansell, D.A. *et al.* (2009) 'Dissolved organic matter in the ocean: A controversy stimulates new insights', *Oceanography*, 22(4), pp. 202–211.

Hansell, D.A. and Orellana, M.V. (2021) 'Dissolved Organic Matter in the Global Ocean: A Primer', *Gels*, 7(3). Available at: https://doi.org/10.3390/gels7030128.

Hansen, A.M. *et al.* (2016) 'Optical properties of dissolved organic matter (DOM): Effects of biological and photolytic degradation', *Limnology and Oceanography*, 61(3), pp. 1015–1032. Available at: https://doi.org/10.1002/lno.10270.

Hao, Z., Gao, Y. and Yang, T. (2017) 'Seasonal variation of DOM and associated stoichiometry for freshwater ecosystem in the subtropical watershed: Indicating the

optimal C: N: P ratio', *Ecological Indicators*, 78, pp. 37–47. Available at: https://doi.org/10.1016/j.ecolind.2017.03.004.

Harshman, R. A. (1970) 'Foundations of the PARAFAC procedure: models and conditions for an "explanatory" multimodal factor analysis'.

Harshman, R.A. (1984) 'How can I know if it's real?', *A catalog of diagnostics for use with three-mode factor analysis and multidimensional scaling*, pp. 566–591.

Harshman, R.A. and Lundy, M.E. (1994) 'PARAFAC: Parallel factor analysis', *Computational Statistics & Data Analysis*, 18(1), pp. 39–72. Available at: https://doi.org/10.1016/0167-9473(94)90132-5.

Heinze, C. *et al.* (2015) 'The ocean carbon sink – impacts, vulnerabilities and challenges', *Earth System Dynamics*, 6(1), pp. 327–358. Available at: https://doi.org/10.5194/esd-6-327-2015.

Helms, J.R. *et al.* (2008) 'Absorption spectral slopes and slope ratios as indicators of molecular weight, source, and photobleaching of chromophoric dissolved organic matter', *Limnology and Oceanography*, 53(3), pp. 955–969. Available at: https://doi.org/10.4319/lo.2008.53.3.0955.

Helms, J.R. *et al.* (2013) 'Photochemical bleaching of oceanic dissolved organic matter and its effect on absorption spectral slope and fluorescence', *Marine Chemistry*, 155, pp. 81–91. Available at: https://doi.org/10.1016/j.marchem.2013.05.015.

Holdway, P.A., Watson, R.A. and Moss, B. (1978) 'Aspects of the ecology of Prymnesium parvum (Haptophyta) and water chemistry in the Norfolk Broads, England', *Freshwater Biology*, 8(4), pp. 295–311. Available at: https://doi.org/10.1111/j.1365-2427.1978.tb01451.x.

Hong, H. *et al.* (2021) 'Trace metal pollution risk assessment in urban mangrove patches: Potential linkage with the spectral characteristics of chromophoric dissolved organic matter', *Environmental Pollution*, 272, p. 115996. Available at: https://doi.org/10.1016/j.envpol.2020.115996.

Hope, D. *et al.* (1997) 'EXPORTS OF ORGANIC CARBON IN BRITISH RIVERS', *Hydrological Processes*, 11(3), pp. 325–344. Available at: https://doi.org/10.1002/(SICI)1099-1085(19970315)11:3<325::AID-HYP476>3.0.CO;2-I.

Hudson, N. *et al.* (2008) 'Can fluorescence spectrometry be used as a surrogate for the Biochemical Oxygen Demand (BOD) test in water quality assessment? An example

from South West England', *Science of The Total Environment*, 391(1), pp. 149–158. Available at: https://doi.org/10.1016/j.scitotenv.2007.10.054.

Hudson, N., Baker, A. and Reynolds, D. (2007) 'Fluorescence analysis of dissolved organic matter in natural, waste and polluted waters—a review', *River Research and Applications*, 23(6), pp. 631–649. Available at: https://doi.org/10.1002/rra.1005.

Huguet, A. *et al.* (2009) 'Properties of fluorescent dissolved organic matter in the Gironde Estuary', *Organic Geochemistry*, 40(6), pp. 706–719. Available at: https://doi.org/10.1016/j.orggeochem.2009.03.002.

Hydes, D.J. *et al.* (2004) 'External and internal control of winter concentrations of nutrients (N, P and Si) in north-west European shelf seas', *Estuarine, Coastal and Shelf Science*, 59(1), pp. 151–161. Available at: https://doi.org/10.1016/j.ecss.2003.08.004.

IAEA (2005) *Fluvial sediment transport: analytical techniques for measuring sediment load.* Vienna: International Atomic Energy Agency.

Imbeau, E. *et al.* (2021) 'Hidden Stores of Organic Matter in Northern Lake Ice: Selective Retention of Terrestrial Particles, Phytoplankton and Labile Carbon', *Journal of Geophysical Research: Biogeosciences*, 126(8), p. e2020JG006233. Available at: https://doi.org/10.1029/2020JG006233.

Indivero, J., Myers-Pigg, A.N. and Ward, N.D. (2021) 'Seasonal Changes in the Drivers of Water Physico-Chemistry Variability of a Small Freshwater Tidal River', *Frontiers in Marine Science*, 8, p. 766. Available at: https://doi.org/10.3389/fmars.2021.607644.

Islam, M.J. *et al.* (2019) 'C : N : P stoichiometry of particulate and dissolved organic matter in river waters and changes during decomposition', *Journal of Ecology and Environment*, 43(1), p. 4. Available at: https://doi.org/10.1186/s41610-018-0101-4.

Jaffé, R. *et al.* (2008) 'Spatial and temporal variations in DOM composition in ecosystems: The importance of long-term monitoring of optical properties', *Journal of Geophysical Research*, 113(G4). Available at: https://doi.org/10.1029/2008jg000683.

Jennings, S. *et al.* (1999) 'Distribution, diversity and abundance of epibenthic fauna in the North Sea', *Journal of the Marine Biological Association of the United Kingdom*. 2001/04/04 edn, 79(3), pp. 385–399. Available at: https://doi.org/10.1017/S0025315498000502.

Jiao, N. *et al.* (2010) 'Microbial production of recalcitrant dissolved organic matter: long-term carbon storage in the global ocean', *Nature Reviews Microbiology*, 8(8), pp. 593–599. Available at: https://doi.org/10.1038/nrmicro2386.

Jiao, N. *et al.* (2014) 'Mechanisms of microbial carbon sequestration in the ocean – future research directions', *Biogeosciences*, 11(19), pp. 5285–5306. Available at: https://doi.org/10.5194/bg-11-5285-2014.

Jickells *et al.* (2000) 'Nutrient Fluxes through the Humber Estuary: Past, Present and Future', p. 7.

Jickells, T.D. *et al.* (2014) 'Nutrient transport through estuaries: The importance of the estuarine geography', *Estuarine, Coastal and Shelf Science*, 150, pp. 215–229. Available at: https://doi.org/10.1016/j.ecss.2014.03.014.

Johnson, M.T. *et al.* (2013) 'Characterising the seasonal cycle of dissolved organic nitrogen using Cefas SmartBuoy high-resolution time-series samples from the southern North Sea', *Biogeochemistry*, 113(1–3), pp. 23–36. Available at: https://doi.org/10.1007/s10533-012-9738-8.

Jolliffe, I. (2005) 'Principal Component Analysis', in *Encyclopedia of Statistics in Behavioral Science*. John Wiley & Sons, Ltd. Available at: https://doi.org/10.1002/0470013192.bsa501.

Jones, T.G. *et al.* (2015) 'Transformations in DOC along a source to sea continuum; impacts of photo-degradation, biological processes and mixing', *Aquatic Sciences*, 78(3), pp. 433–446. Available at: https://doi.org/10.1007/s00027-015-0461-0.

Josse, J., Pagès, J. and Husson, F. (2011) 'Multiple imputation in principal component analysis', *Advances in Data Analysis and Classification*, 5(3), pp. 231–246. Available at: https://doi.org/10.1007/s11634-011-0086-7.

Josse, J. and Husson, F. (2016) 'missMDA: A Package for Handling Missing Values in Multivariate Data Analysis', *Journal of Statistical Software*, 70(1), pp. 1–31. Available at: https://doi.org/10.18637/jss.v070.i01.

Jutaporn, P., Armstrong, M.D. and Coronell, O. (2020) 'Assessment of C-DBP and N-DBP formation potential and its reduction by MIEX® DOC and MIEX® GOLD resins using fluorescence spectroscopy and parallel factor analysis', *Water Research*, 172, p. 115460. Available at: https://doi.org/10.1016/j.watres.2019.115460.

Karl, D.M. and Björkman, K.M. (2015) 'Chapter 5 - Dynamics of Dissolved Organic Phosphorus', in D.A. Hansell and C.A. Carlson (eds) *Biogeochemistry of Marine*

Dissolved Organic Matter (Second Edition). Boston: Academic Press, pp. 233–334. Available at: https://doi.org/10.1016/B978-0-12-405940-5.00005-4.

Kassambara and Mundt (2020) *Extract and Visualize the Results of Multivariate Data Analyses*. Available at: https://cran.r-project.org/web/packages/factoextra/factoextra.pdf (Accessed: 10 March 2022).

Kaul, L.W. and Froelich, P.N. (1984) 'Modeling estuarine nutrient geochemistry in a simple system', *Geochimica et Cosmochimica Acta*, 48(7), pp. 1417–1433. Available at: https://doi.org/10.1016/0016-7037(84)90399-5.

Kellerman, A.M. *et al.* (2018) 'Unifying Concepts Linking Dissolved Organic Matter Composition to Persistence in Aquatic Ecosystems', *Environmental Science & Technology*, 52(5), pp. 2538–2548. Available at: https://doi.org/10.1021/acs.est.7b05513.

Kelso, J.E. and Baker, M.A. (2022) 'Organic matter sources and composition in four watersheds with mixed land cover', *Hydrobiologia* [Preprint]. Available at: https://doi.org/10.1007/s10750-022-04884-y.

Kida, M. *et al.* (2019) 'Origin, distributions, and environmental significance of ubiquitous humic-like fluorophores in Antarctic lakes and streams', *Water Research*, 163, p. 114901. Available at: https://doi.org/10.1016/j.watres.2019.114901.

Kitidis, V. and Uher, G. (2008) 'Photochemical Mineralisation of Dissolved Organic Nitrogen', in, pp. 131–156.

Kitidis, V. *et al.* (2019) 'Winter weather controls net influx of atmospheric CO2 on the north-west European shelf', *Scientific Reports*, 9(1), p. 20153. Available at: https://doi.org/10.1038/s41598-019-56363-5.

Komada, T. and Reimers, C.E. (2001) 'Resuspension-induced partitioning of organic carbon between solid and solution phases from a river–ocean transition', *Marine Chemistry*, 76(3), pp. 155–174. Available at: https://doi.org/10.1016/S0304-4203(01)00055-X.

Kothawala, D.N. *et al.* (2012) 'Selective loss and preservation of lake water dissolved organic matter fluorescence during long-term dark incubations', *Science of The Total Environment*, 433, pp. 238–246. Available at: https://doi.org/10.1016/j.scitotenv.2012.06.029.

Kothawala, D.N. *et al.* (2014) 'Controls of dissolved organic matter quality: evidence from a large-scale boreal lake survey', *Global Change Biology*, 20(4), pp. 1101–1114. Available at: https://doi.org/10.1111/gcb.12488.

Kotlash, A.R. and Chessman, B.C. (1998) 'Effects of water sample preservation and storage on nitrogen and phosphorus determinations: implications for the use of automated sampling equipment', *Water Research*, 32(12), pp. 3731–3737. Available at: https://doi.org/10.1016/S0043-1354(98)00145-6.

Kowalczuk, P. *et al.* (2003) 'Characterization of CDOM in an organic-rich river and surrounding coastal ocean in the South Atlantic Bight', *Aquatic Sciences*, 65(4), pp. 384–401. Available at: https://doi.org/10.1007/s00027-003-0678-1.

Kowalczuk, P. *et al.* (2013) 'Composition of dissolved organic matter along an Atlantic Meridional Transect from fluorescence spectroscopy and Parallel Factor Analysis', *Marine Chemistry*, 157, pp. 170–184. Available at: https://doi.org/10.1016/j.marchem.2013.10.004.

Kreus, M. *et al.* (2015) 'Variations in the elemental ratio of organic matter in the central Baltic Sea: Part I—Linking primary production to remineralization', *Continental Shelf Research*, 100, pp. 25–45. Available at: https://doi.org/10.1016/j.csr.2014.06.015.

Krvavica, N., Travaš, V. and Ožanić, N. (2017) 'Salt-Wedge Response to Variable River Flow and Sea-Level Rise in the Microtidal Rječina River Estuary, Croatia', *Journal of Coastal Research*, 33(4), pp. 802–814. Available at: https://doi.org/10.2112/JCOASTRES-D-16-00053.1.

Kubista, M. *et al.* (1994) 'Experimental correction for the inner-filter effect in fluorescence spectra', *The Analyst*, 119(3), pp. 417–419. Available at: https://doi.org/10.1039/AN9941900417.

Laane, R.W.P.M. and Kramer, K.J.M. (1990) 'Natural fluorescence in the North Sea and its major estuaries', *Netherlands Journal of Sea Research*, 26(1), pp. 1–9. Available at: https://doi.org/10.1016/0077-7579(90)90052-I.

Laane et al. (1993) 'Nutrients P, N, Si) in the Channel and the Dover Strait : seasonal and year-to-year variation and fluxes to the North Sea', p. 10.

Lakowicz, J.R. (2008) 'Principles of Fluorescence Spectroscopy, Third Edition', *Journal of Biomedical Optics*, 13(2), p. 029901. Available at: https://doi.org/10.1117/1.2904580.

Lambert, T. *et al.* (2016) 'Shift in the chemical composition of dissolved organic matter in the Congo River network', *Biogeosciences*, 13(18), pp. 5405–5420. Available at: https://doi.org/10.5194/bg-13-5405-2016.

Lambert, T. *et al.* (2017) 'Effects of human land use on the terrestrial and aquatic sources of fluvial organic matter in a temperate river basin (The Meuse River, Belgium)', *Biogeochemistry*, 136(2), pp. 191–211. Available at: https://doi.org/10.1007/s10533-017-0387-9.

Lan, F. *et al.* (2021) 'Effects of Suspended Particulate Reactive Phosphorus on Phosphorus Cycle in the Pearl River Estuary', *Estuaries and Coasts*, 44(5), pp. 1310–1319. Available at: https://doi.org/10.1007/s12237-020-00863-5.

Lapierre, J.-F. and del Giorgio, P.A. (2014) 'Partial coupling and differential regulation of biologically and photochemically labile dissolved organic carbon across boreal aquatic networks', *Biogeosciences*, 11(20), pp. 5969–5985. Available at: https://doi.org/10.5194/bg-11-5969-2014.

Lawaetz, A.J. and Stedmon, C. (2009) 'Fluorescence intensity calibration using the Raman scatter peak of water', *Applied spectroscopy*, 63(8), pp. 936–940.

Lê, S., Josse, J. and Husson, F. (2008) 'FactoMineR: An R Package for Multivariate Analysis', *Journal of Statistical Software*, 25(1), pp. 1–18. Available at: https://doi.org/10.18637/jss.v025.i01.

Lee, D. *et al.* (2018) 'Characteristics of intracellular algogenic organic matter and its reactivity with hydroxyl radicals', *Water Research*, 144, pp. 13–25. Available at: https://doi.org/10.1016/j.watres.2018.06.069.

Lee, W. and Westerhoff, P. (2005) 'Dissolved Organic Nitrogen Measurement Using Dialysis Pretreatment', *Environmental Science & Technology*, 39(3), pp. 879–884. Available at: https://doi.org/10.1021/es048818y.

Leenheer and Croué (2003) 'Charcaterising aquatic dissolved organic matter', p. 9.

Legendre, L. *et al.* (2015) 'The microbial carbon pump concept: Potential biogeochemical significance in the globally changing ocean', *Progress in Oceanography*, 134, pp. 432–450. Available at: https://doi.org/10.1016/j.pocean.2015.01.008.

Legge, O. *et al.* (2020) 'Carbon on the Northwest European Shelf: Contemporary Budget and Future Influences', *Frontiers in Marine Science*, 7, p. 143. Available at: https://doi.org/10.3389/fmars.2020.00143.

Legrand, C. *et al.* (2003) 'Allelopathy in phytoplankton - biochemical, ecological and evolutionary aspects', *Phycologia*, 42(4), pp. 406–419. Available at: https://doi.org/10.2216/i0031-8884-42-4-406.1.

Lenhart, H.J. *et al.* (2004) *Investigation on the trophic state of the North Sea for three years (1994–1996) simulated with the ecosystem model ERSEM – the role of a sharp NAOI decline*. preprint. Available at: https://doi.org/10.5194/bgd-1-725-2004.

Letscher, R.T. *et al.* (2015) 'Variable C : N : P stoichiometry of dissolved organic matter cycling in the Community Earth System Model', *Biogeosciences*, 12(1), pp. 209–221. Available at: https://doi.org/10.5194/bg-12-209-2015.

Li, P. and Hur, J. (2017) 'Utilization of UV-Vis spectroscopy and related data analyses for dissolved organic matter (DOM) studies: A review', *Critical Reviews in Environmental Science and Technology*, 47(3), pp. 131–154. Available at: https://doi.org/10.1080/10643389.2017.1309186.

Li, X. *et al.* (2019) 'Distribution of organic phosphorus species in sediment profiles of shallow lakes and its effect on photo-release of phosphate during sediment resuspension', *Environment International*, 130, p. 104916. Available at: https://doi.org/10.1016/j.envint.2019.104916.

Little, S. *et al.* (2017) 'Unbounded boundaries and shifting baselines: Estuaries and coastal seas in a rapidly changing world', *Estuarine, Coastal and Shelf Science*, 198, pp. 311–319. Available at: https://doi.org/10.1016/j.ecss.2017.10.010.

Liu, C. *et al.* (2019) 'Exchanges of nitrogen and phosphorus across the sediment-water interface influenced by the external suspended particulate matter and the residual matter after dredging', *Environmental Pollution*, 246, pp. 207–216. Available at: https://doi.org/10.1016/j.envpol.2018.11.092.

Liu, J.T. *et al.* (2021) 'Coupling between physical processes and biogeochemistry of suspended particles over the inner shelf mud in the East China Sea', *Marine Geology*, 442, p. 106657. Available at: https://doi.org/10.1016/j.margeo.2021.106657.

Liu, K.-K. *et al.* (2000) 'Exploring continental margin carbon fluxes on a global scale', *Eos, Transactions American Geophysical Union*, 81(52), pp. 641–644. Available at: https://doi.org/10.1029/EO081i052p00641-01.

Liu, Y. *et al.* (2021) 'Fluorescence Characteristics of Chromophoric Dissolved Organic Matter in the Eastern Indian Ocean: A Case Study of Three Subregions', *Frontiers in Marine Science*, 8. Available at: https://www.frontiersin.org/article/10.3389/fmars.2021.742595.

Lloyd, C.E.M. *et al.* (2016) 'Using hysteresis analysis of high-resolution water quality monitoring data, including uncertainty, to infer controls on nutrient and sediment

transfer in catchments', *Science of The Total Environment*, 543, pp. 388–404. Available at: https://doi.org/10.1016/j.scitotenv.2015.11.028.

Longnecker, K. and Kujawinski, E.B. (2011) 'Composition of dissolved organic matter in groundwater', *Geochimica et Cosmochimica Acta*, 75(10), pp. 2752–2761. Available at: https://doi.org/10.1016/j.gca.2011.02.020.

Longobardi, A. and Villani, P. (2008) 'Baseflow index regionalization analysis in a mediterranean area and data scarcity context: Role of the catchment permeability index', *Journal of Hydrology*, 355(1–4), pp. 63–75. Available at: https://doi.org/10.1016/j.jhydrol.2008.03.011.

Lorenzo-Seva, U. and ten Berge, J.M.F. (2006) 'Tucker's Congruence Coefficient as a Meaningful Index of Factor Similarity', *Methodology*, 2(2), pp. 57–64. Available at: https://doi.org/10.1027/1614-2241.2.2.57.

Mackenzie, F.T., De Carlo, E.H. and Lerman, A. (2011) 'Coupled C, N, P, and O Biogeochemical Cycling at the Land–Ocean Interface', in *Treatise on Estuarine and Coastal Science*. Elsevier, pp. 317–342. Available at: https://doi.org/10.1016/B978-0-12-374711-2.00512-X.

Maie, N. *et al.* (2007) 'Composition of a protein-like fluorophore of dissolved organic matter in coastal wetland and estuarine ecosystems', *Water Research*, 41(3), pp. 563–570. Available at: https://doi.org/10.1016/j.watres.2006.11.006.

Mantoura, R.F.C. and Woodward, E.M.S. (1983) 'Conservative behaviour of riverine dissolved organic carbon in the Severn Estuary: chemical and geochemical implications', *Geochimica et Cosmochimica Acta*, 47(7), pp. 1293–1309. Available at: https://doi.org/10.1016/0016-7037(83)90069-8.

Markager, S., Stedmon, C.A. and Søndergaard, M. (2011) 'Seasonal dynamics and conservative mixing of dissolved organic matter in the temperate eutrophic estuary Horsens Fjord', *Estuarine, Coastal and Shelf Science*, 92(3), pp. 376–388. Available at: https://doi.org/10.1016/j.ecss.2011.01.014.

Martin, J.B., Thomas, R.G. and Hartl, K.M. (2004) 'An inexpensive, automatic, submersible water sampler', *Limnology and Oceanography: Methods*, 2(12), pp. 398–405. Available at: https://doi.org/10.4319/lom.2004.2.398.

Massicotte, P. *et al.* (2017) 'Global distribution of dissolved organic matter along the aquatic continuum: Across rivers, lakes and oceans', *Sci Total Environ*, 609, pp. 180–191. Available at: https://doi.org/10.1016/j.scitotenv.2017.07.076.

Mathers, S.J. *et al.* (2014) 'GB3D – a framework for the bedrock geology of Great Britain', *Geoscience Data Journal*, 1(1), pp. 30–42. Available at: https://doi.org/10.1002/gdj3.9.

Mcknight, D. *et al.* (2001) 'Spectrofluorometric Characterization of Dissolved Organic Matter for Indication of Precursor Organic Material and Aromaticity', *Limnology and Oceanography*, 46, pp. 38–48. Available at: https://doi.org/10.4319/lo.2001.46.1.0038.

McMillan, A.A. (2002) 'Onshore Quaternary geological surveys in the 21st century—a perspective from the British Geological Survey', *Quaternary Science Reviews*, 21(8), pp. 889–899. Available at: https://doi.org/10.1016/S0277-3791(01)00064-6.

McQuatters-Gollop, A. *et al.* (2007) 'A long-term chlorophyll dataset reveals regime shift in North Sea phytoplankton biomass unconnected to nutrient levels', *Limnology and Oceanography*, 52(2), pp. 635–648. Available at: https://doi.org/10.4319/lo.2007.52.2.0635.

Met Office (2022) *Coltishall (Norfolk) UK climate averages*, *Met Office*. Available at: https://www.metoffice.gov.uk/research/climate/maps-and-data/uk-climate-averages/u12unggmv (Accessed: 22 June 2022).

Miranda, M.L. *et al.* (2018) 'Influence of solar radiation on biogeochemical parameters and fluorescent dissolved organic matter (FDOM) in the sea surface microlayer of the southern coastal North Sea', *Elem Sci Anth*, 6(1), p. 15. Available at: https://doi.org/10.1525/elementa.278.

Molinero, J. and Burke, R.A. (2009) 'Effects of land use on dissolved organic matter biogeochemistry in piedmont headwater streams of the Southeastern United States', *Hydrobiologia*, 635(1), pp. 289–308. Available at: https://doi.org/10.1007/s10750-009-9921-7.

Monaghan, E.J. and Ruttenberg, K.C. (1999) 'Dissolved organic phosphorus in the coastal ocean: Reassessment of available methods and seasonal phosphorus profiles from the Eel River Shelf', *Limnology and Oceanography*, 44(7), pp. 1702–1714. Available at: https://doi.org/10.4319/lo.1999.44.7.1702.

Monbet, P., McKelvie, I.D. and Worsfold, P.J. (2009) 'Dissolved organic phosphorus speciation in the waters of the Tamar estuary (SW England)', *Geochimica et Cosmochimica Acta*, 73(4), pp. 1027–1038. Available at: https://doi.org/10.1016/j.gca.2008.11.024.

Mori, C. *et al.* (2019) 'Non-conservative Behavior of Dissolved Organic Matter and Trace Metals (Mn, Fe, Ba) Driven by Porewater Exchange in a Subtropical Mangrove-Estuary', *Frontiers in Marine Science*, 6. Available at: https://doi.org/10.3389/fmars.2019.00481.

Morin, J. and Morse, J.W. (1999) 'Ammonium release from resuspended sediments in the Laguna Madre estuary', *Marine Chemistry*, 65(1), pp. 97–110. Available at: https://doi.org/10.1016/S0304-4203(99)00013-4.

Mostofa, K. *et al.* (2013) 'Fluorescent Dissolved Organic Matter in Natural Waters', in *Environmental Science and Engineering (Subseries: Environmental Science)*, pp. 429–559. Available at: https://doi.org/10.1007/978-3-642-32223-5_6.

Mostofa, K.M.G. *et al.* (2013) 'Dissolved Organic Matter in Natural Waters', in K.M.G. Mostofa et al. (eds) *Photobiogeochemistry of Organic Matter*. Berlin, Heidelberg: Springer Berlin Heidelberg (Environmental Science and Engineering), pp. 1–137. Available at: https://doi.org/10.1007/978-3-642-32223-5_1.

Murphy, K.R. *et al.* (2006) 'Optimized Parameters for Fluorescence-Based Verification of Ballast Water Exchange by Ships', *Environmental Science & Technology*, 40(7), pp. 2357–2362. Available at: https://doi.org/10.1021/es0519381.

Murphy, K.R. *et al.* (2008) 'Distinguishing between terrestrial and autochthonous organic matter sources in marine environments using fluorescence spectroscopy', *Marine Chemistry*, 108(1), pp. 40–58. Available at: https://doi.org/10.1016/j.marchem.2007.10.003.

Murphy, K.R. *et al.* (2011) 'Organic Matter Fluorescence in Municipal Water Recycling Schemes: Toward a Unified PARAFAC Model', *Environmental Science & Technology*, 45(7), pp. 2909–2916. Available at: https://doi.org/10.1021/es103015e.

Murphy, K.R. *et al.* (2013) 'Fluorescence spectroscopy and multi-way techniques. PARAFAC', *Analytical Methods*, 5(23), p. 6557. Available at: https://doi.org/10.1039/c3ay41160e.

Murphy, K.R. *et al.* (2014) 'OpenFluor– an online spectral library of auto-fluorescence by organic compounds in the environment', *Anal. Methods*, 6(3), pp. 658–661. Available at: https://doi.org/10.1039/C3AY41935E.

Murphy, K.R., Bro, R. and Stedmon, C.A. (2014) 'Chemometric Analysis of Organic Matter Fluorescence', in A. Baker et al. (eds) *Aquatic Organic Matter Fluorescence*. Cambridge: Cambridge University Press (Cambridge Environmental Chemistry

Series), pp. 339–375. Available at: https://doi.org/10.1017/CBO9781139045452.016.

Nagata, T. (2000) 'Production mechanisms of dissolved organic matter', *Microbial ecology of the oceans* [Preprint].

National River Flow Archive, Accessed in 2021 and 2022 at: https://nrfa.ceh.ac.uk/data/search.

Neal, C. and Robson, A.J. (2000) 'A summary of river water quality data collected within the Land–Ocean Interaction Study: core data for eastern UK rivers draining to the North Sea', *Science of The Total Environment*, 251–252, pp. 585–665. Available at: https://doi.org/10.1016/s0048-9697(00)00397-1.

Nedwell, D.B. *et al.* (2002) 'Variations of the Nutrients Loads to the Mainland U.K. Estuaries: Correlation with Catchment Areas, Urbanization and Coastal Eutrophication', *Estuarine, Coastal and Shelf Science*, 54(6), pp. 951–970. Available at: https://doi.org/10.1006/ecss.2001.0867.

Niemistö, J. and Lund-Hansen, L.C. (2019) 'Instantaneous Effects of Sediment Resuspension on Inorganic and Organic Benthic Nutrient Fluxes at a Shallow Water Coastal Site in the Gulf of Finland, Baltic Sea', *Estuaries and Coasts*, 42(8), pp. 2054–2071. Available at: https://doi.org/10.1007/s12237-019-00648-5.

NOAA PMEL Carbon Group (2022) *Coastal Carbon Dynamics*. Available at: https://www.pmel.noaa.gov/co2/story/Coastal+Carbon+Dynamics (Accessed: 9 August 2022).

Obernosterer, I. and Herndl, G.J. (2000) 'Differences in the optical and biological reactivity of the humic and nonhumic dissolved organic carbon component in two contrasting coastal marine environments', *Limnology and Oceanography*, 45(5), pp. 1120–1129. Available at: https://doi.org/10.4319/lo.2000.45.5.1120.

Opsahl, S. and Benner, R. (1997) 'Distribution and cycling of terrigenous dissolved organic matter in the ocean', *Nature*, 386(6624), p. 480.

Opsahl, S. and Benner, R. (1998) 'Photochemical reactivity of dissolved lignin in river and ocean waters', *Limnology and Oceanography*, 43(6), pp. 1297–1304. Available at: https://doi.org/10.4319/lo.1998.43.6.1297.

Ortiz-Hernández, M.C. *et al.* (2004) 'Contribution of sedimentary resuspension to non-conservative fluxes of dissolved inorganic phosphorus in San Quintin Bay, Baja

California: An experimental estimate', *Ciencias Marinas*, 30(1A), pp. 75–88. Available at: https://doi.org/10.7773/cm.v30i11.119.

Osburn, C.L. and Stedmon, C.A. (2011a) 'Linking the chemical and optical properties of dissolved organic matter in the Baltic–North Sea transition zone to differentiate three allochthonous inputs', *Marine Chemistry*, 126(1), pp. 281–294. Available at: https://doi.org/10.1016/j.marchem.2011.06.007.

Osburn, C.L. *et al.* (2011b) 'Dissolved organic matter composition and photoreactivity in prairie lakes of the U.S. Great Plains', *Limnology and Oceanography*, 56(6), pp. 2371–2390. Available at: https://doi.org/10.4319/lo.2011.56.6.2371.

Osburn, C.L. *et al.* (2016) 'Predicting Sources of Dissolved Organic Nitrogen to an Estuary from an Agro-Urban Coastal Watershed', *Environmental Science & Technology*, 50(16), pp. 8473–8484. Available at: https://doi.org/10.1021/acs.est.6b00053.

Otto, L. *et al.* (1990) 'Review of the physical oceanography of the North Sea', *Netherlands Journal of Sea Research*, 26(2), pp. 161–238. Available at: https://doi.org/10.1016/0077-7579(90)90091-T.

Outram, F.N. *et al.* (2016) 'Antecedent conditions, hydrological connectivity and anthropogenic inputs: Factors affecting nitrate and phosphorus transfers to agricultural headwater streams', *Science of The Total Environment*, 545–546, pp. 184–199. Available at: https://doi.org/10.1016/j.scitotenv.2015.12.025.

Painter, S.C. *et al.* (2018) 'Terrestrial dissolved organic matter distribution in the North Sea', *Science of The Total Environment*, 630, pp. 630–647. Available at: https://doi.org/10.1016/j.scitotenv.2018.02.237.

Panton, A. *et al.* (2020) 'The impact of rainfall events, catchment characteristics and estuarine processes on the export of dissolved organic matter from two lowland rivers and their shared estuary', *Science of The Total Environment*, 735, p. 139481. Available at: https://doi.org/10.1016/j.scitotenv.2020.139481.

Para, J. *et al.* (2010) 'Fluorescence and absorption properties of chromophoric dissolved organic matter (CDOM) in coastal surface waters of the northwestern Mediterranean Sea, influence of the Rhône River', *Biogeosciences*, 7(12), pp. 4083–4103. Available at: https://doi.org/10.5194/bg-7-4083-2010.

Park, G.S. (2007) 'The role and distribution of total suspended solids in the macrotidal coastal waters of Korea', *Environmental Monitoring and Assessment*, 135(1–3), pp. 153–162. Available at: https://doi.org/10.1007/s10661-007-9640-3.

Parlanti, E. *et al.* (2000) 'Dissolved organic matter fluorescence spectroscopy as a tool to estimate biological activity in a coastal zone submitted to anthropogenic inputs', *Organic Geochemistry*, 31(12), pp. 1765–1781. Available at: https://doi.org/10.1016/S0146-6380(00)00124-8.

Parmenter, W.B. and Melcher, J. (2012) 'Watershed and Drainage Delineation by Pour Point in ArcMap 10', p. 16.

Pasquier et al. (2018) 'An integrated 1D–2D hydraulic modelling approach to assess the sensitivity of a coastal region to compound flooding hazard under climate change'. Available at: https://core.ac.uk/reader/196592785 (Accessed: 27 July 2021).

Passow, U. and Carlson, C. (2012) 'The biological pump in a high CO<sub>2 world', *Marine Ecology Progress Series*, 470, pp. 249–271. Available at: https://doi.org/10.3354/meps09985.

Pavlov, A.K. *et al.* (2014) 'Marine CDOM accumulation during a coastal Arctic mesocosm experiment: No response to elevated pCO2 levels', *Journal of Geophysical Research: Biogeosciences*, 119(6), pp. 1216–1230. Available at: https://doi.org/10.1002/2013JG002587.

Peacock, M. *et al.* (2015) 'Investigations of freezing and cold storage for the analysis of peatland dissolved organic carbon (DOC) and absorbance properties', *Environmental Science: Processes & Impacts*, 17(7), pp. 1290–1301. Available at: https://doi.org/10.1039/C5EM00126A.

Peeters, J.C.H. *et al.* (1991) 'Limiting Factors for Phytoplankton in the North Sea', *Water Science and Technology*, 24(10), pp. 261–267. Available at: https://doi.org/10.2166/wst.1991.0299.

Pejrup, M. and Edelvang, K. (1996) 'Measurements of in situ settling velocities in the Elbe estuary', *Journal of Sea Research*, 36(1), pp. 109–113. Available at: https://doi.org/10.1016/S1385-1101(96)90779-0.

Peleato, N.M. *et al.* (2016) 'Fluorescence spectroscopy for monitoring reduction of natural organic matter and halogenated furanone precursors by biofiltration', *Chemosphere*, 153, pp. 155–161. Available at: https://doi.org/10.1016/j.chemosphere.2016.03.018.

Pereira, R. *et al.* (2014) 'Mobilization of optically invisible dissolved organic matter in response to rainstorm events in a tropical forest headwater river', *Geophysical Research Letters*, 41(4), pp. 1202–1208. Available at: https://doi.org/10.1002/2013GL058658.

Porter, E., Mason, R. and Sanford, L. (2010) 'Effect of tidal resuspension on benthic–pelagic coupling in an experimental ecosystem study', *Marine Ecology Progress Series*, 413, pp. 33–53. Available at: https://doi.org/10.3354/meps08709.

Potter, I.C. *et al.* (2010) 'The concept of an estuary: A definition that incorporates systems which can become closed to the ocean and hypersaline', *Estuarine, Coastal and Shelf Science*, 87(3), pp. 497–500. Available at: https://doi.org/10.1016/j.ecss.2010.01.021.

Prandle, D. *et al.* (1997) 'The Seasonal Cycles of Temperature, Salinity, Nutrients and Suspended Sediment in the Southern North Sea in 1988 and 1989', *Estuarine, Coastal and Shelf Science*, 45(5), pp. 669–680. Available at: https://doi.org/10.1006/ecss.1996.0227.

Ptacnik, R., Andersen, T. and Tamminen, T. (2010) 'Performance of the Redfield Ratio and a Family of Nutrient Limitation Indicators as Thresholds for Phytoplankton N vs. P Limitation', *Ecosystems*, 13(8), pp. 1201–1214. Available at: https://doi.org/10.1007/s10021-010-9380-z.

Pucher, M. *et al.* (2021) 'Complex interactions of in-stream dissolved organic matter and nutrient spiralling unravelled by Bayesian regression analysis', *Biogeosciences*, 18(10), pp. 3103–3122. Available at: https://doi.org/10.5194/bg-18-3103-2021.

Queste, B.Y. *et al.* (2016) 'Drivers of summer oxygen depletion in the central North Sea', *Biogeosciences*, 13(4), pp. 1209–1222. Available at: https://doi.org/10.5194/bg-13-1209-2016.

R Core Team (2020) *R: A language and environment for statistical computing.* Vienna, Austria: R Foundation for Statistical Computing.

Raymond, P.A. and Bauer, J.E. (2001) 'DOC cycling in a temperate estuary: A mass balance approach using natural ^{14}C and ^{13}C isotopes', *Limnology and Oceanography*, 46(3), pp. 655–667. Available at: https://doi.org/10.4319/lo.2001.46.3.0655.

Redfield, A.C., Ketchum, B.H. and Richards, F.A. (1963) 'The influence of organisms on the composition of sea-water', in.

Regnier, P., Friedlingstein, P., *et al.* (2013a) 'Anthropogenic perturbation of the carbon fluxes from land to ocean', *Nature Geoscience*, 6(8), pp. 597–607. Available at: https://doi.org/10.1038/ngeo1830.

Regnier, P., Arndt, S., *et al.* (2013b) 'Modelling Estuarine Biogeochemical Dynamics: From the Local to the Global Scale', *Aquatic Geochemistry*, 19(5–6), pp. 591–626. Available at: https://doi.org/10.1007/s10498-013-9218-3.

Regnier, P. *et al.* (2022) 'The land-to-ocean loops of the global carbon cycle', *Nature*, 603(7901), pp. 401–410. Available at: https://doi.org/10.1038/s41586-021-04339-9.

Ren, W. *et al.* (2021) 'Characteristics of dissolved organic matter in lakes with different eutrophic levels in southeastern Hubei Province, China', 39, p. 21.

Rennie, S. *et al.* (2017) 'UK Environmental Change Network (ECN) stream water chemistry data: 1992-2015'. NERC Environmental Information Data Centre. Available at: https://doi.org/10.5285/fd7ca5ef-460a-463c-ad2b-5ad48bb4e22e.

Riedel, T. *et al.* (2016) 'Molecular Signatures of Biogeochemical Transformations in Dissolved Organic Matter from Ten World Rivers', *Frontiers in Earth Science*, 4, p. 85. Available at: https://doi.org/10.3389/feart.2016.00085.

Riou, P. *et al.* (2007) 'Microbial impact of small tributaries on water and shellfish quality in shallow coastal areas', *Water Research*, 41(12), pp. 2774–2786. Available at: https://doi.org/10.1016/j.watres.2007.03.003.

The Rivers Trust, 'Sewage Map'. Accessed in 2021 at: https://theriverstrust.org/key-issues/sewage-in-rivers

Roberts, E.J. and Cooper, R.J. (2018) 'Riverbed sediments buffer phosphorus concentrations downstream of sewage treatment works across the River Wensum catchment, UK', *Journal of Soils and Sediments*, 18(5), pp. 2107–2116. Available at: https://doi.org/10.1007/s11368-018-1939-x.

Roegner, G.C., Seaton, C. and Baptista, A.M. (2011) 'Climatic and Tidal Forcing of Hydrography and Chlorophyll Concentrations in the Columbia River Estuary', *Estuaries and Coasts*, 34(2), pp. 281–296. Available at: https://doi.org/10.1007/s12237-010-9340-z.

Rothwell, J.J. *et al.* (2010) 'A spatial and seasonal assessment of river water chemistry across North West England', *Science of The Total Environment*, 408(4), pp. 841–855. Available at: https://doi.org/10.1016/j.scitotenv.2009.10.041.

Sarmiento, J.L. & Gruber, N. (2002) Sinks for Anthropogenic Carbon. *Physics Today*. [Online] 55 (8), 30–36. Available from: doi:10.1063/1.1510279.

Schittich, A.-R. *et al.* (2018) 'Investigating Fluorescent Organic-Matter Composition as a Key Predictor for Arsenic Mobility in Groundwater Aquifers', *Environmental Science & Technology*, 52(22), pp. 13027–13036. Available at: https://doi.org/10.1021/acs.est.8b04070.

Schlesinger, W.H. and Bernhardt, E.S. (2020) 'Chapter 6 - Biogeochemical Cycling on Land', in W.H. Schlesinger and E.S. Bernhardt (eds) *Biogeochemistry (Fourth Edition)*. Academic Press, pp. 183–248. Available at: https://doi.org/10.1016/B978-0-12-814608-8.00006-2.

Seidel, M. *et al.* (2015) 'Molecular-level changes of dissolved organic matter along the Amazon River-to-ocean continuum', *Biogeochemistry of dissolved organic matter*, 177, pp. 218–231. Available at: https://doi.org/10.1016/j.marchem.2015.06.019.

Sharma, P. *et al.* (2017a) 'Compositional characteristics of organic matter and its water-extractable components across a profile of organically managed soil', *Geoderma*, 286, pp. 73–82. Available at: https://doi.org/10.1016/j.geoderma.2016.10.014.

Sharma, P. *et al.* (2017b) 'Green manure as part of organic management cycle: Effects on changes in organic matter characteristics across the soil profile', *Geoderma*, 305, pp. 197–207. Available at: https://doi.org/10.1016/j.geoderma.2017.06.003.

Shen, Y. *et al.* (2015) 'Origins and bioavailability of dissolved organic matter in groundwater', *Biogeochemistry*, 122(1), pp. 61–78. Available at: https://doi.org/10.1007/s10533-014-0029-4.

Sheng, Y. *et al.* (2021) 'The partitioning behavior of PAHs between settled dust and its extracted water phase: Coefficients and effects of the fluorescent organic matter', *Ecotoxicology and Environmental Safety*, 223, p. 112573. Available at: https://doi.org/10.1016/j.ecoenv.2021.112573.

Shi, Y. *et al.* (2020) 'Influence of land use and rainfall on the optical properties of dissolved organic matter in a key drinking water reservoir in China', *Science of The Total Environment*, 699, p. 134301. Available at: https://doi.org/10.1016/j.scitotenv.2019.134301.

Sholkovitz, E.R. (1976) 'Flocculation of dissolved organic and inorganic matter during the mixing of river water and seawater', *Geochimica et Cosmochimica Acta*, 40(7), pp. 831–845. Available at: https://doi.org/10.1016/0016-7037(76)90035-1.

Shutova, Y. *et al.* (2014) 'Spectroscopic characterisation of dissolved organic matter changes in drinking water treatment: From PARAFAC analysis to online monitoring wavelengths', *Water Research*, 54, pp. 159–169. Available at: https://doi.org/10.1016/j.watres.2014.01.053.

Siegel, D.A. *et al.* (2002) 'Global distribution and dynamics of colored dissolved and detrital organic materials', *Journal of Geophysical Research: Oceans*, 107(C12), pp. 21-1-21–14. Available at: https://doi.org/10.1029/2001JC000965.

Sierra, J.P. *et al.* (2002) 'Spatial distribution of nutrients in the Ebro estuary and plume', *Fluxes Across a Narrow Shelf*, 22(2), pp. 361–378. Available at: https://doi.org/10.1016/S0278-4343(01)00061-9.

Simon, N.S. (1989) 'Nitrogen cycling between sediment and the shallow-water column in the transition zone of the Potomac River and Estuary. II. The role of wind-driven resuspension and adsorbed ammonium', *Estuarine, Coastal and Shelf Science*, 28(5), pp. 531–547. Available at: https://doi.org/10.1016/0272-7714(89)90028-0.

Sipler, R.E. and Bronk, D.A. (2015a) 'Chapter 4 - Dynamics of Dissolved Organic Nitrogen', in D.A. Hansell and C.A. Carlson (eds) *Biogeochemistry of Marine Dissolved Organic Matter (Second Edition)*. Boston: Academic Press, pp. 127–232. Available at: https://doi.org/10.1016/B978-0-12-405940-5.00004-2.

Sipler, R.E. and Bronk, D.A. (2015b) 'Chapter 4 - Dynamics of Dissolved Organic Nitrogen', in D.A. Hansell and C.A. Carlson (eds) *Biogeochemistry of Marine Dissolved Organic Matter (Second Edition)*. Boston: Academic Press, pp. 127–232. Available at: https://doi.org/10.1016/B978-0-12-405940-5.00004-2.

Sipler, R.E. and Bronk, D.A. (2015c) 'Dynamics of Dissolved Organic Nitrogen', in *Biogeochemistry of Marine Dissolved Organic Matter*. Elsevier, pp. 127–232. Available at: https://doi.org/10.1016/B978-0-12-405940-5.00004-2.

SKALAR (2009a) 'SKALAR METHODS ANALYSIS: AMMONIA AND AMMONIUM'.

SKALAR (2009b) 'SKALAR METHODS ANALYSIS: NITRATE + NITRITE'.

SKALAR (2009c) 'SKALAR METHODS ANALYSIS: PHOSPHATE'.

SKALAR (2012) 'SKALAR METHODS ANALYSIS: TOTAL UV dig. PHOSPHATE'.

Smith, C.T. (1966) 'Dutch Peat Digging and the Origin of the Norfolk Broads', *The Geographical Journal*, 132(1), p. 69. Available at: https://doi.org/10.2307/1793055.

Smith, M.A. *et al.* (2021) 'Stormwater Runoff and Tidal Flooding Transform Dissolved Organic Matter Composition and Increase Bioavailability in Urban Coastal

Ecosystems', *Journal of Geophysical Research: Biogeosciences*, 126(7), p. e2020JG006146. Available at: https://doi.org/10.1029/2020JG006146.

Solinger, S., Kalbitz, K. and Matzner, E. (2001) 'Controls on the dynamics of dissolved organic carbon and nitrogen in a Central European deciduous forest', p. 24.

Solomon, S., Dahe, Qin, & Manning, Martin (2007) *Climate change 2007: the physical science basis: contribution of Working Group I to the Fourth Assessment Report of the Intergovernmental Panel on Climate Change*. Intergovernmental Panel on Climate Change (ed.). Cambridge ; New York, Cambridge University Press.

Søndergaard, M. and Thomas, D. (2004) *Dissolved Organic Matter (DOM) in Aquatic Ecosystems: A Study of European Catchments and Coastal Waters*.

Song, K. *et al.* (2017) 'A systematic examination of the relationships between CDOM and DOC in inland waters in China', *Hydrology and Earth System Sciences*, 21(10), pp. 5127–5141. Available at: https://doi.org/10.5194/hess-21-5127-2017.

Spencer, R.G.M. *et al.* (2009) 'Photochemical degradation of dissolved organic matter and dissolved lignin phenols from the Congo River', *Journal of Geophysical Research: Biogeosciences*, 114(G3). Available at: https://doi.org/10.1029/2009JG000968.

Spencer, R.G.M., Butler, K.D. and Aiken, G.R. (2012) 'Dissolved organic carbon and chromophoric dissolved organic matter properties of rivers in the USA', *Journal of Geophysical Research: Biogeosciences*, 117(G3). Available at: https://doi.org/10.1029/2011JG001928.

Statham, P.J. (2012) 'Nutrients in estuaries — An overview and the potential impacts of climate change', *Science of The Total Environment*, 434, pp. 213–227. Available at: https://doi.org/10.1016/j.scitotenv.2011.09.088.

Stedmon, C.A., Markager, S. and Kaas, H. (2000) 'Optical Properties and Signatures of Chromophoric Dissolved Organic Matter (CDOM) in Danish Coastal Waters', *Estuarine, Coastal and Shelf Science*, 51(2), pp. 267–278. Available at: https://doi.org/10.1006/ecss.2000.0645.

Stedmon, C.A. (2003) 'Tracing dissolved organic matter in aquatic environments using a new approach to fluorescence spectroscopy', *Marine Chemistry*, 82(3–4), pp. 239–254. Available at: https://doi.org/10.1016/s0304-4203(03)00072-0.

Stedmon, C.A. and Markager, S. (2005) 'Tracing the production and degradation of autochthonous fractions of dissolved organic matter by fluorescence analysis',

Limnology and Oceanography, 50(5), pp. 1415–1426. Available at: https://doi.org/10.4319/lo.2005.50.5.1415.

Stedmon, C.A. *et al.* (2007a) 'Characteristics of Dissolved Organic Matter in Baltic Coastal Sea Ice: Allochthonous or Autochthonous Origins?', p. 7.

Stedmon, Colin A. *et al.* (2007b) 'Photochemical production of ammonium and transformation of dissolved organic matter in the Baltic Sea', *Marine Chemistry*, 104(3), pp. 227–240. Available at: https://doi.org/10.1016/j.marchem.2006.11.005.

Stedmon, C.A. and Bro, R. (2008) 'Characterizing dissolved organic matter fluorescence with parallel factor analysis: a tutorial: Fluorescence-PARAFAC analysis of DOM', *Limnology and Oceanography: Methods*, 6(11), pp. 572–579. Available at: https://doi.org/10.4319/lom.2008.6.572b.

Stedmon, C.A., Osburn, C.L. and Kragh, T. (2010) 'Tracing water mass mixing in the Baltic–North Sea transition zone using the optical properties of coloured dissolved organic matter', *Estuarine, Coastal and Shelf Science*, 87(1), pp. 156–162. Available at: https://doi.org/10.1016/j.ecss.2009.12.022.

Stedmon, C.A. and Alvarez-Salgado, X.A. (2011a) 'Shedding Light on a Black Box: UV-Visible spectroscopic characterization of marine dissolved organic matter', in *Microbial Carbon Pump in the Ocean*, pp. 62–63.

Stedmon, C.A., Seredyńska-Sobecka, B., *et al.* (2011b) 'A potential approach for monitoring drinking water quality from groundwater systems using organic matter fluorescence as an early warning for contamination events', *Water Research*, 45(18), pp. 6030–6038. Available at: https://doi.org/10.1016/j.watres.2011.08.066.

Stedmon, C.A., Thomas, D.N., *et al.* (2011c) 'Using fluorescence to characterize dissolved organic matter in Antarctic sea ice brines', *Journal of Geophysical Research: Biogeosciences*, 116(G3). Available at: https://doi.org/10.1029/2011JG001716.

Stedmon, C.A. and Cory, R.M. (2014) 'Biological Origins and Fate of Fluorescent Dissolved Organic Matter in Aquatic Environments', in A. Baker et al. (eds) *Aquatic Organic Matter Fluorescence*. Cambridge: Cambridge University Press (Cambridge Environmental Chemistry Series), pp. 278–300. Available at: https://doi.org/10.1017/CBO9781139045452.013.

Stedmon, C.A. and Nelson, N.B. (2015) 'Chapter 10 - The Optical Properties of DOM in the Ocean', in D.A. Hansell and C.A. Carlson (eds) *Biogeochemistry of Marine Dissolved Organic Matter (Second Edition)*. Boston: Academic Press, pp. 481–508. Available at: https://doi.org/10.1016/B978-0-12-405940-5.00010-8.

Stein, R. & Macdonald, R.W. (2004) *Organic Carbon Budget: Arctic Ocean vs. Global Ocean*. In: [Online]. pp. 315–322. Available from: doi:10.1007/978-3-642-18912-8_8.

Stich, H. and Brinker, A. (2005) 'Less is better: Uncorrected versus pheopigment-corrected photometric chlorophyll-a estimation', *Archiv für Hydrobiologie*, 162(1), pp. 111–120.

Stubbins, A., Niggemann, J. and Dittmar, T. (2012) 'Photo-lability of deep ocean dissolved black carbon', *Biogeosciences*, 9(5), pp. 1661–1670. Available at: https://doi.org/10.5194/bg-9-1661-2012.

Takaki, Y., Hattori, K. and Yamashita, Y. (2022) 'Factors Controlling the Spatial Distribution of Dissolved Organic Matter With Changes in the C/N Ratio From the Upper to Lower Reaches of the Ishikari River, Japan', *Frontiers in Earth Science*, 10. Available at: https://www.frontiersin.org/articles/10.3389/feart.2022.826907.

Takasu, H., Uchino, K. and Mori, K. (2020) 'Dissolved and Particulate Organic Matter Dynamics Relative to Sediment Resuspension Induced by the Tidal Cycle in Macrotidal Estuaries, Kyushu, Japan', *Water*, 12(9). Available at: https://doi.org/10.3390/w12092561.

The MathWorks (2020) *Curve Fitting Toolbox*.

Thomas, H. *et al.* (2005) 'The carbon budget of the North Sea', *Biogeosciences*, 2(1), pp. 87–96. Available at: https://doi.org/10.5194/bg-2-87-2005.

Thornton, D.C.O. (2014) 'Dissolved organic matter (DOM) release by phytoplankton in the contemporary and future ocean', *European Journal of Phycology*, 49(1), pp. 20–46. Available at: https://doi.org/10.1080/09670262.2013.875596.

Tiedje, B., Moll, A. and Kaleschke, L. (2010) 'Comparison of temporal and spatial structures of chlorophyll derived from MODIS satellite data and ECOHAM3 model data in the North Sea', *Journal of Sea Research*, 64(3), pp. 250–259. Available at: https://doi.org/10.1016/j.seares.2010.03.003.

Tipping, E. *et al.* (1997) 'Organic carbon in the Humber rivers', *Science of The Total Environment*, 194–195, pp. 345–355. Available at: https://doi.org/10.1016/S0048-9697(96)05374-0.

Trenberth, K.E. (1983) 'What are the Seasons?', *Bulletin of the American Meteorological Society*, 64(11), pp. 1276–1282. Available at: https://doi.org/10.1175/1520-0477(1983)064<1276:WATS>2.0.CO;2.

Trojahn, S. *et al.* (2019) 'THE SCIENTIFIC EVOLUTION OF RIVERINE INVISIBLE DISSOLVED ORGANIC MATTER', p. 2.

Twardowski, M.S. *et al.* (2004) 'Modeling the spectral shape of absorption by chromophoric dissolved organic matter', *CDOM in the Ocean: Characterization, Distribution and Transformation*, 89(1), pp. 69–88. Available at: https://doi.org/10.1016/j.marchem.2004.02.008.

Twomey, L.J., Piehler, M.F. and Paerl, H.W. (2005) 'Phytoplankton uptake of ammonium, nitrate and urea in the Neuse River Estuary, NC, USA', *Hydrobiologia*, 533(1–3), pp. 123–134. Available at: https://doi.org/10.1007/s10750-004-2403-z.

Van Engeland, T. *et al.* (2010) 'Dissolved organic nitrogen dynamics in the North Sea: A time series analysis (1995–2005)', *Estuarine, Coastal and Shelf Science*, 89(1), pp. 31–42. Available at: https://doi.org/10.1016/j.ecss.2010.05.009.

Van Ledden *et al.* (2014) 'AN IDEALIZED METEOROLOGICAL-HYDRODYNAMIC MODEL FOR EXPLORING EXTREME STORM SURGE STATISTICS IN THE NORTH SEA', *Coastal Engineering Proceedings*, 1(34). Available at: https://doi.org/10.9753/icce.v34.management.21.

Vandenbruwane, J. *et al.* (2007) 'Optimization of dissolved organic nitrogen (DON) measurements in aqueous samples with high inorganic nitrogen concentrations', *Science of The Total Environment*, 386(1), pp. 103–113. Available at: https://doi.org/10.1016/j.scitotenv.2007.06.025.

Vines, M. and Terry, L.G. (2020) 'Evaluation of the biodegradability of fluorescent dissolved organic matter via biological filtration', *AWWA Water Science*, 2(5), p. e1201. Available at: https://doi.org/10.1002/aws2.1201.

Visser, M.P. (1970) 'The turbidity of the southern North Sea', *Deutsche Hydrografische Zeitschrift*, 23(3), pp. 97–117. Available at: https://doi.org/10.1007/BF02227174.

Vodacek, A. *et al.* (1997) 'Seasonal variation of CDOM and DOC in the Middle Atlantic Bight: Terrestrial inputs and photooxidation', *Limnology and Oceanography*, 42(4), pp. 674–686. Available at: https://doi.org/10.4319/lo.1997.42.4.0674.

Wagner, S. *et al.* (2015) 'Associations between the molecular and optical properties of dissolved organic matter in the Florida Everglades, a model coastal wetland system', *Frontiers in chemistry*, 3, p. 66.

Wang, G. *et al.* (2017) 'The peak structure and future changes of the relationships between extreme precipitation and temperature', *Nature Climate Change*, 7(4), pp. 268–274. Available at: https://doi.org/10.1038/nclimate3239.

Wang, S. *et al.* (2020) 'Organic Micropollutants in New York Lakes: A Statewide Citizen Science Occurrence Study', *Environmental Science & Technology*, 54(21), pp. 13759–13770. Available at: https://doi.org/10.1021/acs.est.0c04775.

Wang, S. *et al.* (2022) 'Riverine flux of dissolved phosphorus to the coastal sea may be overestimated, especially in estuaries of gated rivers: Implications of phosphorus adsorption/desorption on suspended sediments', *Chemosphere*, 287, p. 132206. Available at: https://doi.org/10.1016/j.chemosphere.2021.132206.

Wang, X. *et al.* (2021) 'Effect of simulated tidal cycle on DOM, nitrogen and phosphorus release from sediment in Dagu River-Jiaozhou Bay estuary', *Science of The Total Environment*, 783, p. 147158. Available at: https://doi.org/10.1016/j.scitotenv.2021.147158.

Ward, N.D. *et al.* (2017) 'Where Carbon Goes When Water Flows: Carbon Cycling across the Aquatic Continuum', *Frontiers in Marine Science*, 4. Available at: https://www.frontiersin.org/articles/10.3389/fmars.2017.00007.

Watts, G. *et al.* (2015) 'Climate change and water in the UK – past changes and future prospects', *Progress in Physical Geography: Earth and Environment*, 39(1), pp. 6–28. Available at: https://doi.org/10.1177/0309133314542957.

Weishaar, J.L. *et al.* (2003) 'Evaluation of Specific Ultraviolet Absorbance as an Indicator of the Chemical Composition and Reactivity of Dissolved Organic Carbon', *Environmental Science & Technology*, 37(20), pp. 4702–4708. Available at: https://doi.org/10.1021/es030360x.

Williamson, J.L. *et al.* (2021) 'Landscape controls on riverine export of dissolved organic carbon from Great Britain', *Biogeochemistry* [Preprint]. Available at: https://doi.org/10.1007/s10533-021-00762-2.

Wilson, H.F. and Xenopoulos, M.A. (2009) 'Effects of agricultural land use on the composition of fluvial dissolved organic matter', *Nature Geoscience*, 2(1), pp. 37–41. Available at: https://doi.org/10.1038/ngeo391.

Wilson, R.J. and Heath, M.R. (2019) 'Increasing turbidity in the North Sea during the 20th century due to changing wave climate', *Ocean Science*, 15(6), pp. 1615–1625. Available at: https://doi.org/10.5194/os-15-1615-2019.

Winterwerp, H. (1999) 'On the dynamics of high-concentrated mud suspensions', *Communications on Hydraulic and Geotechnical Engineering* [Preprint].

Wisha, U.J. and Ondara, K. (2017) 'Total Suspended Solid (TSS) Distributed by Tidal Currents during Low to High Tide Phase in the Waters of Sayung, Demak: Its Relations to Water Quality Parameters', *Journal of Marine and Aquatic Sciences*, 3(2), p. 154. Available at: https://doi.org/10.24843/jmas.2017.v3.i02.154-162.

Withers, P.J.A. and Jarvie, H.P. (2008) 'Delivery and cycling of phosphorus in rivers: A review', *Science of The Total Environment*, 400(1–3), pp. 379–395. Available at: https://doi.org/10.1016/j.scitotenv.2008.08.002.

Worrall, F. *et al.* (2018) 'Declines in the dissolved organic carbon (DOC) concentration and flux from the UK', *Journal of Hydrology*, 556, pp. 775–789. Available at: https://doi.org/10.1016/j.jhydrol.2017.12.001.

Wünsch, U.J., Murphy, K.R. and Stedmon, C.A. (2017) 'The One-Sample PARAFAC Approach Reveals Molecular Size Distributions of Fluorescent Components in Dissolved Organic Matter', *Environmental Science & Technology*, 51(20), pp. 11900–11908. Available at: https://doi.org/10.1021/acs.est.7b03260.

Wurl, O. (2009) *Practical guidelines for the analysis of seawater*. CRC press.

Wurtsbaugh, W.A., Paerl, H.W. and Dodds, W.K. (2019) 'Nutrients, eutrophication and harmful algal blooms along the freshwater to marine continuum', *WIREs Water*, 6(5), p. e1373. Available at: https://doi.org/10.1002/wat2.1373.

Xenopoulos, M.A. *et al.* (2017) 'Headwaters to oceans: Ecological and biogeochemical contrasts across the aquatic continuum', *Limnology and Oceanography*, 62(S1), pp. S3–S14. Available at: https://doi.org/10.1002/lno.10721.

Xenopoulos, M.A. *et al.* (2021) 'How humans alter dissolved organic matter composition in freshwater: relevance for the Earth's biogeochemistry', *Biogeochemistry*, 154(2), pp. 323–348. Available at: https://doi.org/10.1007/s10533-021-00753-3.

Xiaohong, C., Yongqin, C. and Guoyou, L. (2005) 'Modeling transportation of suspended solids in Zhujiang River estuary, South China', *Chinese Journal of Oceanology and Limnology*, 23(1), pp. 1–10. Available at: https://doi.org/10.1007/BF02845136.

Yamashita, Y. and Tanoue, E. (2003) 'Chemical characterization of protein-like fluorophores in DOM in relation to aromatic amino acids', *Marine Chemistry*, 82(3), pp. 255–271. Available at: https://doi.org/10.1016/S0304-4203(03)00073-2.

Yamashita, Y. and Tanoue, E. (2004) 'Chemical characteristics of amino acid-containing dissolved organic matter in seawater', *Organic Geochemistry*, 35(6), pp. 679–692. Available at: https://doi.org/10.1016/j.orggeochem.2004.02.007.

Yamashita, Y., Panton, A., *et al.* (2010a) 'Assessing the spatial and temporal variability of dissolved organic matter in Liverpool Bay using excitation–emission matrix fluorescence and parallel factor analysis', *Ocean Dynamics*, 61(5), pp. 569–579. Available at: https://doi.org/10.1007/s10236-010-0365-4.

Yamashita, Y., Scinto, L.J., *et al.* (2010b) 'Dissolved Organic Matter Characteristics Across a Subtropical Wetland's Landscape: Application of Optical Properties in the Assessment of Environmental Dynamics', *Ecosystems*, 13(7), pp. 1006–1019. Available at: https://doi.org/10.1007/s10021-010-9370-1.

Yamashita, Y., Cory, R.M., *et al.* (2010c) 'Fluorescence characteristics of dissolved organic matter in the deep waters of the Okhotsk Sea and the northwestern North Pacific Ocean', *Ecological and Biogeochemical Interactions in the Dark Ocean*, 57(16), pp. 1478–1485. Available at: https://doi.org/10.1016/j.dsr2.2010.02.016.

Yamashita, Y. *et al.* (2015) 'Linkages among fluorescent dissolved organic matter, dissolved amino acids and lignin-derived phenols in a river-influenced ocean margin', *Frontiers in Marine Science*, 2. Available at: https://doi.org/10.3389/fmars.2015.00092.

Yang, Y.-Y. *et al.* (2022) 'Molecular characterization of dissolved organic nitrogen and phosphorus in agricultural runoff and surface waters', *Water Research*, 219, p. 118533. Available at: https://doi.org/10.1016/j.watres.2022.118533.

Yates, C.A., Johnes, P.J. and Spencer, R.G.M. (2016) 'Assessing the drivers of dissolved organic matter export from two contrasting lowland catchments, U.K', *Science of The Total Environment*, 569–570, pp. 1330–1340. Available at: https://doi.org/10.1016/j.scitotenv.2016.06.211.

Yates, C.A. *et al.* (2019) 'Variation in dissolved organic matter (DOM) stoichiometry in U.K. freshwaters: Assessing the influence of land cover and soil C:N ratio on DOM composition', *Limnology and Oceanography*, 64(6), pp. 2328–2340. Available at: https://doi.org/10.1002/lno.11186.

Yoro, S., Panagiotopoulos, C. and Sempéré, R. (1999) 'Dissolved organic carbon contamination induced by filters and storage bottles', *Water Research - WATER RES*, 33, pp. 1956–1959. Available at: https://doi.org/10.1016/S0043-1354(98)00407-2.

YSI (2009) ‘ysi-556-multiparameter-system-spec-sheet.pdf’. Available at: https://www.xylem-analytics.asia/media/pdfs/ysi-556-multiparameter-system-spec-sheet.pdf (Accessed: 24 June 2022).

Yu, H. *et al.* (2015) ‘Impact of dataset diversity on accuracy and sensitivity of parallel factor analysis model of dissolved organic matter fluorescence excitation-emission matrix’, *Scientific Reports*, 5(1). Available at: https://doi.org/10.1038/srep10207.

Zark, M. and Dittmar, T. (2018) ‘Universal molecular structures in natural dissolved organic matter’, *Nature Communications*, 9(1), p. 3178. Available at: https://doi.org/10.1038/s41467-018-05665-9.

Zhou, Y., Xuan, J. and Huang, D. (2020) ‘Tidal variation of total suspended solids over the Yangtze Bank based on the geostationary ocean color imager’, *Science China Earth Sciences*, 63(9), pp. 1381–1389. Available at: https://doi.org/10.1007/s11430-019-9618-7.

Zsolnay, A. *et al.* (1999) ‘Differentiating with fluorescence spectroscopy the sources of dissolved organic matter in soils subjected to drying’, *Chemosphere*, 38(1), pp. 45–50. Available at: https://doi.org/10.1016/S0045-6535(98)00166-0.

Appendix A

Supplementary material for Chapter 2

A.1 Images of the riverine sampling points

Figure A1. *Estuarine sampling site SEA1 on 24 February 2019. This is the harbour in Great Yarmouth that connects the rivers to the southern North Sea.*

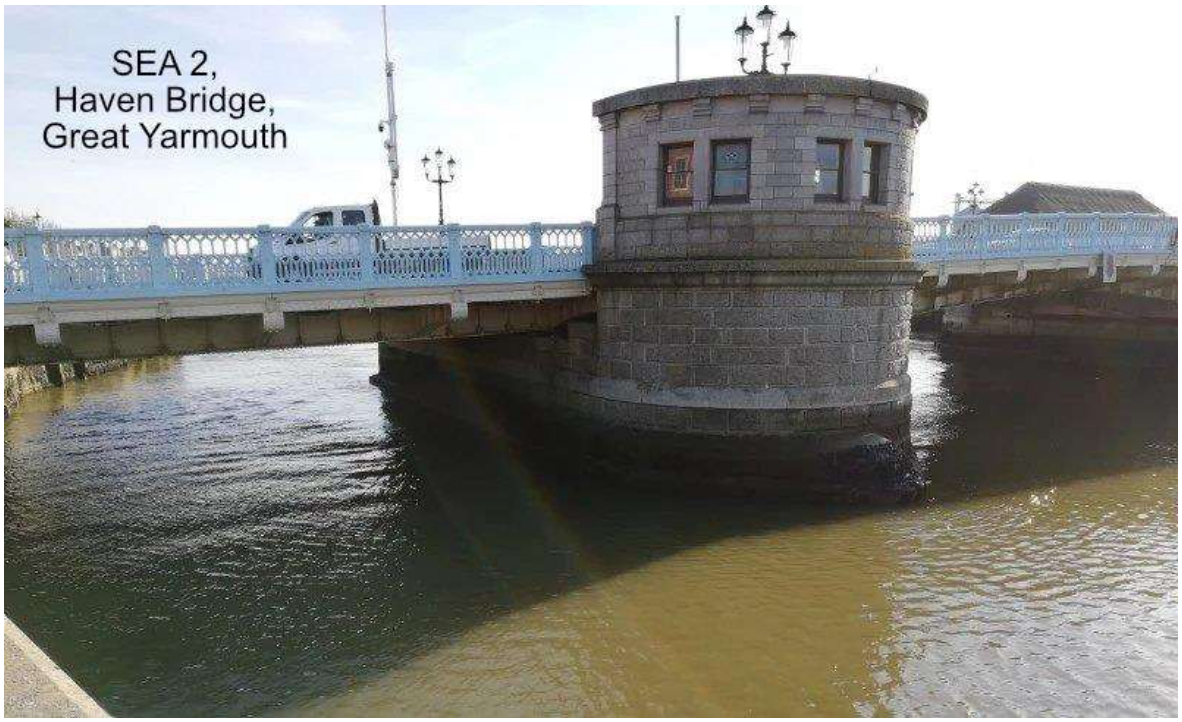

Figure A2. *Estuarine sampling site SEA2 on 17 February 2019. This is Haven Bridge in the city centre of Great Yarmouth.*

Figure A3. *Estuarine sampling point SEA3 on 25 July 2019. This is the estuary Breydon Water near Great Yarmouth. Left is the view on the left of the estuary, and on the right the view on the right of the estuary.*

Figure A4. *Sampling point WAVE4 on the River Waveney on 25 July 2019. This sampling point is located downstream to Burgh Castle, near Marsh view fishery.*

Figure A5. *Sampling site WAVE5 on the River Waveney on 24 February 2019. This sampling point is located near the roman fort at Burgh Castle.*

Figure A6. *Sampling site WAVE6 on the River Waveney on 26 July 2020.*

Figure A7. *Sampling point WAVE7 on the River Waveney on 16 June 2019.*

Figure A8. *Sampling site on the River Yare YAR4 on 17 February 2019. This site is a mooring managed by the Broads Authority, situated near Wickhampton.*

Figure A9. *Sampling point YAR5 at Riverside in Reedham on 17 March 2019.*

Figure A10. *Sampling site YAR6 at Cantley on the River Yare on 20 October 2019. In the picture is visible the sugar factory.*

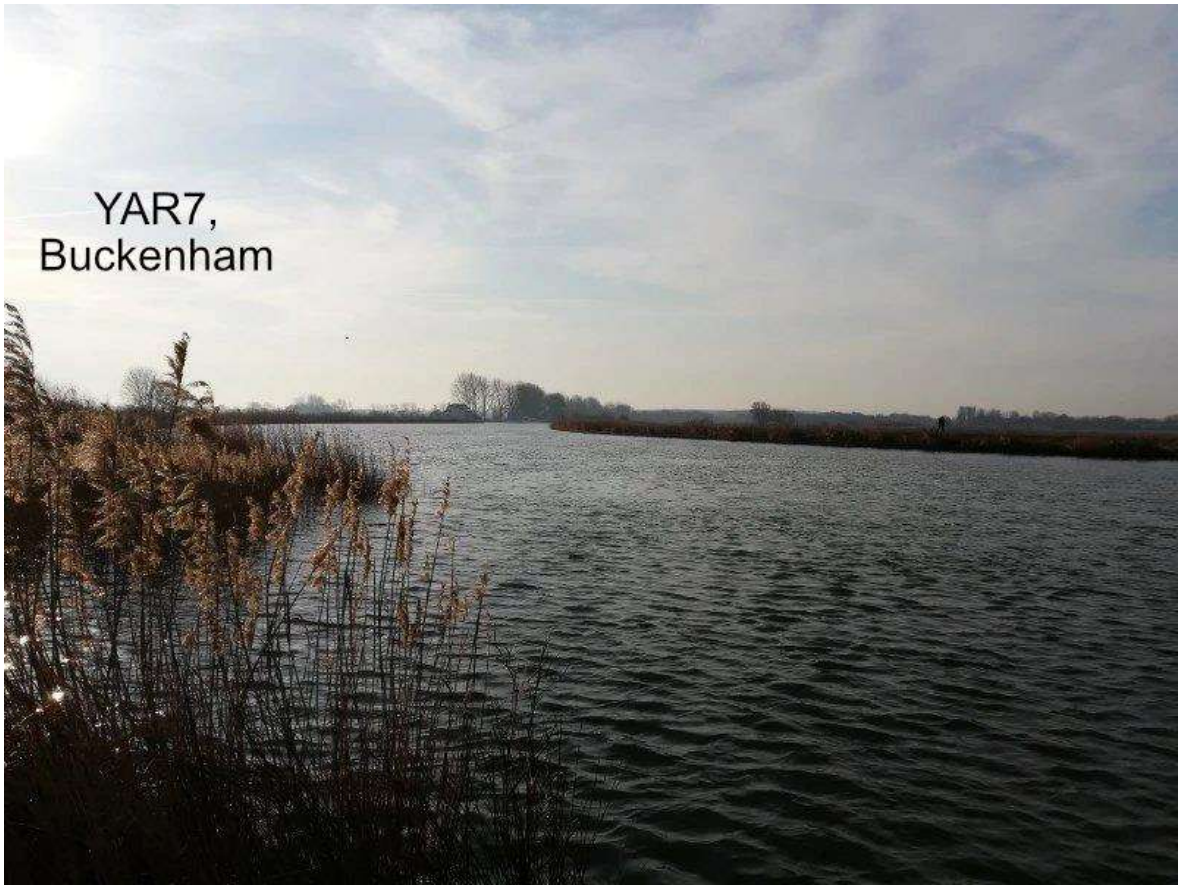

Figure A11. *Sampling point YAR7 at Buckenham on 17 February 2019. This is located in a nature reserve near the Buckenham railway station.*

A.2 Additional information on the riverine sampling

Table A1. *Weather conditions and dates of the riverine sampling.*

Sampling date	River	Weather conditions
15 November 2018	Waveney	Cloudy and windy, and sunny at times
10 December 2018	Yare	Cloudy and sunny
19 December 2018	Waveney	Sunny and windy
13 January 2019	Yare	Very windy, with wind speed reaching 50 mph
20 January 2019	Waveney	Sunny with no wind
17 February 2019	Yare	Sunny, light breeze
24 February 2019	Waveney	Sunny, light breeze
17 March 2019	Yare	Very windy and cloudy. Rain and hail after 12:00
24 March 2019	Waveney	Sunny and windy
11 April 2019	Yare	Cloudy and windy
14 April 2019	Waveney	Windy, cloudy and sunny
19 May 2019	Waveney	Cloudy and light rain
27 May 2019	Yare	Cloudy and windy
12 June 2019	Yare	Cloudy and raining
16 June 2019	Waveney	Windy, cloudy and sunny
22 July 2019	Yare	Sunny and windy
25 July 2019	Waveney	Sunny, light breeze
19 August 2019	Waveney	Windy, cloudy and sunny. Rain after 12:00

22 August 2019	Yare	Sunny and windy
22 September 2019	Waveney	Sunny and windy
28 September 2019	Yare	Windy, cloudy and sunny
13 October 2019	Waveney	Cloudy and windy
20 October 2019	Yare	Sunny and cloudy
16 November 2019	Waveney	Cloudy
24 November 2019	Yare	Cloudy
08 December 2019	Yare	Windy, cloudy and sunny
12 December	Waveney	Cloudy, windy and raining

Appendix B

Supplementary material for Chapter 3

B.1 Correlation between peak T : peak C and water level at Reedham for the River Yare

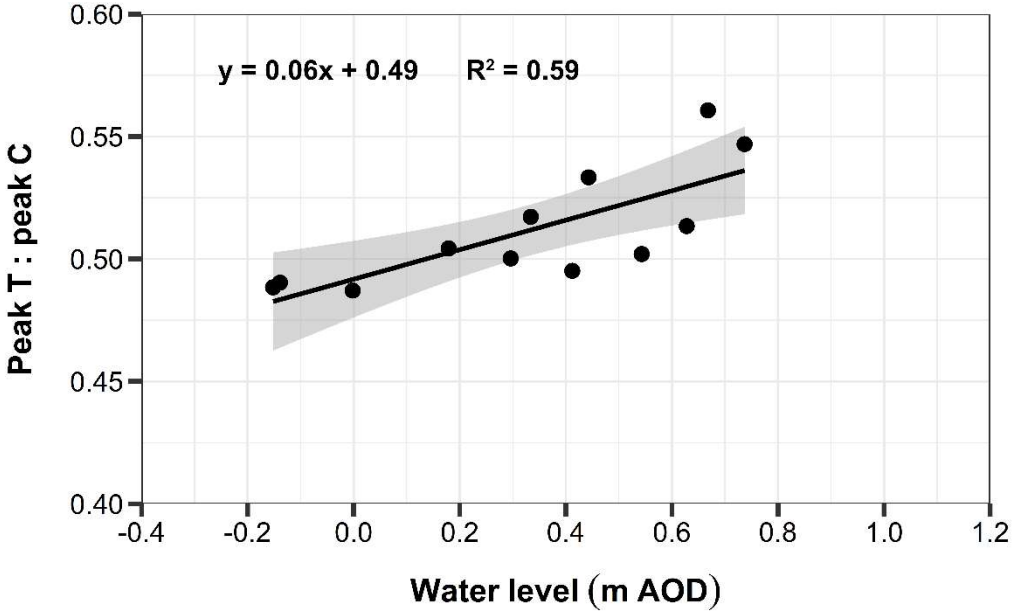

Figure B1. *Linear correlation between peak T : peak C and the water level at Reedham for the samples collected on 21 July 2020 at sampling site YAR4. The grey area indicates the 95% confidence interval for the linear correlation. The p – value is < 0.01.*

B.2 Correlation between TC5 and TC6 with salinity for the River Waveney

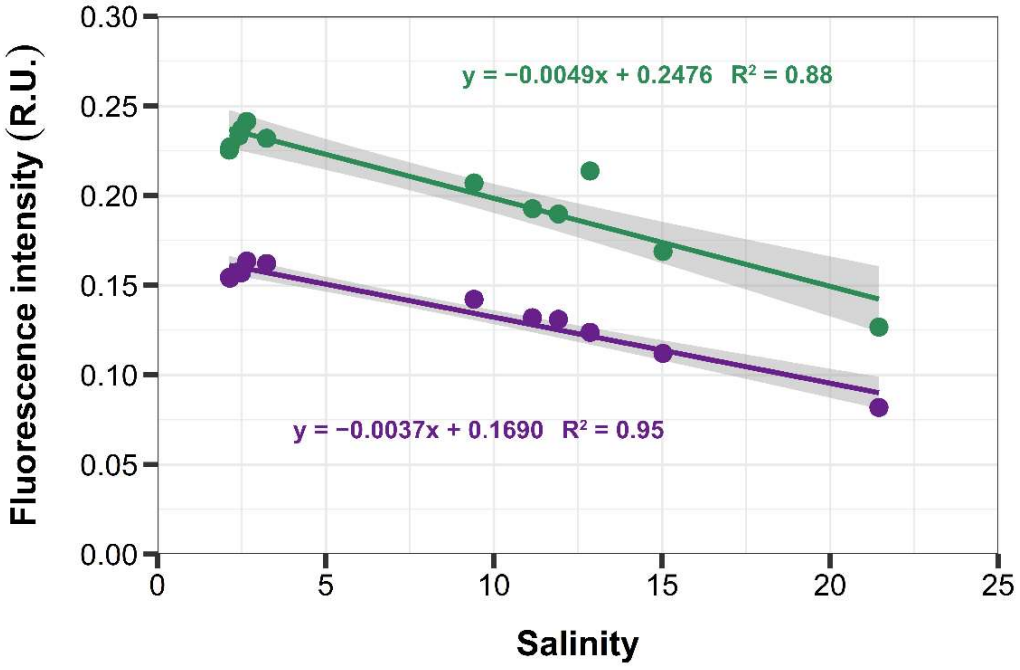

Figure B2. *Linear correlation between the fluorescence intensity (R.U.) for components TC5 and TC6 identified through the PARAFAC model and salinity for the samples collected on 26 July 2020 at sampling site WAVE6. The grey area indicates the 95% confidence interval for the linear correlation. The p-value is < 0.01.*

B.3 Correlation between TSS and chlorophyll-*a* for the River Waveney

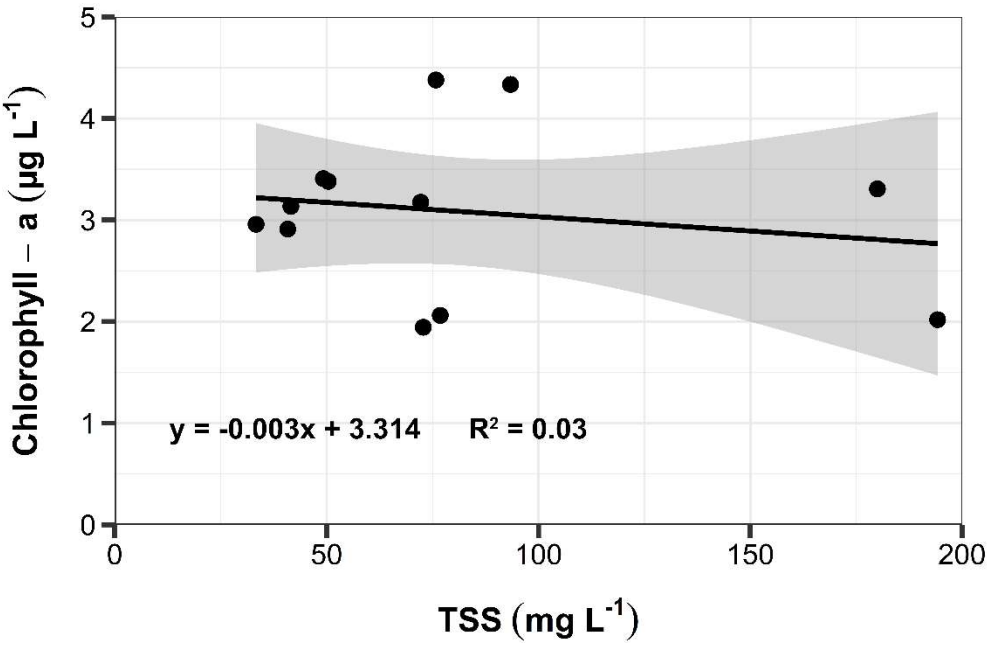

Figure B3. *Linear correlation between chlorophyll-a and TSS for the samples collected on 26 July 2020 at sampling site WAVE6. The grey area indicates the 95% confidence interval for the linear correlation. The p-value is 0.57.*

B.4 Correlation between water levels at Burgh Castle and Haddiscoe with TDN, nitrate plus nitrite, TDP and DOP for the River Waveney

Table B1*. Equations, R^2 and significance for the linear correlations between TDN, nitrate plus nitrite, TDP and DOP with water levels at Burgh Castle and at Haddiscoe for the water samples collected on 26 July 2020 at sampling site WAVE6.*

Variable vs water level at Burgh Castle	Equation linear correlation	R^2	Significance
TDN	$y = -20.25x + 192.71$	0.04	0.55
Nitrate + nitrite	$y = -5.84x + 177.44$	0.01	0.81
TDP	$y = -0.84x + 7.31$	0.11	0.29
DOP	$y = -1.08x + 4.04$	0.12	0.26
Variable vs water level at Haddiscoe	**Equation linear correlation**	**R^2**	**Significance**
TDN	$y = -26.95x + 194.18$	0.03	0.57
Nitrate + nitrite	$y = 2.30x + 172.85$	0.00	0.95
TDP	$y = -1.15x + 7.39$	0.10	0.31
DOP	$y = -1.98x + 4.39$	0.21	0.13

B.5 Statistical significance of the PCA for the quantitative and qualitative data of DOM

The statistical tests performed on the PCA produces four plots summarising its outputs, visualising the comparison between the built null distribution and the observed parameters. The test showed that both PCAs run for this dataset (quantitative and qualitative DOM data) were statistically significant.

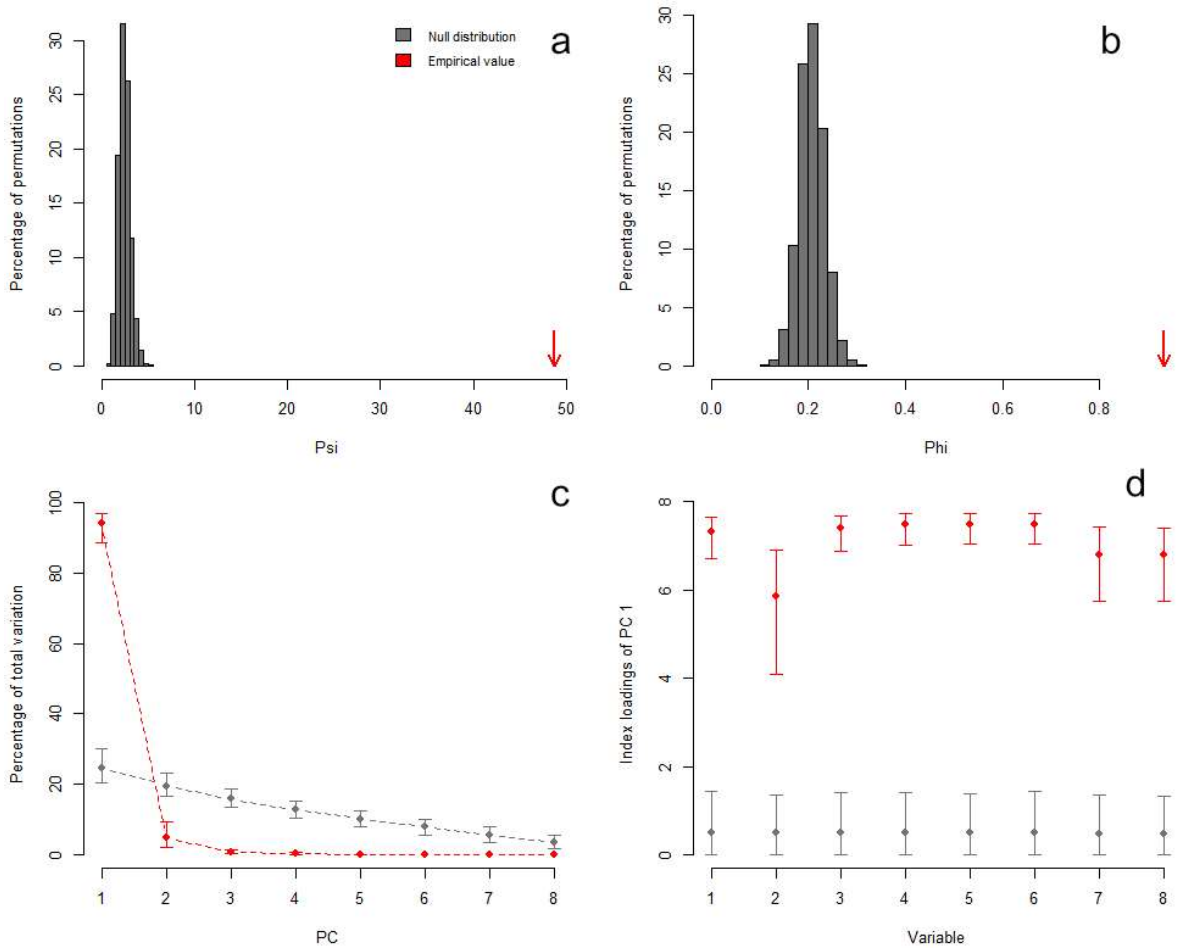

Figure B4. *The outputs from the test on the statistical significance of the PCA run for the quantitative data of DOM for the sampling campaigns of the River Yare and Waveney on 21 and 26 July 2020. Plot a represents the null distribution of the randomised ψ and the empirical values, plot b represents the null distribution of the randomised φ and the empirical values, plot c represents the variation explained by the randomised and empirical components and plot d represents the index loadings of the randomised and empirical values of the significant components. The red dots indicate the mean observed values, whilst the red bars indicate the 95% confidence interval based on 1000 bootstraps replicates. The grey dots indicate the mean values of the random permutations, whilst the grey bars indicate the 95% confidence interval of the same 1000 random permutations.*

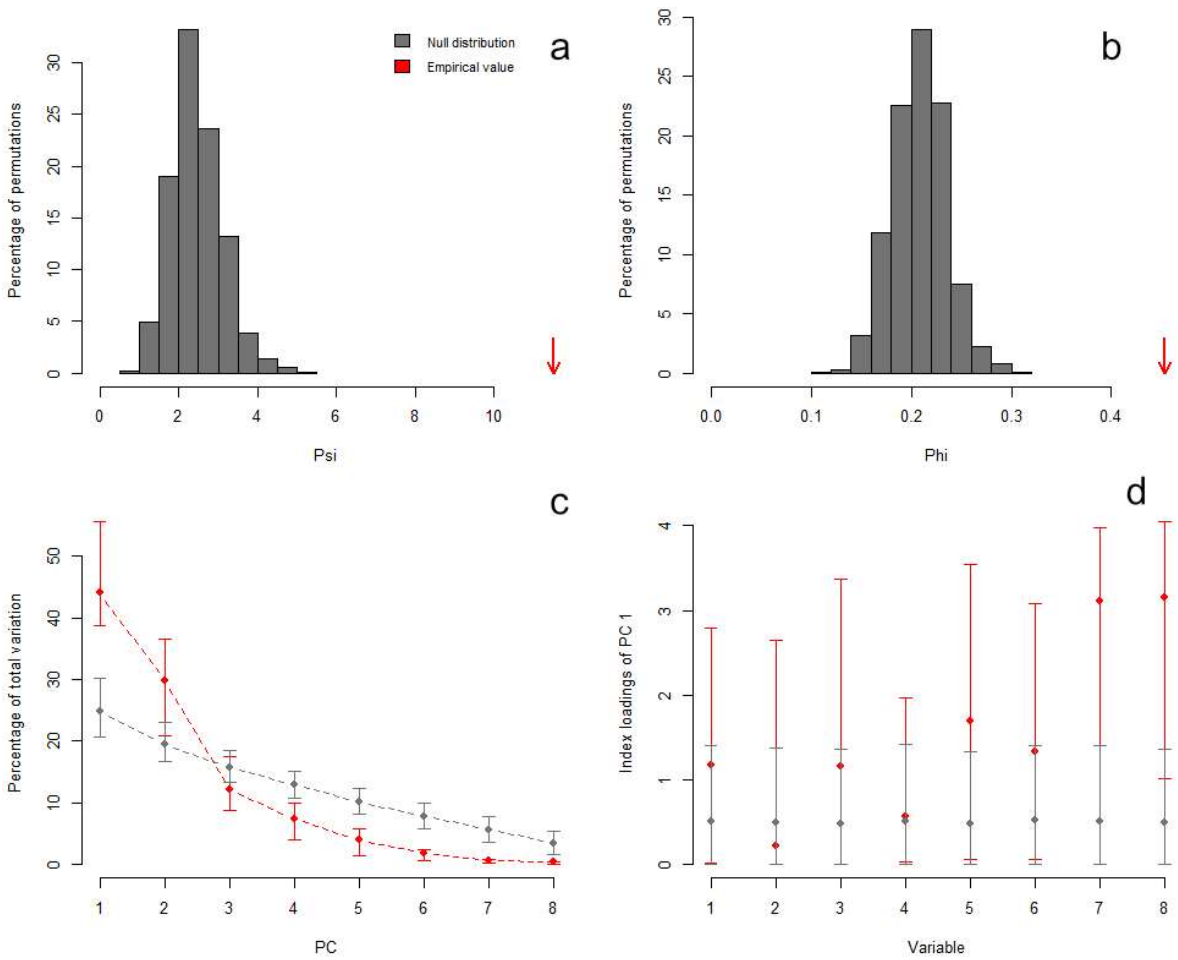

Figure B5. *The outputs from the test on the statistical significance of the PCA run for the qualitative data of DOM for the sampling campaigns of the River Yare and Waveney on 21 and 26 July 2020. Plot a represents the null distribution of the randomised ψ and the empirical values, plot b represents the null distribution of the randomised φ and the empirical values, plot c represents the variation explained by the randomised and empirical components and plot d represents the index loadings of the randomised and empirical values of the significant components. The red dots indicate the mean observed values, whilst the red bars indicate the 95% confidence interval based on 1000 bootstraps replicates. The grey dots indicate the mean values of the random permutations, whilst the grey bars indicate the 95% confidence interval of the same 1000 random permutations.*

Appendix C

Supplementary material for Chapter 4

C.1 Match of the six components identified by the PARAFAC model with the OpenFluor database

Table C1. Description, spectral characterisation and comparison with the OpenFluor database of the components identified and validated by the PARAFAC model of the samples collected between November 2018 and December 2019 in the River Waveney and in the River Yare.

Component	excitation/emission maxima (nm)	Description	OpenFluor database matches	Water type matches
C1	285, 385 / 444	Humic-like of terrestrial origin, photolabile	Borisover et al., 2011; Osburn et al., 2011; Kothawala et al., 2012; Murphy et al., 2014; Lambert, et al., 2016; Chen et al., 2018; Wauthy et al., 2018; Zhou et al., 2019; Groeneveld et al., 2020; Wang et al., 2020; Gullian-Klanian et al., 2021	River Kishon, Israel; Lakes of the Great Plains, U.S.A.; Lakes across south-central Sweden; Horsens fjord, Denmark; River network, Congo; Lakes Taihu and Hongze, China; Circumpolar freshwaters; River to coastal waters, Borneo; Lakes and rivers, Sweden; Lakes in New York; Recirculating aquaponic water system
C2	270 / 466	Humic-like of terrestrial origin, photorefractory	Yamashita et al., 2010; Murphy et al., 2014; Dainard et al., 2015; Chen et al., 2017; Imbeau et al., 2021	Freshwater wetland, U.S.A.; Horsens fjord, Denmark; Sea and ocean waters; Rivers in South Korea; Boreal and Arctic lakes

Component	excitation/emission maxima (nm)	Description	OpenFluor database matches	Water type matches
C3	310 / 392	Humic-like microbially produced	Yamashita et al., 2010; Osburn et al., 2011; Cawley et al., 2012; Lapierre and del Giorgio, 2014; Murphy et al., 2014; Shutova et al., 2014; Li et al., 2015; Yu et al., 2015; Gonçalves-Araujo et al., 2016; Osburn et al., 2016; Wünsch et al., 2017; Wauthy et al., 2018; Wünsch et al., 2018; Gullian-Klanian et al., 2021	Freshwater wetland, U.S.A.; Lakes of the Great Plains, U.S.A.; River to coastal waters, U.S.A.; Boreal aquatic networks; Horsens fjord, Denmark; Drinking water treatment plants; Yangtze estuary, China; Wastewater and algae excretion; Arctic surface waters; Estuaries and coastal waters; Lakes, rivers and ocean waters; Circumpolar freshwaters; Arctic fjords; Recirculating aquaponic water system
C4	285, 410 / 518	Fulvic-like of terrestrial origin, associated with soils	Kowalczuk et al., 2009; Osburn et al., 2011; Wünsch et al., 2017; Gullian-Klanian et al., 2021	Coastal waters, South Atlantic Bight; Lakes of the Great Plains, U.S.A.; Lakes, rivers and ocean waters; Recirculating aquaponic water system
C5*	270, 385 / 466	Between humic- and fulvic-like of terrestrial origin	Stedmon et al., 2011; Harjung et al., 2018; Jutaporn et al., 2020	Drinking water treatment plants; River water, Iberian Peninsula; Wastewater, drinking water and rivers
C6	280 / 340	Protein-like, particularly tryptophan-like produced *in-situ*	Murphy et al., 2008; Borisover et al., 2009; Yamashita et al., 2010; Murphy et al., 2011; Stedmon et al., 2011; Murphy et al., 2014; Peleato et al., 2016; Wheeler et al., 2017; DeFrancesco and Guéguen, 2021; Smith et al., 2021	Marine waters; Lakes and rivers, Israel; Coastal waters, Liverpool Bay; Water treatment plants; Antarctic sea ice brines, Weddell Sea; Horsens fjord, Denmark; River waters, Ontario; Leaf litter leachate; Arctic Ocean; River to coastal waters, U.S.A.

*studies matched shown for C5 have Tucker Congruence Coefficient (TCC) > 0.9. The matches shown for the other components have TCC >0.95.

C.2 Statistical significance of the PCA for the quantitative and qualitative data of DOM

The test showed that both PCAs run (quantitative and qualitative DOM data) were statistically significant.

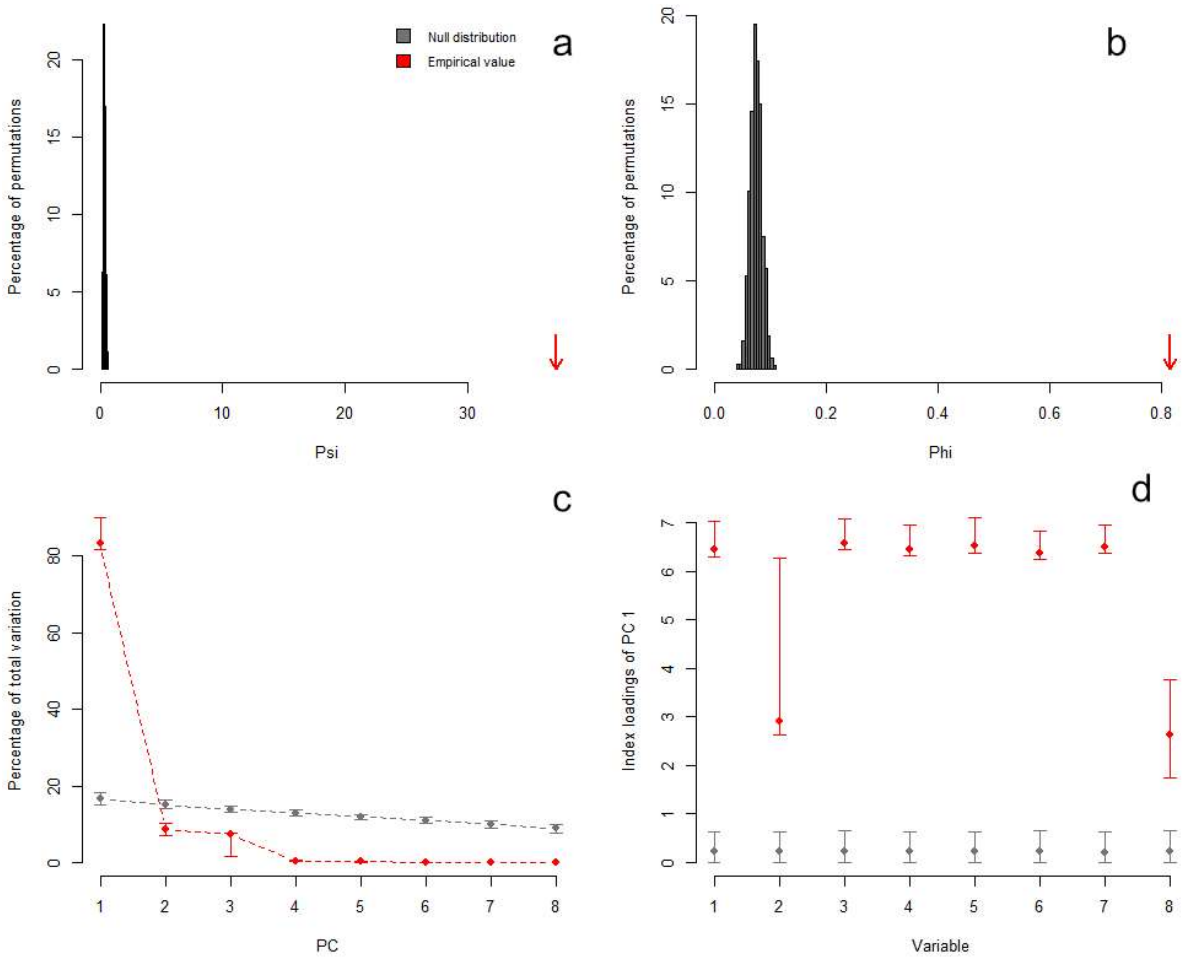

Figure C1. *The outputs from the test on the statistical significance of the PCA run for the quantitative data of DOM for the samples collected in the River Yare and in the River Waveney between November 2018 and December 2019. Plot* ***a*** *represents the null distribution of the randomised ψ and the empirical values, plot* ***b*** *represents the null distribution of the randomised φ and the empirical values, plot* ***c*** *represents the variation explained by the randomised and empirical components and plot* ***d*** *represents the index loadings of the randomised and empirical values of the significant components. The red dots indicate the mean observed values, whilst the red bars indicate the 95% confidence interval based on 1000 bootstraps replicates. The grey dots indicate the mean values of the random permutations, whilst the grey bars indicate the 95% confidence interval of the same 1000 random permutations.*

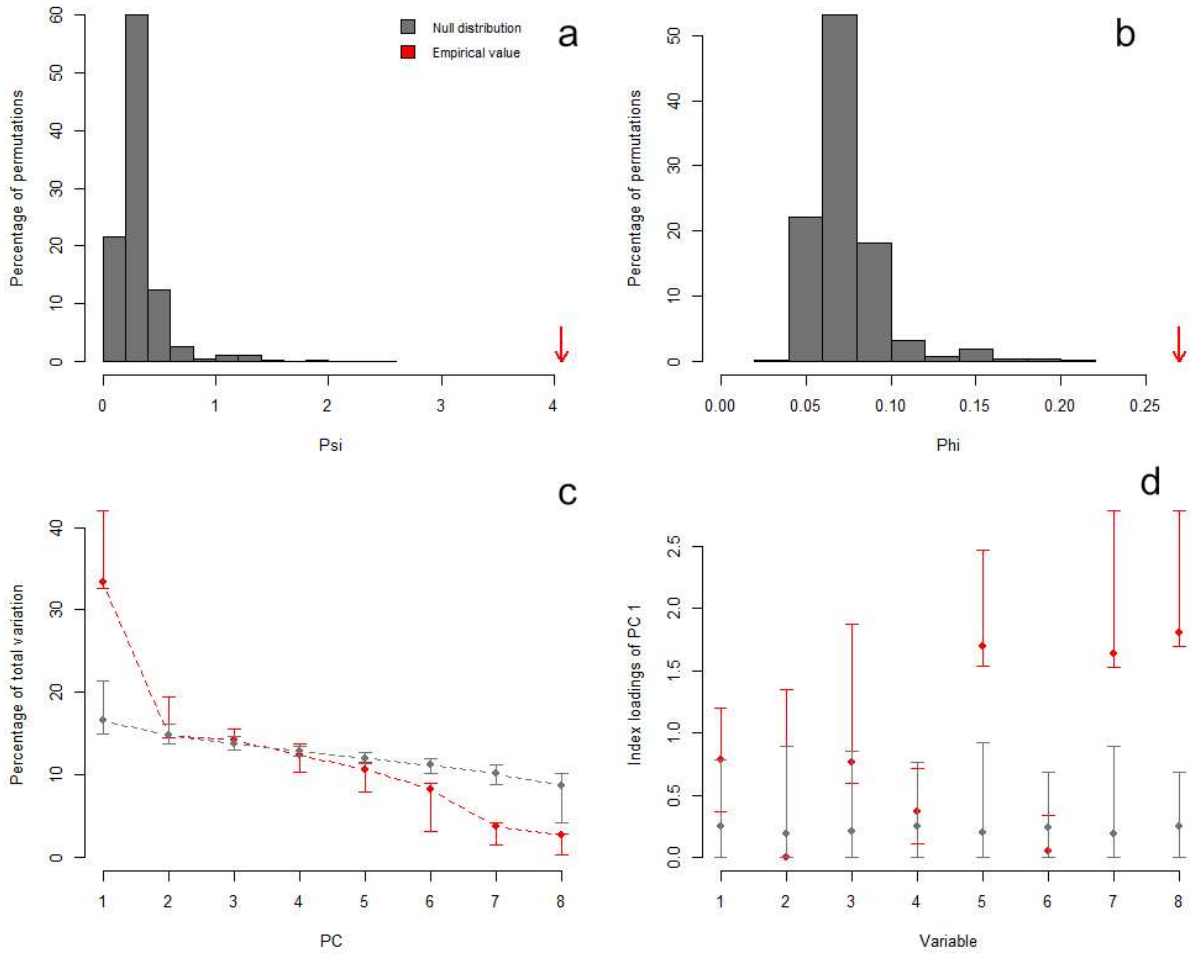

Figure C2. *The outputs from the test on the statistical significance of the PCA run for the qualitative data of DOM for the samples collected in the River Yare and in the River Waveney between November 2018 and December 2019. Plot* ***a*** *represents the null distribution of the randomised ψ and the empirical values, plot* ***b*** *represents the null distribution of the randomised φ and the empirical values, plot* ***c*** *represents the variation explained by the randomised and empirical components and plot* ***d*** *represents the index loadings of the randomised and empirical values of the significant components. The red dots indicate the mean observed values, whilst the red bars indicate the 95% confidence interval based on 1000 bootstraps replicates. The grey dots indicate the mean values of the random permutations, whilst the grey bars indicate the 95% confidence interval of the same 1000 random permutations.*

Appendix D

Supplementary material for Chapter 5

D.1 Match of the six components identified by the PARAFAC model with the OpenFluor database

Table D1. *Description, spectral characteristics and comparison with the OpenFluor database of the five components identified and validated by the PARAFAC model for the 105 samples collected during the cruises onboard the RV Cefas Endeavour between November 2018 and July 2020 in the southern North Sea.*

Component	Excitation/emission maxima λ (nm)	Description	OpenFluor database matches	Water type matches
SC1	270, 360 / 460	Humic-like of terrestrial origin with high aromaticity and molecular weight	Stedmon, 2003; Borisover et al., 2009; Kowalczuk et al., 2009; Yamashita et al., 2010a, 2010b; Dainard and Guéguen, 2013; Shutova et al., 2014; Bittar et al., 2015; Dainard et al., 2015; Gonçalves-Araujo et al., 2015; Chen et al., 2016; Osburn et al., 2016; Sharma et al., 2017a; Chen et al., 2018; Murphy et al., 2018; Schittich et al., 2018; Dainard et al., 2019; García et al., 2019	Estuarine system, Denmark; Lake and rivers, Israel; Coastal waters, U.S.A.; Coastal waters and wetlands; Seawater, North Pacific Arctic Ocean; Drinking water treatment plants; Algal cultures; Seawater, Beaufort Sea, North Atlantic; Seawater, Lena River Delta, Siberia; Sediments, Arctic Ocean; Estuarine systems, North America; Soil samples, Israel; Chukchi Sea, Arctic Ocean; Water samples different environments; Groundwater aquifers, Bengal Basin; Polar mixed waters, Canada Basin; Freshwater, Argentina.
SC2	275, 310 / 406	Humic-like from microbial processing of organic matter of terrestrial origin	Borisover et al., 2009; Kowalczuk et al., 2009; Kothawala et al., 2014; Shutova et al., 2014; Catalá et al., 2015; Gonçalves-Araujo et al., 2016; Lambert et al., 2016; Gao and Guéguen, 2017; Sharma et al., 2017b; Wünsch et al., 2017; Catalán et al., 2018;	Lake and rivers, Israel; Coastal waters, U.S.A.; Boreal lakes, Sweden; Drinking water treatment plants; Dark ocean, >200 m depth; Seawater, Arctic Ocean; River waters, Congo; Seawater, Beaufort Sea; Soil samples, Israel; Lakes, rivers and ocean waters; Headwater streams across Europe;

Component	Excitation/emission maxima λ (nm)	Description	OpenFluor database matches	Water type matches
SC2 continued	275, 310 / 406	Humic-like from microbial processing of organic matter of terrestrial origin	Chen et al., 2018; Murphy et al., 2018; Schittich et al., 2018; Wünsch et al., 2018; Amaral et al., 2020; Kim et al., 2020; Amaral et al., 2021a, 2021b; Du et al., 2021; Imbeau et al., 2021; Wang et al., 2021; Kim et al., 2022	Lake water, China; Water samples different environments; Groundwater aquifers, Bengal Basin; Arctic fjords; Coastal waters, Gulf of Cádiz, Spain; Seawater, western Indian Ocean; Estuarine coastal waters; Lake water, China; Boreal and Arctic lakes; Lake water, U.S.A.; Coastal waters, Jeju Island, Korea.
SC3	275, 400 / 506	Humic-like or fulvic-like of terrestrial origin, linked to soil and sediments but reported also as a product of photodegradation	Kowalczuk et al., 2009; Yamashita et al., 2010; Osburn et al., 2011; Yamashita et al., 2011; Walker et al., 2013; Kothawala et al., 2014; Murphy et al.,2014; Gonçalves-Araujo et al., 2015; Sharma et al., 2017a; Wünsch et al., 2017; Murphy et al., 2018; Schittich et al., 2018; Wünsch et al., 2018; Zhou et al., 2019; Gullian-Klanian et al., 2021; Eder et al., 2022	Coastal waters, U.S.A.; Subtropical wetland: Prairie saline ecosystems, U.S.A.; Headstreams, U.S.A.; Arctic rivers; Boreal lakes, Sweden; Freshwater from rivers, Denmark; Seawater, Lena River Delta, Siberia; Soil samples, Israel; Lakes, rivers and ocean waters; Water samples different environments; Groundwater aquifers, Bengal Basin; Arctic fjords; Rivers, estuaries and coastal waters; Algal cultures; Small agricultural catchment, Austria.

Component	Excitation/emission maxima λ (nm)	Description	OpenFluor database matches	Water type matches
SC4	285 / 350	Protein-like, particularly tryptophan-like from recent *in-situ* biological activity	Murphy et al., 2011; Cawley et al., 2012; Wünsch et al.,2017; Wünsch et al., 2018	Water treatment plants; Coastal waters, Shark Bay, Australia; Lakes, rivers and ocean waters; Arctic fjords.
SC5	275 / 312	Protein-like, particularly tyrosine-like from recent *in-situ* biological activity and degraded proteinaceous material	Murphy et al., 2011; Yamashita et al., 2011; Yamashita et al., 2013; Chen et al., 2017; D'Andrilli et al., 2017; Painter et al., 2018; D'Andrilli et al., 2019; Derrien et al., 2019; Derrien et al., 2020; Pucher et al., 2021	Water treatment plants; Headstreams, U.S.A.; Coastal waters, Florida Keys; River waters, South Korea; Ice cores, western Antarctica; Seawater, North Sea; Plant litter and river water, U.S.A.; Sediment porewater, South Korea; Soil and algae incubations; River water, Austria.

D.2 Linear correlation between chlorophyll-*a* and inorganic and organic nutrients in the Southern North Sea

Table D2. *Equations, R^2 and significance for the linear correlations between chlorophyll-a and TDN, nitrate plus nitrite, TDP, DOP and phosphate for the samples collected during the cruises onboard the RV Cefas Endeavour between November 2018 and July 2020 in the southern North Sea.*

Variable vs chlorophyll-*a*	Equation linear correlation	R^2	Significance
TDN	$y = 0.001x + 0.653$	0.00	0.90
Nitrate + nitrite	$y = -0.014x + 0.829$	0.08	< 0.01
TDP	$y = 0.135x + 0.361$	0.03	> 0.05
DOP	$y = 0.130x + 0.444$	0.04	> 0.05
Phosphate	$y = -0.474x + 0.907$	0.04	> 0.05

D.3 Boxplots for seasonal differences of variables collected in the Southern North Sea between November 2018 and July 2020

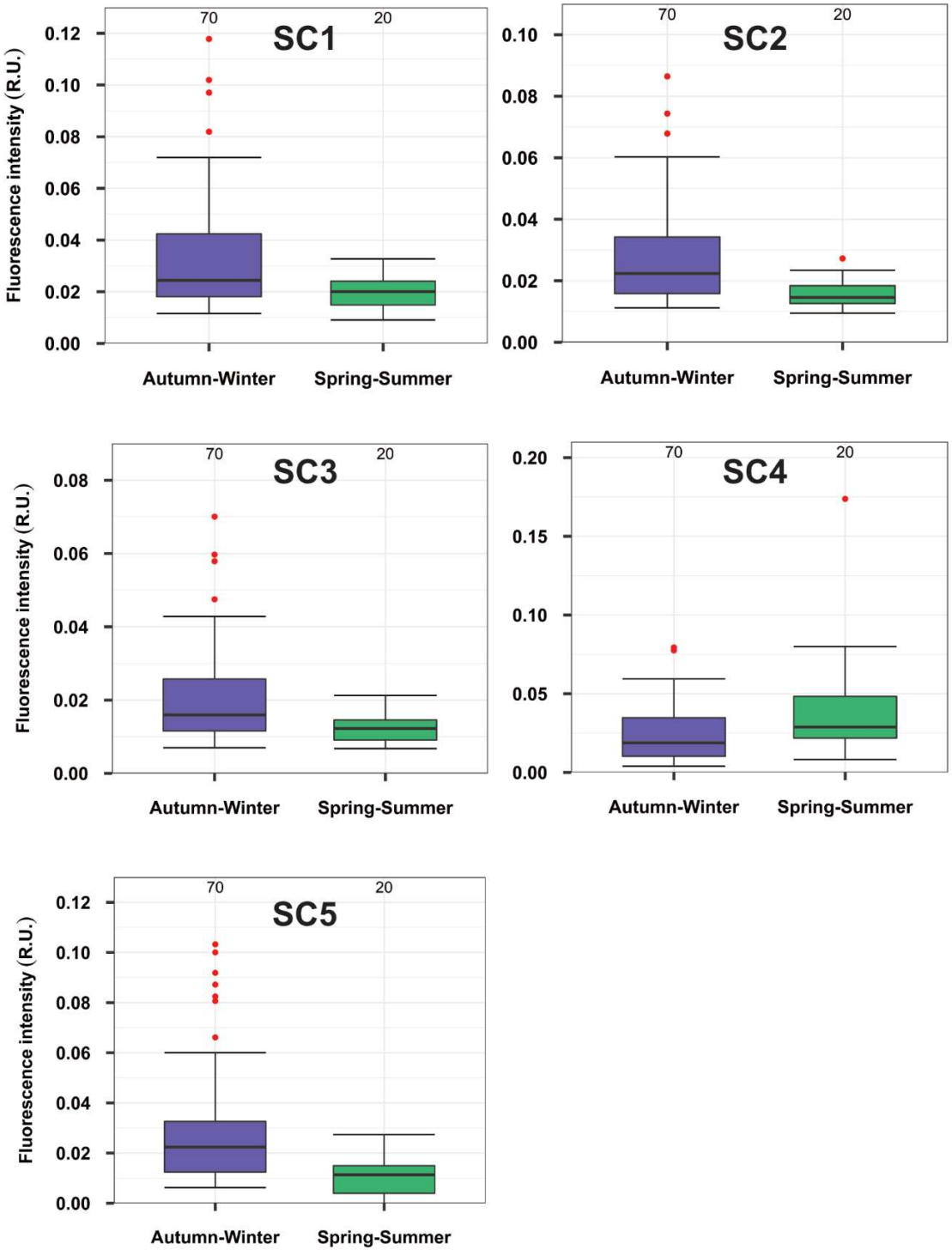

Figure D1. *Boxplot of components SC1 – SC5 identified by the PARAFAC model by season, for the samples collected in the southern North Sea between November 2018 and July 2020. The bars represent the interquartile range with the horizontal line being the median (50th percentile). Below the median is the 25th percentile and above is the 75th percentile. The error bars on top represent the largest value within 1.5 times the range above the 75th percentile, whilst the ones below represent the smallest value within 1.5 times the range below the 25th percentile. The red dots represent values that are > 1.5 times and < 3 times the interquartile range beyond either end of the bars. The numbers at the top of the plot are the number of samples used to create the boxplot.*

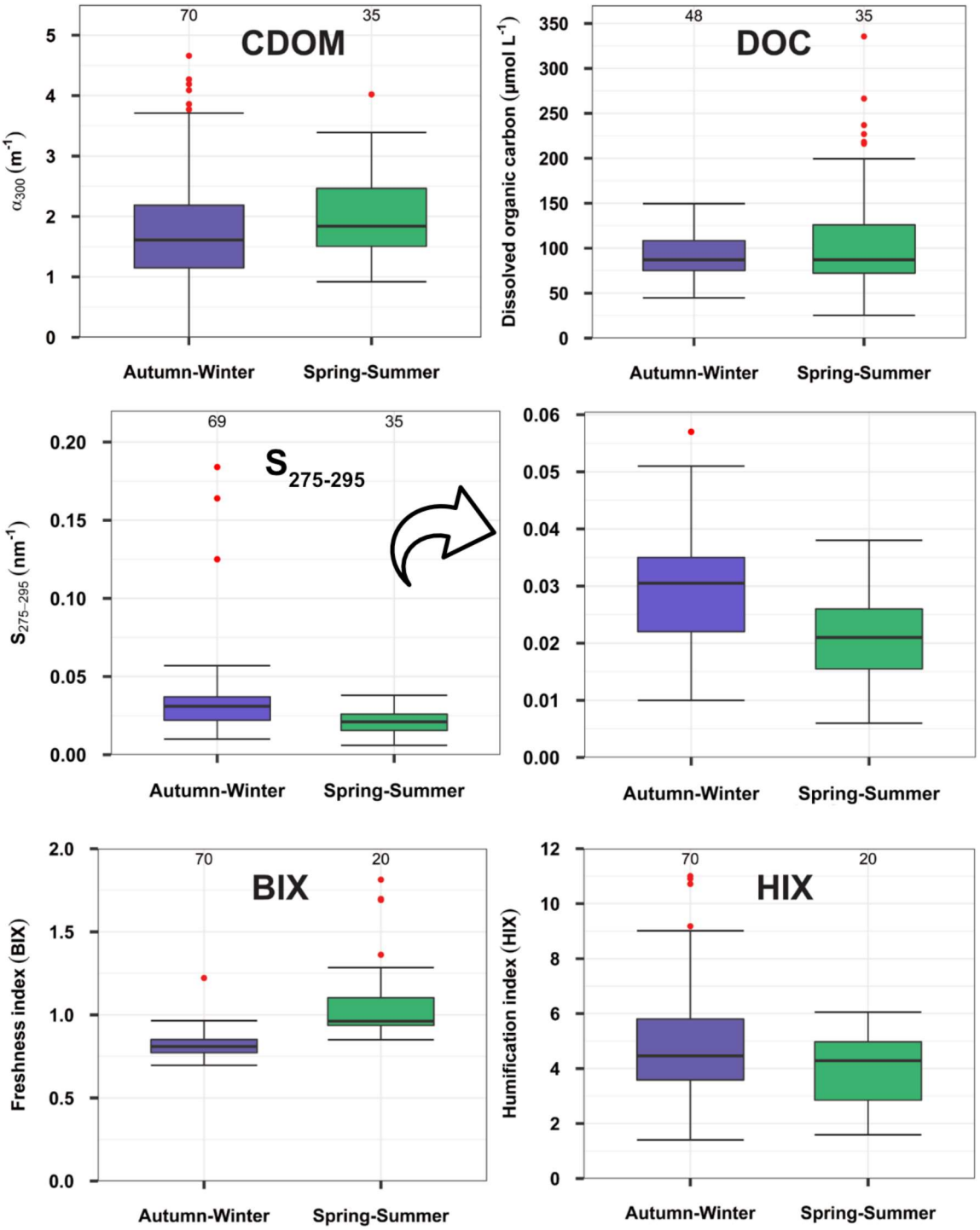

Figure D2. *Boxplot of CDOM, DOC, $S_{275-295}$, BIX and HIX by season, for the samples collected in the southern North Sea between November 2018 and July 2020. See Figure D1 for an explanation of the boxplots.*

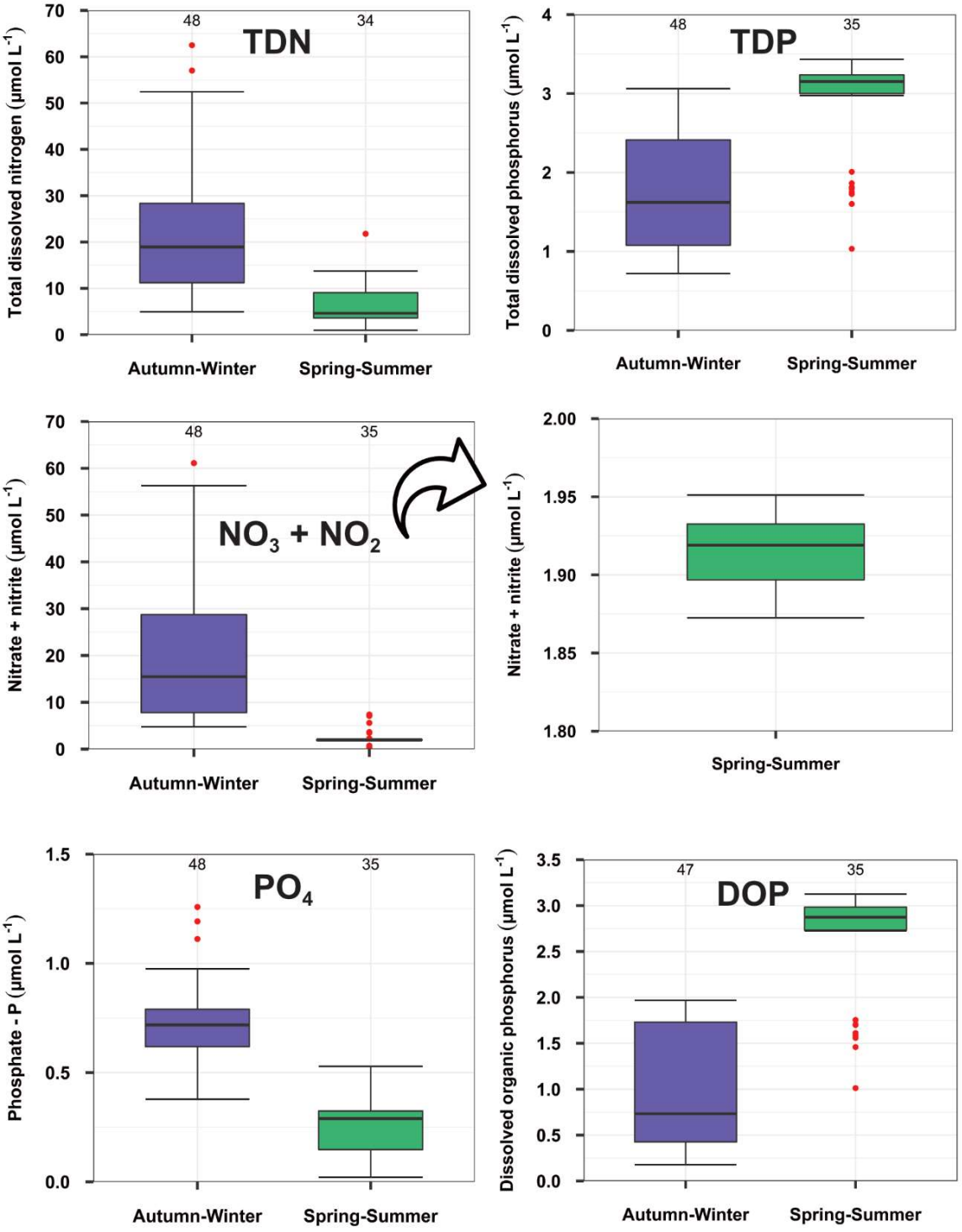

Figure D3. *Boxplot of TDN, TDP, nitrate plus nitrite, phosphate and DOP by season, for the samples collected in the southern North Sea between November 2018 and July 2020. See Figure D1 for an explanation of the boxplots.*

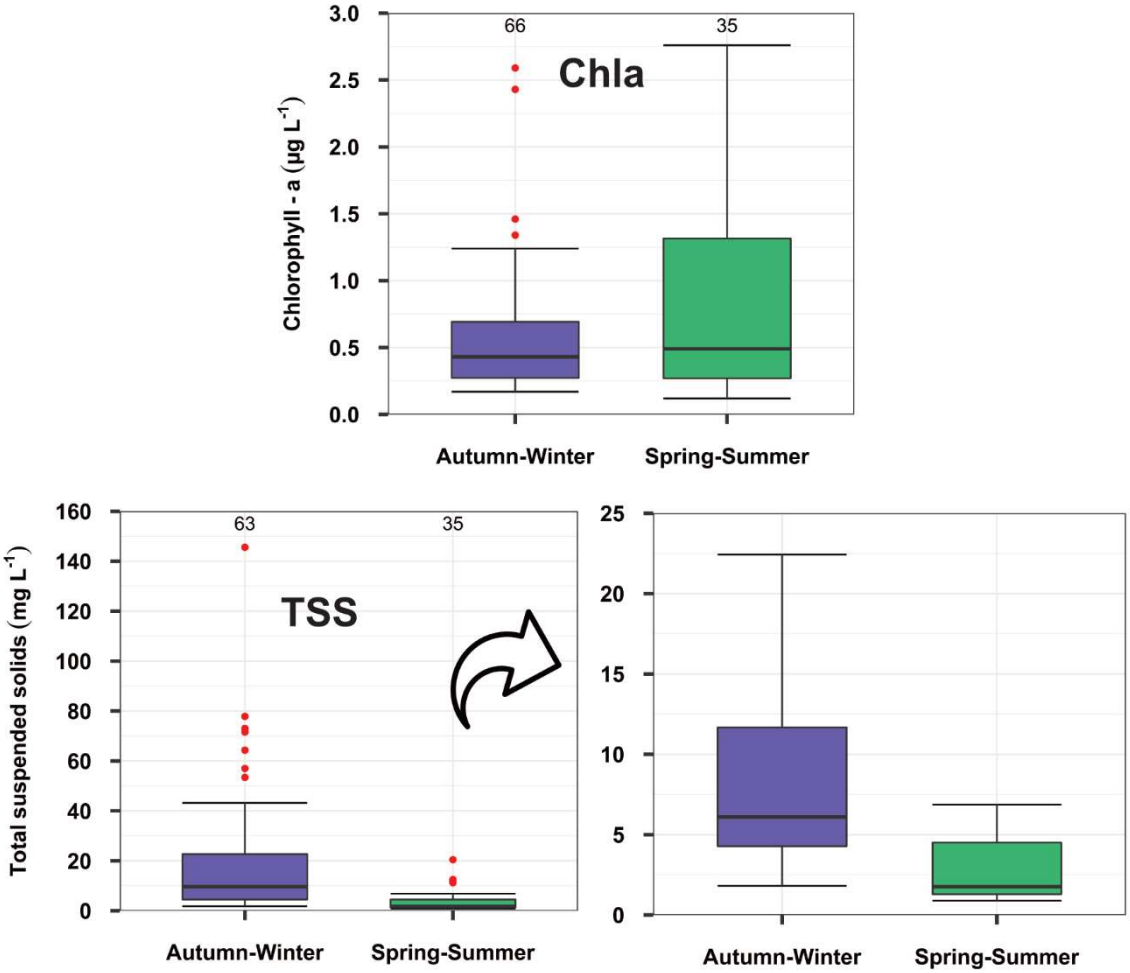

Figure D4. *Boxplot of Chlorophyll-a and TSS by season, for the samples collected in the southern North Sea between November 2018 and July 2020. See Figure D1 for an explanation of the boxplots.*

D.4 Linear correlations of TDN, nitrate plus nitrite, TDP, phosphate and DOP with salinity divided by season

Table D3. *Equations, R^2 and significance for the linear correlations divided by season between salinity and TDN, nitrate plus nitrite, TDP, phosphate and DOP for the samples collected during the cruises onboard the RV Cefas Endeavour between November 2018 and July 2020 in the southern North Sea.*

Season	Variable vs salinity	Equation linear correlation	R^2	Significance
Autumn-winter	TDN	$y = -7.227x + 266.858$	0.29	< 0.001
Spring-summer	TDN	$y = -1.398x + 49.713$	0.01	> 0.05
Autumn-winter	Nitrate + nitrite	$y = -9.821x + 353.352$	0.56	< 0.001
Spring-summer	Nitrate + nitrite	$y = -0.672x + 25.562$	0.02	> 0.05
Autumn-winter	TDP	$y = 0.019x + 1.061$	0.00	> 0.05
Spring-summer	TDP	$y = 1.270x - 40.936$	0.40	< 0.001
Autumn-winter	Phosphate	$y = -0.085x + 3.607$	0.25	< 0.001
Spring-summer	Phosphate	$y = 0.032x - 0.873$	0.01	> 0.05
Autumn-winter	DOP	$y = 0.088x - 1.987$	0.02	> 0.05
Spring-summer	DOP	$y = 1.237x - 40.064$	0.46	< 0.001

D.5 Statistical significance of the PCA for the quantitative and qualitative data of DOM

The test showed that both PCAs run (quantitative and qualitative DOM data) were statistically significant.

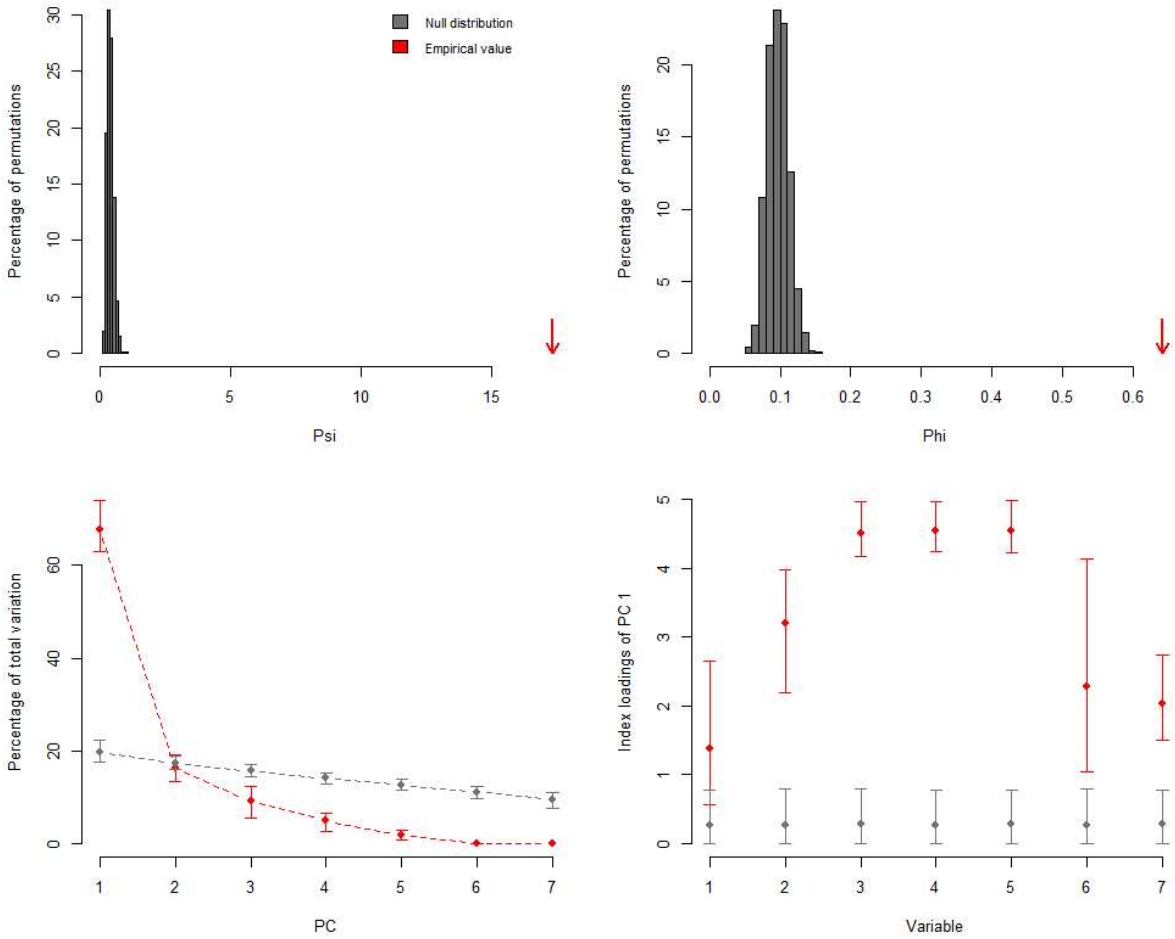

Figure D.5. *The outputs from the test on the statistical significance of the PCA run for the quantitative data of DOM for the samples collected during the cruises onboard the RV Cefas Endeavour between November 2018 and July 2020 in the southern North Sea. Plot* ***a*** *represents the null distribution of the randomised ψ and the empirical values, plot* ***b*** *represents the null distribution of the randomised φ and the empirical values, plot* ***c*** *represents the variation explained by the randomised and empirical components and plot* ***d*** *represents the index loadings of the randomised and empirical values of the significant components. The red dots indicate the mean observed values, whilst the red bars indicate the 95% confidence interval based on 1000 bootstraps replicates. The grey dots indicate the mean values of the random permutations, whilst the grey bars indicate the 95% confidence interval of the same 1000 random permutations.*

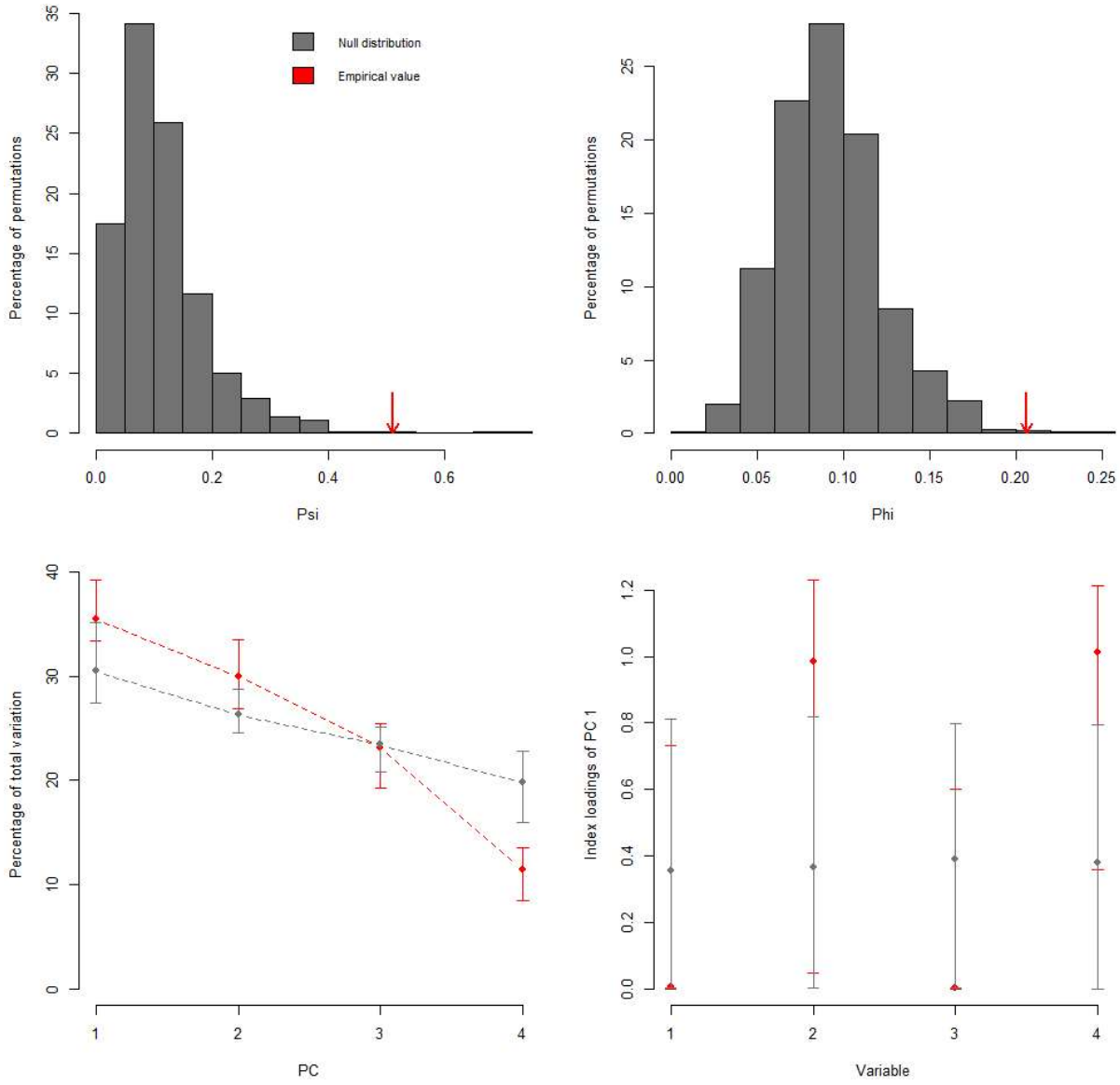

Figure D6. *The outputs from the test on the statistical significance of the PCA run for the qualitative data of DOM for the samples collected during the cruises onboard the RV Cefas Endeavour between November 2018 and July 2020 in the southern North Sea. Plot* ***a*** *represents the null distribution of the randomised ψ and the empirical values, plot* ***b*** *represents the null distribution of the randomised φ and the empirical values, plot* ***c*** *represents the variation explained by the randomised and empirical components and plot* ***d*** *represents the index loadings of the randomised and empirical values of the significant components. The red dots indicate the mean observed values, whilst the red bars indicate the 95% confidence interval based on 1000 bootstraps replicates. The grey dots indicate the mean values of the random permutations, whilst the grey bars indicate the 95% confidence interval of the same 1000 random permutations.*